Interactions involving lipid-based surfaces

From protein adsorption to membrane adhesion

Victoria Maria Latza

Kumulative Dissertation

zur Erlangung des akademischen Grades
"doctor rerum naturalium"
(Dr. rer. nat.)
in der Wissenschaftsdisziplin "Physikalische Chemie"

eingereicht an der
Mathematisch-Naturwissenschaftlichen Fakultät
Institut für Chemie
der Universität Potsdam
und
Max-Planck Institut für Kolloid- und Grenzflächenforschung

Ort und Tag der Disputation: Potsdam, den 21.02.2020

Hauptbetreuer: Prof. Dr. Ilko Bald
Betreuer: Prof. Dr. Emanuel Schneck
Gutachter: Prof. Dr. Ilko Bald, Prof. Dr. Emanuel Schneck, Dr. habil. Aleksandra Szcześ

Published online at the
Institutional Repository of the University of Potsdam:
https://doi.org/10.25932/publishup-44559
https://nbn-resolving.org/urn:nbn:de:kobv:517-opus4-445593

Abstract

Interactions involving biological interfaces such as lipid-based membranes are of paramount importance for all life processes. The same also applies to artificial interfaces to which biological matter is exposed, for example the surfaces of drug delivery systems or implants. This thesis deals with the two main types of interface interactions, namely (i) interactions between a single interface and the molecular components of the surrounding aqueous medium and (ii) interactions between two interfaces. Each type is investigated with regard to an important scientific problem in the fields of biotechnology and biology:

1.) The adsorption of proteins to surfaces functionalized with hydrophilic polymer brushes; a process of great biomedical relevance in context with harmful foreign-body-response to implants and drug delivery systems.

2.) The influence of glycolipids on the interaction between lipid membranes; a hitherto largely unexplored phenomenon with potentially great biological relevance.

Both problems are addressed with the help of (quasi-)planar, lipid-based model surfaces in combination with x-ray and neutron scattering techniques which yield detailed structural insights into the interaction processes. Regarding the adsorption of proteins to brush-functionalized surfaces, the first scenario considered is the exposure of the surfaces to human blood serum containing a multitude of protein species. Significant blood protein adsorption was observed despite the functionalization, which is commonly believed to act as a protein repellent. The adsorption consists of two distinct modes, namely strong adsorption to the brush grafting surface and weak adsorption to the brush itself. The second aspect investigated was the fate of the brush-functionalized surfaces when exposed to aqueous media containing immune proteins (antibodies) against the brush polymer, an emerging problem in current biomedical applications. To this end, it was found that antibody binding cannot be prevented by variation of the brush grafting density or the polymer length. This result motivates the search for alternative, strictly non-antigenic brush chemistries. With respect to the influence of glycolipids on the interaction between lipid membranes, this thesis focused on the glycolipids' ability to crosslink and thereby to tightly attract adjacent membranes. This adherence is due to preferential saccharide-saccharide interactions occurring among the glycolipid headgroups. This phenomenon had previously been described for lipids with special oligo-saccharide motifs. Here, it was investigated how common this phenomenon is among glycolipids with a variety of more abundant saccharide-headgroups. It was found that glycolipid-induced membrane crosslinking is equally observed for some of these abundant glycolipid types, strongly suggesting that this under-explored phenomenon is potentially of great biological relevance.

Kurzfassung

Wechselwirkungen lipid-basierter Oberflächen:

Protein-Adsorption und Membran-Adhäsion

Wechselwirkungen, die von biologischen Grenzflächen wie Lipidmembranen eingegangen werden, haben tiefgreifende Auswirkungen auf alle Lebensprozesse. Dasselbe trifft auf alle künstlichen Grenzflächen zu, die in Kontakt mit biologischer Materie treten. Die Oberflächen von Wirkstoffverabreichungssystemen oder Implantaten sind hierfür prominente Beispiele. Diese Dissertationsschrift behandelt zwei Hauptkategorien von Grenzflächen-Wechselwirkungen: Zum einen die Wechselwirkung zwischen einzelnen Grenzflächen und den molekularen Komponenten des wässrigen Umfelds; zum anderen die Wechselwirkung zwischen zwei Grenzflächen. Jede dieser beiden Wechselwirkungskategorien wurde unter Bezugnahme auf eine wichtige wissenschaftliche Fragestellung aus den Bereichen der Biologie und Biotechnologie untersucht:

1.) Die Adsorption von Proteinen an Oberflächen die mit hydrophilen Polymerbürsten funktionalisiert sind; diese Anlagerung von biologischem Material stellt einen Prozess von äußerster biomedizinischer Relevanz dar, der beispielsweise beim Auftreten der schädlichen Fremdkörperabstoßung von Implantaten oder Wirkstoffverabreichungssystemen eine entscheidende Rolle spielt.
2.) Der Einfluss von Glykolipiden auf Wechselwirkungen zwischen Lipidmembranen, einem bislang größtenteils unerforschten Phänomen von potentiell herausragender biologischer Bedeutung.

Die Bearbeitung beider Fragestellungen erfolgte unter Verwendung (quasi-)planarer, lipid-basierter Modellsysteme in Kombination mit Röntgen- oder Neutronenstreuung, welche detaillierte strukturelle Einblicke von Wechselwirkungsprozessen liefern. In Bezug auf die Adsorption von Proteinen an polymer-funktionalisierte Oberflächen wurde zunächst ein Szenario behandelt, bei dem die Oberflächen menschlichem Blutserum ausgesetzt sind, welches eine Vielzahl verschiedener Proteinspezies enthält. Die verwendete Funktionalisierung gilt gemeinhin als proteinabstoßend. Anders als erwartet zeigte sich dennoch signifikante Adsorption von Blutproteinen auf der Oberfläche. Die gemessene Adsorption weist zwei unterschiedliche Arten auf: Starke Adsorption an die Oberfläche, an die die Polymere kovalent gebunden sind, und schwache Adsorption an die Polymerbürste selbst. Der zweite Aspekt, der beleuchtet wurde, sind die Folgen von Antikörpern gegen die Bürstenpolymere. Deren zunehmendes Vorkommen stellt ein Problem für biomedizinische Anwendungen dar. Die Ergebnisse der Arbeit zeigen, dass die starke Adsorption von Antikörpern nicht durch die Veränderung von Bürstenparametern, wie Anbindungsdichte oder Polymerisationsgrad, aufgehalten werden kann. Diese Erkenntnis motiviert die Suche nach

alternativen, nicht-antigenen Bürstenmaterialien. In der zweiten Wechselwirkungskategorie, dem Einfluss von Glykolipiden auf Wechselwirkungen zwischen Lipidmembranen, wurde die Fähigkeit der Glykolipide zur Membran-Adhäsion und der damit einhergehenden starken Anziehung von aneinander liegenden Membranen beleuchtet. Die Kohäsion erfolgt dabei über anziehende Saccharid-Saccharid-Wechselwirkungen der Kopfgruppen. Dieses Verhalten wurde schon für Lipide mit speziellen Oligosaccharid-Motiven beschrieben. Daher wurde bei der Untersuchung der Adhäsionsfähigkeit besonders die Verbreitung des Phänomens unter Glykolipiden mit häufig vorkommenden Saccharid-Kopfgruppen fokussiert. Es zeigte sich, dass die von Glykolipiden hervorgerufene Adhäsion auch für einige dieser häufig vorkommenden Glykolipidtypen beobachtet werden kann. Dies deutet darauf hin, dass dieses Phänomen von weitreichender Bedeutung für die Biologie ist und daher weiterhin intensiv erforscht werden sollte.

1 Introduction

1.1 Motivation

Biological matter is composed of a diversity of functional biomolecular assemblies of microscopic and nanoscopic dimensions. Typical examples are proteins and protein aggregates, as well as biomembranes in the form of cell outer membranes or intercellular membrane systems such as the Golgi apparatus [1]. Cells in general have to be viewed as densely packed compartments consisting of only about 70 % water, while the rest is constituted by biomolecules and structures assembled thereof. The surface area exposed by these structures to the aqueous medium is enormous. In eukaryotic cells the surface area of the membranes has the magnitude of around·10^5 μm^2, whereas the volume is in the range of around·10^3 μm^3. Interestingly 98 % of the area is constituted from internal membranes and only 2 % from the outer plasma membrane [2]. The characteristics of interfaces are therefore of paramount importance for the function of all biological matter, and phenomena involving interfaces are equally relevant for the artificial interfaces of foreign bodies introduced in an organism, such as drug delivery systems, stents, catheters, and pacemakers [3-7].

Key aspects of the behavior of interfaces are their interactions with the environment. To this end one distinguishes between two basic types of interactions: On one hand, interfaces experience interactions with the components of the aqueous medium, such as ions and water-soluble saccharides, nucleic acids, amino acids, and proteins. On the other hand, interfaces also experience interactions with other interfaces in the crowded environment of biological matter. Prototypical examples of the latter are interactions between neighboring biomembranes [8].

This thesis deals with the structural exploration of these two fundamental interaction phenomena. To be more precise, each of the two phenomena is investigated with regard to an important question in the fields of biotechnology and biology, respectively.

Topic 1 The adsorption of proteins to surfaces with biocompatible functionalization (see Figure 1 A);

Topic 2 The interaction between lipid membranes containing glycolipids (see Figure 1 B);

Although these two processes are scientifically independent cases of interactions involving interfaces, they are addressed in this thesis with a common approach:
The use of experimental (quasi-)planar model interfaces in combination with the deployment of scattering techniques which yield valuable and detailed structural insight; the model systems are designed with a well-controlled architecture based on the self-assembly of phospholipids, a main constituent of biological membranes.

Taking this approach, the thesis not only establishes the usability of phospholipid-based systems in combination with scattering techniques to extract structural information on interaction mechanisms, but also contributes to a deeper understanding of the two scientific cases mentioned before, which will be introduced in more detail in the following.

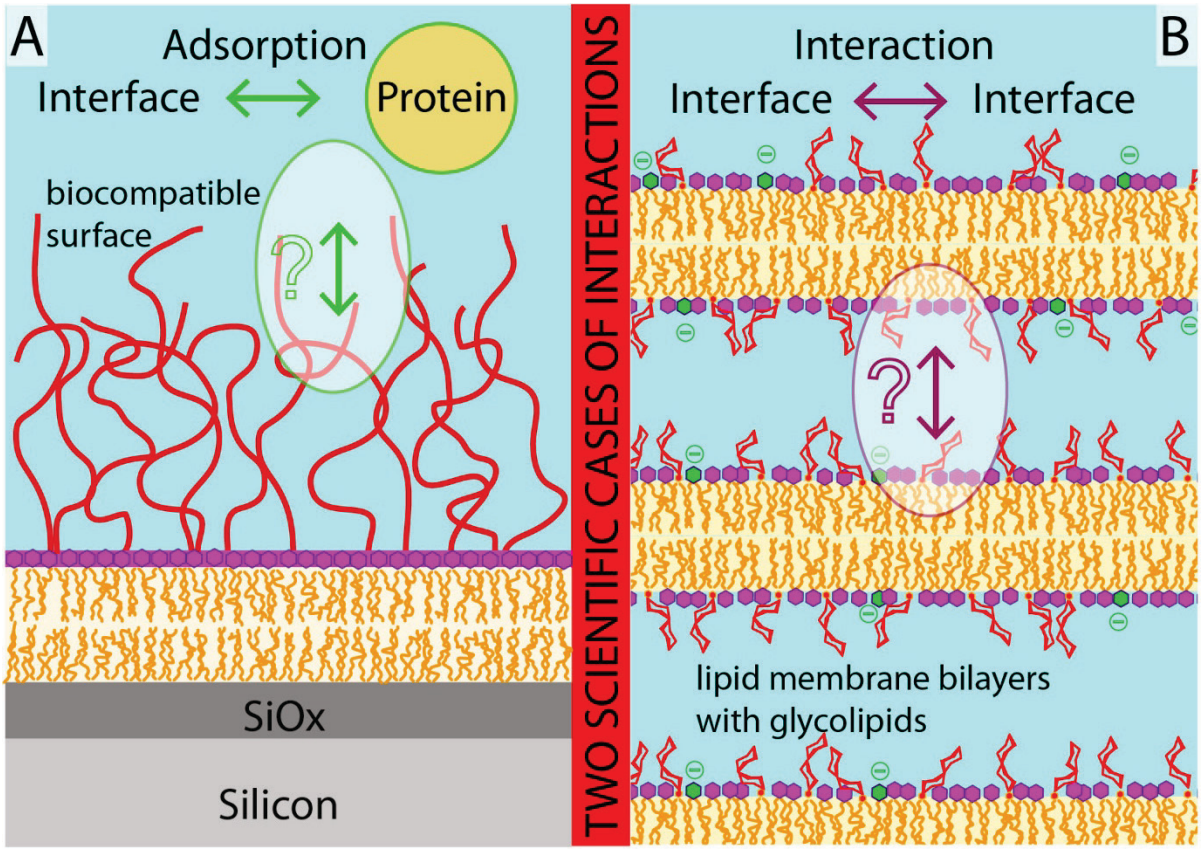

Figure 1 Scheme of the two separate scientific cases studied in this thesis: Left) Adsorption of proteins to phospholipid surfaces with biocompatible functionalization with poly[ethylene glycol] (PEG). Right) Interaction between two adjacent membranes in a multilayer system of phospholipid membranes with incorporated glycolipids.

1.1.1. Adsorption of proteins to surfaces with bio-compatible functionalization

Surface functionalization with polymers has become vastly popular in biotechnology and medical applications but also in other industrial sectors like tools manufacturing, paintings and lacquers and cosmetics [9]. Product quality is aimed to be enhanced by the use of polymers. Polymers exhibit positive characteristics that make paintings less viscous but at the same time more easily spreadable. Tools might be more effective by lessening friction by a surface functionalization with polymers. Massive research efforts are undergone. To that end even screws that can be purchased in a building supply store are possibly covered with polymers. Biomedical applications in clinical practice involving the insertion of foreign bodies into the human organism, such as implants, stents, catheters or drug delivery systems [4-6], are commonly equipped with polymer coatings of hydrophilic polymers, e.g. poly[ethylene glycol] (PEG). The deployment of terminally grafted PEG is widely known as *PEGylation* [10]. It aims to enhance biocompatibility [3, 4, 7] by repressing protein adsorption. Adsorption of proteins is believed to be the initial stage of harmful reactions to a foreign material like blood clotting, inflammation, and immune response [11-14]. The adsorption of proteins onto *PEGylated* surfaces has been subject of research since the 1980s [15-17]. However, it is still unclear why *PEGylation* sometimes works, while on other occasions it does not meet the expectations. In fact, only the applications on the nanoscale, such as *PEGylated* protein drugs [18] and stealth liposomes [4], have led to industrial exploitation on the billion dollar scale [18]. PEG has been initially thought to be fully biocompatible. The term biocompatibility is defined as the *ability of a material to perform with an appropriate host response in a specific situation* [19]. A biocompatible foreign material is able to fulfill its function inside the body, despite certain responses of the body that occur. In the case of PEG it was longtime believed that it can even inhibit certain host responses: The formation of antibodies (anti-immunogenicity), the binding of specific antibodies (non-antigenicity), and the adsorption of proteins, initiating the foreign body reaction (anti-fouling). Starting around the 2000s contradictory evidence appeared: anti-PEG antibodies (Abs) of clinical significance were identified in the blood of test persons in contact with PEG [20-22] and crystallographic data evidenced PEG binding to specific sites of proteins [23, 24].

These aspects were identified as main limitations of this technology and constitute the focus of the first part of this thesis, which deals with protein adsorption to surfaces:

a) (Non-specific) adsorption of proteins from human blood serum (HBS) to *PEGylated* surfaces;

b) The (cap)ability of antibodies to bind specifically to *PEGylated* surfaces (antigenicity);

The human blood contains many different proteins namely 22 abundant and around 10^4 minority species [25], but also components like glucose, mineral ions, carbon dioxide and blood cells. Initially it was commonly believed that the interactions between blood and polymers are merely repulsive [26]. However, these various types of proteins can in principle all interact differently with polymer brushes. The knowledge about structural details of these interactions has remained limited up to today. For that reason this thesis aims to contribute structural details by investigating the distribution of adsorbed proteins in terms of concentration profiles as a function of the altitude (see Figure 1 A).

Moreover, it was found that anti-PEG Abs have become increasingly abundant in the human population [27]. This discovery has a huge impact because anti-PEG Abs are very likely to negate the effect of *PEGylation* in clinical applications. Therefore adsorption of backbone-binding (BB) and end-binding Abs (EB) to planar, solid supported PEG functionalized lipid interfaces (see Figure 1), varying in grafting density σ and polymerization degree N are systematically investigated in this thesis. The spatial distribution of adsorbed Abs at the interface sheds light on mechanisms encoded in the obtained structural information. A key question in this context is how effectively these two types of Ab adsorb to the polymer brush. With the variation of the grafting density σ and polymerization degree N, mechanisms which en- or disable the adsorption can be investigated.

The investigated lipid-based surfaces anchoring the PEG chains (see Figure 1), seem to be well suited models to describe interactions of biomedical devices or drug delivery systems in the human body with molecules in solution mimicking proteins solubilized in the body fluids. The lipid-based model systems are well controlled regarding their composition and lateral density (see also methods section) and allow the variation of parameters in a simple way. Solid supported lipid-monolayers (see Figure 1 A) are formed by self-assembly in lateral direction at the air water interface. Within this technique it is especially easy to change the grafting density σ of the *PEGylated* lipid components and also the length of the polymers by using different PEG-lipids with different polymerization degrees N. Moreover the systems have proven a high degree of reproducibility [28].

In order to access the mentioned protein distributions, that are essential for a deeper understanding of underlying adsorption mechanisms, the scattering technique of neutron reflectometry (NR) was chosen. NR is uniquely suited to structurally characterize protein adsorption to the brush grafting surface. It resolves matter distributions on molecular length scales perpendicular to planar interfaces with high depth resolution. The data obtained by NR yield statistically relevant information because the whole area of the sample is measured.

1.1.2. Interaction between lipid membranes containing glycolipids

Membrane-membrane interactions in a liquid medium include the whole spectrum of interfacial forces such as electrostatic forces, van der Waals forces, inter- and intramolecular hydrogen bonding solvation forces and steric forces [29]. The contribution of each force is determined by the surface chemistry and the components of the liquid medium. Therefore it can be claimed that composition of the surface plays a key role, when looking at interactions between membranes. Phospholipids are for example the main constituent of natural membranes, exhibiting polar headgroups to the surface. Other surface determining components can be charged lipids, hydrophilic polymers, proteins or sugars. These sugargroups originate often from glycolipids that are abundant in biological membranes. Glycolipid rich membranes are present e.g. in the stacked membranes of thylakoids [30], the plants' photosynthetic power station. Strikingly, also in other naturally stacked membrane systems like myelin sheaths [31] high fractions of glycolipids are present. The correlation of high glycolipid fractions in stacked membranes points towards a significant role of glycolipids in membrane adhesion. But little has been actually investigated about the influence of glycolipids on membrane interactions. In this thesis the influence of glycolipids on the interaction of membranes is investigated.

For this purpose mulitlayers of phospholipid membranes with incorporated glycolipids were chosen (see Figure 1 B). The interaction of stacked phospholipid membranes containing defined mole fractions of commercially-available glycolipids with various types of uncharged saccharide headgroups, ranging from mono- to tetra-saccharides is studied. In order to test the stability of the crosslinking against tensile stress, the membranes are further loaded with defined mole fractions of charged phospholipids inducing controlled electrostatic repulsion between the membrane surfaces. The influence of these glycolipids on the interaction between adjacent membranes is quantified with the help of the scattering technique small-angle x-ray scattering (SAXS), which yields the lamellar period of the multilayers. Additional information on the mechanical properties of the interacting membranes is obtained by neutron diffraction (ND) with planar, solid-supported membrane multilayers.

1.2 OUTLINE

In **Chapter 1.3** *State of the art*, the current level of knowledge regarding the research questions, presented in Chapter 1 *Introduction*, is described. For the sake of clarity, there is a subsection for each of the two interaction phenomena. First a general overview about theoretical basic knowledge is given. This part is followed by a short introduction of relevant experimental methods and a short summary of the knowledge gained with exemplary studies from literature using these methods.

In **Chapter 1.4** *Publications*, an overview of publications is provided, divided in first and second author publications. The first author publications constitute this thesis and can be found as reprints in the Appendix I.

In **Chapter 2** *Discussion*, the main results regarding the two research question are discussed and summarized. Also here, there are two subchapters for the phenomena.

Chapter 3 *General summary*, provides an executive summary of Chapter 2, and the main conclusions.

In the **Appendix I** *Manuscript*s, the reprints of the three first author publications, including Supporting information, can be found. In Part **II** of the **Appendix** all the information about the systems can be found regarding *chemicals/materials, sample preparation and scattering techniques*. The scattering techniques were the primary experimental methods of this thesis. There are explained in detail in this section, in order to facilitate the access to the publications. The **Appendix III** contains the citations for the utilized *literature*.

1.3 State of the art

1.3.1 Protein adsorption to functionalized surfaces

Biomedical applications, such as implants, stents, and drug delivery systems [4-6] are often equipped with a coating. In many cases this coating is made from the polymer poly[ethylene glycol] (PEG). The deployment of terminally grafted PEG is widely known as the *PEGylation* technology [10] aiming to repress protein adsorption and is therefore enhancing biocompatibility [3, 4, 7]. Problems that occur due to protein adsorption are e.g. blood clotting, biofouling and immune response [11-14]. However, it is still unclear why *PEGylation* sometimes works, while on other occasions it does not meet the expectations.

1.3.1.1 General background and theory

There are three fundamental modes reported in the literature concerning protein adsorption to polymer brushes (see Figure 2): (i) primary adsorption located at the grafting surface of the brush due to attraction between the proteins and the surface at short length scales [32, 33]. (ii) secondary adsorption occurring at the verge of the brush due to a counterbalance of favorable interactions between proteins and the surface at long length scales and the osmotic barrier upon protein insertion into a brush based on repulsion between polymer and proteins [32-35]. (iii) ternary adsorption located in the brush due to attraction between polymer and proteins [36-38].

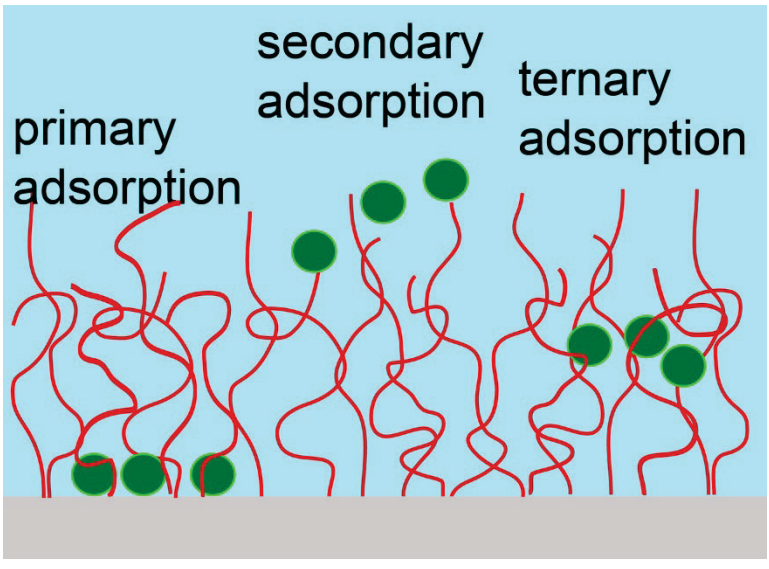

Figure 2 Illustration of the three adsorption modes reported in literature. A PEG polymer brush (red wavy lines) is grafted to a surface (grey block). Green circles represent globular proteins and their location characterizes the adsorption mode: (left) adsorption at the grafting surface: primary adsorption, (middle) adsorption at the brush periphery: secondary adsorption, and (right) adsorption within the brush itself: ternary adsorption.

The successes of *PEGylation*, used since the 1980s [15-17], have been attributed to repulsive interactions between PEG and proteins [26]. Based on experiments, PEG was believed to be a non-immunogenic material [26, 39, 40]. This view of PEG and brushes thereof is widely held to the present although evidence to the contrary emerged from the 2000s onwards:

(i) small angle neutron scattering and light scattering results evidenced weak attraction rather than repulsion between proteins and PEG [41, 42];

(ii) adsorption experiments with proteins exhibiting deviations of the surface mass density with respect to the grafting density σ or the polymerization degree N indirectly revealed ternary adsorption [36, 43];

(iii) crystallography measurements proved the binding of PEG to specific protein binding-sites [23, 24];

(iv) analysis of blood showed the appearance of anti-PEG IgG Abs among the population [20-22];

So far a lot of research in the field of theoretical calculations or simulations and physical chemistry dealing with protein-PEG interactions (non-specific and specific) concerns typically the incubation of interfaces with only one type of protein [39, 44]. In contrast to this scenario, where the concentration and the molecule interacting with PEG are clear beforehand, experiments with blood are more complex. Despite the huge challenge to identify the type of protein adsorbed to a surface from a mixture of 22 abundant proteins and a total of $\approx 10^4$ minority species [25], in dependence of the location in terms of distance to the grafting surface and time (Vroman effect [45]), the study of surfaces in contact with blood is of significant relevance for advancements in biomedicine.

Recently a proteomics technique revealed 147 protein species originating from blood serum adsorbed onto gold nanoparticles covered with PEG brushes [22] and 24 protein species originating from blood plasma adsorbed onto PEG brushes grafted to a planar gold surface [46]. These studies propose that the grafting density and the chemical end-motif of the polymer chain influence the types of proteins that adsorb. Interestingly it was found that fibrinogen (Fbg) and human serum albumin (HSA) bind to PEG when they originate from blood plasma and not from single protein solutions, which reveals an unknown mechanism, where further adsorption is provoked by a different already adsorbed protein type [46]. This sequential mechanism resulting in a layered structure of proteins emphasizes the importance of the location of adsorption. Therefore it is crucial to identify the distribution of adsorbed proteins in terms of concentration profiles as a function of the altitude, meaning the distance to the grafting surface, on a molecular length scale.

1.3.1.2 Experimental techniques characterizing protein adsorption to surfaces

In the following, details about state of the art techniques suitable to investigate protein adsorption to surfaces are described with a particular focus on polymer functionalized surfaces.

1.3.1.2.1 Qualitative techniques

In order to determine an unknown composition and chemical identity of adsorbed proteins polyacrylamide gel electrophoresis (PAGE) or liquid-chromatography mass-spectrometry (LC-MS) are prominent and widely used techniques [46-48]. A special form of LC-MS (high pressure liquid-chromatography-MS) is even claimed to be the most applied technique in the fields of proteomics and pharmaceutical laboratories [49].

Polyacrylamide gel electrophoresis (PAGE)

PAGE is a biochemical method separating macromolecules of different sizes and charges and enables further analyzation via reference bands. In order to split up the components an electric field is applied and the charged molecules start to migrate in the gel matrix: small molecules migrate faster and further than bigger ones. Other parameters influencing the final location of the substance are charge, molar mass, length, conformation and the gel medium itself. The molecules are separated due to their electrophoretic mobility. The different molecules appear as distinct bands and can be classified by direct comparison with the reference bands. The reference bands often stem from a protein standard, containing different proteins with known size and charge. In many applications both standard and sample are visualized in the gel by a dye. In the exemplary experiment shown in Figure 3 a blue and negatively charged staining is utilized.

Experiments determining the adsorbed protein species by PAGE are usually structured in the following way: i) the sample is incubated with protein solution ii) the sample is rinsed (washed) to get rid of unbound proteins iii) bound proteins are detached by special chemicals iv) the obtained solution is analyzed by PAGE. The protocol makes it clear that PAGE is detecting solemnly strongly adsorbed proteins and not the more loosely bound ones.

Schöttler et al. compared protein adsorption from human blood plasma on polymer (PEG and poly(ethyl ethylene phosphate) (PEEP)) functionalized nanocarriers with PAGE and other complementary techniques [47]. The blue bands in Figure 3 obtained by PAGE are direct evidence for the comparatively low adsorption of proteins to the *PEGylated* systems (PS-PEG_{44} and PS-PEG_{110}) and also PEEP-systems, since the bands appear weakly compared to reference bands (right lane). The non-functionalized system exhibits much stronger adsorption (left lane).

This method has the advantage to yield qualitative results at first glance making it extremely suitable to perform a first screening. A drawback is that there is always a reference needed, which might not always be straightforward if components are unknown. Nevertheless the molecular mass of unidentified substances can still be obtained also references. What is more, single bands can be further analyzed by simply cutting the gel, removing the part of interest, subsequent chemical extraction of the components and the final identification by another technique e.g. MS.

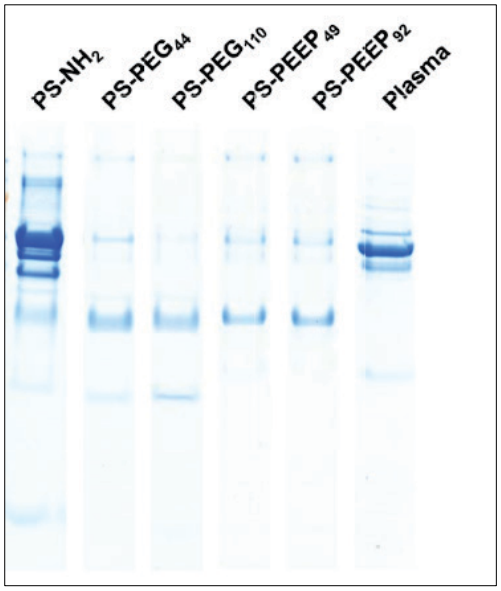

Figure 3 PAGE was used to visualize adsorption of proteins from human blood plasma on polymer functionalized surfaces of investigated nanocarriers. Dilute of adsorbed proteins of the investigated systems was separated into its different components on the gel. For comparison human plasma was loaded (right lane).
Reprinted by permission from Rightslink: [Nature nanotechnology][Protein adsorption is required for stealth effect of poly(ethylene glycol)- and poly(phosphoester)- coated nanocarriers, Schöttler S., Becker G., Winzen S., Steinbach T., Mohr K., Landfester K., Mailänder V.and Wurm F. R.] [Springer Nature] (2016).

Liquid-chromatography mass-spectrometry (LC-MS)

LC-MS is a tandem technique combining LCs ability to separate molecules of different size and charge and MS ability to identify the molecules with even higher specificity and sensitivity [49].

In a recent publication from Riedel et al. relative amounts and identity of proteins adsorbing on a *PEGylated* substrate from blood plasma were analyzed deploying LC-MS (see also the following section 1.2.1.2.2). The group found, that the protein types present in the adsorbed layer did not depend on the molecular weight, which was around 30 to 500 kDa, since the proteins adsorbed in similar amounts. From the identified masses, it was concluded that the adsorbed proteins could not enter the brush [46], and thus did not form a primary adsorption layer. This correlation must be based on the osmotic penalty. (Estimations based on the osmotic penalty, resulted in a molecular mass cutoff of ≈ 8 kDa [50].) Nonetheless, direct structural evidence would be needed to undermine this assumption. As shown in section **Error! Reference source not found.**.1.2.3 such structural insight can be obtained with reflectometry techniques.

1.3.1.2.2 Quantitative techniques

Most common and widely used methods that yield the adsorbed protein amount per unit area, are surface plasmon resonance (SPR), quartz-crystal microbalance (QCM), and ellipsometry.

Surface plasmon resonance (SPR)

SPR is able to measure precisely the dielectric properties of the sample in direct vicinity of the solid surface. This method is based on the excitation of surface plasmons by light [51, 52]. It averages over the first few hundred nanometers adjacent to the surface. Upon protein adsorption the amount of organic sample on the surface is increased and the refractive index of the sample changes, which leads to a shift in the angle of resonance (angle modulation) (see Figure 4 A, general measurement setup), or to a narrow dip in the spectrum of reflected light at a certain wavelength at a fixed angle (wavelength modulation) (see Figure 4 B, calculated spectrum). There are additional measures to enhance the sensitivity of the method.

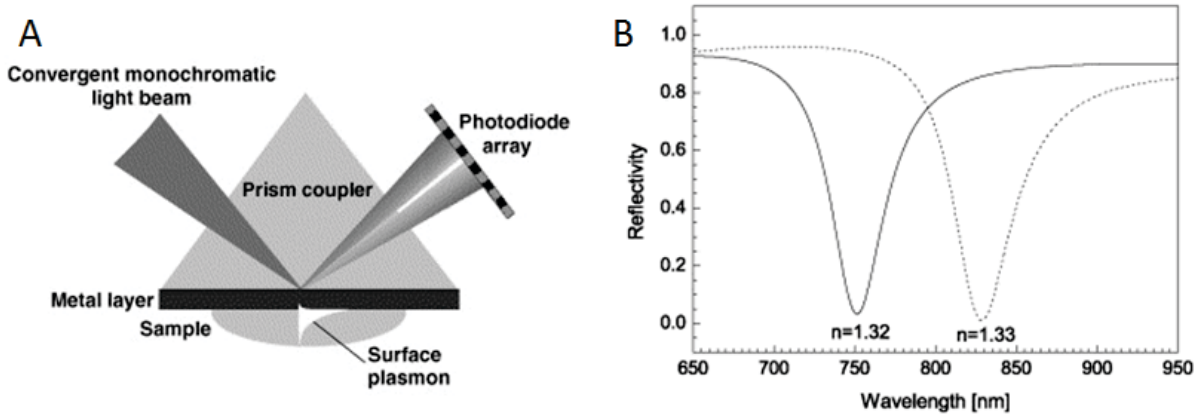

Figure 4 A) Scheme of the SPR experimental geometry in angle modulation mode. The surface plasmons are excited by a convergent beam of monochromatic light and the resonant angle is measured using a photodetector array. B) Calculated spectrum of reflected light obtained by wavelength modulation for two different refractive indices of analyte.
Reprinted with permission from [Homola, J.; Dostalek, J.; Chen, S. F.; Rasooly, A.; Jiang, S. Y.;Yee, S. S., *Spectral surface plasmon resonance biosensor for detection of staphylococcal enterotoxin B in milk.* J. Food Microbiol. 2002, **75**, 61−69.]. Copyright [2002] Elsevier.

A study in 1997 by Green et al. [53] demonstrated that SPR is suitable to follow the kinetics of protein adsorption of blood plasma proteins, albumin, Fbg and IgG to polystyrene (PS) surfaces. The data revealed that the concentration has a major impact on the timescale of adsorption and monolayer formation. Further, the investigated proteins exhibit different kinetics.

Pavey and Olliff [54] showed by SPR that the functionalization of a gold surface with a mixture of long- and short-chain PEG triblock copolymers was more effectively reducing adsorption from bovine serum albumin (BSA), than either long- or short-chain copolymers alone. The angle modulation measurements (see also Figure 5) indicated almost no or strongly reduced protein adsorption when compared to untreated gold surfaces.

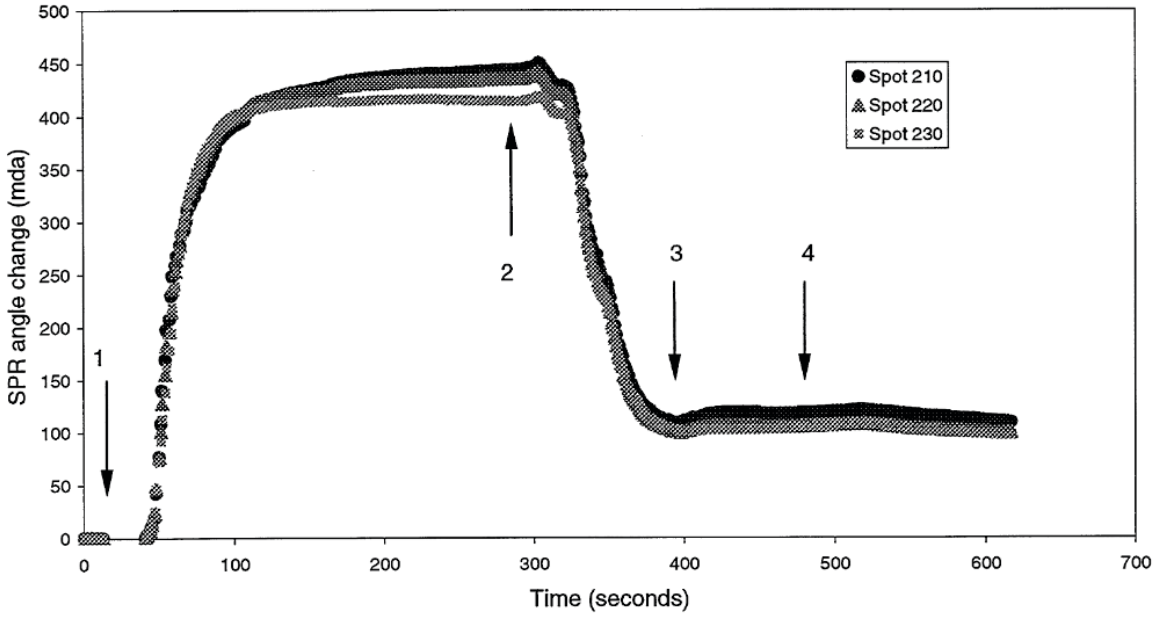

Figure 5 SPR angle change vs. time for an adsorption experiment with bovine serum albumin on a gold surface functionalized with a mixture of long- and short-chain PEG triblock copolymers. The protocol of the experiment is as follows: 1: addition of polymer mixtures in solution, 2: rinsing with buffer, 3: addition of protein, 4: rinsing with buffer. The measurement at three different locations on the sample (spot 210, 220 and 230) showed that addition of proteins (point 3) does not lead to a significant change of the angle compared to the once again rinsed sample (point 4); therefore almost no protein has adsorbed to the surface.
Reprinted with permission from [Pavey, K.D. and C.J. Olliff, *SPR analysis of the total reduction of protein adsorption to surfaces coated with mixtures of long- and short-chain polyethylene oxide block copolymers.* Biomaterials, 1999. **20**(9): p. 885-890.]. Copyright [1999] Elsevier.

In Figure 6 A a graph of the resonance wavelength in dependence of time for a wavelength modulation measurement conducted by Riedel et al. [46] is shown. (Results of this study obtained with LC-MS were presented in section 1.3.1.2.1.) The amount of adsorption from blood plasma and adsorption of HSA, IgG and Fbg on gold surfaces coated with different types of polymer layers was detected. It was shown that all the samples suffered from less adsorption than their reference without polymer (around 3 mg/m^2). For brush functionalized surfaces values between 1.2 mg/m^2 and 0.5 mg/m^2 for adsorption from plasma and between $7.5 \cdot 10^{-2}$ mg/m^2 and zero for adsorption from the single protein component solutions were obtained (see Figure 6 B). A brush from poly[oligo(ethylene glycol) methyl ether methacrylate] (PMeOEGMA) exhibited most excellent properties: 0.48 mg/m^2 for adsorption from plasma and no detectable adsorption from single component solutions. Convincingly the values for different PEG end chemistries (–Me, -OH, and –COOH) are in the same order of magnitude and do not differ significantly (see Figure 6 B).

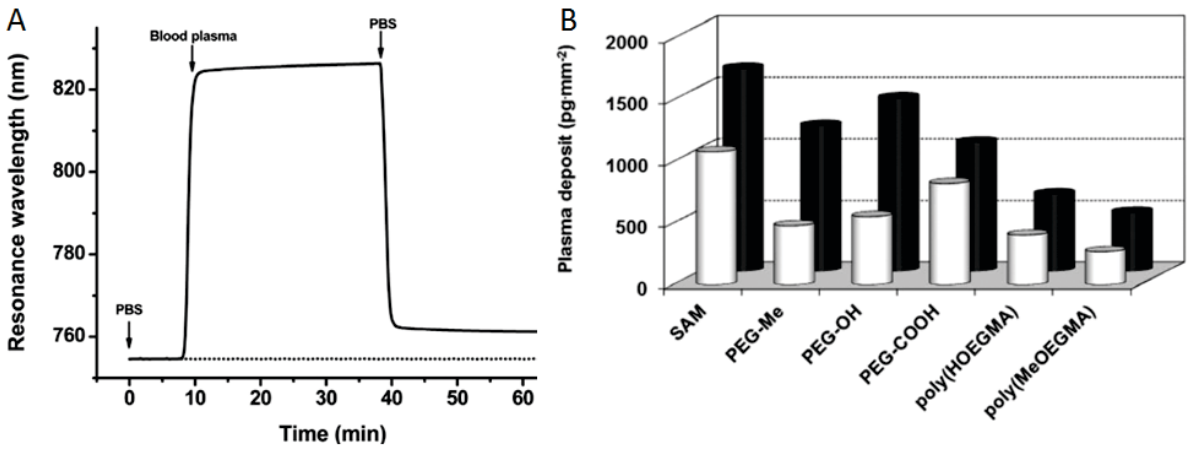

Figure 6 A) SPR wavelength as a function of time measured for PEG-COOH sample in contact with human blood plasma. The protocol of the experiment is as follows and marked by arrows: 1: rinsing with buffer (Phosphate-buffered saline (PBS)), 2: addition of protein (blood plasma), 3: rinsing with buffer (PBS). B) Mass of deposits of blood plasma after 30 min, determined from SPR measurement. Black indicates adsorption from untreated blood plasma. White indicates adsorption of blood plasma, which was ultrafiltered with a 300 kDa cutoff.
Reprinted with permission from [Riedel, T., et al., *Complete Identification of Proteins Responsible for Human Blood Plasma Fouling on Poly(ethylene glycol)-Based Surfaces.* Langmuir, 2013. **29**(10): p. 3388-3397.]. Copyright [2013] American Chemical Society.

Quartz-crystal microbalance (QCM)

QCM measures the mass bound to a crystal surface by detecting changes in the crystal's mechanical resonance frequency. In context with protein adsorption this bound mass represents the mass of the adsorbed proteins per area. In Figure 7 the outcome of such a measurement is shown [55]: Upon injection of proteins (e.g. see label BSA injected) the adsorbed mass is increasing. Rinsing with buffer (see label PBS rinse) leads to a decreasing mass of proteins due to desorption of loosely bound proteins. This technique is frequently used to follow kinetics of protein adsorption [55-57].

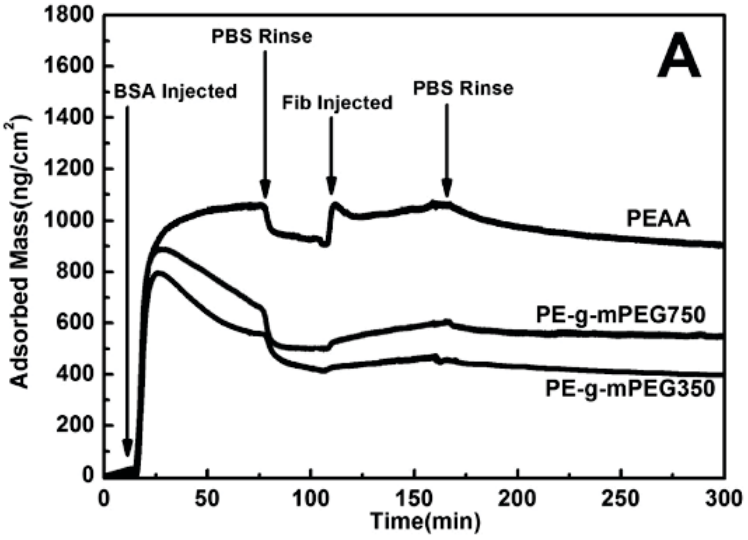

Figure 7 Outcome of QCM measurement: Adsorbed mass versus time.
Three different polymer surfaces (poly(ethylene-co-acrylic acid) (PEAA), PEG750 and PEG350 were injected with BSA and Fbg (denoted as Fib) and rinsed afterwards.
The protocol of the experiment is as follows:
1: addition of protein (BSA) 2: rinsing with buffer (Phosphate-buffered saline (PBS)), 3: addition of protein (Fbg), 4: rinsing with buffer (PBS). The surfaces exhibit different amounts of adsorbed proteins.

Reprinted with permission from [Jin, J., et al., *Plasma Proteins Adsorption Mechanism on Polyethylene-Grafted Poly(ethylene glycol) Surface by Quartz Crystal Microbalance with Dissipation.* Langmuir, 2013. **29**(22): p. 6624-6633.]. Copyright [2013] American Chemical Society.

A study on adsorption of homo-molecular solutions of various proteins on phospholipid bilayers (human Fbg, HSA, horse heart cytochrome *c*, human immunoglobulin and fetal bovine serum) deploying SPR and QCM was conducted by Glasmästar et al. in 2002 [58]. Reversible adsorption of the proteins to the bilayer of phospholipids was detected by QCM. Adsorption was in the range of 0.3 % to 4 % of the saturation coverage on a hydrophobic thiol monolayer on gold. The amounts detected with SPR were slightly higher. The 96 % to 99.7 % reduction of adsorption reveals that the bilayer of phospholipids is highly protein resistant [58].

Another aspect that has been investigated is the role of surface roughness regarding protein adsorption. Molino et al. [59] studied adsorption from BSA and fibronectin to a surface functionalized with a negatively charged polymer. For BSA it was shown that the amount of adsorbed protein is increasing by 50 % for rougher substrates (≈ 9 mg/m^2 compared to ≈ 4.5 mg/m^2). For fibronectin no such evidence was found.

Nagasawa et al. [60] prepared various polymer brushes differing in hydrophilicity and charge (see Figure 8). One important finding was that protein adsorption is prevented by brushes of hydrophilic polymers that interact strongly with surrounding water molecules (see Figure 8). Adsorption for the only hydrophobic poly[benzyl methacrylate] (PBMA) was found to be around 2.2 mg/m^2 for BSA. For most hydrophilic polymers adsorption from BSA was lower. For poly[2-methacryloyloxyethyl phosphorylcholine] (PMPC) adsorption was even below the detection limit. Only poly[2-aminoethyl methacrylate hydrochloride) (PAEMA), which exhibits high charges from amino groups, bound higher amount of BSA of around 4.5 mg/m^2. To conclude, hydrophilic and uncharged surfaces are likely to adsorb small amounts of proteins.

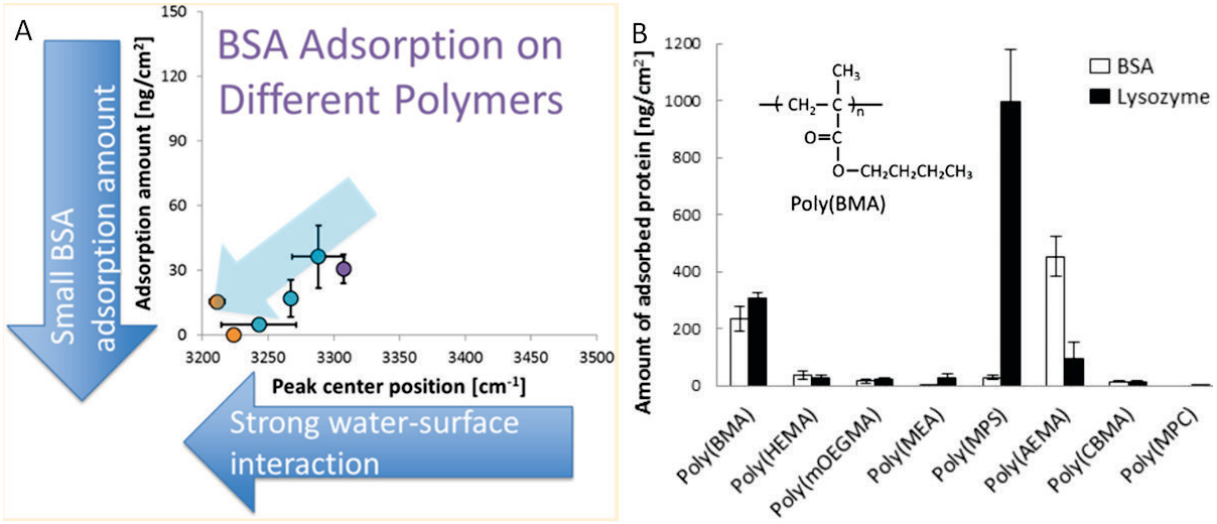

Figure 8 QCM study on the influence of hydrophilicity and charge of polymers on protein adsorption of BSA. A) Schematic illustration of the main findings of this study. Polymers that show stronger water-surface interaction are located further left. Polymers that adsorb only small protein amounts are located further down. The different colors and shapes of the graph stand for different polymers. The light blue arrow indicates that polymers with the strongest water interaction show the smallest amounts of protein adsorption. B) Amount of adsorbed BSA and lysozyme on different polymer brushes obtained by QCM.
Reprinted with permission from [Nagasawa, D., et al., *Role of Interfacial Water in Protein Adsorption onto Polymer Brushes as Studied by SFG Spectroscopy and QCM.* The Journal of Physical Chemistry C, 2015. **119**(30): p. 17193-17201.]. Copyright [2015] American Chemical Society.

Among the studies following the kinetics of protein adsorption to polymer functionalized surfaces by QCM, Tanaka et al. [57] investigated adsorption of the plasma proteins albumin and Fbg. Their results suggests different detachment rates of the proteins for the examined polymers (poly(2-methoxyethylacrylate (PMEA), poly(2-hydroxyethylmethacrylate (PHMEA) and polypropylene (PP)) which correlate with the degree of conformational changes of the proteins (PP < PHEMA < PMEA). This result suggest that the interaction between PMEA and protein is weaker compared to the other polymers. In conclusion, here reversible and irreversible adsorption was observed.

In 2013 Jin et al. [55] investigated the adsorption kinetics of BSA on poly(ethylene-co-acrylic acid) (PEAA) and *PEGylated* surfaces and subsequent of fibrinogen on the same surfaces. Two different polymerization degrees *N* of PEG were examined (see Figure 7 and Figure 9). Here, the grafting density has a strong impact on the nonspecific BSA adsorption. The sparse brush (with 0.4 % covered surface) and comparatively longer chains (PEG-MeOH Mw = 750 with $N \approx 17$) suffers from more protein adsorption (28 mg/m^2) than the denser brush (with 1.7 % covered surface) with comparatively shorter chains (PEG-MeOH Mw = 350 with $N \approx 8$) (11 mg/m^2) (see Figure 9, B). The poly(ethylene-co-acrylic acid) (PEAA) grafting surface suffered from 60 mg/m^2 adsorbed BSA (see Figure 9 B). Therefore, the surface modification with PEG reduced the adsorbed BSA amount to ≈ 1/3. It has to be noted that results of that study might not be meaningful and can hardly be interpreted, because not only grafting density but also the polymerization degree *N* was varied at the same time. Additionally the measured amounts suggest rather multilayers of adsorbed proteins since the amount of 28 mg/m^2 is around five times higher, compared to other studies.

In 2017 Hagiwara et al. [56] investigated the adsorption kinetics behavior of BSA onto a stainless steel surface. Adsorbed amounts were dependent on the BSA concentration and went up to 6 mg/m^2.

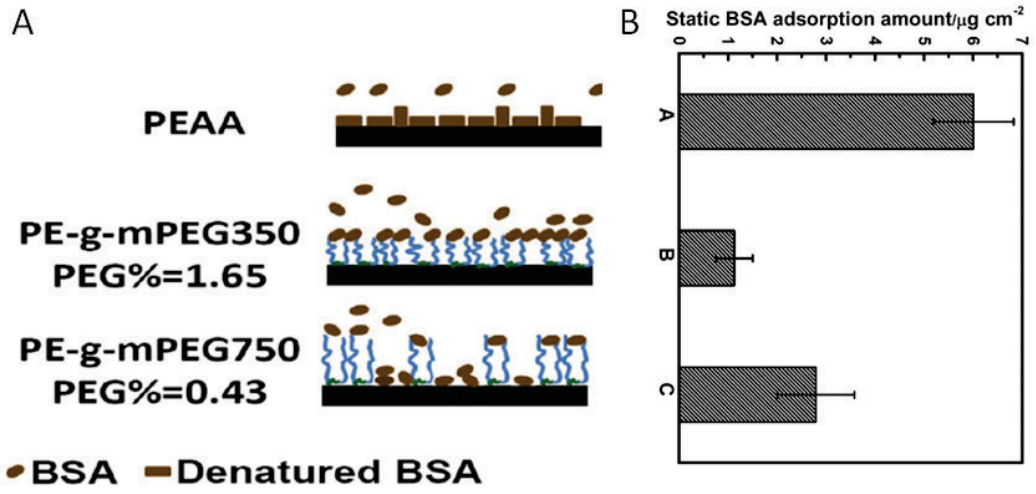

Figure 9 Results of QCM measurement (see Figure 7) of bare and of two PEG functionalized surfaces upon injection of the protein BSA. A) Schematic illustration summarizing main results of the study. The dense brush with shorter chains (PEG350), compared to the other sample (PEG750), suffers from less adsorption from BSA. B) Measured amounts of adsorbed BSA on A: bare PEAA (surface shows highest amount of adsorbed BSA); B: PEG350-sample (shows a reduced amount of adsorbed BSA compared to PEAA and PEG750-sample); C: PEG750-sample (suffers from more adsorption compared to PEG350-sample);
Reprinted with permission from [Jin, J., et al., *Plasma Proteins Adsorption Mechanism on Polyethylene-Grafted Poly(ethylene glycol) Surface by Quartz Crystal Microbalance with Dissipation.* Langmuir, 2013. **29**(22): p. 6624-6633.]. Copyright [2013] American Chemical Society.

Ellipsometry

An optical surface-sensitive technique that yields the thickness of adsorbed protein layers is ellipsometry. It is based on the variation of the polarization state of light from circular or linear to elliptical upon reflection from a surface. This explains why this technique requires reflecting surfaces, like silicon-wafers or titanium films [61]. This polarization modification for a known refractive index depends on the layer thickness and is quantified by the amplitude ratio before and after reflection and the phase difference due to reflection both encoded in the ellipticity of the reflected light [62]. Ellipsometry is a sensitive and non-destructive technique to measure thin films with thicknesses below the wavelength of light. Further it is a fast working technique acquiring data in seconds, which makes it suitable for following real-time kinetics of processes on these thin films [63]. It is also possible to use it for samples in air or liquid environments [64]. In order to obtain precise thicknesses in protein adsorption experiments, the refractive index of the protein layer should be known.

Already in 1987 Gölander and Kiss [65] performed an ellipsometry study elucidating protein adsorption of BSA, IgG, Fbg and lysine to surface functionalized silicon wafers. The surface modifications were realised by attaching polyvynil chloride (PVC), poly(methyl acrylate) (PMA) or PEG films. BSA, IgG and Fbg adsorbed to a higher degree to the hydrophobic PVC, than to hydrophobic PMA or hydrophilic PEG surfaces. Generally low amounts of adsorbed proteins (below 0.5 mg/m^2) were found on PEG films.

Another experiment dealing with protein adsorption on hydrophilic and hydrophobic substrates was conducted by Malmsten et al. [66] in 1994. It was proven that surface hydrophobicity strongly enhances the adsorption of HSA, IgG and Fbg, whereas contrary effects were found for lysozyme.

Guzman et al. [63] measured adsorption of plasma proteins from homo-molecular solutions by ellipsometry on an amphiphilic polymer network with pores. Real time data of adsorption and desorption represented by a thickness change were obtained. This system is very complex and due to the presence of pores the amount of adsorbed proteins is very large and not comparable with other studies that are part of this chapter.

Summary

This chapter has so far dealt with quantitative techniques suitable to investigate protein adsorption to surfaces: SPR, QCM and ellipsometry. There are of course more methods that are not mentioned here. To summarize most important findings from the mentioned studies that determined surface mass densities of the adsorbed proteins, it was found that,

i) hydrophilic surfaces typically exhibit lower adsorption than unfunctionalized or hydrophobic surfaces [46, 60, 65, 66];
ii) the amount of protein adsorption to phospholipid surfaces is in general very low [58];
iii) denser brushes suffer from less protein adsorption, compared to sparse brushes [55];
iv) brushes with comparatively longer polymer chains seem to suffer from more pronounced protein adsorption when at the same time the grafting density is decreased [55];
v) mixtures of long and short polymers may reduce amounts of adsorbed protein [54];
vi) the amount of adsorbed protein increases for rougher substrates [59];

The adsorbed amounts for BSA, a frequently studied protein, varied from values below the detection limit (≈ 0 mg/m^2) (e.g. on a PEG-CHO film [65] or on a PMPC brush [60]) to ≈ 5 mg/m^2 on a PAEMA brush, exhibiting high charges from amino groups [60].

1.3.1.2.3 Structural techniques: Neutron reflectometry

The methods described in the previous chapters bear the limitation of accessing the adsorbed protein amount per unit area without structural information. But indeed information on the structure of the polymer brush and the location of adsorbed proteins with respect to the brush grafting surface are important to further elucidate the adsorption mechanisms. To this end it is of particular importance to discriminate between the different adsorption modes introduced in section 1.3.1.2 (see Figure 2): i) primary adsorption to the grafting surface arising from short-range attraction between the surface and the proteins. ii) secondary adsorption at the border of the brush due to long-range attractions between the surface and the proteins and at the same time repulsion between the polymer and the protein (osmotic penalty) and iii) ternary adsorption within the brush due to attraction between the polymer and the protein [32-38]. Emanating from the positon of protein adsorption, the interaction partners (proteins and grafting surface, or proteins and polymers) can be identified and the mechanisms driving the adsorption can be elucidated.

In general scattering techniques with x-rays and neutrons provide structural information at molecular length scales, like molecular distribution functions or periodicities in crystalline structures. Neutron scattering is a non-destructive method and also x-ray scattering experiments can be designed in a way that is preserving the sample. This is very handy, when probing differences before and after incubation with e.g. proteins. Another powerful aspect is the access to buried and therefore otherwise inaccessible interfaces (see appendix II 3.1). When using scattering techniques it is not necessary to characterize layer by layer beforehand. This has proven to be very practical when handling sensitive samples that are only stable under certain conditions.

A technique that is very useful for structural investigations is neutron reflectivity (NR). Additionally to the adsorbed amount of protein, NR resolves matter distributions perpendicular to planar interfaces with high depth resolution. Therefore it is uniquely suited to structurally characterize protein adsorption to polymer brushes.

Early reflectivity studies have proven that this method has the ability to characterize solid surfaces and determine the structure and composition of the adsorbed material. In 1990 Rennie et al. [67] have been among the first to establish the use of NR to resolve structures at the solid/water interface. The investigated structure was not resolved in every detail, but it was shown that the surfactant hexadecyltrimethylammonium bromide (C_{16}TAB) adsorbs as a thick bilayer of ≈ 5 nm to the silicon surface (see Figure 10). In the model the hydrocarbon core, and the headgroups of the surfactant, water molecules, bromide ions, and the solid support were distinguished.

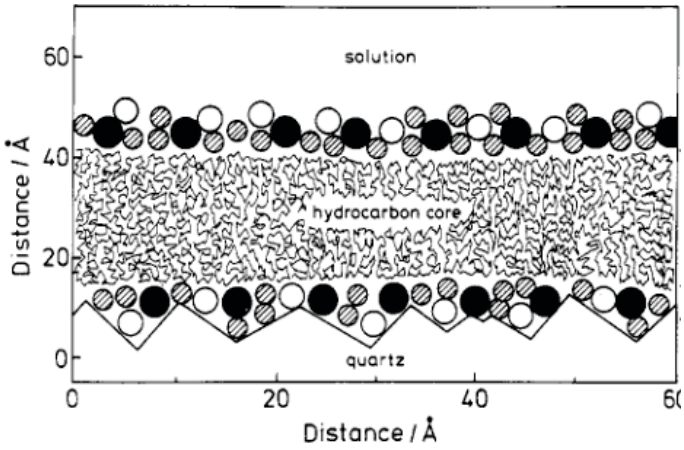

Figure 10 Schematic illustration of the structure of adsorbed C_{16}TAB on a silicon substrate. The filled black circles represent the surfactant headgroups, the unfilled circles the bromide ions and the shaded circles the water molecules.
Reprinted with permission from [Rennie, A.R., et al., *Structure of a cationic surfactant layer at the silica-water interface.* Langmuir, 1990. **6**(5): p. 1031-1034.]. Copyright [1990] American Chemical Society.

Deploying isotopic labeling of the water and the introduction of a hydrophobic layer of octadecyltrichlorosilane (OTS) further improved the method [68] (see Figure 11 A). In 1996 Fragneto and coworkers revealed the structure of a surfactant layer adsorbed at the solid/water interface in detail [69] (see Figure 11 B).

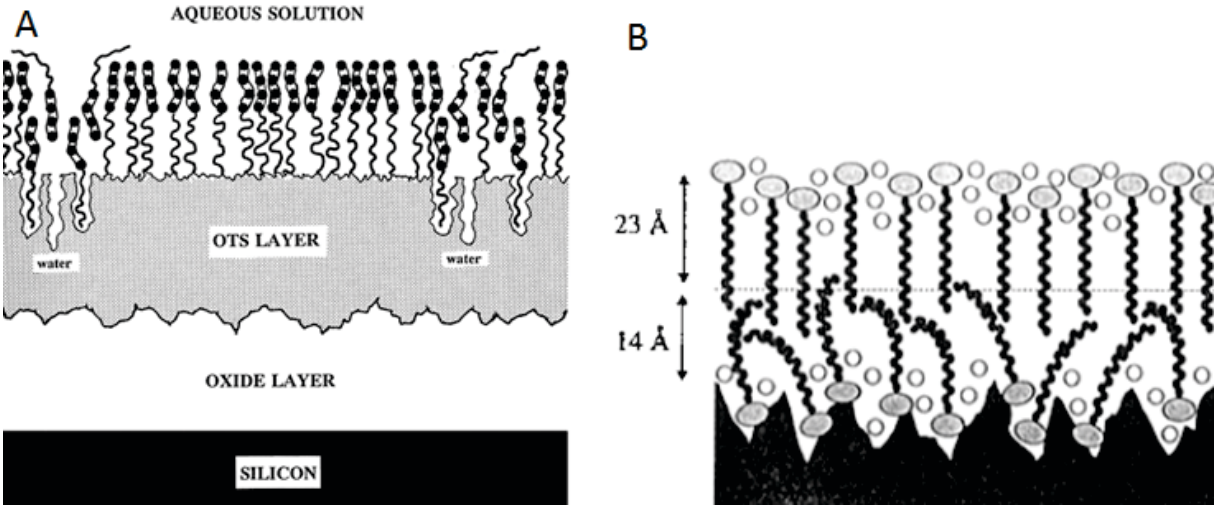

Figure 11 Schematic representation of the systems A) Surfactant tetraethylene glycol monodecyl ether adsorbed as monolayer to silicon substrate with hydrophobic OTS layer in aqueous solution. B) The surfactant C_{16}TAB is adsorbed to silicon oxide layer. In the model headgroup and hydrocarbon layer of the surfactant were distinguished. The inner and outer layers are found to be different. The inner layer is less dense.
Panel A reprinted with permission from [Fragneto, G., et al., *Structure of Monolayers of Tetraethylene Glycol Monododecyl Ether Adsorbed on Self-Assembled Monolayers on Silicon: A Neutron Reflectivity Study.* Langmuir, 1996. **12**(2): p. 477-486.]. Copyright [1996] American Chemical Society. Panel B reprinted with permission from [Fragneto, G., et al., *Neutron Reflection from Hexadecyltrimethylammonium Bromide Adsorbed on Smooth and Rough Silicon Surfaces.* Langmuir, 1996. **12**(25): p. 6036-6043.]. Copyright [1996] American Chemical Society.

Brouette et al. investigated adsorption of the globular protein myoglobin to poly(N-isopropylacrylamide) (PNIPAM) brushes [70], OTS surfaces and PS films [71]. Small amounts or even no protein adsorption to PINAM was found. Adsorption of myoglobin onto hydrophobic OTS and PS surfaces was characterized in terms of the layer thickness. In both cases two distinct protein layers were found (see Figure 12). The first adsorption layer is composed of denaturated proteins, whereas the proteins of the second layer are still intact.

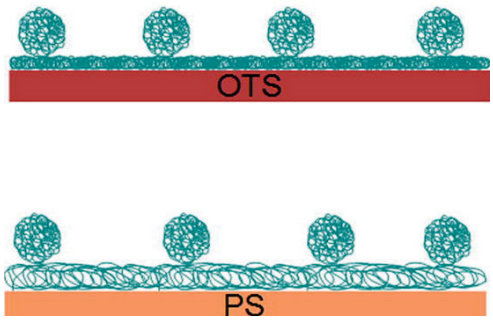

Figure 12 Schematic drawing of adsorbed myoglobin on OTS and PS surface. There are two layers of primarily adsorbed myoglobin. The first layer is denaturated. The second layer is similar in both cases.
Reprinted with permission from [Brouette, N., et al., *A neutron reflection study of adsorbed deuterated myoglobin layers on hydrophobic surfaces.* Journal of Colloid and Interface Science, 2013. **390**(1): p. 114-120.]. Copyright [2013] Elsevier.

Later on the NR approach using contrast variation was applied to protein adsorption to PEG brushes [28, 72]. A state-of-the-art volume-fraction based analysis methodology was developed, allowing the comprehensive investigation of these rather complex systems. Concentration profiles of primary adsorbed myoglobin PEG brushes grafted to hydrophobic surfaces (see Figure 13 A) could be revealed [72]. This was first structural data to identify and characterize primary adsorption to the brush grafting surface. What is more, in 2014 Schneck et al. [28] found evidence for ternary adsorption of anti-PEG antibodies binding specifically to the end segments of PEG brushes (see Figure 13 B).

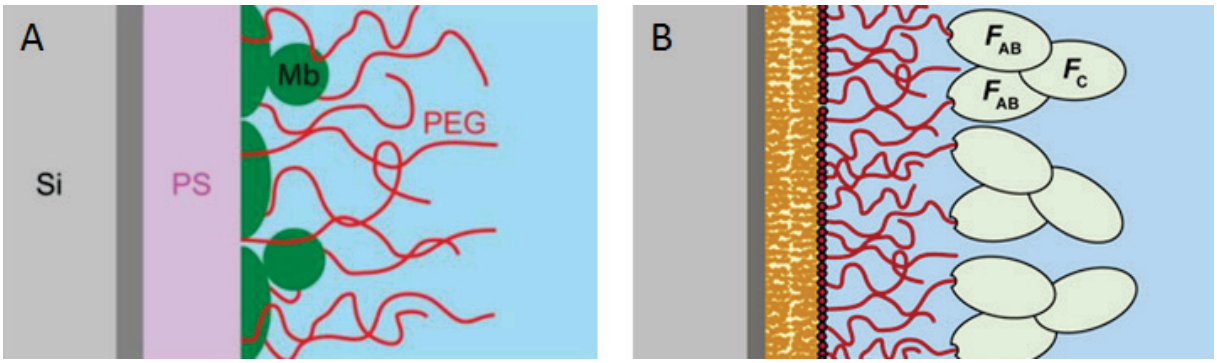

Figure 13 Schematic representation of the investigated system A) Myoglobin adsorbed to a PS grafting surface equipped with PEG brushes. B) Anti-PEG Abs adsorbing onto PEG brush immobilized to a lipid monolayer.
Panel A is reprinted with permission from [Schneck, E., et al., *Neutron Reflectometry Elucidates Density Profiles of Deuterated Proteins Adsorbed onto Surfaces Displaying Poly(ethylene glycol) Brushes: Evidence for Primary Adsorption.* Langmuir, 2013. **29**(46): p. 14178-14187.]. Copyright [2013] American Chemical Society. Panel B is reprinted with permission from [Schneck E., et al., *Neutron reflectometry from poly(ethylene glycol) brushes binding anti-PEG antibodies: Evidence of ternary adsorption.* Biomaterials, 2015. **46**: p. 95-104.]. Copyright [2015] Elsevier.

This work that combined knowledge about protein adsorption onto polymer functionalized surfaces and the ability to structurally reveal underlying mechanisms by NR lay the foundation of the here presented biological relevant studies constituting this thesis.

1.3.2 Influence of glycolipids on membrane interactions

Membrane interactions are strongly dominated by the chemistry of the headgroup layer, which forms the accessible surface of the system. Glycolipids possess headgroups known to play a key role in the interactions in naturally occurring membrane systems (see section 1.1.2). Noteworthy, glycolipids are present in abundancy in stacked membrane systems such as the thylakoids [30] of plants or the myelin sheaths [31], located in the neural system of vertebrates. This correlation suggests a significant impact of glycolipids to membrane stacking, a situation where membranes are adhered to one another.

1.3.2.1 General background and theory

1.3.2.1.1 Membrane interactions and force balance

Membrane interactions in a liquid medium include the whole range of interfacial forces such as electrostatic forces, van der Waals forces, entropic forces, solvation forces, undulation forces, and steric forces [29]. The equilibrium distance d_w between two adjacent uncharged zwitterionic PC bilayer-membranes, separated by a layer of aqueous medium, mainly results from the force balance of van der Waals attraction and hydration repulsion. At larger separation, contributions from undulation repulsion become important. When the membranes are charged additional electrostatic repulsion occurs.

Van der Waals forces

The van der Waals interaction is a combination of i) the orientation force, resulting from the orientation of permanent dipoles, ii) the induction force, resulting from the interaction between permanent dipoles and induced dipoles and iii) the dispersion force, resulting from the interaction among induced dipoles [29]. In general the outcome of this combination, in terms of the so-called Hamaker constant [29], can be attractive or repulsive. In the investigated case of adjacent lipid membranes with the same thickness, separated by a layer of the aqueous medium, the interaction is always attractive [73]. Demé et al. deployed a double film model (with one Hamaker constant $A = 5.1 \cdot 10^{21}$ J) to calculate van der Waals attraction between PC lipid membranes in fluid L_α-phase [74]:

$$\Pi_{vdW}(d_w) = -\frac{A}{6\pi}\left[\frac{1}{d_w^3} - \frac{2}{(d_w + d_H)^3} + \frac{1}{(d_w + 2d_H)^3}\right] \quad (1)$$

Here, d_w denotes the thickness of the aqueous layer (membrane separation) and d_H denotes the thickness of the hydrocarbon tails of the lipids (hydrophobic thickness).

Electrostatic forces

In interacting membrane systems with charges resulting from charged headgroups or surface-adsorbed ions, electrostatic interactions are present. For symmetric membrane systems the forces are repulsive and decay approximately exponentially with d_w under the salt conditions used in this thesis.

Hydration force

The repulsive hydration force between hydrophilic surfaces results from the preferential interaction of the surface with water molecules and other mechanisms involving the H-bond network of the aqueous medium in the vicinity of the surface. For lipid bilayers, the repulsion was empirically found to approximately obey an exponential decay [29]:

$$\Pi_{hyd}(d_w) = \Pi_0 exp\left(-\frac{d_w}{\lambda_{hyd}}\right), \quad (2)$$

where Π_0 denotes the extrapolated pressure at $d_w = 0$, and λ_{hyd} denotes the decay length.

$\Pi_0 = 4.5 \cdot 10^9\ Pa$ is a commonly used value for interacting PC lipid membranes where the membranes have the same thickness d_H, and are separated by a layer of aqueous medium with a thickness of d_w [74]. In the literature $\lambda_{hyd} \approx 2$ Å were reported [75-77].

Undulation force

The repulsive undulation force is caused by the suppression of thermal membrane undulations when the membrane separation d_w decreases. These out-of-plane undulations depend on the bending rigidity modulus κ. This entropic contribution can be neglected in multilayer systems of lipids forming stiff membranes [74]. In general the repulsive undulation interaction has a high impact at larger membrane separations, where the contributions from other forces are weaker. The undulation pressure for a solid-supported multilayer system can be determined to:

$$\Pi_{und}(d_w) = \alpha_\infty \frac{2(k_B T)^2}{\kappa d_w^3}, \quad (3)$$

where $\alpha_\infty \approx 0.23$ [78, 79] or $\alpha_\infty \approx 0.104$ [80] are values reported in literature, first derived by Helfrich [78, 79].

1.3.2.1.2 Current knowledge

Already in the 1980s experiments with glycolipid-rich phospholipid membranes have been conducted revealing spontaneous vesicle aggregation. These first in-vitro experiments used a mixture of glycolipids originating from natural thylakoid lipid extracts [81]. Ten years later, in 1990, a study using phospholipid membranes with high amounts of a single glycolipid (which is still a mixture of different chains originating from the plant thylakoids as well) [82] showed membrane stacking. These findings were based on fluorescence emission spectra coupled with electron microscopy to visualize the aggregates. Interestingly, these results suggested that cations, e.g. Mg^{2+}, induce the stacking of membranes. The role of the glycolipids was presumably underestimated at this time.

Later on differences in pressure distance curves of glycolipids and phospholipids were observed. The so-called hydration repulsion, i.e., the dehydrating pressure required to bring adjacent membranes to close proximity, was found to decay much more rapidly with the membrane separation for glycolipids [83, 84] than for commonly studied phospholipids with phosphatidylcholine (PC) headgroups [85].

Recently, Kanduč et al. quantitatively reproduced the interaction characteristics of glycolipid and PC lipid membranes in solvent-explicit atomistic molecular dynamics simulations[86]. The study revealed that the repulsion mechanisms responsible for the comparatively longer hydration repulsion range of PC lipid membranes are inoperative for the glycolipid membranes. On the basis of an interplay between long-range van der Waals attraction and hydration repulsion [87, 88], the adhesion energy for the glycolipid was thus estimated to be enhanced by a factor of approximately six with respect to PC lipids [86]. Within this picture, the tight cohesion between glycolipid membranes is rationalized solely on the basis of a shorter ranged hydration repulsion. In other words, it does not explicitly invoke attraction between the saccharide groups belonging to the opposing membrane surfaces.

Other studies have, however, demonstrated that already small fractions of glycolipids can induce pronounced cohesion between lipid membranes. For example, attractive forces were measured between lipid vesicles displaying low surface densities of membrane-bound *LewisX* [89], a trisaccharide motif known to be involved in cell adhesion processes during embryonic development [90]. Later on, neutron diffraction (ND) on membrane multilayers showed that *LewisX* glycolipids effectively cross-link adjacent membranes even against repulsive membrane interactions[91]. It was found that *LewisX* glycolipids lead to a strong confinement of the membrane separation around a value dictated by the lipids' saccharide head groups. However, in the literature one also finds indication that not only the specific trisaccharide motif *LewisX*, but also other motifs are able to crosslink membranes. Surprisingly strong attractive interactions were observed, for instance, for PC lipid membranes containing a glycolipid with a lactose disaccharide head group (N-Hexadecanoyl-

lactosylceramide, *LacCer*) at ≈ 10 mol % [92]. This finding is consistent with the observation that membrane-bound lactose has a similar effect on membrane adhesion as membrane-bound *LewisX* [89].

Little has been actually investigated concerning the abundancy of this phenomenon among glycolipids. In this thesis the influence of glycolipids on the interaction of membranes is investigated systematically.

1.3.2.2 Experimental approaches to study membrane interactions

1.3.2.2.1 Pressure distance curves

Pressure-distance curves quantify the interaction of extended surfaces and liquids by relating the interaction pressure *Π* to the surface separation or solvent layer thickness d_w.

The so called surface force apparatus (SFA), going back to Israelachvili [93], is an instrument that yields force-distance profiles $F(d_w)$, the normal force *F* between two immobilized hard and curved surfaces upon separation d_w. The force-distance profiles exhibit an 1 Å resolution in distance and a 10 pN resolution in force [94]. In order to obtain pressure-distance curves, $\Pi(d_w)$ is approximated from $F(d_w)$ via mathematical considerations [29]. Typically, SFA is used deploying mica (group of minerals belonging to the layered sheet-silicates) substrates [94].

SFA, developed in the 1970s, is a versatile technique that is still widely used to study interfacial interactions. In 2013, Orozco-Alcaraz and Kuhl [94] obtained force-distance profiles by SFA to compare interactions between two bilayer membranes formed by the lipid 1,2-dipalmitoyl-sn-glycero-3-phosphocholine (DPPC) supported on SiO_2-covered mica or bare mica (see Figure 14). Van der Waals attraction was measured upon separation of the membranes in both systems (SiO_2-covered mica or bare mica supported bilayers). For different ionic strength (salt concentrations of the aqueous media of 0.5 and 1.5 M KNO_3) an adhesion of ≈ 0.65 mN/m and an adhesive minimum of ≈ 30 Å were found. Reduced long-range repulsion with rising salt concentration suggests the presence of electrostatic interactions.

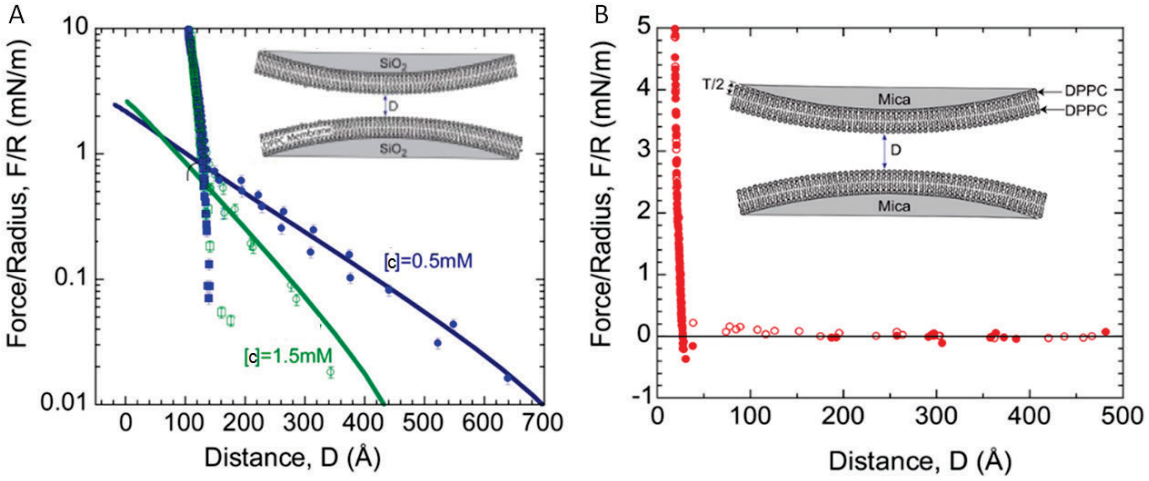

Figure 14 SFA measurements yield force-distance curves. DPPC membrane interactions are compared for A) SiO_2-covered mica solid support and B) Bare mica solid support. A) Measurement of DPPC membrane on SiO_2 was conducted at different ionic strengths (salt concentrations of 0.5 M and 1.5 M KNO_3). In the graph D = 0 is defined as the contact between bare SiO_2- SiO_2 surfaces in 0.5 M KNO_3. B) Measurement of DPPC membrane on mica was conducted at a salt concentration of 0.5 M KNO_3. In the graph d_w is denoted as D, where D = 0 is defined as the contact between two non-hydrated bilayers;
Reprinted with permission from [Orozco-Alcaraz, R. and T.L. Kuhl, *Interaction Forces between DPPC Bilayers on Glass.* Langmuir, 2013. **29**(1): p. 337-343.]. Copyright [2013] American Chemical Society.

In order to determine interactions between self-assembled multi-bilayer membrane structures other techniques are applied more commonly. X-ray or neutron diffraction experiments at controlled humidity and therefore at known equivalent osmotic pressures Π yield d_w. Similar to SFA, this method was established in the 1970s when Parsegian and coworkers performed measurements of membrane multilayers that quantified for the first time the hydration force [76, 77, 85], which acts between hydrophilic surfaces at short interaction distances (see also section 1.3.2.1.1). For uncharged PC lipid membranes the hydration decay length was found to be ≈ 0.3 nm [77]. More recently, a much shorter decay length of ≈ 0.1 nm was found for glycolipid membranes [83]. With increasing interaction distance the repulsive pressure decays much faster for glycolipid membranes compared to PC lipid membranes [86].

1.3.2.2.2 Interacting membranes at full hydration

In contrast to the approach discussed above there is also the possibility to investigate membrane multilayers at zero osmotic pressure *Π*, realized by full hydration of the sample. The bilayers are separated by the equilibrium distance d_w, whose response upon variation of external parameters such as salt concentration, pH or temperature gives insight into the interaction potential and its components (e.g. van der Waals attraction, electrostatic repulsion, or undulation repulsion). The equilibrium distance d_w can be probed via x-ray and neutron scattering techniques such as small angle x-ray scattering (SAXS) or neutron diffraction (ND).

In various studies the equilibrium distance of periodic multilayer systems upon presence of free molecules has been interpreted in terms of interaction forces.

Aroti et al. [95] characterized structural parameters of multilamellar 1,2-dipalmitoyl-sn-glycero-3-phosphocholine (DPPC) lipid bilayers in the presence of different concentrations of salt in the aqueous medium by SAXS and calculated pressure-distance curves. The swelling of d_w upon rising salt concentrations revealed electrostatic repulsion due to an adsorbed layer of ions in the headgroup region.

Demé et. al. [74] characterized the maximal swelling of the lamellar L_α-phase of 1,2-Dimyristoyl-sn-glycero-3-phosphocholine (DMPC) upon addition of rising concentrations of glucose, a small, soluble carbohydrate by SAXS (see Figure 15 A). The total force (see Figure 15 B, right) is hypothesized to be a combination of van der Waals (see Figure 15 B, left), hydration, and undulation forces. A shift of the Bragg peaks in the 2D patterns towards lower angles (see Figure 15 A, from left to right) is due to an increase of the water layer thickness d_w, occurring as combined effect of van der Waals attraction and membrane fluctuations (see Figure 15 B). At high carbohydrate concentrations the membranes are softened and show larger distances, leading to a rising contribution of undulation repulsion (see Figure 15 B, right).

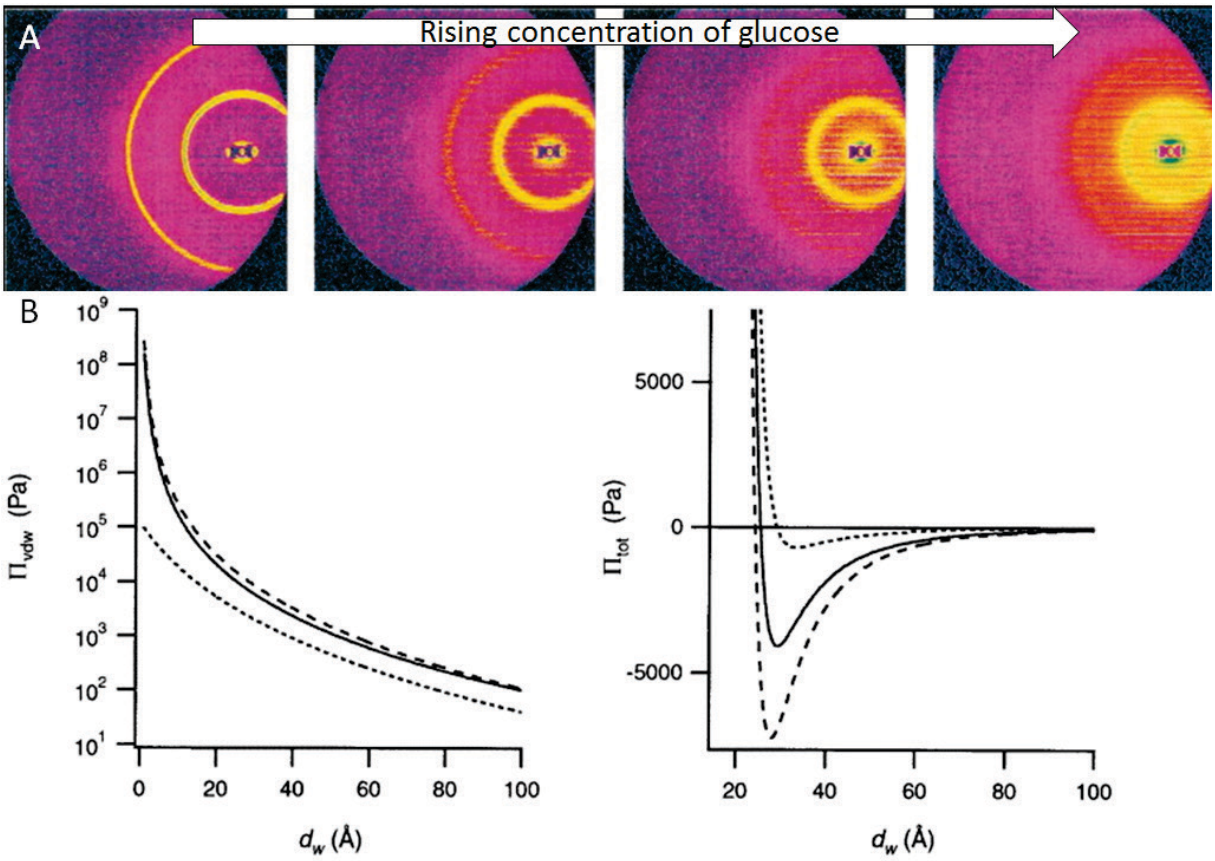

Figure 15 A) SAXS 2D patterns of a multilayer system of DMPC with rising concentration of glucose in the aqueous medium (from left to right) B) left: Van der Waals pressure right: Total pressure-distance curve resulting from the sum of van der Waals, hydration and undulation contributions. The zero of the x-axis corresponds to the lipid headgroup/aqueous medium interface. The zero on the y-axis corresponds to the equilibrium pressure. The style of the lines represents the outcome of different calculation models.
Reprinted with permission from [Demé, B., M. Dubois, and T. Zemb, *Swelling of a lecithin lamellar phase induced by small carbohydrate solutes.* Biophys. J., 2002. **82**(1): p. 215-225.]. Copyright [2002] Elsevier.

1.4 Publications

First author publications

Manuscript I

Latza V. M., Rodriguez-Loureiro I., Kiesel I., Halperin A., Fragneto G.and Schneck E., Neutron Reflectometry Elucidates Protein Adsorption from Human Blood Serum onto PEG Brushes. *Langmuir*, 2017, **33**, 44, 12708-12718.

Manuscript II

Latza V. M., Rodriguez-Loureiro I., Fragneto G. and Schneck E., End Point Versus Backbone Specifity Governs Characteristics of Antibody Binding to Poly(Ethylene Glycol) Brushes. *Langmuir*, 2018, **34**, 46, 13946-13955.

Manuscript III

Latza V. M., Demé B., Schneck E., Membrane adhesion via glycolipids occurs for abundant saccharide chemistries. *Biophysical Journal,* accepted.

The experiments were designed by Emanuel Schneck and myself and conducted by myself with the help of Ignacio Rodriguez-Loureiro and Emanuel Schneck. Experiments were supported by Giovanna Fragneto and Bruno Demé. The data were evaluated and interpreted by myself with support of Emanuel Schneck, Bruno Demé and Avi Halperin. The drafts for the manuscript were written by myself and finalised with the support of Emanuel Schneck and the other co-authors.

Second Author publications

Rodriguez-Laureiro I., Latza V. M., Fragneto G., Schneck E., Conformation of Single and Interacting Lipopolysaccharide Surfaces Bearing O-Side Chains *Biophysical Journal*, 2018, **114**, 1624-1635.

Stefaniu C., Latza V. M., Gutowski O., Fontaine P., Brezesinski G., Schneck E., Headgroup-Ordered Monolayers of Uncharged Glycolipids Exhibit Selective Interactions with Ions. *The Journal of Physical Chemistry Letters*, 2019, **10**, 8, 1684-1690.

I was part of the experimental team and contributed a considerable part of the experimental data published.

2 Discussion

In this thesis, interaction phenomena involving lipid-based surfaces in aqueous environments were investigated. One generally distinguishes between two types of surface interaction phenomena (see Figure 16 A), namely surface interactions with the components of their aqueous surroundings (see Figure 16, left and middle columns) and interactions between two surfaces (see Figure 16, right column). As pointed out in the introduction, both types of interactions are of great biotechnological or biological importance.

Here, lipid-based surfaces (see Figure 16 B) were used to create well-defined mimics of biomembrane surfaces and of the surfaces of functionalized materials for biomedical applications (see Figure 16 C). With the help of these well-defined experimental model systems (see Figure 16 C), two important problems in the fields of biotechnology and membranes biophysics, respectively, were addressed:

Topic 1

The interaction of proteins with polymer-functionalized (*PEGylated*) surfaces (see Figure 16 C a/b);

To this end, the PEG "brushes" with different polymerization degree *N* and grafting densities σ were either exposed to human blood serum (HBS) (see Figure 16 B a/b and C a) or to aqueous solutions of anti-PEG antibodies (Abs) (see Figure 16 B a/b and C b). The studied anti-PEG antibodies (Abs) were IgG Abs binding specifically to endpoints (EB Abs) and IgG Abs binding specifically to the backbone (BB Abs) of PEG.

Topic 2

The interaction between lipid membranes containing glycolipids (see Figure 16 C c);

For this purpose phospholipid membranes incorporated with a range of various glycolipids exhibiting headgroups with one to four saccharides, were investigated (see Figure 16 B c).

In order to gain valuable structural insight into these processes, scattering techniques with x-rays and neutrons were utilized, which yield detailed information on molecular length scales in a perturbation-free manner (see Figure 16 D). In context with protein adsorption, neutron reflectometry revealed the volume fraction profiles of proteins from human blood serum HBS (see Figure 16 E a) and of anti-PEG antibodies with either high affinity to the terminal group (EB Abs) or to the backbone (BB Abs) (see Figure 16 E b) to *PEGylated* lipid-based surfaces. In context with interacting lipid membranes small-angle x-ray scattering revealed the lamellar period of phospholipid membrane multilayers with various fractions of glycolipids (see Figure 16 E c).

In the following, the obtained results are summarized and discussed. The main results are also summarized in Figure 16 F and G in the form of short bullet points. The respective publications of the here presented results are depicted in Figure 16 E, and can be found in the Appendix I. A complete list of the publications is also available in section 1.4.

A Classification of topics

Surface interaction phenomena

Topic 1: Interactions with components of aqueous sourrounding: Adsorption of proteins to biocompatible functionalized surfaces

- Human Blood Serum (HBS)
- Anti-PEG IgG antibodies (EB and BB Abs)

Topic 2: Interactions between two surfaces: lipid membranes containing glycolipids

B Systems

functionalization	fraction	Incubation-proteins	
PEG-lipid-22	0.1		+BB, BB & EB
PEG-lipid-114	0.01		+BB, EB*
PEG-lipid-114	0.02		+EB*
PEG-lipid-114	0.05		+BB, EB*
PEG-lipid-114	0.1	+HBS	+BB, EB*
PEG-lipid-455	0.01		+BB
non-functionalized		+HBS	

* obtained from [28]

glycolipid	headgroup	matrixlipid
MGDG-sat	Monosaccharide	DMPC
MGDG-unsat	Monosaccharide	POPC
Psyc-sat	Monosaccharide	DMPC
DGDG-sat	Disaccharide	DMPC
DGDG-unsat	Disaccharide	POPC
LacCer-sat	Trisaccharide	DMPC
Trihexo-sat	Trisaccharide	DMPC
TetraG-sat	Tetrasaccharide	DPPC

C Schemes

a

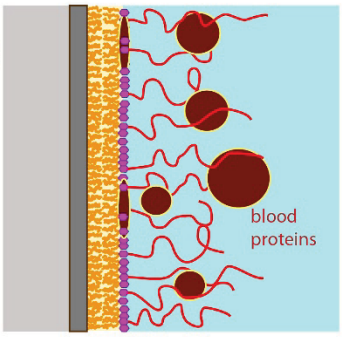

b

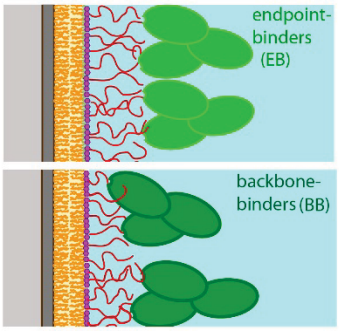

c

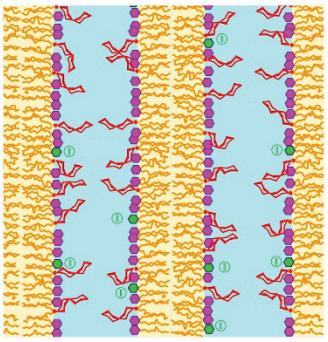

D Scattering techniques

neutron reflectivity

small and wide angle x-ray scattering

neutron diffraction

E Representative graphs

a

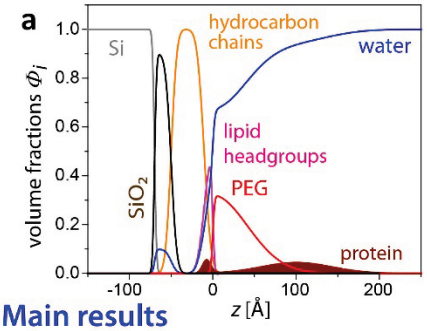

b

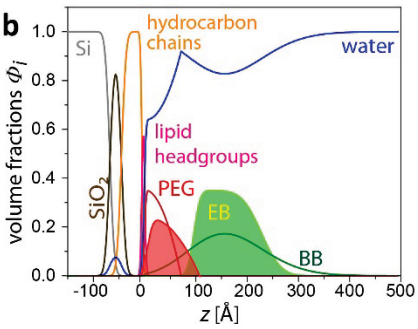

c

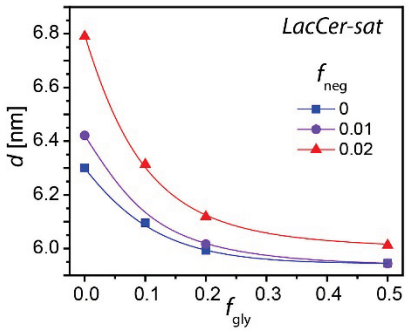

F Main results

Serum proteins adsorb strongly to headgroup layer in *Pegylated* and non-*Pegylated* systems

Diffuse layer of serum proteins adsorbs weakly at brush periphery

PEG profile is not altered upon adsorption; Brush is still functional

AB profiles from EB and BB differ for all samples

AB amounts are substantial for all samples

Brush parameter variation insufficient to avoid AB adsorption

PEG profile is altered upon adsorption; Brush is dysfunctional

Glycolipid mediated interactions:

Monosaccharides: no crosslinking, sterical hindrance

Di- and Trisaccharides: crosslinking is abundant phenomen

Tetrasaccharides: no crosslinking, steric repulsion

G Interactions

Ternary adsorption
-covalent binding of PEG and Ab

Primary adsorption in headgroup region
-strong attraction of lipids and HSB proteins

Ternary adsorption in PEG brush region
-weak attraction of PEG and HSB proteins

Van der Waals attraction

v.s.

Undulation repulsion
Hydration repulsion
Electrostatic repulsion

H Publications

Latza V. M. et al., *Langmuir*, **2017**, 33,12708.

Latza V. M. et al., *Langmuir*, **2018**, 34,13946.

Latza V. M. et al., *Biophysical Journal*, **2020**, mansucript accepted.

Figure 16 Overview: A) Scheme of the classification of surface interaction phenomena that were dealt with in this thesis. B) Investigated systems and their components C) Schematic illustrations of systems a) Solid-supported lipid membrane with PEG brush functionalization and adsorbed blood proteins immersed in aqueous medium (according to volume fraction profiles see graph E a)) b) Solid-supported lipid membranes with PEG brush functionalization and adsorbed EB or BB Abs immersed in aqueous medium (according to volume fraction profiles see graph E b)) c) Multilayer membrane system comprising PC lipids, glycolipids and negatively charged lipids immersed in aqueous medium D) Utilized scattering methods: Topic 1 was studied with neutron reflectometry; Topic 2 was studied with small and wide angle x-ray scattering and neutron diffraction. E) Representative graphs of data: a) Volume fraction profile of blood proteins adsorbed to solid-supported lipid membrane with PEG brush functionalization b) Volume fraction profile of EB and BB Abs adsorbed to solid-supported lipid membranes with PEG brush functionalization c) Distance of adjacent lipid membranes as function of the glycolipid mole fraction at different mole fractions of negatively charged lipids F) Summary of main results G) Summary of main interactions found in the different systems upon adsorption of proteins (Topic 1) or membrane adhesion (Topic 2) H) Respective publications, regarding adsorption of proteins (Topic 1) or membrane adhesion (Topic 2)
Panels C a) and E a) are reprinted with permission from [Latza, V.M., et al., *Neutron Reflectometry Elucidates Protein Adsorption from Human Blood Serum onto PEG Brushes.* Langmuir, 2017. **33**(44): p. 12708-12718.]. Copyright [2017] American Chemical Society. Panels C b) and E b) are reprinted with permission from [Latza, V.M., et al., *End Point Versus Backbone Specifity Governs Characteristics of Antibody Binding to Poly(ethylene glycol) Brushes.* Langmuir, 2018. **34**(46): p. 13946-13955.]. Copyright [2018] American Chemical Society. Panels C c) and E c) are reprinted from [Latza, V.M., Demé B. Schneck E., *Membrane adhesion via glycolipids occurs for abundant saccharide chemistries.* Biophysical Journal, accepted.].

2.1. Protein adsorption to PEG functionalized surfaces

As explained in the motivation (section 1), *PEGylation* is widely used as "gold standard" in biomedical applications such as implants, pace makers, or stents, with the aim to suppress undesired protein adsorption. Despite the omnipresence of *PEGylated* materials, structural knowledge about protein adsorption has remained limited up to today. Adsorption of proteins to surfaces can be explained in three different scenarios that depend on the predominant interactions and are characterized by the location of the adsorption (see Section XY and Figure 2): i) primary adsorption to the grafting surface due to favorable short-range interactions between the surface and the proteins. ii) secondary adsorption at the brush periphery due to long-range interactions between the surface and the proteins and at the same time repulsive interactions between the polymer and the protein, which occur whenever the proteins penetrate the brush. Upon penetration the brush would have to make room for the proteins, which would be energetically unfavorable for the brush, because the system would lose entropy. This free energy barrier resulting from the brush resistance to insertion of proteins, is called osmotic penalty. And iii) ternary adsorption within the brush due to attractive interactions between the polymer and the protein [37, 38]. This classification, where the location of the adsorbed layer already points towards predominant interactions, highlights the importance of structural insight about adsorption processes. Adsorption from human blood serum (HBS) and of anti-PEG antibodies to *PEGylated* systems is of great significance in the field of biotechnology (see section 1). Therefore the structural behavior of anti-PEG antibodies (see Figure 17 right) and of human blood serum (HBS) (see Figure 17 left) to PEG anchored to lipid interfaces was examined.

The utilized model system is schematically drawn in Figure 17: The basis is a silicon block, covered with a natural layer of silicon oxide (SiO_x) which is hydrophobically functionalized with a layer of hydrocarbon chains (stemming from the molecule trichloroocatdecylsilan (OTS)). The hydrophobic layer supports the monolayer of lipids. For the reason of data evaluation, lipids are described in the model in terms of hydrocarbon chains and headgroups (see Figure 17). The lipid monolayer anchors the PEG brush, immersed in aqueous media. The modular sample architecture allows adjusting of the brush parameters (grafting density σ and polymerization degree N) in a precise manner. This is explained in more detail in chapter 1.1.1.

In the following the main results of the thesis, regarding the adsorption of human blood serum (HBS) proteins and of anti-PEG antibodies to the planar lipid-based model systems in terms of structural information will be discussed (see Figure 17).

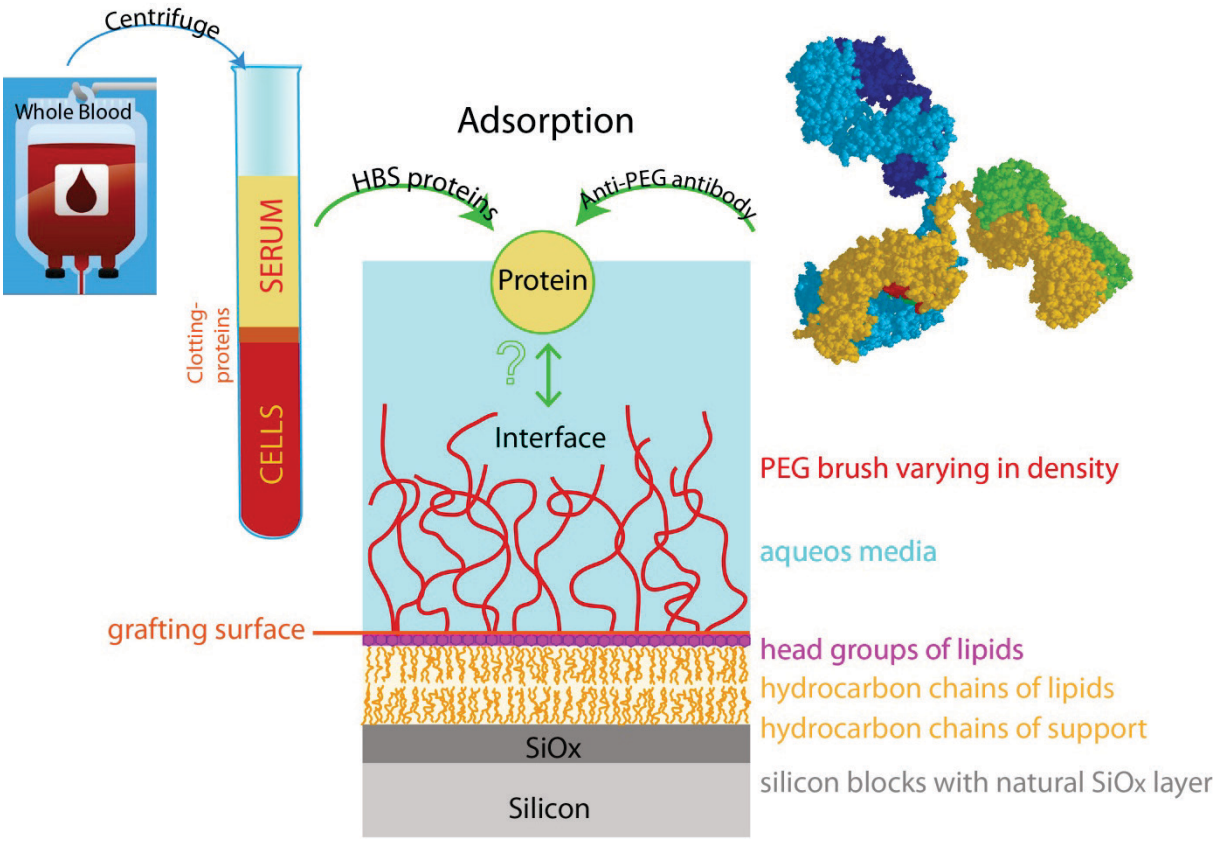

Figure 17 Model system consisting of solid supported lipid layer functionalized with a PEG-brush; the sample exhibits a layered structure of silicon, silicon oxide, hydrocarbon chains of the support for the lipids and of the lipids, headgroups of lipids and PEG chains in aqueous solution. The model system was used to study adsorption from proteins on the grafting layer. The examined proteins were proteins from anti-PEG antibodies and whole human blood serum (HBS).

2.1.1 Adsorption of proteins from whole human blood serum

Earlier work had already established that *PEGylation* is able to reduce the amount of adsorbed protein from HBS [46-48] or single component blood protein solutions [54, 55] (see section 1.3), but those studies did not reveal depth profiles of the adsorbed proteins. Obtaining structural results is highly desirable but also correlates with the difficulty to investigate a complex solution like blood, with the plasma proteome comprising a mixture of 22 abundant and around 10^4 minority protein species [25]. Every single component might in principle adsorb in a different way.

In order to gain structural insight into protein adsorption, in this thesis solid supported PEG functionalized lipid interfaces were systematically brought into contact with non-diluted and diluted HBS and were measured by means of neutron reflectivity (NR) (see also Figure). The polymerization degree of PEG was N = 114. The utilized brush was dense having a defined grafting density σ corresponding to a PEG-lipid mole fraction of f = 0.1. This means that the sample exhibited a homogenous layer of 10 mol % of PEG-lipid and of 90 mol % of phospholipid. Actually this is the densest brush that can be reliably produced in terms of homogeneity of lipid and PEG-lipid distribution. As non-*PEGylated* reference the pure phospholipid surface was equally treated.

A first important finding was that the PEG profile is not altered by incubation of HSB proteins and subsequent adsorption. This means that the structural characteristics of the brush stay intact. It is therefore justified to assume that the function of the brush in general is not affected by attached HBS proteins.

For the interpretation of the protein profiles, the three adsorption modes of primary, secondary and ternary adsorption have to be recalled (see section 1.3.1.1 and Figure 2)). Primary adsorption at the grafting surface was found to be present at the grafting layer of *PEGylated* and non-*PEGylated* samples as well. Unexpectedly the amount of adsorbed proteins is comparable for the *PEGylated* and non-*PEGylated* samples. The layer is very thin with a thickness of around 10 Å and is penetrating the headgroup region. The thickness of the headgroup region is not affected by adsorption of proteins. Before incubation with proteins the headgroup layer contained around 50 % water. Upon adsorption the water molecules are swamped out and the volume is occupied by the proteins. The adsorbed layer resists rinsing with aqueous media, which was performed for contrast variation (see Appendix II 3.1). Therefore this layer of primary adsorption is characterized by strong adhesion to the grafting layer.

From this presence of the primary layer of proteins in *PEGylated* and non-*PEGylated* samples with same characteristics, it is concluded that PEG does not suppress primary adsorption. This finding is contradictory to many studies on *PEGylated* surfaces showing that PEG is reducing protein adsorption. This structural revelation is pivotal for our understanding of the working principle of *PEGylation* and will therefore be discussed in detail later on.

An additional type of adsorption was identified, which occurs while the samples are still in contact with serum: ternary adsorption to the PEG brush itself. The ternary adsorption mode points directly towards weak attraction between PEG and proteins.

Experimentally, contrast variation was necessary to measure adsorption with the intended accuracy. To investigate processes while the sample is still in contact with HBS, dilution of the serum with the wished contrasts was performed. The contrast solutions were H_2O- and D_2O-buffer solutions and mixtures thereof (see also methods section). Considering that regular HBS contains around 7 % proteins diluted in aqueous medium, the concentration of proteins was reduced down to around 0.7 % by the utilized 10-fold dilution with the contrast solutions. This has to be kept in mind when comparing rinsed and unrinsed adsorption profiles. The unrinsed protein profile reveals a diffuse layer penetrating the PEG brush, while the proteins in large part stay at the brush periphery at a distance of around 100 Å with respect to the grafting surface. We find an amount of adsorbed protein of around 0.6 mg/m^2, which is surprisingly high considering the dilution of the solution and constitutes around 1/4th of the amount of the primary adsorption of the rinsed sample. Therefore this effect is considered to be very important.

This suggests that ternary adsorption is a significant process which has been vastly neglected in the experimental literature up to now. Hence it is a largely unexplored phenomenon with potentially far reaching consequences with regard to the reaction of the organisms to *PEGylated* surfaces.

To summarize, searching for structural aspects of brush failure two main adsorption modes on *PEGylated* systems were found: Strong primary and weak ternary adsorption. Primary adsorption on the *PEGylated* system was comparable to the primary adsorption on the non-*PEGylated* system, suggesting no effect of PEG in this case. These results will alter the understanding for the basic working principle of *PEGylation*.

2.1.2 Adsorption of anti-PEG antibodies

The second aspect of the interaction of *PEGylated* surfaces with blood that was studied in this thesis is the implication of PEG's antigenicity. Earlier studies have shown that the human blood can contain immunoglobulin (IgG) antibodies against PEG (anti-PEG Abs) [20-22] (see Section 1). Some of them suggest increasing amounts in the population upon frequent contact with PEG in cosmetics [9], drug delivery systems [4, 5], or implants [6]. There are different kinds of Abs exhibiting high affinity either to the endgroup of PEG (EB Abs) or to the backbone of PEG (BB Abs), respectively.

A main question in this thesis was how effective anti-PEG Abs adsorb to PEG when it assumes the typical brush configuration of *PEGylated* surfaces. In order to cover systematically the possible scenarios, adsorption of BB Abs and of EB Abs to the *PEGylated* model surface was investigated. The utilized IgG Abs exhibit a molecular mass of around 150 kDa and are Y-shaped molecules comprising two antigen binding arms and one effector binding arm [96, 97] (see Figure 17, right). The antigen binding arms of EB Abs attach to the terminal methoxy group and the adjacent 16 monomers with an affinity of 1.58 nm [18, 20], whereas the antigen binding arms of BB Abs attach to the backbone chain of PEG exhibiting a repeating unit of $-OC_2H_4-$. The planar, solid-supported, PEG-functionalized lipid interfaces (see Figure 17) varied in grafting density σ corresponding to PEG-lipid mole fractions of $f = 0.01$, 0.02, 0.05, and 0.1 and in polymerization degree $N = 22$, 114, and 455. The two parameters σ and N were thus varied systematically. Adsorption of EB Abs had already been studied earlier (see Figure 18 B) for $N = 114$ [28] and the acquired data was used for this work.

The first step undergone was to perform BB Ab adsorption experiments on *PEGylated* surfaces. Adsorption of BB Abs to the backbone of PEG had not been described before in terms of structural information on sub-nanometer scale.

The grafting density σ of the brush was varied for a middle sized length of the polymer chains ($N = 114$) from very sparse ($f = 0.01$) to very dense ($f = 0.1$) (see Figure 18 A and B). For a sample with low grafting density the PEG chains are relatively far apart and for high grafting densities, closer together. It was found that EB and BB Abs adsorb substantially to PEG at all grafting densities (see Figure 18 A and B). To conclude, both investigated types of Abs adsorb to various grafting densities.

In the case of a dense brush Abs have to penetrate a region which is heavily occupied with PEG chains in order to bind. Abs have to overcome a repulsive interaction of PEG and Abs, which occurs whenever the Abs penetrate the brush. This repulsion is stronger for denser brushes. Upon penetration the PEG chains would have to make space for the Abs, which would be energetically unfavorable for the brush, due to the loss of entropy. The free energy barrier resulting from the brush resistance to insertion of Abs, is called osmotic penalty. To conclude, dense brushes impose a high osmotic penalty upon Ab insertion into the brush. The fact that Abs adsorption occurs to very dense brushes shows that the binding of Abs to PEG is strong and overcomes parts of this energetic barrier. One main conclusion from this result is that a simple variation of brush parameters in terms of σ or N is insufficient to fully suppress anti-PEG Ab adsorption. To design a brush which exhibits a high enough osmotic penalty to prevent BB Abs to partially insert into the brush by counteracting the high binding affinity of the Abs to PEG is a future challenge.

The variation of the second essential parameter N was further studied: short PEG chains with 22 monomers (studied with f = 0.1), middle sized chains with 114 monomers (studied with f = 0.01, 0.05, and 0.1) and long chains with 455 monomers (studied with f = 0.01) were used for the surface modifications. Also here considerable BB Ab adsorption was present for all polymerization degrees N. In Figure 18 C and D the volume fraction profiles for the middle sized polymer chains (N = 114) and the very long ones (N = 455) with equally low PEG fraction of f = 0.01 are illustrated for comparison. In the brush formed by the medium PEG (N = 114) the BB Abs form a pronounced layer, close to the grafting surface (see Figure 18 C). The brush exhibiting long PEG chains (N = 455) exhibits even more pronounced adsorption with very high amounts (see Figure 18 D). It is located further away from the grafting surface and is also more extended. This is due to the abundance of binding sites for the BB Abs, already at the brush periphery. In this brush Abs can insert without noteworthy resistance, due to a very small osmotic penalty.

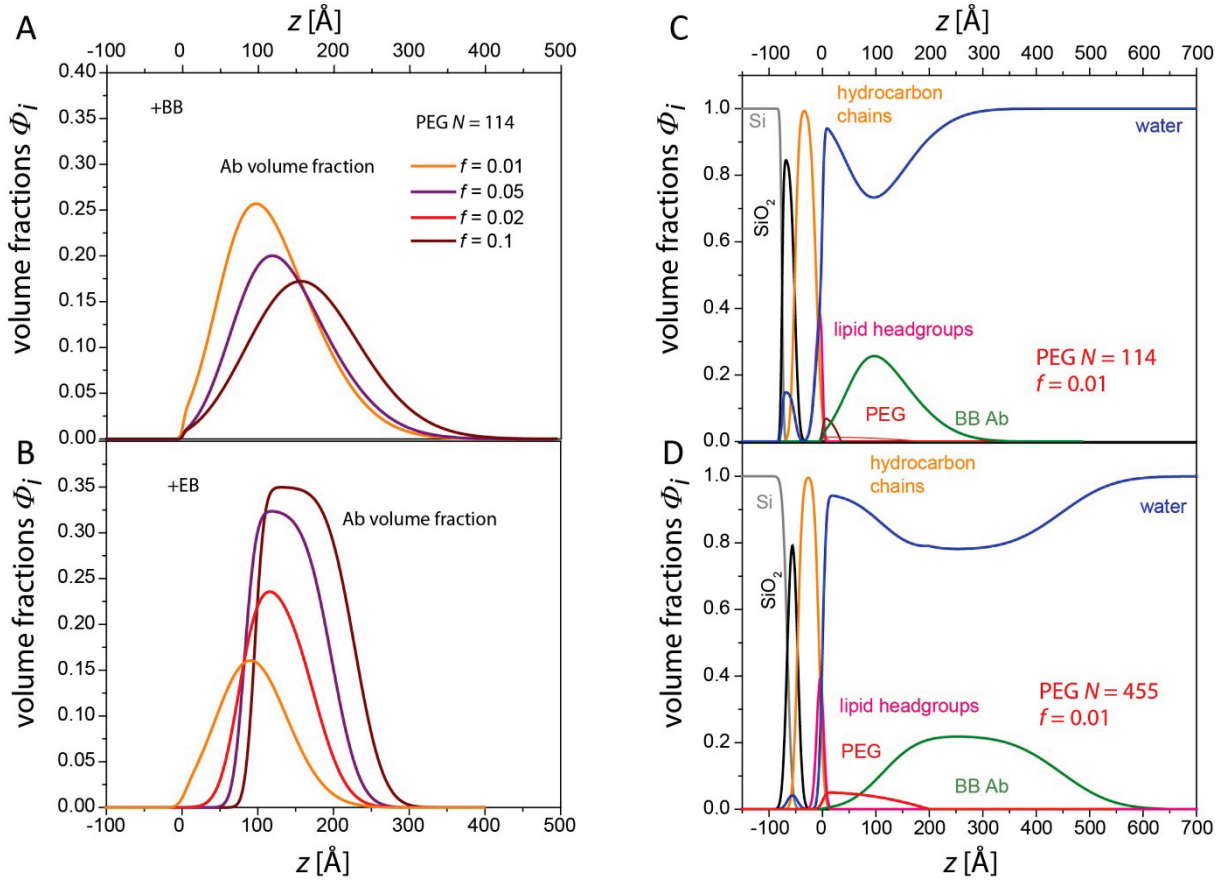

Figure 18 Volume fractions of Abs as function of the distance to the grafting surface. A) BB and B) EB Ab volume fractions adsorbed to model systems with different grafting densities f = 0.1, 0.02, 0.05 and 0.01. C) BB Ab adsorption volume fraction and volume fractions of model system with PEG-lipid-114 and f = 0.01. D) BB Ab adsorption volume fraction and volume fractions of model system with PEG-lipid-455 and f = 0.01.
Panel B is adapted with permission from [Schneck E., et al., *Neutron reflectometry from poly(ethylene glycol) brushes binding anti-PEG antibodies: Evidence of ternary adsorption.* Biomaterials, 2015. **46**: p. 95-104.]. Copyright [2015] Elsevier. Panels C and D are reprinted with permission from [Latza V. M., et al., *End Point Versus Backbone Specifity Governs Characteristics of Antibody Binding to Poly(ethylene glycol) Brushes.* Langmuir, 2018. **34**(46): p. 13946-13955.]. Copyright [2018] American Chemical Society.

When comparing adsorption for both investigated Ab types, it was found that BB adsorption shows different features than EB adsorption irrespective of the brush parameters (Figure 18 A and B). The profiles of BB and EB Ab adsorption are dissimilar in terms of the maximal extension of the distribution. Volume fraction profiles Φ shown in Figure 18 A and B are extended to around 350 Å to 400 Å for BB Abs and to around 250 Å to 300 Å for EB Abs. In turn the values obtained for the maximal volume fraction Φ_{AB}^{max} are higher for EB Abs for the denser brushes (f = 0.1 and f = 0.05). Values are $\Phi_{AB}^{max} \approx 0.35$ for EB Abs and $\Phi_{AB}^{max} \approx 0.2$ for BB Abs (see Figure 18 A and B). For the sparse brush (f = 0.01) Φ_{AB}^{max} for BB Abs is higher with $\Phi_{AB}^{max} \approx 0.25$ for BB Abs compared to $\Phi_{AB}^{max} \approx 0.15$ for EB Abs. The adsorbed amount and structural parameters have different dependence on σ (see [98], Figure 4) for both cases.

In the following the influence of σ will be exemplarily discussed with regard to the number of adsorbed Abs per PEG chain n_{AB} which highlights the differences of BB and EB Abs (Figure 19). In this context it has to be recalled that the utilized Abs exhibit two antigen binding arms, with high affinity either to the terminal group (EB) or to the backbone (BB) of the polymer chains respectively.

For EB Abs the theoretical maximum number of n_{AB} is 1 when monovalent, and 0.5 when divalent binding is assumed. This follows from the limitation of one antigen binding site per PEG chain and the in principal two binding sites of the Ab. In the experiment indeed the maximum value is $n_{AB} = 0.5$ for EB Abs adsorbing on PEG-lipid-114 with a low grafting density of $f = 0.01$. This number suggests divalent binding where the two antigen binding arms of one Ab molecule bind two PEG chain end segments. The experimental value of $n_{AB} = 0.5$ further suggests that Ab adsorption is diffusion-limited and occurs one-by-one with a slow time scale for the initial binding and a fast timescale for the binding of the second antigen-binding arm. This surface with a grafting density of $f = 0.01$ exhibits a distance of two PEG chain grafting points close enough for the Ab molecule to reach with the two antigen-binding arms. For even lower grafting density one could expect a value of $n_{AB} = 1$. Due to large distances of PEG chain anchor points, Abs are likely to merely bind with one of their antigen binding arms. This scenario was not investigated experimentally and would be true for a slow in-plane mobility of the PEG anchors compared to the time scale of adsorption. For higher σ the experimental value for EB Abs is decreasing from $n_{AB} = 0.5$ to $n_{AB} = 0.12$. This is due to sterical reasons. There is simply not enough space for the Abs to bind to all PEG chain endpoints. To summarize, for EB Abs divalent binding and a decrease of bound PEG chain end points with increasing σ was found. The maximum value of n_{AB} is therefore limited by σ.

In contrast, for BB Abs the theoretical maximum number of n_{AB} is not limited by the end points of the polymer but by the mere length of PEG chains, defined by N. BB Abs bind simultaneously with two antigen-binding arms to one PEG-chain. If the PEG-chains are long enough, also several BB Abs are likely to bind simultaneously to a single PEG-chain.

For the brush formed by the medium PEG ($N = 114$) a maximum value of $n_{AB} = 1.0$ at the lowest grafting density corresponding to a PEG mole fraction of $f = 0.01$ was found for BB Abs. This value suggests divalent binding where the two antigen-binding arms of one Ab molecule bind one PEG-chain. In conclusion the osmotic penalty imposed by the brush is not strong enough to prevent substantial insertion of BB Abs into the brush.

Similar to EB Abs, the experimental n_{AB} value for BB Abs is decreasing from $n_{AB} = 1.0$ to $n_{AB} = 0.08$, when increasing σ. Here the limitation is probably a mixture of the rising osmotic pressure of the denser brushes and again a sterical hindrance of further Ab binding.

In addition, for surfaces with long PEG chains (N = 455) with a sparse grafting density σ corresponding to a mole fraction of f = 0.01 a value of n_{AB} = 1.92 is observed. This number suggests divalent binding where the two antigen-binding arms of two Ab molecules bind one PEG-chain. Interestingly, the observed value for short PEG chains (N = 22 and f = 0. 1) is similar to the value for the medium chains (N = 114 and f = 0. 1): $n_{AB} \approx 0.1$. This finding strengthens the assumption of the high osmotic penalty hindering the BB Ab adsorption to the backbone. The influence of N is negligible at high σ.

To summarize, for BB Abs divalent binding and a decrease of bound PEG-chain end-points with increasing σ was found. The maximum value of n_{AB} is therefore limited by σ. At low σ n_{AB} values are constrained by N. Comparing n_{AB} for EB and BB Abs, it can be stated that BB Abs bind more effectively to PEG at lower σ, because binding sites for EB Abs are limited in this case. Opposingly EB Abs bind more effectively at higher σ, since EB adsorb at the brush periphery. BB Abs need to penetrate the brush and are therefore more affected by higher σ and a resulting higher osmotic penalty.

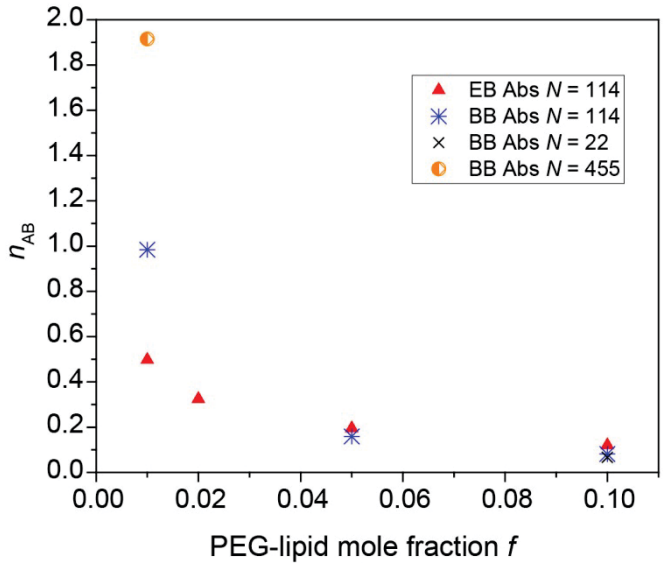

Figure 19 Number of adsorbed Abs per PEG chain as a function of the grafting density for Δ) PEG-lipid-114 incubated with EB Ab; *) and PEG-lipid-114 incubated with BB Ab; **x**) PEG-lipid-22 incubated with BB Ab; ○) PEG-lipid-455 incubated with BB Ab.
Adapted with permission from [Latza V. M., et al., *End Point Versus Backbone Specifity Governs Characteristics of Antibody Binding to Poly(ethylene glycol) Brushes.* Langmuir, 2018. **34**(46): p. 13946-13955.]. Copyright [2018] American Chemical Society.

The discussion of the elementary differences of the structural parameters, such as Ab mass per area, center of mass position of Abs, maximal Ab volume fraction, width of Ab volume fraction, and number of adsorbed Abs per PEG chain in dependence of σ reveals profound information on the adsorption behavior of the two types of Abs. Further these parameters bring to light the structural difference in adsorption of the Ab types. For medium PEG-chain lengths (N = 114) the center of mass position of the Ab distribution alone is similar for both Ab types. The center of mass position is therefore independent of Ab specificity and mainly driven by the osmotic energy barrier.

Coming back to the initial research question on the biomedical implications of specific Abs binding to PEG brushes, important statements can be made: First, adsorption of Abs cannot be prevented by merely changing the brush design parameters σ and N. Even for the densest brushes that can be reproducibly prepared, the imposed energy barrier is not high enough to prevent Ab binding. This is due to the strength of the specific bonds established between Ab and PEG. Second, comparison of EB and BB Ab adsorption profiles revealed that the osmotic penalty and Ab size are crucial effects for Ab adsorption to PEG brushes.

Based on the structural knowledge of adsorption of two types of IgG Abs, conclusions for new approaches in biomedical applications utilizing *PEGylation* can be drawn. In this context it should be recalled that PEG raised suspicion to provoke immune responses in the body e.g. the formation of antibodies against PEG [20, 21]. Results of the presented study suggest that variation of σ and N alone is insufficient to fully prevent Ab adsorption to PEG. A possible way to hinder adsorption of EB Abs is the chemical modification of the end-motif of the PEG-chains. This change means avoiding the antigen and therefore avoiding an immune response. Still, the risk that these new terminal groups provoke immune responses with anew formed Abs should be taken into account. What is more, the end-modification of PEG cannot prevent adsorption from BB Abs. One possibility to overcome BB Ab adsorption might be the substitution of PEG with other polymers. These substituting polymers would need to fulfil the general requirements for the formation of polymer brushes such as exhibiting one main chain without side chains, very good solvent solubility, and no interacting forces between chains. Bio-polymers consisting of chemical motifs that are already present in human organisms could be ideal replacements. In contrast, if PEG would be substituted by another non-biological chemistry, the emergence of Abs against this chemistry in the long run is not unlikely. Therefore the use of a biological material is suggested, against which the organism cannot develop immune response without developing auto-immune reaction at the same time. Such a material could be poly-phosphocholine (poly-PC), because it combines the chemically necessary requirements (flexible, highly hydrophilic) with the fact that it is a biological motif. Recently a study utilizing poly-PC incorporated into a PC lipid vesicle membrane was published [99]. Poly-PC acted as sterical stabilizer hindering aggregation, which is commonly aimed for with the help of PEG. Such vesicles could serve as stable vectors in biomedical applications and possibly replace *PEGylated* systems. In any case, the development of biocompatible functionalization would strongly benefit from accompanying clinical tests on the long-term antigenicity of the involved chemicals.

2.1.3 Summary and conclusions

The general approach of this part of the presented thesis was to investigate systematically the adsorption of proteins to lipid-based *PEGylated* surfaces with well-defined brush parameters with regard to grafting density and polymer length (polymerization degree). To that end NR was utilized, constituting a method that reveals depth profiles of PEG and of the adsorbed proteins. NR thereby delivers unique insights into the mode and characteristics of adsorption.
In summary, the following insights into the adsorption of proteins to *PEGylated* surfaces were gained within the scope of this thesis:

1)
The study of *PEGylated* surfaces brought into contact with HBS, evidenced the formation of a thin layer of primary adsorbed proteins to the brush grafting surface. De facto the presence of *PEGylation* has no influence on the formation of this layer. This primary layer can only be constituted from small proteins, because only small sized molecules can overcome the osmotic barrier imposed by the brush. This result manifests, that the complete suppression of protein adsorption cannot be the working principle of *PEGylation*.

2)
Based on the assumption that *PEGylation* prevents the recognition of the primary layer by the immune system, another working principle of the *PEGylated* surface can be hypothesized. Indeed, components of the immune system like special cells or proteins are quite large [25] and are therefore unlikely to surmount the osmotic energy barrier which was estimated to be around 8 kDa [50]. This was also shown in this thesis for Immunoglobulin antibodies.

3)
Ternary adsorption to the PEG brush itself was observed for *PEGylated* surfaces during contact with (diluted) HBS for the first time. The role of this adsorption mode regarding the working principle of the *PEGylated* surface is unknown. However the presented work shows that this mode of adsorption has potentially great significance for future design of surface modifications.

4)

The investigation of binding of PEG specific Abs to *PEGylated* surfaces revealed that different Abs with distinctive affinities to the end-group and to the backbone, exhibit deviating adsorption profiles. Still, the key finding is that adsorption amounts for both types are significant for practically accessible brush characteristics in terms of grafting density and polymerization degree. This can be explained by the fact that EB Abs do bind to antigens located at the brush outer edge and therefore evade the osmotic barrier. BB Abs exhibit a strong binding affinity that overcomes the osmotic barrier partially and therefore bind substantially to the brush.

5)

In any case, a brush loses its function when significant Ab binding occurs. In principle adsorption of Abs with high affinity to the terminal group, can be hindered by chemical modification thereof. This would not change the brush characteristics in a significant manner. In contrast this procedure would not prevent BB Ab adsorption, since the PEG backbone is not altered. It is therefore necessary to alter the chemistry of the surface functionalization completely. In order to hinder immune responses, the most sustainable solution would be the utilization of biological motifs, which would be ideally flexible and hydrophilic polymers.

2.2 Influence of glycolipids on membrane interactions

2.2.1 Interactions between lipid membranes containing glycolipids

This thesis deals with interaction phenomena involving lipid-based surfaces in aqueous environments. Regarding interactions between two such surfaces, interactions between phospholipid membranes containing glycolipids were studied. As pointed out in section 1.1, the interaction between membranes is of great importance in the crowded environment of cells and tissues and depends on the chemical composition of the membrane surface. Interestingly, in stacked membrane systems of plants and vertebrates high fractions of glycolipids are present [30, 31]. This fact is already pointing towards the unique role of glycolipids for the formation and/or stabilization of membrane stacks. There are several studies verifying this hypothesis, e.g. it could be shown that there is more attraction between glycolipid membranes compared to phospholipid membranes [83-85]. This view was based on diminished hydration repulsion between such membranes containing glycolipids. Other studies have however shown that there is even attraction between these membrane systems. Crosslinking induced by attractive forces was first measured for the *LewisX* glycolipid, which can even withstand induced repulsive forces [89, 91]. It was longtime believed that this crosslinking ability is unique for *LewisX* glycolipids. This behavior was especially attributed to the trisaccharide motif of the headgroup. Interestingly attractive forces were also found for membrane systems containing the glycolipid N-hexadeanoyl-lactosyl-ceramide (*LacCer*) with a disaccharide headgroup [92]. So far little has been actually investigated concerning the abundancy of this phenomenon among glycolipids with different headgroups. In this thesis the ability of glycolipids with different headgroup types to establish crosslinks between membranes is investigated. For this purpose, multilayer membrane systems composed of phospholipids incorporated with a range of various glycolipids were investigated (see Figure 20). The studied glycolipids possess various saccharide-headgroups comprising mono-, di-, tri- or tetra-saccharides. In Figure 20 the components and the formed multilayered membrane system interacting in an aqueous environment are depicted. Additionally the adherence of the membranes against repulsive forces was probed by further incorporation of charged phospholipids into the membrane.

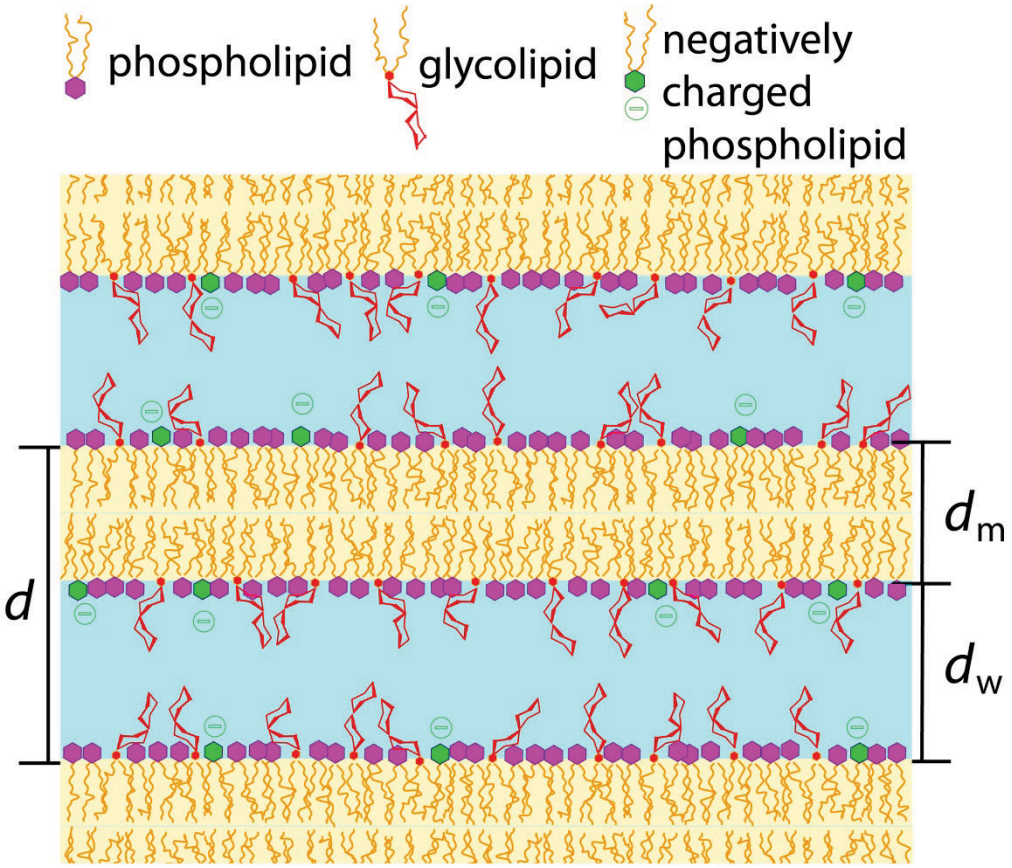

Figure 20 Schematic drawing of multilayered membranes: The lipids consist of hydrocarbon chains (orange) and headgroups that are depicted in different colors/shapes according to the chemistry. The phospholipids are the matrix lipids, compromising the largest mole fraction of the membrane components. The headgroup is depicted as pink hexagon. The membranes are incorporated with different mole fractions of glycolipids. The glycolipid headgroup is depicted as red dihexose. Additionally also different mole fractions of negatively charged lipids are incorporated. The PG or PS headgroup is depicted as green hexagon with minus symbol. The lamellar period *d* is composed of d_m (membrane thickness) plus d_w (water layer thickness).
Reprinted from [Latza, V.M., Demé B. Schneck E., *Membrane adhesion via glycolipids occurs for abundant saccharide chemistries.* Biophysical Journal, Manuscript submitted for publication.].

A detailed overview of the investigated membrane systems is given in the Appendix II 2.1 (see **Table 3**). In general, the samples are composed of phosphatidylcholine (PC) lipids with a mole fraction of $f_{PC} = 1 - f_{gly} -$ (where 1 corresponds to 100 mol %). The glycolipid mole fraction was varied (f_{gly} = 0, 0.1, 0.2, 0.5) together with the negatively charged lipid mole fraction (comprising phosphatidylserine (PS) or phosphatidylglycerol (PG) headgroups) (f_{neg} = 0, 0.01, 0.02, 0.05).

By measuring wide angle x-ray scattering (WAXS) the phase of the lipid membranes is accessible and it could be confirmed that all the investigated membrane multilayers were in the biologically relevant fluid L_α–phase. By probing the lamellar period *d* (see Figure 20) of the multilayered membranes with small angle x-ray scattering (SAXS), the ability of the glycolipids to crosslink adjacent membranes was quantified. The lamellar period *d* is dictated by the equilibrium between the effective interfacial

forces: van der Waals attraction, hydration repulsion [85, 91], undulation repulsion, and electrostatic repulsion. Attractive interactions between two adjacent membranes, resulting in crosslinked membranes, lead to a reduction of *d*. For this reason, the monitoring of *d* offers information on the crosslinking ability of glycolipids comprising different saccharide-headgroups.

The lamellar period *d* (see Figure 20) is composed of the distance between the adjacent membrane surfaces (here: water layer thickness) d_w and the membrane thickness d_m:

$$d = d_m + d_w$$

Decreasing *d* values with increasing f_{gly} suggest rising attraction between the adjacent membranes. Contrary, increasing *d* values show a rising repulsion between the membranes. Comparably, higher f_{neg} which lead to an increase in *d* values, show the repulsion resulting from their electrostatic contributions.

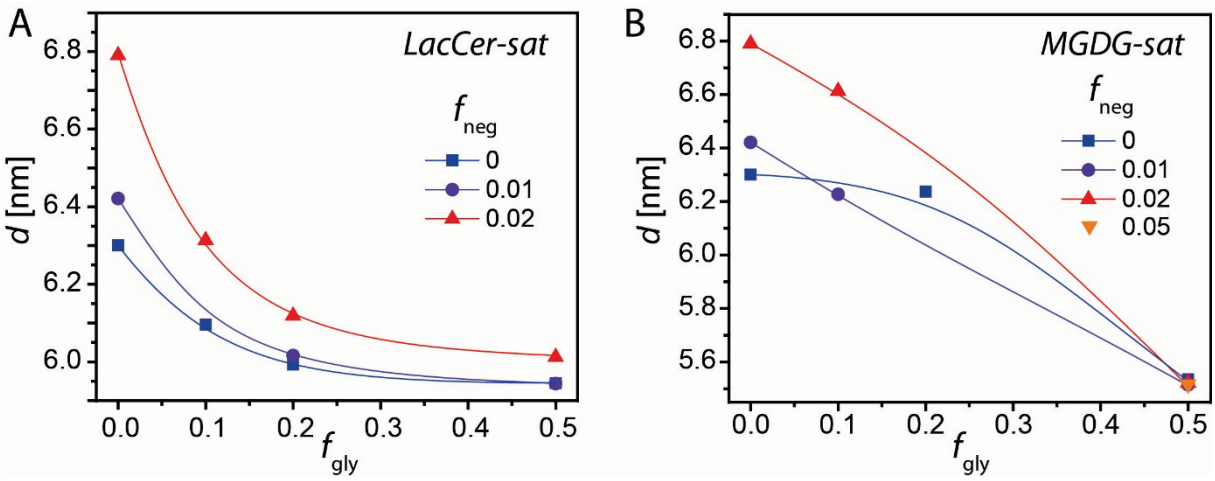

Figure 21 A) Lamellar period *d* of *LacCer-sat* incorporated into a PC membrane forming a multilayer membranes system. Different mole fractions of negatively charged lipids (f_{neg}) were further incorporated in the membranes. B) Lamellar period *d* of *MGDG-sat* incorporated into a PC membrane. Different mole fractions of negatively charged lipids (f_{neg}) were further incorporated in the membranes.
Reprinted from [Latza, V.M., Demé B. Schneck E., *Membrane adhesion via glycolipids occurs for abundant saccharide chemistries.* Biophysical Journal, Manuscript submitted for publication.].

Repulsive interactions upon insertion of negatively charged lipids are most prominent for pure PC membranes as can be seen in Figure 21 A. At $f_{gly} = 0$ *d* is increasing stronger than for the other samples.

Exemplarily, $d(f_{gly})$ for N-hexadeanoyl-lactosyl-ceramide (*LacCer-sat*) incorporated into a PC multilayer membrane system is shown in Figure 21 A. With increasing f_{gly}, d is decreasing. Interestingly already low *LacCer-sat* fractions are able to reduce d significantly. This is also true when $f_{neg} \neq 0$. This behavior is very similar to the *LewisX* trisaccharide crosslinking, which was reported earlier [85, 91]. It is hence suggested, that the crosslinking arises from binding of saccharide-headgroups between adjacent membranes (homotypic inter-membrane binding). Crosslinking was found mainly for headgroups containing the disaccharide *lactose*. For this disaccharide a decreased water-solubility (≈ 19 g/dL) [100] is reported, compared to other disaccharides like *sucrose* (≈ 200 g/dL) [101], *maltose* (≈ 110 g/dL), or *trehalose* (≈ 70 g/dL) [102], which indicates strong binding between *lactose* groups of adjacent membranes. In contrast, the investigated membranes with glycolipids comprising saccharide-headgroupds with mono-saccharides, do not show this behavior (see exemplarily Figure 21 B). This might be due to the comparatively small size of monosaccharides, which are most likely not able to protrude from the phospholipids' headgroup region. Glycolipids with large saccharide-headgroups, like tetra-saccharides, seem to have high contributions from steric repulsion in the balance of interfacial forces, influencing d.

In the course of this thesis it was also investigated to what extent crosslinking via glycolipids has an influence on the mechanical properties of the interacting membranes. This was done with the help of specular and off-specular neutron diffraction (ND) which is sensitive to the thermal undulations of the membranes [84, 103]. The characteristics of these fluctuations are governed by two mechanical parameters [104]: The first one is the bending modulus κ of the individual membranes. High bending moduli suppress undulations with short wavelengths but tolerate undulations with long wavelengths. The second one is the interaction modulus (also known as compression modulus) B, which represents the strength of the interaction of each membrane with its two neighboring membranes. High interaction moduli lead to a strong positional confinement of each membrane, so that its distance to both its neighbors is always very similar (low local variations in the water layer thickness d_w). In contrast, low interaction moduli correspond to more pronounced local variations in d_w. Significant in-plane interactions of glycolipid headgroups can be assumed to affect the membrane bending modulus, whereas the formation of crosslinks may lead to an increase in the interaction modulus, as reported earlier [91]. The results of the ND experiments performed in this thesis indicate that the presence of crosslinks between adjacent membranes have no significant influence on the membrane bending modulus. The obtained values were similar for a non-crosslinked and a crosslinked system. The values for the interaction modulus could not be interpreted conclusively, because the contribution of the crosslinks to B is likely not the dominant one when additional osmotic pressures are exerted. Overall, the obtained results indicate that glycolipid-mediated membrane adhesion is a highly abundant phenomenon, which is therefore potentially of great biological relevance.

2.2.2 Summary and conclusions

The general approach of this part of the thesis was, to investigate systematically the ability of glycolipids with different saccharide-headgroups to form crosslinks. SAXS was used to quantify the effect, because it yields the lamellar period, resulting from the force balance between the membranes, which is influenced by the attractive forces induced by the glycolipids. Complementary ND experiments give further insights into the influence of crosslinking induced by the investigated glycolipids on the mechanical parameters of the interacting membranes.

In summary, the following insights into the influence on glycolipids on membrane interactions were gained within the scope of this thesis:

1)
Some of the investigated glycolipid types are found to crosslink adjacent membranes. This interaction even resists electrostatic repulsive forces, induced by incorporation of charged phospholipids into the membranes. From this result it is concluded that glycolipid-induced crosslinking occurs abundantly in nature.

2)
The investigated glycolipids with a mono-saccharide-headgroups do not crosslink adjacent membranes. It can be speculated that the headgroup is too small to protrude from the headgroup region of the matrix lipids and therefore cannot establish inter-membrane crosslinking.

3)
For glycolipids with large oligo-saccharide-headgroups, such as tetra-saccharides, the influence on membrane interaction seems to be dominated by steric repulsion, such that their crosslinking ability can hardly be assessed.

4)
Among the investigated glycolipids there is no significant effect due to crosslinking influencing mechanical parameters of the interacting membranes:

i) the values obtained for the bending modulus do not differ for crosslinked and non-crosslinked membranes;
ii) in presence of dehydrating osmotic pressures, the influence of crosslinking on the interaction modulus could not be unambiguously determined;

3 General summary and conclusions

Due to the crowded state of most living matter, interactions between interfaces and their environment must be considered key aspects of biological processes. This thesis deals with two fundamental interaction phenomena and their structural investigation: Interactions of interfaces with the components of their aqueous surroundings or and interactions between two biological interfaces. Each of these interaction types was studied with regard to an important scientific problem in the fields of biotechnology and biology.

The first topic was the adsorption of proteins to surfaces with biocompatible functionalization (see Figure 1 A). This phenomenon is of great biomedical relevance because undesired protein adsorption to surfaces is believed to be the initial step of harmful foreign-body-response to implants and drug delivery systems. The second topic was the influence of glycolipids on the interaction between lipid membranes (see Figure 1 B). As demonstrated in this thesis, this phenomenon is likely of great relevance for fundamental membrane biophysics and cell biology, but had been largely neglected so far.

Both topics were adressed with one common approach: The utilization of self-assembled (quasi-) planar lipid interfaces and the use of x-ray and neutron scattering techniques which yield highly detailed structural information. The results of this thesis demonstrate that lipid-based model-systems in combination with scattering methods are extremely useful in order to obtain structural knowledge on interaction mechanisms. The gained results contribute to deepen insights into interaction phenomena involving biological and biomedically relevant interfaces.

Regarding the adsorption of proteins to surfaces with biocompatible functionalization, *PEGylated* surfaces were chosen. *PEGylation*, a surface functionalization with end-grafted brushes of the polymer poly[ethylene glycol] (PEG), is a frequently used technique in biotechnology and therefore is of great relevance. The adsorption of proteins from human blood serum (HBS) and of specific antibodies (Abs) on PEG brushes anchored to a lipid-based model system was investigated. In order to resolve the structural details of the adsorption, neutron reflectometry (NR) was utilized.

It was found that blood proteins adsorb to the surfaces to a considerable extent, despite functionalization with a PEG brush. This adsorption consists of two distinct modes: i) strong adsorption to the brush grafting surface (termed primary adsorption), which persists also after rinsing; ii) weak adsorption to the brush itself (termed ternary adsorption), which does not persist after rinsing. The unprecedented structural insight obtained allows assessing the consequences of both adsorption types for the biomedical performance of the PEG brushes. To this end, it was concluded that the primary adsorption layer may be protected by the brush from being identified and attacked by the immune system.

This thesis also addressed the adsorption of PEG-specific antibodies, namely backbone-binding (BB) and end-binding (EB) Abs to *PEGylated* surfaces varying in brush grafting density σ and PEG polymerization degree *N.* At first, the phenomenology of BB Ab adsorption to PEG brushes was described in terms of the experimental Ab volume fraction profiles perpendicular to the interface for defined brush parameters, Ab types, and Ab concentrations. These results are valuable for theoretical model calculations of the specificity of interactions between surface and proteins. Second, the characteristic profiles obtained for adsorption of BB Abs were compared to EB Ab adsorption profiles. The data reveal that adsorption of BB and EB Abs to the surfaces, varying in brush parameters, differs significantly. The amount of adsorbed Abs and the structural parameters depend qualitatively differently on the grafting density. Ab binding is found to be substantial for all brush parameters investigated, even for the densest brushes which impose a considerable osmotic penalty to Ab insertion. It thus appears unlikely that Ab adsorption to PEG brushes can be practically prevented through variation of the parameters σ and *N*. The findings therefore motivate further efforts in the search for alternative brush chemistries, since in contrast to EB Ab adsorption, BB Ab adsorption cannot easily be suppressed by modifying the chemistry of the terminal polymer segment. These results constitute a valuable basis for further research aiming to enhance biocompatibility of medical applications, where either new design rules for *PEGylation* or alternative functionalization chemistries are in focus.

Regarding the interaction between lipid membranes, glycolipids are of special interest because they were found in high fractions in stacked membrane systems occurring in nature. Their role was longtime underestimated. It is known now that some glycolipids influence membrane interactions strongly namely, the *LewisX* and N-hexadecanonyl-lactosyl-ceramide (*LacCer*). Attraction between the membranes was found for multilayer systems containing these glycolipids. In this thesis the abundancy of attractive forces and their strength as well as the influence of the headgroup chemistry was investigated. A range of glycolipids with different saccharide-headgroups was incorporated into lipid membranes, where the mole fraction of glycolipids was varied. Furthermore negatively charged lipids were additionally incorporated into these membranes with varying mole fractions. This was done to introduce electrostatic repulsive forces acting as tensile stress, testing the crosslinking strength. The obtained results show that some of the investigated saccharide-headgroup types are able to tightly bind adjacent membranes together, also called crosslinking. For glycolipids with monosaccharide headgroups, no such crosslinking is observed, likely because they are too small to protrude from the headgroup layer of the matrix lipids.

Overall, the results suggest that glycolipid-mediated membrane adhesion is a highly abundant phenomenon with great biological relevance. Glycolipids are versatile molecules that are not only found in high fractions in stacked membrane systems, but are also found in low fractions e.g. in the plasma membranes of cells, where they are known to e.g. mediate signal pathways or act as receptors for toxins or bacteria. Possibly the found phenomenon of glycolipid induced membrane adhesion has further implications on these processes and the knowledge of the existence of the crosslinking ability will uncover new processes in biological research fields.

Appendix

I Manuscripts

Manuscript I

Neutron Reflectometry Elucidates Protein Adsorption from Human Blood Serum onto PEG Brushes

Latza V. M., Rodriguez-Loureiro I., Kiesel I., Halperin A., Fragneto G. and Schneck E.

Neutron Reflectometry Elucidates Protein Adsorption from Human Blood Serum onto PEG brushes

Victoria M. Latza[a], Ignacio Rodriguez-Loureiro[a], Irena Kiesel[b,c], Avraham Halperin[d], Giovanna Fragneto[b], and Emanuel Schneck[a,*]

[a]Max Planck Institute of Colloids and Interfaces, Am Mühlenberg 1, 14476 Potsdam, Germany

[b]Institut Laue-Langevin, 71 avenue des Martyrs, 38042 Grenoble Cedex 9, France

[c]TU Dortmund University, Otto-Hahn-Straße 4a, 44227 Dortmund, Germany

[d]Univ. Grenoble Alpes, CNRS, LIPhy, 38000 Grenoble France

[*]Corresponding author: schneck@mpikg.mpg.de, Phone: +49-331567-9404, Fax: +49-331567-9402

Keywords: surfaces and interfaces, biocompatibility, PEG brushes, lipids, neutron reflectometry

Abstract

Poly[ethylene glycol] (PEG) brushes are reputed for their ability to prevent undesired protein adsorption to material surfaces exposed to biological fluids. Here, protein adsorption out of human blood serum onto PEG brushes anchored to solid-supported lipid monolayers was characterized by neutron reflectometry, yielding volume fraction profiles of lipid headgroups, PEG, and adsorbed proteins at sub-nanometer resolution. For both PEGylated and non-PEGylated lipid surfaces, serum proteins adsorb as a thin layer of approximately 10 Å, overlapping with the head-group region. This layer corresponds to primary adsorption at the grafting surface and resists rinsing. A second, diffuse protein layer overlaps with the periphery of the PEG brush and is attributed to ternary adsorption due to protein-PEG attraction. This second layer disappears upon rinsing thus providing a first observation of the structural effect of rinsing on protein adsorption to PEG brushes.

Introduction

The deployment of brushes of terminally grafted poly[ethylene glycol] (PEG) is recognized since the 1980s as a method of repressing protein adsorption[1-3]. This approach is of great interest in applications where protein adsorption triggers undesirable processes such as blood clotting, bio-fouling, and immune response[4-14]. The broad protein "repellency" of PEG was initially attributed to the absence of protein-binding sites and to repulsive monomer-protein interactions. Based on this

picture and experimental observations, PEG was also considered non-immunogenic[15-17]. This view of PEG and brushes thereof is widely held to the present although evidence to the contrary emerged from the 2000s onwards. The evidence includes: (i) Crystallographic data on PEG binding to specific sites of proteins[18, 19]. (ii) Small angle neutron scattering and light scattering data suggesting that protein-PEG interactions are weakly attractive rather than repulsive[20, 21]. (iii) Identification of anti-PEG antibodies of clinical significance capable of binding specifically to the backbone or to terminal groups[22-24]. (iv) Indirect evidence for ternary protein adsorption within PEG brushes as deduced from the variation of the surface mass density of the adsorbed protein, Γ_{pro}, with the number of PEG polymers per unit area, σ, or the polymerization degree N[25, 26]. (v) Neutron reflectometry experiments resolving interfacial concentration profiles to identify primary adsorption at the grafting surface[27] and ternary adsorption within the PEG brush itself[28] demonstrating, in particular, binding of anti-PEG antibodies[28]. Theory efforts and physical chemistry experiments concerning the interactions of PEG brushes with proteins typically focused on surfaces contacting single component protein solutions when the identity and concentration of the adsorbing moiety are known[15, 17]. Adsorption out of blood serum/plasma is of greater significance to biomedical applications but its study confronts difficulties associated with the determination of the composition of the adsorbed proteins as it varies with altitude, i.e. distance from the grafting surface, and time (Vroman effect[29]). The scope of these difficulties relates to the size of the plasma proteome comprising 22 abundant proteins and a total of $\approx 10^4$ minority species[30] whose adsorption may be nevertheless important. A proteomics technique enabling the identification of the adsorbed proteins and the determination of their relative abundance is *nanoscale liquid chromatography coupled to tandem mass spectrometry* (nanoLC-MS/MS)[31]. It was recently deployed to characterize protein adsorption onto PEG brushes displayed by gold nanoparticles contacting blood serum[32] and onto PEG brushes grafted to planar gold surfaces contacting blood plasma[33] identifying, respectively, 147 and 24 adsorbed species. The results suggest that the composition of the adsorbed proteins varies with the grafting density and with the nature of the end-group. Importantly, fibrinogen (Fbg) and human serum albumin (HSA) were reported to adsorb from plasma but not from the corresponding single component solutions. This implies a hitherto unrecognized mechanism involving adsorption mediated by another adsorbing species[33]. This picture suggests spatial organization with the mediating species located between the gold surface and the adsorbed Fbg/HSA. In turn, it highlights the need to characterize the concentration profile of the adsorbing proteins within the PEG brush contacting blood serum or blood plasma on a sub-nanometer scale. Since nanoLC-MS/MS does not provide structural information regarding the adsorbed layer this problem lends itself to neutron reflectometry (NR).

In the following we report a first NR study of the protein and PEG concentration profiles as a function of altitude for PEG brushes immersed in human blood serum. The system studied comprised silicon blocks coated by two types of lipid monolayers: pure lipid monolayers and lipid monolayers anchoring PEG-lipids bearing a methoxy-terminated PEG chain comprising $N = 114$ monomers such that the PEG chains overlap and form a brush. The systems were characterized by NR (i) prior to incubation in serum, (ii) after incubation in whole serum and rinsing with buffer and (iii) during contact with serum diluted 10 times with buffers containing various D_2O fractions for contrast variation. The PEG volume fraction profile was not modified by protein adsorption. Primary adsorption in the form of an approximately 10 Å thin layer overlapping with the lipid head group region was observed for both incubation protocols and for both PEGylated and non-PEGylated surfaces. Ternary adsorption within the PEG brush was detected in un-rinsed samples during contact with diluted serum. It is manifested as a diffuse layer overlapping with the PEG brush and attaining a maximum at its periphery. While rinsing does not affect the primary adsorption, it removes the protein undergoing ternary adsorption. As we shall elaborate in the Discussion, the combination of nanoLC-MS/MS and NR holds much promise for the determination of the composition and spatial distribution of the adsorbing proteins thus helping in the formulation of design rules for PEGylation[13].

Experimental Section

Chemicals and Sample preparation

Unless stated otherwise the utilized chemicals were purchased from Sigma-Aldrich (St. Luis, MO, USA) and used without further purification. The PEG brushes are assembled from two amphiphilic molecules (see Fig. 1A), purchased from Avanti Polar Lipids (Alabaster, AL, USA): the lipids 1,2-distearoyl-*sn*-glycero-3-phosphocholine (DSPC) and 1,2-distearoyl-*sn*-glycero-3-phosphoetanolamine-N-[methoxy(polyethylene glycol)-5000] (PEG-lipid). PEG-lipid consists of a PEG-chain with a polymerization degree of $N = 114$ bound to the headgroup of 1,2-distearoyl-*sn*-glycero-3-phosphoetanolamine (DSPE). At neutral pH it carries one negative charge. Human blood serum is used either in the pure form or 10-times diluted in aqueous buffer solutions containing 150 mM NaCl and 20 mM Tris-aminomethan (Tris) at pH 7. Silicon single (111) crystal blocks, 50 mm x 50 mm x 10 mm in size, polished on one large face and coated with a thin layer of native silicon oxide (SiO_2), were purchased from Synchrotronix (Annemasse, France) and used as planar solid supports for the PEG brushes. The blocks were cleaned by washing with the organic solvents chloroform, acetone, and ethanol and by subsequent UV-ozone treatment for 30 min. Their surfaces were then rendered hydrophobic via covalent functionalization with trichloro(octadecyl)silane (OTS). For this purpose, the blocks were immersed in freshly prepared OTS solutions in dry hexadecane at a concentration of 1

mM for 1 h. Free and polymerized OTS were removed by washing with hexadecane and ethanol. Lipid monolayers anchoring the PEG brushes were deposited onto the hydrophobized substrates via the Langmuir-Schaefer (LS) technique[34]. For this purpose, either pure DSPC (when the mol fraction of PEG lipids is $f = 0$) or a mixture of 10 mol% ($f = 0.1$) PEG-lipid and 90 mol% DSPC in chloroform at an overall concentration of 2 mg/mL was prepared and spread at the air-water interface in a Teflon Langmuir trough (Nima Technology, Coventry, UK) containing H_2O-based buffer. After compression to a lateral pressure of $\Pi_{lat} = 35$ mN/m the monolayer was transferred onto the hydrophobic OTS by LS. For $f = 0.1$, the average PEG grafting density σ (i.e. the number of PEG chains per unit area) is approximately $\sigma \approx f/A_{lip} = 21 \times 10^{-4}$ Å^{-2}, as determined from the average area per DSPC at $\Pi_{lat} = 35$ mN/m, $A_{lip} = 47$ Å^2 [35], and as was experimentally confirmed earlier[28]. This grafting density was chosen because it is close to the highest density for which homogeneous PEG-lipid monolayers can be reliably prepared. For this high density one expects clear effects concerning a system of biomedical relevance. The in-plane interaction between PEG-lipids in a phospholipid matrix can be considered purely repulsive. In fact, the lateral repulsion between the polymers is directly seen in the pressure/area isotherms of DSPC/PEG-lipid mixtures (See Supporting Information). After the NR characterization of the bare non-PEGylated ($f = 0$) and PEGylated ($f = 0.1$) surfaces in aqueous buffer, they were either (i) incubated with whole human blood serum for at least 5 h and re-characterized by NR after rinsing with buffer solutions or (ii) re-characterized by NR during exposure with 10-times diluted serum after initial incubation of at least 5 h. Surfaces functionalized with pure DSPC monolayers were used as reference systems. Similar experiments using lipid/lipopolymer monolayers at the air/water interface can be conceived, however a number of practical issues e.g., rinsing should be taken into account.

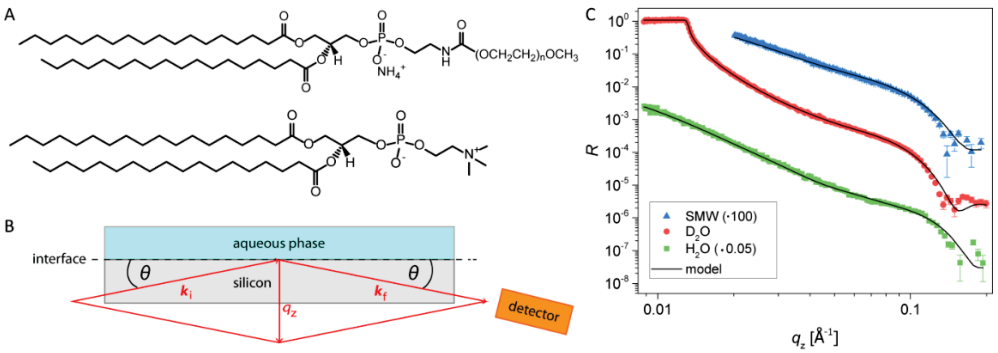

Figure 1: (A) Chemical structures of PEG-lipid (top) and DSPC (bottom), the constituents of the solid-supported PEG brushes. (B) Geometry of the NR experiments. The reflectivity R is recorded as a function of the component q_z of the scattering vector perpendicular to the interface. (C) Representative set of reflectivity curves in three water contrasts, D_2O, SMW, and H_2O. The solid lines indicate the simulated reflectivities corresponding to the best-matching model.

Neutron reflectometry

NR was performed with the reflectometers D17 and FIGARO of Institute Laue-Langevin (Grenoble, France). All measurements were carried out using "solid/liquid-cells" at a controlled temperature of T = 30°C. The geometry of specular neutron reflection is schematically depicted in Fig. 1B. After passing through the silicon block the incident beam hits the solid-liquid interface with an incident angle θ and is reflected at the same angle. The reflectivity, i.e. the intensity ratio R between reflected and incident beams, with wave vectors $\boldsymbol{k}_i$ and $\boldsymbol{k}_f$, respectively, is recorded as a function of $q_z = (4\pi/\lambda)\sin\theta$, the scattering vector component perpendicular to the interface. The neutron wavelength is denoted with λ. The measurements were conducted in the time-of-flight (TOF) mode using two fixed incident angles θ_1 = 0.8° and θ_2 = 3.0° (D17) or θ_2 = 3.2° (FIGARO). The wavelength range was 2.5 Å < λ < 25 Å (D17) or 2 Å < λ < 22 Å (FIGARO). The corresponding q_z-ranges are q_z < 0.26 Å^{-1} (D17) and q_z < 0.35 Å^{-1} (FIGARO). Data points above q_z < 0.20 Å^{-1} were, however, discarded, because the background level was reached. The relative q_z-resolution in terms of the full width at half maximum (FWHM), $\Delta q_z/q_z$, corresponds to the finite angular and wavelength resolutions, is q_z-dependent, and varies between 2% and 10%. In modeling the experimental data this aspect was taken into account via convolution (for further details see ref.[28]). The reflectivity curves $R(q_z)$ depend on the interfacial scattering length density (SLD) profiles $\rho(z)$. The latter in turn are obtained from the interfacial volume fraction profiles of all chemical components i, each having a characteristic and known SLDs ρ_i:

$$\rho_i = \frac{1}{v_i}\sum_k N_k^i b_k \qquad (1)$$

Here b_k is the coherent scattering length of an atomic nucleus of type k and N_k^i the number of such nuclei in component i per volume v_i (Footnote 1). For crystalline silicon, silicon oxide, and PEG we have, respectively, ρ_{Si} = 2.07 x 10^{-6} Å^{-2} , ρ_{SiO2} = 3.4 x 10^{-6} Å^{-2}, and ρ_{PEG} = 0.6 x 10^{-6} Å^{-2} [36]. The SLDs of lipids and proteins are discussed below. With Eq. 1, all volume fraction profiles can be reconstructed from the measured $R(q_z)$. Contrast variation is commonly applied in NR to eliminate ambiguities and enhance sensitivity to the chemical components: The SLD of the aqueous medium is varied by replacing H_2O with D_2O or defined H_2O/D_2O mixtures of known SLD. Contrast variation in a wide SLD-range is possible due to the large difference of the scattering length of the hydrogen isotopes H and D. In our measurements, we use up to four contrasts, H_2O (ρ_w = -0.56 x 10^{-6} Å^{-2}), D_2O (ρ_w = 6.37 x 10^{-6} Å^{-2}), 4-matched water (4MW, ρ_w = 4 x 10^{-6} Å^{-2}), and water matching the SLD of the silicon substrate (SMW, ρ_w = 2.07 x 10^{-6} Å^{-2}). Minor deviations in ρ_w can occur due to incomplete exchange of the aqueous medium inside the cell during the rinsing procedure. This was taken into account by

allowing for small variations in ρ_w in the data analysis, a procedure which has negligible influence on the relevant model parameters concerning PEG and protein distributions. The SLD of the serum proteins, ρ_{pro}, was estimated using the program "Biomolecular Scattering Length Density Calculator" of ISIS (Rutherford Laboratory, UK, http://psldc.isis.rl.ac.uk/Psldc/). Due to the dynamic H/D exchange of "labile" protein hydrogens, ρ_{pro} is dependent on the SLD of the aqueous medium and for typical proteins it is approximated by

$$\rho_{pro} = 2.0 \times 10^{-6} Å^{-2} + 0.19\rho_w \quad (2)$$

[37, 38]. As a result we obtain $\rho_{pro}(H_2O) = 1.9 \cdot 10^{-6}$ Å^{-2}, $\rho_{pro}(D_2O) = 3.3 \cdot 10^{-6}$ Å^{-2}, $\rho_{pro}(4MW) = 2.8 \cdot 10^{-6}$ Å^{-2} and $\rho_{pro}(SMW) = 2.4 \cdot 10^{-6}$ Å^{-2}. The fact that all reflectivity curves can be modeled consistently using Eq. 2 (see Results section) corroborates the commonly accepted picture that adsorption layers from blood serum are largely proteinaceous.

Data analysis

A representative set of reflectivity curves, from a PEGylated surface incubated in serum diluted with D_2O, SMW, and H_2O, is shown in Fig. 1C. The solid lines indicate the simulated reflectivity curves corresponding to the best-matching common model for all contrasts. The model, schematically illustrated in Fig. 2, is formulated in terms of the volume fraction profiles of all chemical components at altitude z along the normal to the interface, $\Phi_i(z)$[27]. A similar approach was used by Heinrich & Lösche to study proteins associated with lipid bilayers[39]. The $z = 0$ plane is defined as the interface between the lipid headgroups and the aqueous medium accommodating the hydrated PEG brush and proteins. The model consistently describes the reflectivity curves of a sample for all measurement conditions, i.e. before and after exposure to serum and in all contrast fluids. The SLD profile of each condition is defined as:

$$\rho(z) = \Phi_{Si}(z)\rho_{Si} + \Phi_{SiO2}(z)\rho_{SiO2} + \Phi_{hc}(z)\rho_{hc} + \Phi_{hg}(z)\rho_{hg} + \Phi_{PEG}(z)\rho_{PEG} + \Phi_{pro}(z)\rho_{pro} + \Phi_w(z)\rho_w \quad (3)$$

where Φ_{Si}, Φ_{SiO2}, Φ_{hc}, Φ_{hg}, Φ_{PEG}, Φ_{pro}, and Φ_w, denote the volume fractions of silicon, SiO_2, hydrocarbon chains (belonging to both OTS and lipids), lipid headgroups, PEG, proteins, and water, respectively. By definition, the sum of all volume fractions equals unity at each z:

$$\sum_i \Phi_i(z) \equiv 1 \quad (4)$$

The silicon substrate is modeled as semi-infinite continuum with constant SLD ρ_{Si}. The SiO_2, hydrocarbon chain and lipid headgroup layers are represented as homogeneous slabs with adjustable thicknesses d_{SiO2}, d_{hc}, and d_{hg}, respectively. To account for interfacial roughness, the profiles of all slabs are modulated by error functions with adjustable roughness parameters δ_i. Uncertainties introduced with adjustable roughness parameters have negligible influence on the parameters concerning PEG and protein distributions. The SLD of SiO_2 is kept at the literature value ρ_{SiO2}. However, in line with earlier reports[27, 28, 40, 41], we account for oxide hydration effects by allowing for a finite water content in the SiO_2 layer, characterized by an adjustable parameter Φ_w^{SiO2}. In contrast, the water content in the hydrophobic hydrocarbon layer is assumed to be negligible. The SLD of the hydrocarbon chains ρ_{hc} is allowed to vary in the range 0 to $-0.5\cdot10^{-6}$ Å^{-2}, corresponding to a wide range of possible packing densities. For the headgroup SLD we use the literature value $\rho_{hg} = 1.75\cdot10^{-6}$ Å^{-2} [42].

The volume fraction of the PEG brush grafted to the lipid/water interface is modeled as

$$\Phi_{PEG}(z) = I_{hg/w}(z)\cdot\Phi_m(z) \tag{5}$$

where $I_{hg/w}(z)$ accounts for the topographic roughness of the grafting surface in the form of an error function characterized by the roughness parameter $\delta_{hg/w}$. The monomer profile of a planar brush is phenomenologically described by a stretched exponential

$$\Phi_m(z) = \Phi_m^0 e^{-|z/\Lambda|^n} \tag{6}$$

In this description, Λ denotes the decay length of the monomer volume fraction profile and n is a stretching exponent. For a given Λ, n, and brush grafting density σ, the pre-factor Φ_m^0 is not an independent parameter, but is determined by the normalization condition:

$$\int \Phi_{PEG}(z)dz = N\sigma v_{EG} \tag{7}$$

where $v_{PEG} = 69$ Å^3 is the volume per ethylene glycol monomer, consistent with the value of ρ_{PEG}. In earlier studies, we utilized simpler parabolic brush profiles, as suggested by self-consistent-field (SCF). These were sufficient to describe reflectivity curves of similar brushes at a satisfactory level [27, 28]. Here we use the mathematically more complex stretched exponential description for two reasons: First, introducing an additional parameter reproduces the shape of the brush volume fraction profiles including the tail at the outer edge in a superior way. Second, varying the stretching exponent yields a wide variety of shapes, from box-like to slowly decaying, thus rendering this functional form suitable to empirically fit the profiles of brushes perturbed by adsorbed serum proteins.

Consequently, two independent sets of Λ and n are considered, corresponding to the brush before and after protein adsorption.

Regarding the protein profiles, we simultaneously allow for three different protein adsorption modes discussed in the literature: primary adsorption to the grafting surface[43, 44], secondary adsorption at the outer edge of the brush[43-45], and ternary adsorption within the brush itself due to protein-polymer attraction[25, 46, 47]. The protein volume fraction distribution $\Phi_{pro}(z)$ in each sample after protein adsorption is described as the sum of up to three Gaussian distributions

$$\Phi_{pro}(z) = I_{hc/hg}(z) \cdot \sum_k \Phi_k^{pro}(z) \qquad \text{with} \qquad \Phi_k^{pro}(z) = \Phi_k^{\max} \cdot \exp\left[-\left(\frac{z - z_k^{pro}}{2 w_k^{pro}} \right)^2 \right] \tag{8}$$

where each Gaussian represents one adsorption mode. In Eq. 8, z_k^{pro}, w_k^{pro}, and $\Phi_k^{\max}$ denote, respectively, the center position, width, and scale factor for each mode. To satisfactorily reproduce the experimental reflectivity curves after exposure to the serum it is necessary to allow for protein penetration into the headgroup region of the lipid layer at the grafting surface (see Fig. 2 and Results Section). The protein distribution is therefore truncated only at the hydrocarbon/headgroup interface, via multiplication with $I_{hc/hg}(z)$ which accounts for the interfacial roughness $\delta_{hc/hg}$ as in Eq. 5. Finally, water occupies all the space free of the other components so that $\Phi_w(z)$ follows directly from Eq. 4.

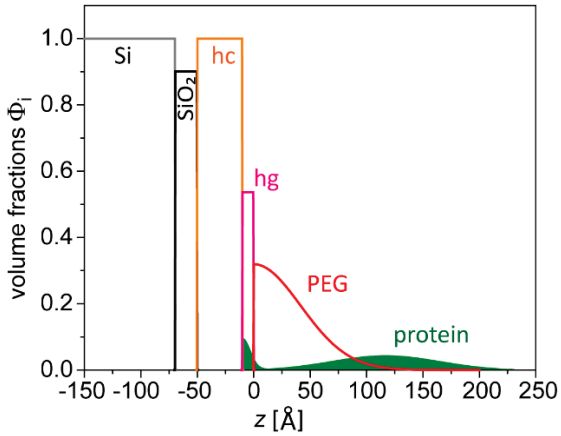

Figure 2: Schematic illustration of the model describing the sample structure in terms of the volume fraction profiles $\Phi_i(z)$ of all chemical components: Silicon (Si), silicon oxide (SiO_2), hydrocarbon chains (hc), lipid head groups (hg), PEG, and proteins (pro). For the sake of clarity, the interfacial roughness of the SiO_2, hc, and hg slabs is neglected in this illustration. The PEG and protein profiles as described by their fitting functions (Eqs. 6 and 8) are intrinsically smooth.

The set of model parameters with the best agreement with the experimental reflectivity data is obtained as follows: starting from initial parameter values specified in the Supporting Material, we first employ Eq. 3 to calculate each sample's interfacial SLD profiles ρ(z) corresponding to all measurement conditions (i.e. the same sample before and after protein adsorption and in each contrast fluid.) In the next step, we calculate the reflectivity curves corresponding to the $\rho(z)$ profiles using dynamical reflection theory. To this end the profiles are discretized into hundreds of thin slabs of 1 Å thickness and of constant SLD. The q_z-dependent intensities are then calculated via application of Fresnel's reflection laws at each slab/slab interface using the iterative recipe of Parratt and the outcome is compared to the experimental data. In the last step, the parameters are varied until the best simultaneous agreement with all experimental reflectivity curves, characterized by the minimal chi-square deviation χ^2, was reached. For the studied sample architecture, the H_2O contrast is most sensitive to the protein distributions (see further below). The statistical weight of this contrast was thus purposefully increased by a factor of 3, to prevent the fit from being dominated by the D_2O contrast, which is less sensitive to the protein distributions but has more data points and smaller error bars. We consider this treatment justified, although consistent results are obtained also without it, see Supporting Information. The volume fraction profiles obtained for various samples are shown in Figs. 3B and E and 4A and discussed below.

Results and Discussion

This study primarily deals with the adsorption of proteins from human blood serum onto non-PEGylated and PEGylated surfaces as characterized by the adsorbed protein mass per unit area, Γ_{pro}, and the corresponding protein density profiles $\Phi_{\text{pro}}(z)$. Nevertheless, it is instructive to first discuss the structure of the non-PEGylated and PEGylated surfaces prior to protein adsorption since these are at the basis of all subsequent analysis.

Non-PEGylated and PEGylated surfaces prior to protein adsorption

The thickness of the silicon oxide layer is obtained as d_{SiO2} = 18 ± 1 Å, where the error represents the standard deviation over all samples characterized. The content of water in the oxide is Φ_w^{SiO2} = 14 ± 4 vol% (Footnote 2). Differences among the structures of the oxide layers reflect the individual history of the silicon blocks but do not significantly affect the surface functionalization. The thickness of the hydrocarbon layer, jointly formed by OTS and the alkyl chains of the phospholipid layer, is determined to be d_{hc} = 38 ± 2 Å. All these results are consistent with the values reported in

earlier studies[28, 48]. The thickness of the layer formed by the hydrated lipid headgroups, which was neglected in our earlier work, is found to be d_{hg} = 12 ± 4 Å. The roughness of the headgroup-water interface, which acts as grafting surface for the PEG brush, is $\delta_{hg,w}$ = 6 ± 3 Å. The structure of the PEG brushes present on the PEGylated surfaces, with the grafting density specified, is discerned best in the D_2O contrast[28]. The brushes are modeled according to Eqs. 5-7 and the fit yields Λ = 70 ± 10 Å and n = 0.93 ± 0.06, where the former is comparable to the values obtained in an earlier work assuming parabolic brush profiles[28] (Footnote 3).

Protein Adsorption

Non-PEGylated surface after contact with whole serum and subsequent rinsing

The sample preparation procedure (see Experimental Section) of the non-PEGylated samples yields an outer boundary of densely packed phospholipid headgroups contacting the blood serum. This layer serves as anchoring surface for the PEG brush and in pure form it serves as a reference state. Its role as a reference state benefits from the relatively low protein adsorption onto phospholipid layers[49, 50] as compared to commonly studied surfaces such as polystyrene (PS) or iron oxide[51-53]. This is advantageous because it avoids masking of additional adsorption modes by extensive primary adsorption onto the grafting surface. This system is also of interest because PEGylated phospholipid layers closely resemble the surfaces of stealth liposomes[7]. Fig. 3A shows reflectivity curves in H_2O contrast of a non-PEGylated surface before and after incubation with whole blood serum and subsequent rinsing. The complete data sets including D_2O, 4MW, and SMW contrasts are shown in the Supporting Information. While the reflectivity curves for all four water contrasts change upon protein adsorption, the H_2O contrast is shown because it is most sensitive to the adsorption of proteins. This is because the SLDs of H_2O and of the hydrocarbon layer are both low, thus enhancing the signature of headgroup + protein layer, which stands out because of its higher SLD (see insets of Fig. 3 A and D). The solid line indicates the simulated reflectivity obtained using the best-matching parameters of the common model. The characteristic features of the curve measured before protein adsorption, namely a dip at $q_z \approx 0.06$ Å^{-1} and a maximum around $q_z \approx 0.10$ Å^{-1}, are related to a maximum in the SLD profile $\rho(z)$ due to the headgroup layer. These features are enhanced upon protein adsorption thus suggesting significant adsorption of proteins that accumulate in the headgroup region such that the SLD maximum becomes more pronounced. Indeed, the reflectivity data after protein adsorption and rinsing are well reproduced by the simulated curves when assuming a narrow unimodal protein distribution overlapping with the headgroup distribution (see Fig. 3B). The corresponding sample structure is schematically illustrated in Fig. 3C. As shown in the

Supporting Information, only a scenario in which the protein layer fully overlaps with the headgroup layer reproduces the experimental reflectivity data. Note that this structure is obtained after extensive rinsing with neat solution, so that the binding of the adsorbed proteins to the surface is effectively irreversible. Interactions between proteins and lipids generally reflect a subtle interplay of electrostatic, van der Waals, hydrophobic, and solvation forces[54]. The total adsorbed protein mass per unit area is specified by

$$\Gamma_{pro} = \frac{m_{pro}}{v_{pro}} \int \Phi_{pro}(z) dz \qquad (9)$$

where $m_{pro}/v_{pro} \approx 1.4$ g/cm^3 is the mass density of protein estimated using the "Biomolecular Scattering Length Density Calculator". Note that this estimate is strictly consistent with the above estimation of the protein SLD. For the non-PEGylated surface after incubation with serum and subsequent rinsing we find: $\Gamma_{pro} = 0.43 \pm 0.05$ mg/m^2, where the error approximately reflects the parameter variation throughout the evolution and refinement of the model description, i.e. it reflects the robustness of the parameters with respect to the model. The obtained value is low when compared to the extent of protein adsorption reported for commonly studied surface types like polystyrene (PS) or iron oxide (typically $\gtrsim 0.5$ mg/m^2 for at least one abundant protein species)[51-53] and consistent with earlier studies reporting low protein adsorption to phospholipid surfaces[49, 50]. In contrast to earlier studies of adsorption out of serum/plasma that utilized surface plasmon resonance (SPR)[33], quartz-crystal microbalance (QCM)[55, 56] or ellipsometry[57], our NR measurements yield not only Γ_{pro}, but also the structural details of the adsorbed protein layer. The adsorbed protein layer thickness, defined as the full width at half the maximum (FWHM) of the protein volume fraction distribution, is approximately 12 Å, corresponding to $w^{pro} \approx 5$ Å in Eq. 8. In view of considerable interfacial roughness, the actual local thickness of the protein layer is probably thinner than 10 Å. This finding indicates that the adsorbed serum proteins are small or strongly denaturated. It thus excludes scenarios in which the adsorbed layer is formed by large, sparsely adhering globular proteins. Adsorption of polypeptides into the headgroup region of phospholipid surfaces has been reported in experimental[58] and computer simulation[59] studies. It should be noted that the details of the adsorbed protein layer in terms of composition and structure depend on the chemical nature of the surface and thus cannot be generalized. For example, adsorbed protein double-layers were reported for hydrophobic surfaces [60].

PEGylated surface after contact with whole serum and subsequent rinsing

Large proteins can only approach the grafting surface by compressing the brush. Small proteins can penetrate the brush with only local effect on the brush structure. For spherical proteins, the crossover between the two regimes occurs when the protein radius is comparable to the brush thickness. Three different adsorption modes were postulated for small proteins interacting with polymer brushes: (i) Primary adsorption at the brush grafting surface due to favorable short-range protein-surface interactions such as hydrophobic attraction, electrostatic attraction, or hydrogen bonding[43, 44]. (ii) Secondary adsorption at the brush periphery due to an equilibrium between long-range protein-surface attraction and the osmotic penalty incurred by inserting the protein into a brush when the polymer-protein interactions are repulsive[43-45, 61]. (iii) Ternary adsorption within the brush itself due to protein-polymer attraction. Within this last scenario it is helpful to distinguish between adsorption due to specific PEG binding sites and adsorption attributed to proteins having uniform and weakly attractive surfaces[25, 46, 47]. The weak ternary adsorption of serum albumin and lysosome was demonstrated in earlier experimental work providing indirect evidence and suggesting weak, non-specific protein-polymer attraction[26, 52]. Subsequent experiments yielded direct, structural evidence for strong, specific protein-polymer binding of anti-PEG antibodies[28].

As elaborated in the Experimental Section, the analysis of the reflectivity data in the present work can account for several concurrent protein distributions. In other words, the functional form adopted for the trial function allows fitting a brush undergoing both primary and ternary adsorption. Fig. 3D shows reflectivity curves in H_2O contrast of a PEGylated surface before and after incubation with whole blood serum and subsequent rinsing. This is the counterpart of the experiment involving the non-PEGylated surface as discussed before (Fig. 3A-C). The complete data sets including D_2O, 4MW, and SMW contrasts are shown in the Supporting Information. The solid line again indicates the simulated reflectivity using the best-matching parameters of the common model. The H_2O contrast, the most sensitive to primary protein adsorption, again reveals distinct changes. As in the non-PEGylated case, the features at $q_z \approx 0.06$ Å^{-1} and $q_z \approx 0.10$ Å^{-1} are enhanced, suggesting adsorption at the grafting surface. Indeed, the reflectivity data can be well reproduced assuming a single, narrow protein sub-monolayer overlapping with the headgroup region (see Fig. 3E). The reflectivity fits cannot be further improved by addition of a second protein distribution within the brush or at its periphery. In fact, the fit deteriorates when additional protein distributions are invoked. The experimental data are best reproduced by setting these additional contributions to zero. Accordingly, we observe pure primary adsorption to the grafting surface, as was reported earlier for single component protein solutions[27]. Note however, that in the present case the adsorbed layer may comprise a number of different proteins in contrast to the case of adsorption out of single component solutions. The corresponding sample structure is schematically illustrated in Fig. 3F. As in case of the non-PEGylated surface, the adsorption of the protein layer is effectively irreversible in

that it resists rinsing with aqueous buffers. The total adsorbed protein mass per unit area according to Eq. 9 is Γ_{pro} = 0.41 ± 0.05 mg/m^2. This is much lower than the amount of primary adsorption reported earlier for the primary adsorption of myoglobin onto PEGylated, hydrophobic PS surfaces[27], but comparable to the corresponding value for the non-PEGylated surface discussed above, Γ_{pro} = 0.43 ± 0.05 mg/m^2. Furthermore, within the experimental error the structure of the primary adsorption layer as observed by NR is identical to the structure of the protein layer adsorbed to the non-PEGylated surface (compare Fig. 3B and E). This result demonstrates that the influence of the negative charge carried by each PEG lipid is only minor, presumably due to the low charge density. Note however that these measurements cannot exclude differences in the protein composition of the two systems. In case of the PEGylated surface, one may argue that the adsorption layer comprises small proteins because of the osmotic penalty associated with the insertion of large proteins into the brush. To first approximation, this penalty is $G \approx v_{pro}\Pi$, as estimated within the Alexander step like model. The osmotic pressure for athermal solvent is $\Pi \approx k_BT/\xi^3$, where $\xi \approx \sigma^{-1/2}$ is the blob size. For $\sigma \approx 21 \times 10^{-4}$ Å^{-2} we obtain $\Pi \approx 4 \times 10^5$ Pa, so that $G > k_BT$ for $v_{pro} > \xi^3 \approx 10000$ Å^3. Using $m_{pro}/v_{pro} \approx 1.4$ g/cm^3, $G \approx k_BT$ corresponds roughly to $m_{pro} \approx 8$ kDa. Osmotic exclusion of proteins from a polymer brush has been observed earlier[28]. Based on this argument it is highly unlikely that serum albumin ($m_{pro} \approx 67$ kDa), globulins ($m_{pro} > 36$ kDa), or transferrin ($m_{pro} \approx 75$ kDa), which are all among the most abundant serum proteins[62], contribute to the primary adsorption layer. On the other hand, serum amyloids are potential candidates since they are smaller ($m_{pro} \approx 12$ kDa), comparatively abundant in the serum[63], and reported to have an affinity for phosphatidylcholine (PC) lipids[64]. Conversely, the structural similarity of the adsorbed protein layers at PEGylated and non-PEGylated phospholipid surfaces suggests that small protein adsorption is dominant in both cases. Our discussion of this scenario invoked the "small" protein limit when an inserted protein causes small local perturbation in the brush structure. Within our model the brush structure as characterized by $\Phi_{PEG}(z)$ is set by Λ and n. Both parameters change slightly upon protein adsorption, from Λ = 73 Å and n = 0.83 prior to adsorption to Λ = 80 Å and n = 0.93 after. These differences are, however, insignificant because the estimated parameter errors are ± 10 Å for Λ and ± 0.06 for n. Accordingly, within our analysis the PEG profile is only weakly perturbed by protein adsorption as was initially assumed.

In summary, the PEGylation of the studied surface does not affect the amount of adsorbed protein following rinsing or the corresponding protein layer structure. In fact, the adsorbed protein layer resulting from exposure to serum following by a rinse is structurally unaffected by the presence of the brush, although the composition profile of the adsorbed proteins may be different. We reemphasize that this result may well depend on the nature of the grafting surface.

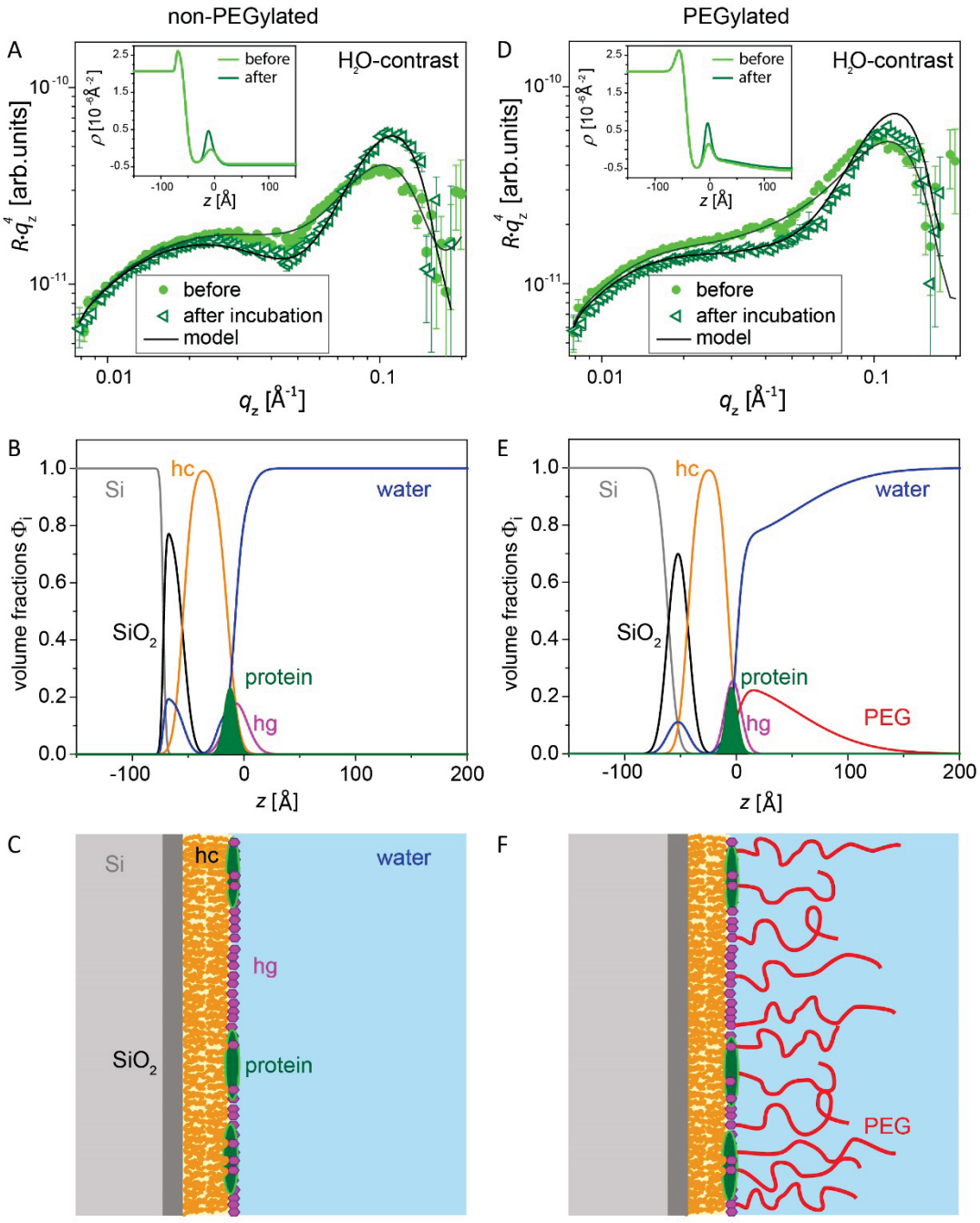

Figure 3: (A and D) Reflectivity curves of non-PEGylated (A) and PEGylated (D) surfaces in H_2O contrast before and after incubation with human blood serum and subsequent rinsing. Solid lines represent the simulated intensities corresponding to the best-matching parameters in the common models. Insets: SLD profiles in H_2O contrast before (light solid lines) and after (dark solid lines) incubation and rinsing. (B and E) The volume fraction profiles $\Phi(z)$ of all chemical components (Si, SiO_2, hydrocarbon chains, headgroups, PEG, protein, and water) for non-PEGylated (B) and PEGylated (E) surfaces after incubation with human blood serum and subsequent rinsing. The protein volume fraction distributions are unimodal in both cases. The different widths of the headgroup volume fraction profiles mainly reflect differences in the surface roughness. (C and F) Schematic illustration of the structures of non-PEGylated (C) and PEGylated (F) surfaces after incubation with human blood serum and subsequent rinsing, as suggested by the volume fraction profiles in panels B and E.

PEGylated and non-PEGylated surfaces in contact with dilute serum without rinsing

In the earlier sections, we discussed protein adsorption as observed after rinsing the samples thus removing weakly adsorbed proteins. While such strongly bound proteins are important, it is also of interest to characterize the structure of surfaces carrying weakly adsorbed proteins. We therefore carried out NR measurements of non-PEGylated and PEGylated surfaces in contact with serum. Human serum in which H_2O is replaced with D_2O is not commercially available and non-trivial to prepare. Nevertheless, in order to implement contrast variation, we diluted whole serum by a factor of 10 with aqueous buffers based on D_2O, H_2O, or defined mixtures thereof. The dilution has two noteworthy implications. First, even when diluted with D_2O buffer, the resulting SLD of the diluted serum serving as aqueous bulk medium does not reach the SLD of pure D_2O. Second, as we shall see, the dilution reduces Γ_{pro}. To the extent that mass action law applies this reduction follows from the reduction of the reactants concentration. A similar effect is expected for kinetic control. A much simpler effect of dilution is the reduction in the total amount of protein available for adsorption in the sample cell. Thus, if the adsorbing species is a minority component, a 10 times dilution may result in a situation whereby the adsorption of all the available minority species will give rise to Γ_{pro} lower than the value obtained upon contacting the whole serum.

The volume fraction profiles of proteins adsorbed to the non-PEGylated surface in presence of diluted serum are qualitatively similar to those obtained upon incubation in whole serum and subsequent rinsing. The reflectivity curves measured in three contrasts (see Supporting Information) are again well reproduced with a model incorporating a single, narrow protein distribution in the headgroup region. The best-matching volume fraction profiles are shown in the Supporting Information. The amount of protein adsorbed in the narrow headgroup layer ($\Gamma_{pro} \approx 0.05$ mg/m^2) is significantly lower in comparison to the corresponding case of incubation in whole serum ($\Gamma_{pro} = 0.43 \pm 5$ mg/m^2) for an identical period. $\Phi_{pro}(z)$ as obtained on a PEGylated surface in presence of diluted serum is superficially unimodal. At first glance, the reflectivity curves measured in three contrasts can be reproduced satisfactorily assuming pure primary adsorption with a single, narrow layer of proteins in the headgroup region. However, the fit quality is significantly improved, when the model allows for ternary protein adsorption. The absolute χ^2 value of the global model in this case decreases by more than 400 (from 5608 to 5176), which is highly significant[65] by the standard statistical criteria (Footnote 4) and also by alternative, stricter criteria, requiring for instance a 5% difference in χ^2 (ref. [66]). The reflectivity curves and this fit are presented in the Supporting Information, where we also show a comparison of the H_2O reflectivity data with model reflectivity curves excluding and including ternary adsorption. The best-matching model for $\Phi_{pro}(z)$ yields an additional ternary adsorption term $\Phi_{tern}^{pro}(z)$ overlapping on the exterior side with the tail of the PEG

brush, see Fig. 4 A. The center of $\Phi_{tern}^{pro}(z)$ is located at z_{tern}^{pro} ≈ 100 Å above the grafting surface, its width in terms of the FWHM is approximately 90 Å (corresponding to w_{tern}^{pro} ≈ 40 Å in Eq. 8), and its maximal value is approximately 5 vol%. As in the cases discussed previously, the PEG volume fraction profile is not affected by the protein adsorption. From a structural viewpoint alone it is difficult to attribute the broad peripheral $\Phi_{pro}(z)$ to secondary or ternary adsorption. Both adsorption modes can give rise to qualitatively similar profiles. It is however clear that we are dealing with ternary adsorption. If secondary adsorption resulting from long-range attraction between the grafting surface and the proteins played a role in the present case it would give rise to a relatively thick multilayer of adsorbed proteins on the non-PEGylated surface. As discussed earlier, protein adsorption within the brush is considered ternary whenever it is induced by protein-polymer attraction. In view of the documented significant preferential adsorption of PEG to the hydrophobic air/water interface, one can speculate that the observed protein-PEG attraction is at least partially of hydrophobic nature. The protein mass per surface area in the primary and ternary adsorption modes is specified by

$$\Gamma_{prim}^{pro} = \frac{m_{pro}}{v_{pro}} \int \Phi_{prim}^{pro}(z) dz \qquad \text{and} \qquad \Gamma_{tern}^{pro} = \frac{m_{pro}}{v_{pro}} \int \Phi_{tern}^{pro}(z) dz \tag{10}$$

leading to Γ_{prim}^{pro} ≈ 0.1 mg/m^2 and Γ_{tern}^{pro} ≈ 0.6 mg/m^2. The amount of protein in the layer of primary adsorption is lower than the one observed for the same surface type after incubation with whole serum and subsequent rinsing (Γ_{pro} = 0.41 ± 0.05 mg/m^2, see above), following the trend observed also for the non-PEGylated surfaces. The overall amount of protein adsorbed to the PEGylated surface in presence of diluted serum, $\Gamma_{pro} = \Gamma_{pro}^{prim} + \Gamma_{pro}^{tern}$ ≈ 0.7 mg/m^2, is dominated by the ternary mode. In contrast to the primary adsorption layer, the proteins adsorbed ternarily are only weakly bound and do not resist rinsing (see above).

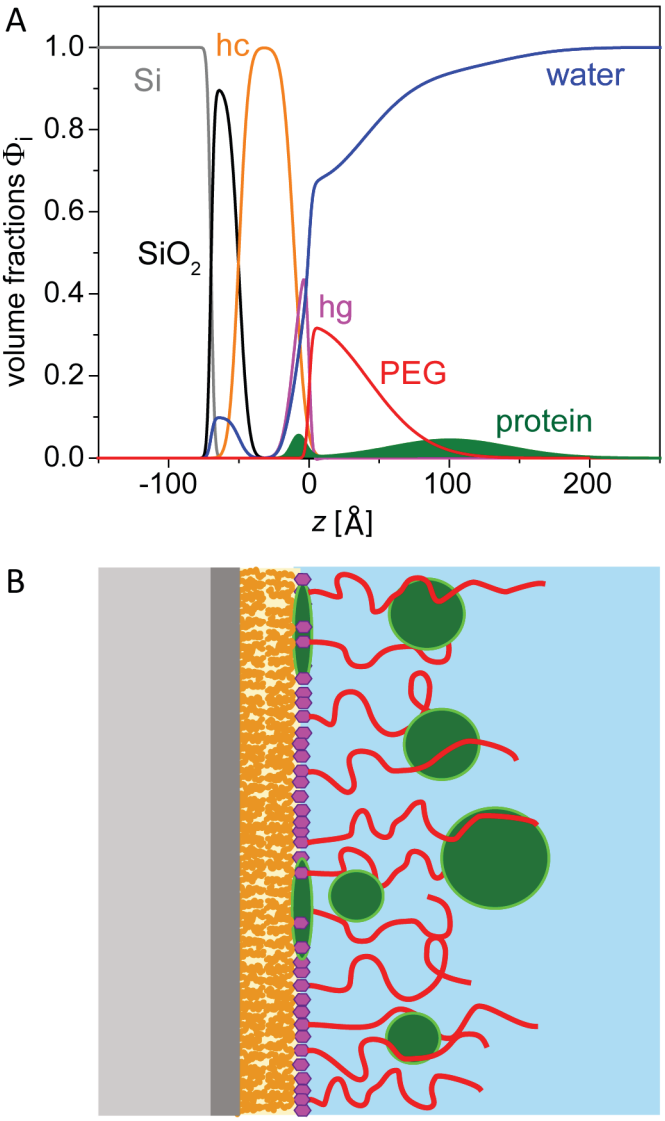

Figure 4: (A) Best-matching volume fraction profiles $\Phi(z)$ of all chemical components for PEGylated surfaces during incubation in 10-times diluted human blood serum. The protein distribution is bimodal. (B) Schematic illustration of the structures according to the volume fraction profiles in panel A. Primary protein adsorption to the brush-grafting surface coexists with ternary adsorption to the brush periphery.

Discussion

In this work, we utilized NR to investigate protein adsorption from blood serum onto PEG brushes anchored to lipid monolayers, surfaces closely resembling stealth liposomes[7]. The brush comprises chains of polymerization degree N = 114 with an area per chain $\Sigma = 1/\sigma = 470$ Å^2, i.e. with distance of approximately 21 Å between grafting sites. The NR measurements yielded interfacial volume density profiles at sub-nanometer resolution. We identified the following features: (i) Primary adsorption, at the grafting surface, manifested as an approximately 10 Å thick layer overlapping with the headgroup

region of the lipids anchoring the PEG chains. The headgroup layer in its bare state has a comparable thickness and comprises approximately 50 % water. It is thus able to accommodate the adsorbed protein. Such primary adsorbed protein layers were observed in PEGylated and non-PEGylated surfaces irrespective of the serum dilution or whether the samples were rinsed by neat buffer or not. The thickness of the corresponding protein layer suggests adsorption of small proteins in their native state or of larger proteins undergoing denaturation. Since the PEG brush penalizes the primary adsorption of large proteins our results suggest that the primary adsorption involves small proteins. (ii) Ternary adsorption within the PEG brush manifested as diffuse protein layer having a maximum at a distance of approximately 100 Å from the grafting surface. This layer is sensitive to rinsing and is totally removed upon washing by neat buffer. The term ternary adsorption is utilized because we attribute this layer to PEG-protein attraction. We rule out secondary adsorption due long-ranged protein-surface attraction because there is no protein adsorption at similar altitudes for the non-PEGylated surface.

In vague terms, the results are consistent with theory ideas[25, 43-47, 61, 67]: For proteins small in comparison to the brush thickness insertion into PEG brushes incurs an osmotic penalty Πv_{pro}, proportional to the osmotic pressure in the bare brush Π and the volume of the protein v_{pro}. This penalty counteracts the adsorption energy at the surface. A PEG brush thus acts as a semipermeable membrane that selects proteins of lower v_{pro} for adsorption at the surface. Within this picture a surface displaying a brush with Σ = 470 Å^2 preferentially adsorbs proteins having volume lower than approximately 10^4 Å^3, corresponding to molecular weights below 8 kDa. In this molecular weight range, the osmotic penalty is below k_BT and thus negligible. It is interesting to note that the proteins adsorbed at the grafting surface are shielded from contact with large blood proteins because the brush functions as a semipermeable barrier selectively blocking approach by large proteins. The potential role of this effect remains to be explored. Larger proteins having attractive interaction to PEG are adsorbed throughout the PEG layer. The ternary adsorption reflects the interplay of PEG binding mode (to the PEG back bone or terminal groups), the binding energy and the variation in the osmotic penalty that decreases with increasing z. We note here the evidence that attractive PEG-protein interactions[19] are not rare and may thus be well represented in the serum proteome. This suggests that the observed adsorption reflects contributions from many protein species. This scenario is also supported by results suggesting that the composition of the adsorbed proteins varies with the PEG grafting density[32]. Altogether, these points suggest that the adsorbed layers comprise many proteins with composition that may well vary with z. The z dependence of the composition profile is of special interest in view of the results of Riedel et al.[33] suggesting the possibility that

proteins that are nonadsorbing on their own do adsorb out of multicomponent solution because of interactions mediated by adsorbing species.

The direct identification of the adsorbing proteins as a function of z is currently impossible. Furthermore, the interaction energies with PEG and the grafting surface are established only for a small minority of the relevant proteins. It is thus not even possible to identify the adsorbing species by inspecting the serum proteome. With these reservations in mind there are several promising research directions to explore. Our interpretation suggests that a minimal model system can exhibit similar adsorption behavior. Based on earlier experimental results[25, 52, 68] and theory[25, 43-47, 61, 67] we speculate that the "serum adsorption scenario", combining primary and ternary modes, should be reproduced upon contacting a PEGylated surface with a binary solution of monomeric insulin and HSA. HSA is the bigger protein ($m_{pro} \approx 67$ kDa, $v_{pro} \approx 8 \times 10^4$ Å^3) and it is known to undergo ternary adsorption onto PEG. Monomeric insulin (see *insulin-lispro*, http://www.sigmaaldrich.com/), on the other hand, is a small protein ($m_{pro} \approx 5$ kDa, $v_{pro} \approx 6 \times 10^3$ Å^3) that was not reported to adsorb onto PEG and is known to adsorb to lipid layers[69]. Accordingly, a PEG brush contacting a binary insulin/HSA solution is expected to manifest a "serum like" profile with insulin at the grafting surface and HSA adsorbed within the brush. Exploring this direction affords the advantage that the ingredients are well characterized and commercially available. Another direction utilizes depleted serum (http://www.fishersci.com/). Comparing the NR reflectivity curves of serum with the corresponding depleted serum curves is expected to shed light on the contribution of the depleted component to Γ_{prot} and its spatial distribution within the brush. A complementary, though labor-intensive approach requires deuterated proteins. The formulation of this strategy is straightforward for the case of HSA because of the consistent evidence that HSA is one of the proteins adsorbing on PEG brushes[25, 32, 33, 52]. One may thus replace the HSA from the HSA-depleted serum by deuterated HSA. NR of the PEGylated surface following incubation with the selectively deuterated serum should help resolve the spatial distribution of the adsorbed HSA.

As noted in the Introduction, NR complements nanoLC-MS/MS. The latter enables to identify the adsorbing proteins and their abundance but provides no information on the structure of the adsorbed layer[32, 33]. NR, on the other hand, probes the structure of the adsorbed layer but does not permit to identify the adsorbing species. In an ideal situation, the samples will be characterized using both techniques. Note however that (i) nanoLC-MS/MS does not currently guarantee the identification of all adsorbed species[31] and (ii) the sample preparation protocol for nanoLC-MS/MS measurements involves a rinsing step and this method thus cannot characterize the "washable" component.

The adsorption of proteins onto PEGylated surfaces remains a subject of active research despite 40 years of activity[1-3]. There is need for this research because PEGylation sometimes works, while on other occasions it is a promising approach that does not lead to the results hoped for. Thus, PEGylation applications were investigated on both nano and macroscopic scales. Yet, only the nano applications, such as PEGylated protein drugs[70] and stealth liposomes[7], led to industrial exploitation with sales in the multibillion $ range[70]. When PEGylation does work it sometimes deploys PEG brushes as suggested by physical chemistry. For example, stealth liposomes display PEG brushes[7]. However, PEGylated protein drugs such as PEG-interferon are functionalized by a single PEG chain, i.e. they are located in the mushroom regime where physical chemistry arguments suggest weak effect. Altogether the mechanisms underlying the successes and failures of PEGylation remain to be clarified and the nature of the interaction of PEG brushes with proteins is thought to be, now as in the past, a key ingredient.

	Incubation with whole serum and subsequent rinsing		**Incubation with diluted serum without rinsing**	
	non-PEGylated	PEGylated	non-PEGylated	PEGylated
d_{SiO2} [Å]	18 ± 2	18 ± 2	17 ± 2	20 ± 2
Φ_w^{SiO2} [%]	20 ± 5	14 ± 5	13 ± 5	10 ± 5
d_{hc} [Å]	39 ± 2	36 ± 2	39 ± 2	40 ± 2
ρ_{hc} [10^{-6}Å^{-2}]	-0.4 ± 0.1	-0.5 ± 0.1	-0.5 ± 0.1	-0.5 ± 0.1
d_{hg} [Å]	> 10	7 ± 3	> 10	10 ± 3
$D_{hg} = \int \Phi_{hg}(z)dz$ [Å]	5 ± 1	5 ± 1	7 ± 1	5 ± 1
$\delta_{sub/SiO2}$ [Å]	< 5	7 ± 3	7 ± 3	< 5
$\delta_{SiO2/hc}$ [Å]	7 ± 3	7 ± 3	5 ± 3	5 ± 3
$\delta_{hc/hg}$ [Å]	8 ± 3	6 ± 3	10 ± 3	7 ± 3
$\delta_{hg,w}$ [Å]	10 ± 3	7 ± 3	6 ± 3	< 7
Λ before inc. [Å]	-	73 ± 10	-	64 ± 10
n before inc.	-	0.83 ± 0.06	-	0.98 ± 0.06
Λ after inc [Å]	-	80 ± 10	-	59 ± 10
n after inc.	-	0.93 ± 0.06	-	1.00 ± 0.06
Γ_{prim}^{pro} [mg/m^2]	0.43 ± 0.05	0.41 ± 0.05	≈ 0.05	≈ 0.10
FWHM $\Phi_{prim}^{pro}(z)$ [Å]	12 ± 3	13 ± 3	18 ± 5	13 ± 5
Γ_{term}^{pro} [mg/m^2]	-	-	-	0.60 ± 0.05
z_{tern}^{pro} [Å]	-	-	-	100 ± 10
w_{tern}^{pro} [Å]	-	-	-	40 ± 10
χ^2	6423	5234	2420	5176
χ_{red}^2	8.25	6.11	2.25	4.64

Table 1: Best-matching model parameters specified by the simultaneous fits to the reflectivity curves obtained in various water contrasts before and after serum exposure.

Summary and Conclusions

PEG brushes anchored to lipid monolayers adsorb blood proteins upon contacting human serum. The resulting structure was clarified by use of neutron reflectometry. The adsorption involves two components: (i) rinsing-resistant primary adsorption at the grafting surface involving apparently small proteins. Similar adsorption is observed on the bare lipid layers and on their PEGylated counterparts. (ii) ternary adsorption within the PEG brush that is eliminated by rinsing. This is a first structural observation of the effect of rinsing on protein adsorption to PEG brushes.

Footnote 1: The volume v_i in Eq. 1 equally applies to the volume of a molecule, to that of a crystal unit cell, or to an arbitrary unit volume in an amorphous material, if the numbers of nuclei, N_k^i, are used consistently.

Footnote 2: Strictly, Φ_w^{SiO2} must be considered an effective quantity, because the measurements do not distinguish between H_2O/D_2O exchange and the H/D exchange in silanols.

Footnote 3: Λ defines the decay of the distribution to 1/e. Applying this criterion to the profile of a parabolic brush with height *H* yields $\Lambda = H\sqrt{1-e^{-1}}$ ≈ 0.8 *H*.

Footnote 4: The 95% (two-sigma) statistical confidence interval is reached already for a difference in χ^2 of 4.

Associated content

Supporting information

(1) Description of the initial parameter values of the simultaneous fits (2) Volume fraction profiles and schematic illustration of the structures of non-PEGylated surfaces in contact with dilute serum without rinsing; Corresponding reflectivity curves (3) Reflectivity curves of PEGylated surfaces in contact with dilute serum without rinsing

Acknowledgements

The authors thank Institute Laue-Langevin (ILL) for beam time allocation (dois: 10.5291/ILL-DATA.9-11-1679 and 10.5291/ILL-DATA.9-13-545), the ILL/PSCM laboratories for support during sample preparation and pre-characterization, Richard Campbell for support during beamtimes, and Samantha Micciulla and Ernesto Scoppola for insightful comments. Financial support by the Max Planck Society, by NMI3, by RESOLV, and by Deutsche Forschungsgemeinschaft (DFG) via Emmy-Noether grant (SCHN 1396/1) is gratefully acknowledged.

References

1. Abuchowski, A.; McCoy, J. R.; Palczuk, N. C.; van Es, T.; Davis, F. F., Effect of covalent attachment of polyethylene glycol on immunogenicity and circulating life of bovine liver catalase. *Journal of Biological Chemistry* **1977,** 252, (11), 3582-6.
2. Abuchowski, A.; van Es, T.; Palczuk, N. C.; Davis, F. F., Alteration of immunological properties of bovine serum albumin by covalent attachment of polyethylene glycol. *Journal of Biological Chemistry* **1977,** 252, (11), 3578-81.
3. Merrill, E. W.; Salzman, E. W., Polyethylene oxide as a biomaterial. *ASAIO Journal* **1983,** 6, 60-64.
4. Bridges, A. W.; García, A. J., Anti-Inflammatory Polymeric Coatings for Implantable Biomaterials and Devices. *Journal of diabetes science and technology (Online)* **2008,** 2, (6), 984-994.
5. Chen, H.; Yuan, L.; Song, W.; Wu, Z.; Li, D., Biocompatible polymer materials: role of protein-surface interactions. *Progress in Polymer Science* **2008,** 33, (11), 1059-1087.
6. Elbert, D. L.; Hubbell, J. A., Surface Treatments of Polymers for Biocompatibility. *Annual Review of Materials Science* **1996,** 26, (1), 365-394.
7. Immordino, M. L.; Dosio, F.; Cattel, L., Stealth liposomes: review of the basic science, rationale, and clinical applications, existing and potential. *International Journal of Nanomedicine* **2006,** 1, (3), 297-315.
8. Li, S.; Henry, J. J. D., Nonthrombogenic approaches to cardiovascular bioengineering. *Annual review of biomedical engineering* **2011,** 13, 451-475.
9. Pasut, G.; Veronese, F. M., State of the art in PEGylation: the great versatility achieved after forty years of research. *Journal of Controlled Release* **2012,** 161, (2), 461-472.
10. Shi, J.; Xiao, Z.; Kamaly, N.; Farokhzad, O. C., Self-Assembled Targeted Nanoparticles: Evolution of Technologies and Bench to Bedside Translation. *Accounts of Chemical Research* **2011,** 44, (10), 1123-1134.
11. Shin, H.-S.; Park, K.; Kim, J. H.; Kim, J.-J.; Han, D. K.; Moon, M.-W.; Lee, K.-R.; Shin, J. H., Biocompatible PEG Grafting on DLC-coated Nitinol Alloy for Vascular Stents. *Journal of Bioactive and Compatible Polymers* **2009,** 24, (4), 316-328.
12. Teramura, Y.; Iwata, H., Islet encapsulation with living cells for improvement of biocompatibility. *Biomaterials* **2009,** 30, (12), 2270-2275.
13. Walkey, C. D.; Chan, W. C. W., Understanding and controlling the interaction of nanomaterials with proteins in a physiological environment. *Chemical Society Reviews* **2012,** 41, (7), 2780-2799.
14. Yu, M.; Urban, M. W., Polymeric Surfaces with Anticoagulant, Antifouling, and Antimicrobial Attributes. *Macromolecular Symposia* **2009,** 283–284, (1), 311-318.
15. Currie, E. P. K.; Norde, W.; Cohen Stuart, M. A., Tethered polymer chains: surface chemistry and their impact on colloidal and surface properties. *Adv. Colloid Sci.* **2003,** 100-102, 205-265.

16. Harris, J. M., *Poly(Ethylene Glycol) Chemistry: Biotechnical and Biomedical Applications*. Plenum Press: New York, 2003.
17. Leckband, D.; Sheth, S.; Halperin, A., Grafted poly(ethylene oxide) brushes as nonfouling surface coatings. *Journal of Biomaterials Science, Polymer Edition* **1999,** 10, (10), 1125-1147.
18. Becker, A.; Schlichting, I.; Kabsch, W.; Schultz, S.; Wagner, A. F. V., Structure of peptide deformylase and identification of the substrate binding site. *Journal of Biological Chemistry* **1998,** 273, (19), 11413-11416.
19. Hasek, J., Poly (ethylene glycol) interactions with proteins. *Zeitschrift fur Kristallographie Supplements* **2006,** 2006, 613-618.
20. Abbott, N. L.; Blankschtein, D.; Hatton, T. A., Protein partitioning in two-phase aqueous polymer systems. 3. A neutron scattering investigation of the polymer solution structure and protein-polymer interactions. *Macromolecules* **1992,** 25, (15), 3932-3941.
21. Bloustine, J.; Virmani, T.; Thurston, G. M.; Fraden, S., Light scattering and phase behavior of lysozyme-poly (ethylene glycol) mixtures. *Physical review letters* **2006,** 96, (8), 087803.
22. Armstrong, J. K., The occurrence, induction, specificity and potential effect of antibodies against poly (ethylene glycol). In *Pegylated protein drugs: Basic science and clinical applications*, Springer: 2009; pp 147-168.
23. Armstrong, J. K.; Hempel, G.; Koling, S.; Chan, L. S.; Fisher, T.; Meiselman, H. J.; Garratty, G., Antibody against poly (ethylene glycol) adversely affects PEG-asparaginase therapy in acute lymphoblastic leukemia patients. *Cancer* **2007,** 110, (1), 103-111.
24. Schellekens, H.; Hennink, W. E.; Brinks, V., The immunogenicity of polyethylene glycol: facts and fiction. *Pharmaceutical research* 30, (7), 1729-1734.
25. Currie, E. P. K.; van der Gucht, J.; Borisov, O. V.; Cohen Stuart, M. A., Stuffed brushes: theory and experiment. *Pure Appl. Chem.* **1999,** 71, 1227-1241.
26. Gon, S.; Fang, B.; Santore, M. M., Interaction of cationic proteins and polypeptides with biocompatible cationically-anchored PEG brushes. *Macromolecules* **2011,** 44, (20), 8161-8168.
27. Schneck, E.; Schollier, A.; Halperin, A.; Moulin, M.; Haertlein, M.; Sferrazza, M.; Fragneto, G., Neutron reflectometry elucidates density profiles of deuterated proteins adsorbed onto surfaces displaying poly (ethylene glycol) brushes: evidence for primary adsorption. *Langmuir* **2013,** 29, (46), 14178-14187.
28. Schneck, E.; Berts, I.; Halperin, A.; Daillant, J.; Fragneto, G., Neutron reflectometry from poly (ethylene-glycol) brushes binding anti-PEG antibodies: Evidence of ternary adsorption. *Biomaterials* **2015,** 46, 95-104.
29. Vroman, L.; Adams, A.; Fischer, G.; Munoz, P., Interaction of high molecular weight kininogen, factor XII, and fibrinogen in plasma at interfaces. *Blood* **1980,** 55, (1), 156-159.
30. Nanjappa, V.; Thomas, J. K.; Marimuthu, A.; Muthusamy, B.; Radhakrishnan, A.; Sharma, R.; Ahmad Khan, A.; Balakrishnan, L.; Sahasrabuddhe, N. A.; Kumar, S.; Jhaveri, B. N.; Sheth, K. V.; Kumar Khatana, R.; Shaw, P. G.; Srikanth, S. M.; Mathur, P. P.; Shankar, S.; Nagaraja, D.; Christopher, R.; Mathivanan, S.; Raju, R.; Sirdeshmukh, R.; Chatterjee, A.; Simpson, R. J.; Harsha, H. C.; Pandey, A.; Prasad, T. S. K., Plasma Proteome Database as a resource for proteomics research: 2014 update. *Nucleic Acids Research* **2014,** 42, D959-D965.
31. Bantscheff, M.; Schirle, M.; Sweetman, G.; Rick, J.; Kuster, B., Quantitative mass spectrometry in proteomics: a critical review. *Analytical and Bioanalytical Chemistry* **2007,** 389, (4), 1017-1031.
32. Walkey, C. D.; Olsen, J. B.; Guo, H.; Emili, A.; Chan, W. C. W., Nanoparticle Size and Surface Chemistry Determine Serum Protein Adsorption and Macrophage Uptake. *Journal of the American Chemical Society* **2012,** 134, (4), 2139-2147.
33. Riedel, T.; Riedelova-Reicheltova, Z.; Majek, P.; Rodriguez-Emmenegger, C.; Houska, M.; Dyr, J. E.; Brynda, E., Complete identification of proteins responsible for human blood plasma fouling on poly (ethylene glycol)-based surfaces. *Langmuir* **2013,** 29, (10), 3388-3397.
34. Tamm, L.; McConnell, H. M., Supported phospholipid bilayers. *Biophys. J.* **1984,** 47, 105-113.
35. Hermelink, A.; Brezesinski, G., Do unsaturated phosphoinositides mix with ordered phosphadidylcholine model membranes? *Journal of lipid research* **2008,** 49, (9), 1918-1925.

36. Loizou, E.; Porcar, L.; Schexnailder, P.; Schmidt, G.; Butler, P., Shear-Induced Nanometer and Micrometer Structural Responses in Nanocomposite Hydrogels. *Macromolecules* **2010,** 43, 1041-1049.
37. Harroun, T. A.; Wignall, G. D.; Katsaras, J., Neutron scattering for biology. In *Neutron Scattering in Biology*, Springer: 2006; pp 1-18.
38. Timmins, P. A.; Zaccai, G., Low resolution structures of biological complexes studied by neutron scattering. *European Biophysics Journal* **1988,** 15, (5), 257-268.
39. Heinrich, F.; Lösche, M., Zooming in on disordered systems: neutron reflection studies of proteins associated with fluid membranes. *Biochimica et Biophysica Acta (BBA)-Biomembranes* **2014,** 1838, (9), 2341-2349.
40. Fragneto, G.; Thomas, R. K.; Rennie, A. R.; Penfold, J., Neutron reflection study of bovine beta-casein adsorbed on OTS self-assembled monolayers. *Science* **1995,** 267, (5198), 657-660.
41. McDermott, D. C.; Lu, J. R.; Lee, E. M.; Thomas, R. K.; Rennie, A. R., Study of the adsorption from aqueous solution of hexaethylene glycol monododecyl ether on silica substrates using the technique of neutron reflection. *Langmuir* **1992,** 8, (4), 1204-1210.
42. Dabkowska, A. P.; Talbot, J. P.; Cavalcanti, L.; Webster, J. R. P.; Nelson, A.; Barlow, D. J.; Fragneto, G.; Lawrence, M. J., Calcium mediated interaction of calf-thymus DNA with monolayers of distearoylphosphatidylcholine: a neutron and X-ray reflectivity study. *Soft Matter* **2013,** 9, (29), 7095-7105.
43. Halperin, A., Polymer Brushes that Resist Adsorption of Model Proteins: Design Parameters. *Langmuir* **1999,** 15, 2525-2533.
44. Szleifer, I., Protein Adsorption on Surfaces with Grafted Polymers: A Theoretical Approach. *Biophys. J.* **1997,** 72, 595-612.
45. Jeon, S. I.; Andrade, J. D., Protein-surface interactions in the presence of polyethylene oxide: II. Effect of protein size. *Journal of colloid and interface science* **1991,** 142, (1), 159-166.
46. Halperin, A.; Fragneto, G.; Schollier, A.; Sferrazza, M., Primary versus Ternary Adsorption of Proteins onto PEG Brushes. *Langmuir* **2007,** 23, 10603-10617.
47. Halperin, A.; Kroeger, M., Ternary Protein Adsorption onto Brushes: Strong versus Weak. *Langmuir* **2009,** 25, 11621-11634.
48. Rodriguez-Loureiro, I.; Scoppola, E.; Bertinetti, L.; Barbetta, A.; Fragneto, G.; Schneck, E., Neutron reflectometry yields distance-dependent structures of nanometric polymer brushes interacting across water. *Soft Matter* **2017**.
49. Glasmästar, K.; Larsson, C.; Höök, F.; Kasemo, B., Protein adsorption on supported phospholipid bilayers. *Journal of colloid and interface science* **2002,** 246, (1), 40-47.
50. Malmsten, M., Protein adsorption at phospholipid surfaces. *Journal of colloid and interface science* **1995,** 172, (1), 106-115.
51. Arai, T.; Norde, W., The behavior of some model proteins at solid—liquid interfaces 2. Sequential and competitive adsorption. *Colloids and Surfaces* **1990,** 51, 17-28.
52. Norde, W.; Gage, D., Interaction of Bovine Serum Albumin and Human Blood Plasma with PEO-Tethered Surfaces: Influence of PEO Chain Length, Grafting Density, and Temperature *Langmuir* **2004,** 20, 4162-4167.
53. Norde, W.; Lyklema, J., The adsorption of human plasma albumin and bovine pancreas ribonuclease at negatively charged polystyrene surfaces. *Journal of Colloid and Interface Science* **1978,** 66, (2), 257-265.
54. Norde, W., *Colloids and interfaces in life sciences and bionanotechnology*. CRC Press: 2011.
55. Hagiwara, T.; Nattawut, P.; Shibata, M.; Sakiyama, T., Monitoring of adsorption behaviors of bovine serum albumin onto a stainless steel surface by the quartz crystal microbalance based on admittance analysis. *Bioscience, Biotechnology, and Biochemistry* **2017,** 81, (4), 783-789.
56. Jin, J.; Jiang, W.; Yin, J.; Ji, X.; Stagnaro, P., Plasma Proteins Adsorption Mechanism on Polyethylene-Grafted Poly(ethylene glycol) Surface by Quartz Crystal Microbalance with Dissipation. *Langmuir* **2013,** 29, (22), 6624-6633.

57. Guzman, G.; Bhaway, S. M.; Nugay, T.; Vogt, B. D.; Cakmak, M., Transport-Limited Adsorption of Plasma Proteins on Bimodal Amphiphilic Polymer Co-Networks: Real-Time Studies by Spectroscopic Ellipsometry. *Langmuir* **2017,** 33, (11), 2900-2910.
58. Ladokhin, A. S.; Selsted, M. E.; White, S. H., Bilayer interactions of indolicidin, a small antimicrobial peptide rich in tryptophan, proline, and basic amino acids. *Biophysical journal* **1997,** 72, (2), 794-805.
59. Hsu, J. C. Y.; Yip, C. M., Molecular dynamics simulations of indolicidin association with model lipid bilayers. *Biophysical journal* **2007,** 92, (12), L100-L102.
60. Brouette, N.; Fragneto, G.; Cousin, F.; Moulin, M.; Haertlein, M.; Sferrazza, M., A neutron reflection study of adsorbed deuterated myoglobin layers on hydrophobic surfaces. *J. Colloid Interface Sci.* **2013,** 390, 114-120.
61. Jeon, S. I.; Lee, J. H.; Andrade, J. D.; De Gennes, P. G., Protein-surface interactions in the presence of polyethylene oxide: I. Simplified theory. *J. Colloid Interface Sci.* **1991,** 142, 149-158.
62. Adkins, J. N.; Varnum, S. M.; Auberry, K. J.; Moore, R. J.; Angell, N. H.; Smith, R. D.; Springer, D. L.; Pounds, J. G., Toward a Human Blood Serum Proteome: Analysis By Multidimensional Separation Coupled With Mass Spectrometry. *Molecular & Cellular Proteomics* **2002,** 1, (12), 947-955.
63. Hijmans, W.; Sipe, J. D., Levels of the serum amyloid A protein (SAA) in normal persons of different age groups. *Clinical and experimental immunology* **1979,** 35, (1), 96.
64. Bausserman, L. L.; Herbert, P. N.; Forte, T.; Klausner, R. D.; McAdam, K. P.; Osborne, J. C.; Rosseneu, M., Interaction of the serum amyloid A proteins with phospholipid. *Journal of Biological Chemistry* **1983,** 258, (17), 10681-10688.
65. Bevington, P. R.; Robinson, D. K., *Data Reduction and Error Analysis for the Physical Sciences*. Mcgraw-Hill: New York, 2003.
66. Gutfreund, P.; Wolff, M.; Maccarini, M.; Gerth, S.; Ankner, J. F.; Browning, J.; Halbert, C. E.; Wacklin, H.; Zabel, H., Depletion at solid/liquid interfaces: Flowing hexadecane on functionalized surfaces. *The Journal of chemical physics* **2011,** 134, (6), 064711.
67. Satulovsky, J.; Carignano, M. A.; Szleifer, I., Kinetic and thermodynamic control of protein adsorption. *Proceedings of the National Academy of Sciences* **2000,** 97, (16), 9037-9041.
68. Malmsten, M.; Emoto, K.; Van Alstine, J. M., Effect of chain density on inhibition of protein adsorption by poly (ethylene glycol) based coatings. *Journal of colloid and interface science* **1998,** 202, (2), 507-517.
69. Mauri, S.; Pandey, R.; Rzeznicka, I.; Lu, H.; Bonn, M.; Weidner, T., Bovine and human insulin adsorption at lipid monolayers: a comparison. *Frontiers in Physics* **2015,** 3, (51).
70. Veronese, F. M., *PEGylated Protein Drugs: Basic Science and Clinical Applications: Basic Science and Clinical Applications*. Springer: 2009.

Neutron Reflectometry Elucidates Protein Adsorption from Human Blood Serum onto PEG brushes

Victoria M. Latza[a], Ignacio Rodriguez-Loureiro[a], Irena Kiesel[b,c], Avraham Halperin[d], Giovanna Fragneto[b], and Emanuel Schneck[a,*]

[a]Max Planck Institute of Colloids and Interfaces, Am Mühlenberg 1, 14476 Potsdam, Germany

[b]Institut Laue-Langevin, 71 avenue des Martyrs, 38042 Grenoble Cedex 9, France

[c]TU Dortmund University, August-Schmidt-Straße 4, 44227 Dortmund, Germany

[d]Univ. Grenoble Alpes, CNRS, LIPhy, 38000 Grenoble France

[*]Corresponding author: schneck@mpikg.mpg.de, Phone: +49-331567-9404, Fax: +49-331567-9402

Supporting information

Table of content

1.) Initial parameter values for the common model

Initial values for all parameters concerning the layered structure of the functionalized solid surface including the brush-grafting lipid monolayer were taken from the best-matching results obtained in a previous study [1]. The decay length Λ of the PEG brush was initially set to $\Lambda = H\sqrt{1-e^{-1}} \approx 0.8\,H$ (see main text), where *H* is the best-matching parabolic brush height obtained in the same study [1]. The stretching exponent *n* was initially set to 2, corresponding to a Gaussian distribution. Regarding the protein volume fraction profiles, various sets of initial parameters for z_k^{pro}, w_k^{pro}, and $\Phi_k^{\max}$ were tested. When they were taken from a suitable range, the parameter values during the fitting procedure converged to the values presented in the main text, for which the experimental data are well reproduced. In all other cases, the fitting procedure resulted in vanishing protein volume fraction profiles, for which the experimental data are poorly reproduced.

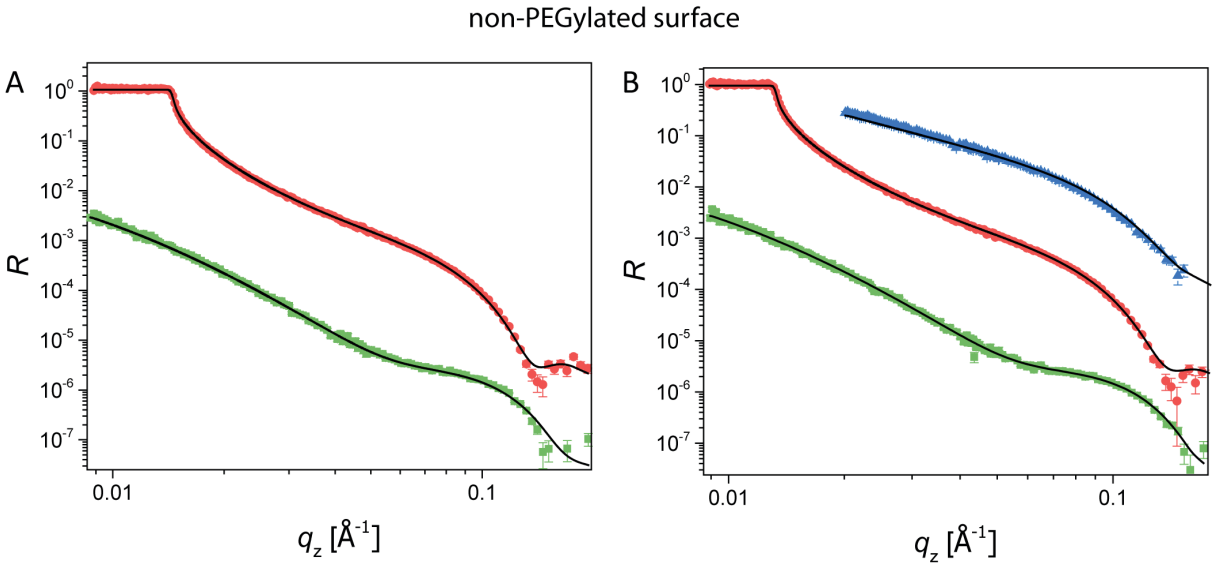

Figure S1: Set of reflectivity curves for non-PEGylated surfaces in various water contrasts. The solid lines indicate the simulated reflectivities corresponding to the best-matching model. (A) Reflectivity curves prior to contact with diluted serum in D_2O (top) and H_2O (bottom). (B) Reflectivity curves during contact with diluted serum in D_2O (middle), SMW (top), and H_2O (bottom). The curves are vertically shifted for clarity.

2.) Non-PEGylated surfaces in contact with dilute serum without rinsing

The reflectivity curves (Fig. S1) measured during exposure to diluted serum in three contrasts are again well reproduced with a model incorporating a single, narrow protein distribution in the headgroup region. The volume fraction profiles of proteins adsorbed to the non-PEGylated surface in presence of diluted serum (Fig. S2) are qualitatively similar to those obtained upon incubation in whole serum and subsequent rinsing.

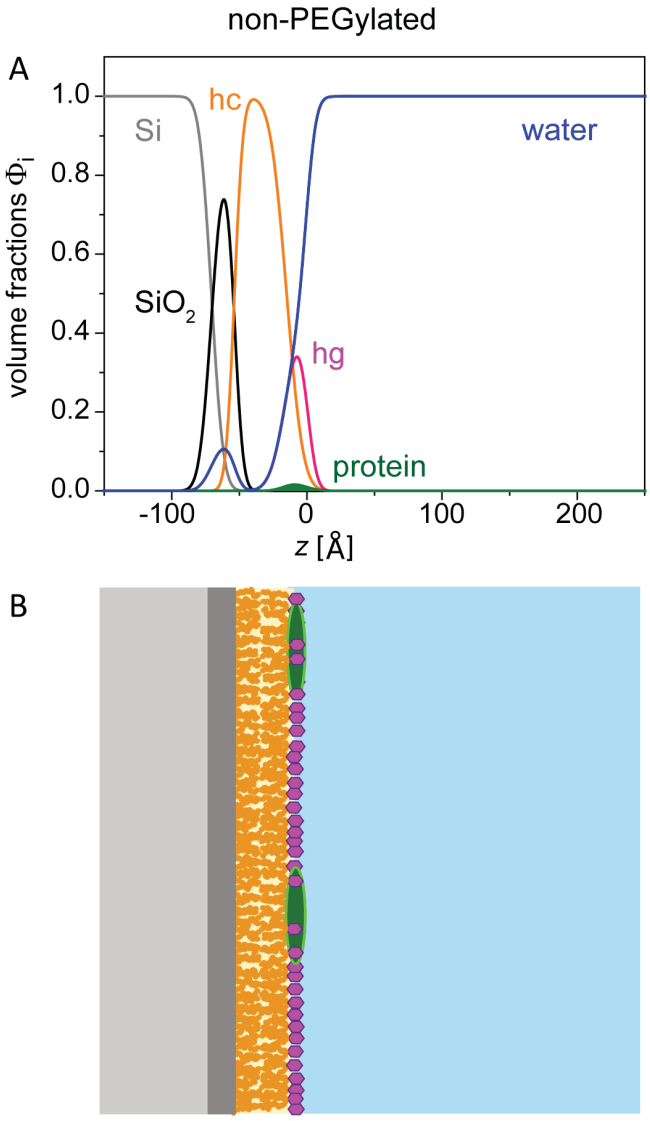

Figure S2: (A) The volume fraction profiles $\Phi(z)$ of all chemical components (Si, SiO_2, hydrocarbon chains, headgroups, PEG, protein, and water) for non-PEGylated surfaces during incubation with diluted human blood serum. The protein volume fraction distribution is unimodal. (B) Schematic illustration of the structures of non-PEGylated surfaces during incubation with dilute human blood serum, as suggested by the volume fraction profiles in panel B.

3.) PEGylated surfaces in contact with diluted serum without rinsing

Fig. S3 shows reflectivity curves in three contrasts of a PEGylated surface before and during exposure to 10 x diluted human serum together with the simulated reflectivities corresponding to the best-matching model allowing for simultaneous primary and ternary adsorption.

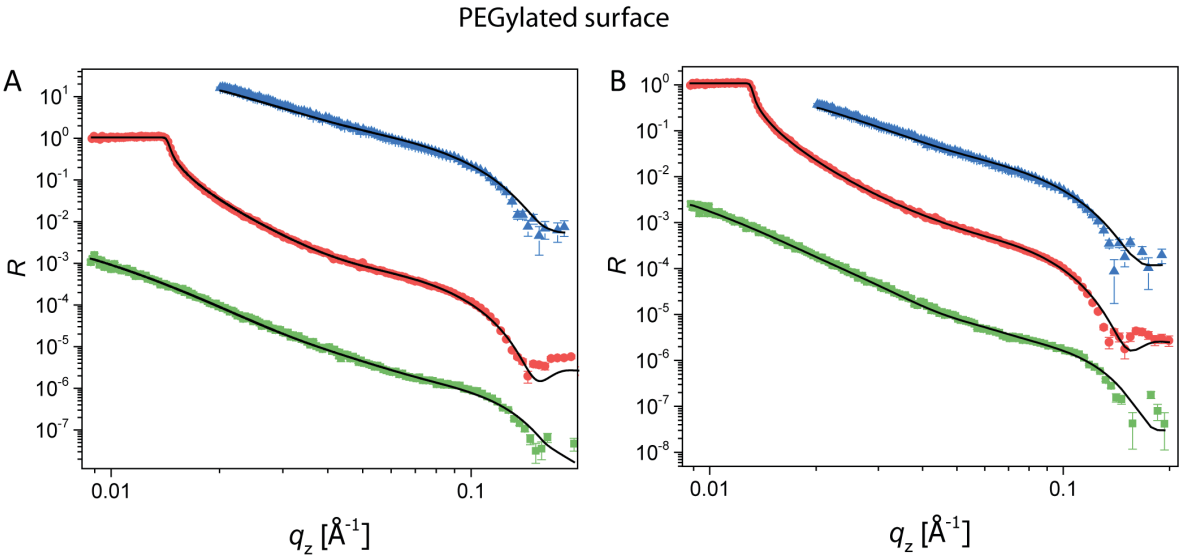

Figure S3: Set of reflectivity curves for a PEGylated surface in various water contrasts. The solid lines indicate the simulated reflectivities corresponding to the best-matching model. (A) Reflectivity curves prior to contact with 10 x diluted human serum in D_2O (middle), SMW (top), and H_2O (bottom). (B) Reflectivity curves during contact with dilute serum in D_2O (middle), SMW (top), and H_2O (bottom).

4.) Pressure/area isotherm of a DSPC/PEG-lipid mixture

Fig. S4 shows the influence of 10 mol% (f = 0.1) PEG-lipid on the pressure/area isotherm of DSPC at the air/water interface at room temperature. It is seen that the presence of the PEG chains leads to significant lateral repulsion between the molecules. Only at the lowest areas per lipid the steric repulsion between the hydrocarbon chains becomes dominant and the two curves converge again.

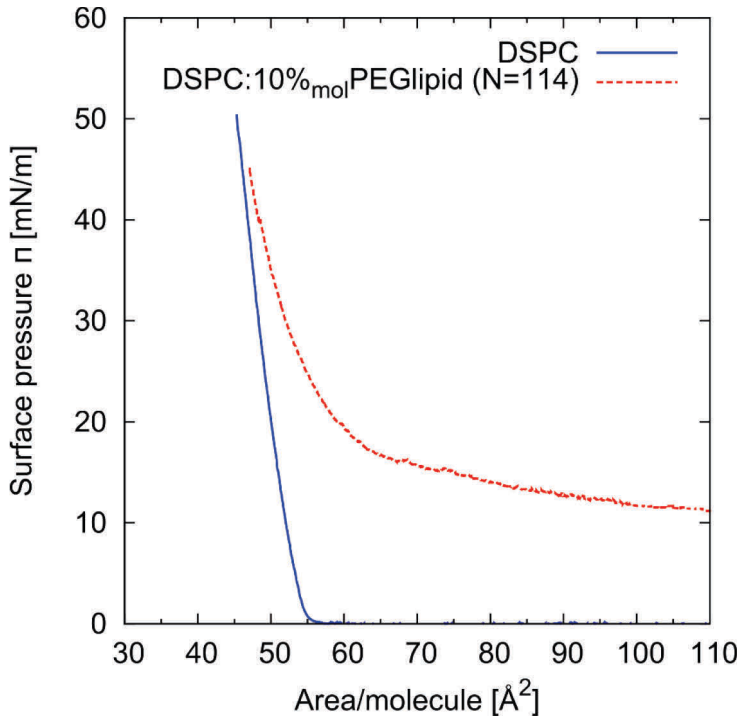

Figure S4: Pressure/area isotherms of DSPC with and without 10 mol% (f = 0.1) PEG-lipid at the air/water interface at room temperature.

5.) Comparison of various adsorption scenarios

Fig. S5 shows a comparison of various protein adsorption scenarios to phospholipid surfaces, differing only in the protein layer position with respect to the headgroup layer but not in the adsorbed amount. It is clearly seen that only the scenario in which the protein layer fully overlaps with the headgroup layer (see panel B) reproduces the experimental reflectivity data (see panel A) obtained after incubation with whole serum and subsequent rinsing.

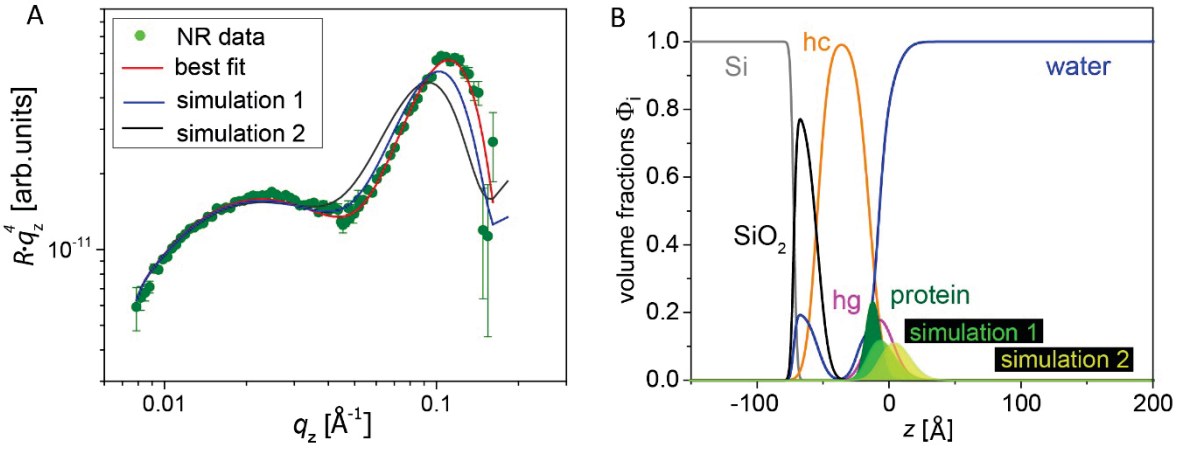

Figure S5: (A) Experimental reflectivity data (symbols) obtained after incubation of a non-PEGylated phospholipid surface with whole serum and subsequent rinsing. The solid lines represent the best-matching model and two alternative scenarios (simulations 1 and 2). (B) Volume fraction profiles according to the best-matching model together with two alternative scenarios of the protein profiles (simulations 1 and 2).

6.) Complete sets of reflectivity curves and fits obtained with non-PEGylated and PEGylated surfaces before and after incubation with whole serum and subsequent rinsing

Fig. S6 shows reflectivity curves in D_2O, 4MW, SMW, and H_2O contrasts of non-PEGylated and PEGylated surfaces before and after incubation with whole serum and subsequent rinsing, together with the simulated reflectivities corresponding to the best-matching models.

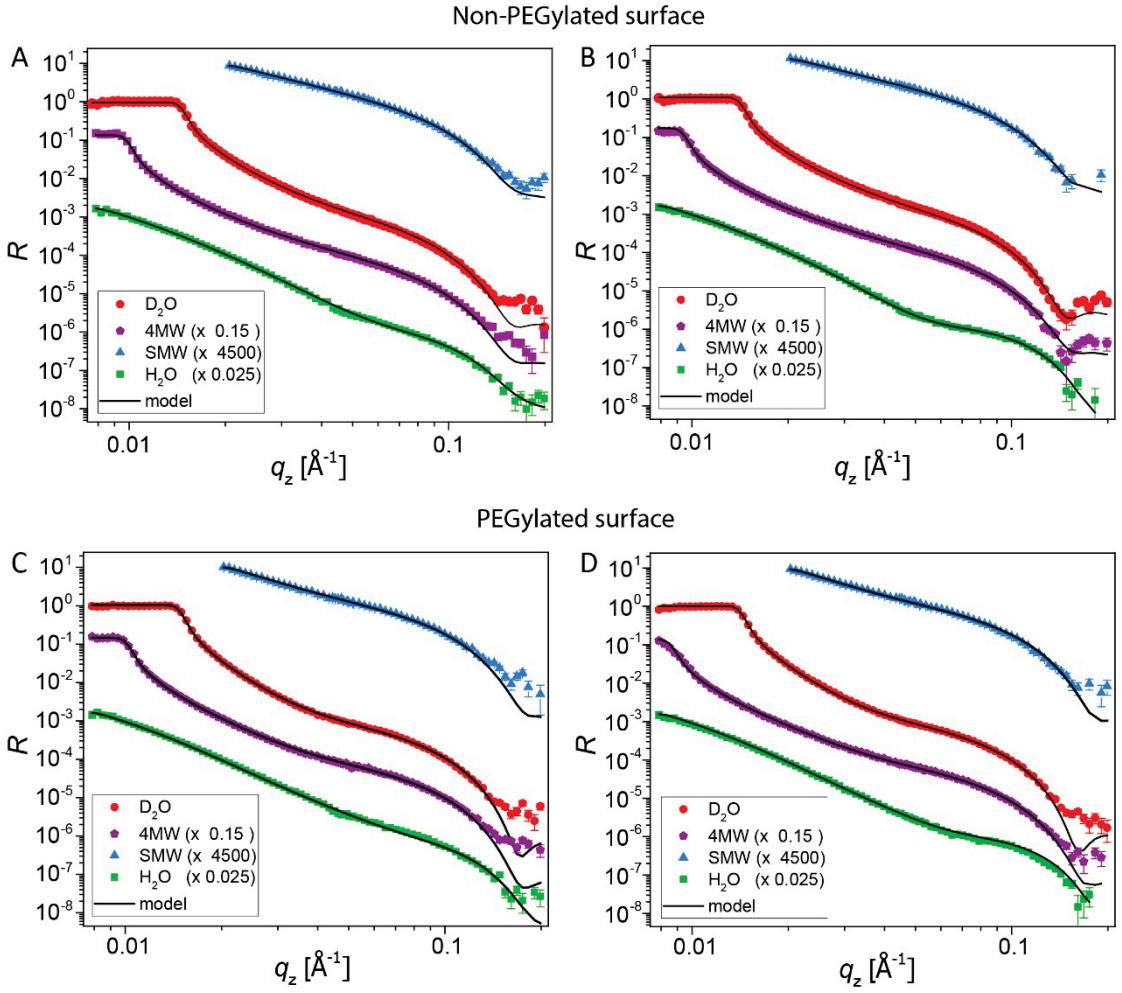

Figure S6: Reflectivity curves of non-PEGylated (top) and PEGylated (bottom) surfaces in D_2O, 4MW, SMW, and H_2O contrasts before (left) and after (right) incubation with whole serum and subsequent rinsing. The solid lines indicate the simulated reflectivities corresponding to the best-matching model.

7.) Influence of the enhanced statistical weighting of the H_2O contrast

Fig. S7 shows reflectivity curves in D_2O, SMW, and H_2O contrasts of a PEGylated surface before and during incubation with 10x diluted serum, together with the simulated reflectivities corresponding to the best-matching model obtained in reflectivity fits without enhanced H_2O weighting. Fig. S8 shows the corresponding volume fraction profiles. It is seen that the resulting profiles are largely consistent with those obtained with enhanced H_2O weighting (see main article).

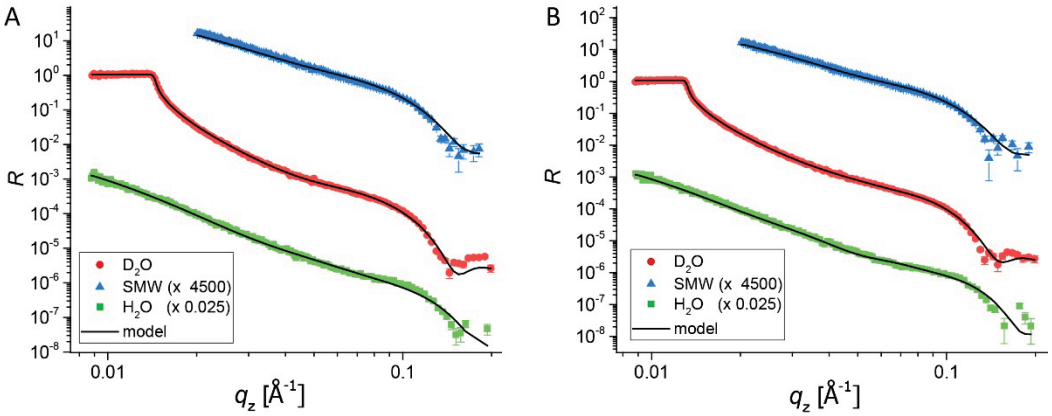

Figure S7: (A) Experimental reflectivity curves in various water contrasts (symbols) of a PEGylated surface before (left) and during (right) incubation with 10x diluted serum. The solid lines represent the best-matching model obtained in reflectivity fits without enhanced H_2O weighting.

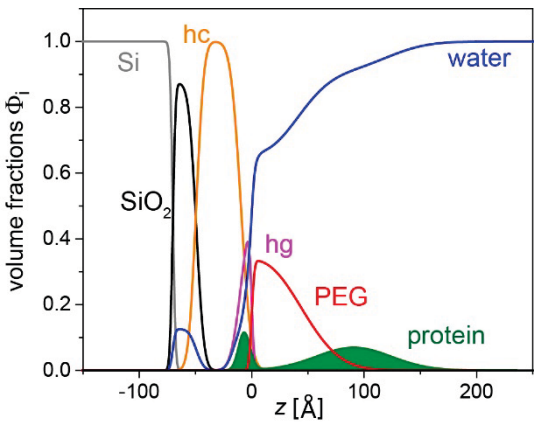

Figure S8: Volume fraction profiles of a PEGylated surface during incubation with 10x diluted serum deduced from a reflectivity fit without enhanced H_2O weighting.

8.) Comparison of models excluding and including ternary adsorption

Fig. S9 (right) shows reflectivity data obtained with a PEGylated surface during incubation with 10 times diluted serum in H_2O contrast. The data are smoothed using 5-point adjacent averaging. The solid lines indicate the simulated reflectivity curves according to the best-matching models excluding and including ternary adsorption. The comparison conveys the better match of the model including ternary adsorption, as it better captures the q_z-scaling of the intensity in the relevant q_z-range between low and intermediate q_z. Fig. S9 (left) shows the corresponding SLD profiles.

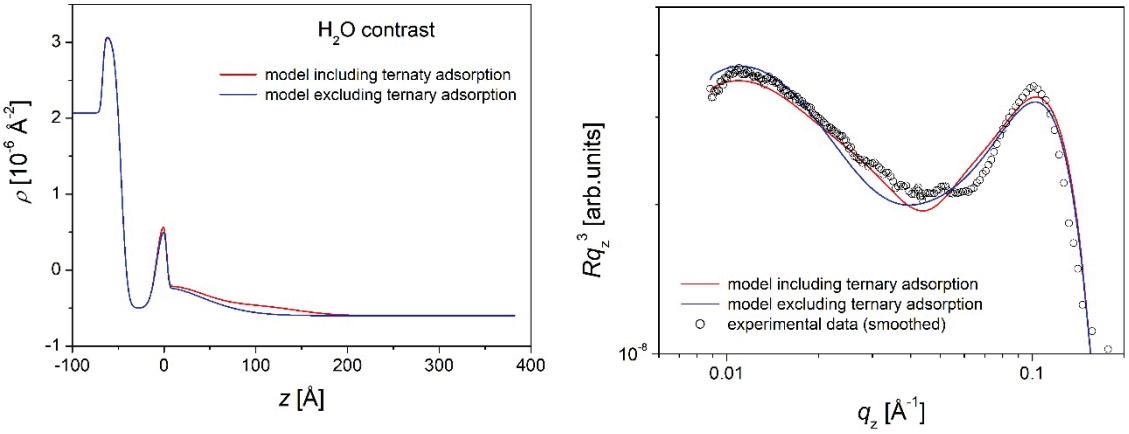

Figure S9: (left) SLD profiles in H_2O contrast according to the best-matching models excluding and including ternary adsorption. (right) Reflectivity data obtained with a PEGylated surface during incubation with 10x diluted serum in H_2O contrast. The data are smoothed using 5-point adjacent averaging. The solid lines indicate the simulated reflectivity curves according to the best-matching models excluding and including ternary adsorption.

References

1. Schneck, E.; Berts, I.; Halperin, A.; Daillant, J.; Fragneto, G. Neutron reflectometry from poly (ethylene-glycol) brushes binding anti-PEG antibodies: Evidence of ternary adsorption. *Biomaterials* **2015,** *46*, 95-104.

Manuscript II

End Point Versus Backbone Specifity Governs Characteristics of Antibody Binding to Poly(Ethylene Glycol) Brushes

Latza V. M., Rodriguez-Loureiro I., Kiesel I., Fragneto G. and Schneck E.

End point vs. backbone specificity governs characteristics of antibody binding to poly(ethylene glycol) brushes

Victoria M. Latza[a], Ignacio Rodriguez-Loureiro[a], Giovanna Fragneto[b], and Emanuel Schneck[a,*]

[a]Max Planck Institute of Colloids and Interfaces, Am Mühlenberg 1, 14476 Potsdam, Germany

[b]Institut Laue-Langevin, 71 avenue des Martyrs, 38042 Grenoble Cedex 9, France

[*]Corresponding author: schneck@mpikg.mpg.de, Phone: +49-331567-9404, Fax: +49-331567-9402

Keywords: surfaces and interfaces, biocompatibility, PEGylation, lipids, neutron reflectometry

Abstract

End-grafted poly[ethylene glycol] (PEG) brushes are widely used in order to suppress undesired protein adsorption to surfaces exposed to blood or other biological fluids. The specific adsorption of antibodies (Abs) to PEG brushes associated with PEG's antigenicity is drawing increasing attention because it can affect clinical applications. Here, the adsorption to PEG brushes of two Ab types, specifically binding the polymer backbone and the polymer endpoints, respectively, is structurally characterized by neutron reflectometry. The measurements yield volume fraction profiles of PEG and of the adsorbed Abs with sub-nanometer resolution perpendicular to the surface. For all brush parameters in terms of grafting density and polymerization degree, the Ab profiles clearly differ between backbone-binders and endpoint-binders. The adsorbed Ab amount per unit area is substantial for both Ab types and for all brush parameters investigated, even for dense brushes, which impose a considerable osmotic barrier to Ab insertion. The results therefore indicate that variation of brush parameters alone is insufficient to prevent undesired Ab adsorption. Instead, our work motivates further efforts in the search for non-antigenic brush chemistry.

Introduction

Biomedical applications involving the insertion of foreign bodies, such as implants, stents, or drug delivery systems[1-3], into the human organism are commonly equipped with polymer coatings of hydrophilic polymers, often poly[ethylene glycol] (PEG). The deployment of terminally grafted PEG is widely known as *PEGylation*[4]. It aims to enhance biocompatibility[1, 5, 6] by repressing protein adsorption, which is believed to constitute the initial stage of harmful reactions like blood clotting, inflammation, and immune response[7-10]. The adsorption of proteins onto PEGylated surfaces has

been subject of research since the 1980s[11-13]. However, it is still unclear why PEGylation sometimes works, while on other occasions it does not meet the expectations. In fact, only the applications on the nanoscale, such as PEGylated protein drugs[14] and stealth liposomes[1], have led to industrial exploitation in the multibillion $ range[14].

With regard to brush-failure, three different modes of protein adsorption to polymer brushes have been described in the literature: (i) Primary adsorption at the brush grafting surface due to favorable short-range protein-surface interactions[15, 16]; (ii) Secondary adsorption at the brush periphery due to an equilibrium between long-range protein-surface attraction and the osmotic penalty incurred by inserting the protein into a brush when the polymer-protein interactions are repulsive[15-18]; (iii) Ternary adsorption within the brush itself due to favorable protein-polymer interactions[19-21]. Traditionally, the interaction of proteins with PEG has been considered purely repulsive[22]. This view is widely held to the present and ternary adsorption to PEG brushes is thus commonly neglected, although evidence to the contrary emerged from the 2000s onwards. For example, small angle neutron scattering (SANS) and light scattering data indicated that protein-PEG interactions are weakly attractive rather than repulsive[23, 24]. It should be noted, however, that such observations made in bulk solutions are not necessarily fully transferable to surface-grafted brushes, which assume different chain conformations and mobilities. Indirect evidence for ternary protein adsorption within PEG brushes was further deduced from the variation of the surface mass density of the adsorbed proteins with the PEG grafting density and the polymerization degree[19, 25, 26]. More recently, neutron reflectometry (NR) provided direct evidence of weak ternary adsorption of blood proteins to PEG brushes[27].

Of particular biomedical relevance is ternary protein adsorption involving strong, specific binding. While PEG has been initially believed to be non-immunogenic[28-30], crystallographic data evidenced PEG binding to specific sites of proteins[31, 32]. Later on, anti-PEG antibodies (Abs) of clinical significance were identified, capable of binding specifically to the backbone or to the polymer end points[33-35]. More recently it was found that such anti-PEG antibodies have become highly abundant in the human population[36]. This notion has far-reaching consequences, because anti-PEG Abs threaten to impede the performance of PEGylation in clinical applications. A key question in this context is how effective Ab binding to PEG is when the latter is in a brush configuration.

We have recently used NR to study the specific adsorption of end-binding antibodies to PEG brushes of variable grafting density σ and constant polymerization degree N (ref. [37]). In contrast to conventional methods that merely yield the adsorbed protein amount per unit area, like surface plasmon resonance (SPR)[38], quartz-crystal microbalance (QCM)[39, 40], or ellipsometry[41], NR resolves matter distributions perpendicular to planar interfaces with high depth resolution and is therefore

uniquely suited to structurally characterize protein adsorption to polymer brushes. The technique was therefore used to identify and characterize primary adsorption to the brush grafting surface[42] as well as weak[27] and strong[37] ternary adsorption within the PEG brush itself.

In the present work we systematically investigate by NR the adsorption of backbone-binding (BB) and end-binding (EB) Abs to planar, solid-supported PEG brushes varying in grafting density σ and polymerization degree *N*. The motivation is twofold. At first, we characterize the phenomenology of BB Ab adsorption to PEG brushes, which has not yet been described and, in contrast to EB Ab adsorption, cannot easily be suppressed by modifying the chemistry of the terminal polymer segment. Secondly, we provide high-resolution experimental Ab volume fraction profiles perpendicular to the interface for defined brush parameters, Ab types, and Ab concentrations. This set of quantitative experimental data constitutes a valuable basis for the theoretical description of specific protein-brush interactions on the continuum level[21] and beyond[43]. Our experiments reveal that BB and EB Ab adsorption has different features for all brush parameters investigated. The adsorbed amount and the structural parameters have qualitatively different dependence on σ. Ab binding is found to be substantial for all brush parameters investigated, even for the densest brushes which impose a considerable osmotic penalty to Ab insertion. It thus appears unlikely that Ab adsorption to PEG brushes can be practically prevented through variation of the parameters σ and *N*, and our work motivates further efforts in the search for alternative brush chemistry[44].

Materials and Methods

Chemicals and sample preparation

Unless stated otherwise, all chemicals were purchased from Sigma-Aldrich (St. Luis, MO, USA) and used without further purification. The PEG brushes are composed of the phospholipid 1,2-distearoyl-*sn*-glycero-3-phosphocholine (DSPC) and of lipopolymers based on 1,2-distearoyl-*sn*-glycero-3-phosphoetanolamine (DSPE) comprising PEG polymers of various polymerization degrees ($N = 22$, $N = 114$, or $N = 455$): DSPE-N-[methoxy(polyethylene glycol)-1000] (PEG-lipid-22), DSPE-N-[methoxy(polyethylene glycol)-5000] (PEG-lipid-114), or DSPE-N-[methoxy(polyethylene glycol)-20000] (PEG-lipid-455). The chemical structures of DSPC and the PEG-lipids are shown in Fig. 1A. DSPC, PEG-lipid-22, and PEG-lipid-114 were from Avanti Polar Lipids (Alabaster, USA) and PEG-lipid-455 from Nanocs (Boston, USA). IgG1 3.3 anti-PEG monoclonal antibody with high affinity to the PEG backbone (backbone-binder Ab, BB Ab) was purchased from Institute of Biomedical Sciences, Academia Sinica (Taipei, Taiwan). IgG anti-PEG Rabbit Monoclonal Antibody (clone ID: PEG-B-47) with high affinity to the methoxy end group (end-binder Ab, EB Ab) was purchased from Epitomics, Inc. (Burlingame, California, USA). According to the literature, the antibodies have no cross reactions with

non-specific targets in serum or blood[45, 46]. They were shipped and stored in buffer solutions. Prior to the experiments they were diluted with H_2O buffer solution yielding an overall concentration of 0.1 mg/mL. The buffer solutions were based on H_2O or D_2O or mixtures thereof for contrast variation (see further below) and contained 150 mM NaCl and 20 mM Tris at pH 7. Silicon single (111) crystal blocks, 80 mm x 50 mm x 15 mm in size, polished on one large face and terminated with a thin layer of native silicon oxide (SiO_2), were purchased from Synchrotronix (Annemasse, France) and used as planar solid supports for the PEG brushes. The blocks were first cleaned with the organic solvents chloroform, acetone, and ethanol and subsequently treated in a plasma cleaner for 30 min. Their surfaces were then rendered hydrophobic via covalent functionalization with octadecyl-trichloro-silane (OTS): the blocks were immersed in freshly prepared OTS solutions in dry hexadecane at a concentration of 1 mM for 1 h. Free and polymerized OTS was removed by extensive washing with hexadecane and ethanol. Lipid monolayers anchoring the PEG brushes were deposited onto the hydrophobized substrates via the Langmuir-Schaefer (LS) technique[47]. For this purpose, mixtures of DSPC and PEG-lipid (PEG-lipid-22, PEG-lipid-114, or PEG-lipid-455) in chloroform at an overall concentration of 2 mg/mL were prepared and spread at the air-water interface in a Teflon Langmuir trough (Nima Technology, Coventry, UK) containing H_2O-based buffer. The PEG-lipid mole fractions f ranged between f = 0.01 (1 mol% PEG-lipid) and f = 0.1 (10 mol% PEG-lipid). After compression to a lateral pressure of Π = 35 mN/m the monolayer was transferred onto the OTS-functionalized blocks by LS. The PEG grafting density σ (i.e., the number of PEG chains per unit area) realized in this way is approximately $\sigma \approx f/A_{lip}$, as follows from the average area per DSPC at 35 mN/m, A_{lip} = 47 Å^2 (ref. [48]), and as was experimentally confirmed earlier[37]. The characteristics of all the types of PEG brushes prepared and investigated are summarized in Table 1. After the characterization by NR of the bare PEG brushes in aqueous buffer, incubation with BB Ab for 1.5 h followed (Tables 1 and 2), and the samples were re-characterized by NR after rinsing with buffer. One sample (PEG-lipid-22, f = 0.1) was subsequently incubated with EB Ab for 1.5 h and re-characterized after rinsing with buffer.

Sample	N	σ [10^{-4} Å^{-2}]	Σ [Å^2]	D_{PEG} [Å]	Γ_{PEG} [mg/m^2]	σ/σ_{OT}	antibodies
PEG-lipid-22, f = 0.1	22	21.3	470	3.2	0.34	1.5	BB, BB+EB
PEG-lipid-114, f = 0.01	114	2.1	4700	1.7	0.18	1.1	BB, EB[37]
PEG-lipid-114, f = 0.02	114	4.3	2350	3.3	0.35	2.1	EB[37]
PEG-lipid-114, f = 0.05	114	10.6	940	8.4	0.88	5.3	BB, EB[37]
PEG-lipid-114, f = 0.1	114	21.3	470	16.7	1.77	10.6	BB, EB[37]
PEG-lipid-455, f = 0.01	455	2.1	4700	6.7	0.71	5.5	BB

Table 1: List of PEG brushes investigated, their characteristics in terms of polymerization degree N, grafting density σ, reduced brush density σ/σ_{OT}, area per polymer chain Σ, PEG amount and mass per unit area, D_{PEG} and Γ_{PEG}, respectively, and the types of antibodies they were incubated with. Results obtained with EB Abs alone are from an earlier study[37].

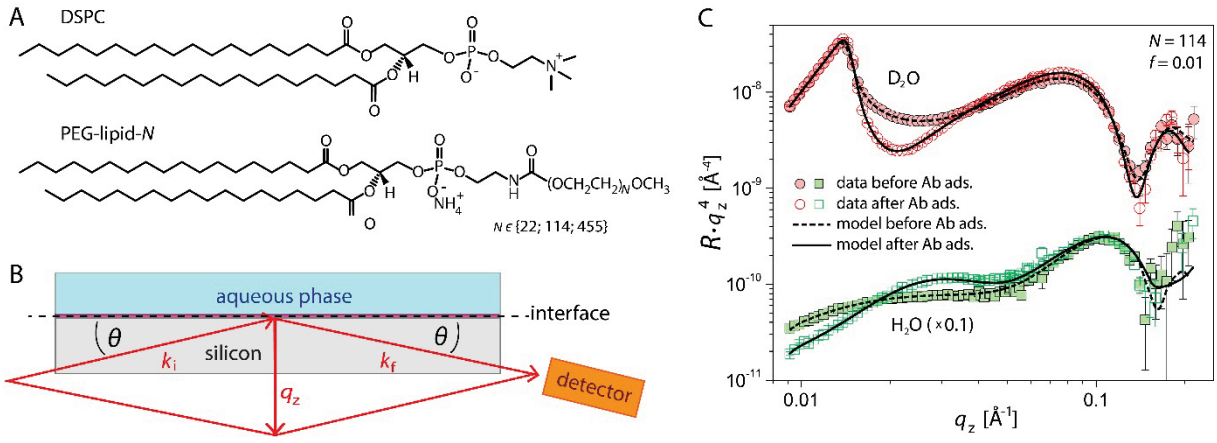

Figure 1: (A) Chemical structures of DSPC (top) and PEG-lipid with $N \in \{22; 114; 455\}$ (bottom), the constituents of the solid-supported PEG brushes. (B) Geometry of the NR experiments. The reflectivity R is recorded as a function of the component q_z of the scattering vector perpendicular to the interface. (C) Exemplary set of reflectivity curves (PEG-lipid-114, $f = 0.01$) in two water contrasts (D_2O, and H_2O) before and after Ab adsorption. Note that the analysis in general involves also reflectivity curves in other water contrasts (see Methods section). Dashed and solid lines represent the simulated intensities corresponding to the best-matching parameters in the common model.

Neutron reflectometry

NR was performed with the reflectometers D17 and FIGARO of Institut Laue-Langevin (ILL, Grenoble, France)[49, 50]. All measurements were carried out using "solid/liquid-cells" at a controlled temperature of $T = 30$°C. In Fig. 1B the geometry of specular neutron reflection is schematically depicted. After passing through the silicon block the incident beam hits the solid-liquid interface with an angle θ and is reflected at the same angle. The reflectivity, i.e., the intensity ratio R between reflected and incident beams, with wave vectors $\boldsymbol{k}_i$ and $\boldsymbol{k}_f$, respectively, is recorded as a function of $q_z = |\boldsymbol{k}_f - \boldsymbol{k}_i| = (4\pi/\lambda)\sin\theta$, the scattering vector component perpendicular to the interface (see Fig. 1B). The neutron wavelength is denoted with λ. The measurements were conducted in the time-of-flight (TOF) mode using two fixed incident angles $\theta_1 = 0.8°$ and $\theta_2 = 3.0°$ (D17) or $\theta_2 = 3.2°$ (FIGARO). The wavelength range was 2.5 Å < λ < 25 Å (D17) and 2 Å < λ < 20 Å (FIGARO). The relative q_z-resolution in terms of the full width at half maximum (FWHM), $\Delta q_z/q_z$, corresponds to the finite angular and wavelength resolutions, is q_z-dependent, and varied between 2% and 10%. While modeling the experimental data this aspect was considered via convolution, as explained in a previous publication[42]. The reflectivity curves $R(q_z)$ depend on the interfacial scattering length density (SLD) profiles $\rho(z)$, which in turn follow from the interfacial distribution of all chemical components i having their characteristic and known SLDs ρ_i:

$$\rho_i = \frac{1}{v_i}\sum_k N_k^i b_k \,, \qquad (1)$$

where b_k is the coherent scattering length of an atomic nucleus of type k and N_k^i the number of such nuclei in component *i* per volume v_i. The SLD strictly refers to the anhydrous chemical components and their solvent-excluded volume. With that, the distributions of all components can be reconstructed from $R(q_z)$. To avoid ambiguities in this procedure, and to enhance sensitivity to the chemical components of interest, a technique called contrast variation is commonly applied in NR: The SLD of the aqueous medium is varied by replacing H_2O with D_2O or defined H_2O/D_2O mixtures of known SLD. Contrast variation in a wide SLD-range is possible due to the large difference of the scattering length of the hydrogen isotopes H and D. Here, we use up to four contrasts, H_2O (ρ_w = -0.56 x 10^{-6} Å^{-2}), D_2O (ρ_w = 6.35 x 10^{-6} Å^{-2}), 4-matched water (4MW, ρ_w = 4.00 x 10^{-6} Å^{-2}), and water matching the SLD of the silicon substrate (SMW, ρ_w = 2.07 x 10^{-6} Å^{-2}). Minor deviations in ρ_w can occur due to incomplete exchange of the aqueous medium inside the cell during the rinsing procedure. This was accounted for by allowing for small variations in ρ_w in the data analysis (see further below). Most of the chemical components of which the samples are composed are constant. This applies to crystalline silicon (ρ_{Si} = 2.07 x 10^{-6} Å^{-2}), silicon oxide (ρ_{oxi} = 3.41 x 10^{-6} Å^{-2}), hydrocarbon chains of OTS and lipids (-0.5 x 10^{-6} Å^{-2} < ρ_{hc} < 0), lipid headgroups (ρ_{hg} = 1.75 x 10^{-6} Å^{-2}), and PEG (ρ_{PEG} = 0.6 x 10^{-6} Å^{-2}), as was established earlier[27, 37]. Due to the dynamic H/D exchange of "labile" hydrogens, however, the SLD of the antibodies, ρ_{ab}, depends on the SLD ρ_w of the aqueous medium[37]:

$$\rho_{Ab} = 2.0 \text{ x } 10^{-6}\text{Å}^{-2} + 0.19\rho_w \,, \qquad (2)$$

and we obtain $\rho_{Ab}(H_2O)$ = 1.9·10^{-6} Å^{-2}, $\rho_{Ab}(D_2O)$ = 3.3·10^{-6} Å^{-2}, ρ_{Ab}(4MW) = 2.8·10^{-6} Å^{-2} and ρ_{Ab}(SMW) = 2.4·10^{-6} Å^{-2}.

Data analysis

An exemplary set of reflectivity curves from a sample before and after incubation with antibodies measured in D_2O, and H_2O is shown in Fig. 1C. Antibody binding affects the interfacial SLD profiles and thus clearly changes the shapes of the reflectivity curves. The solid lines indicate the simulated reflectivity curves corresponding to a common model. The model (see Fig. 2) is based on the volume fraction profiles, $\Phi_i(z)$, of all chemical components perpendicular to the interface, and simultaneously describes the reflectivity curves of a sample for all measurement conditions, i.e., before and after incubation with antibodies and in all water contrasts.

The SLD profile for each condition follows as:

$$\rho(z) = \Phi_{Si}(z)\rho_{Si} + \Phi_{oxi}(z)\rho_{oxi} + \Phi_{hc}(z)\rho_{hc} + \Phi_{hg}(z)\rho_{hg} + \Phi_{PEG}(z)\rho_{PEG} + \Phi_{Ab}(z)\rho_{Ab} + \Phi_{w}(z)\rho_{w}\,, \quad (3)$$

where Φ_{Si}, Φ_{oxi}, Φ_{hc}, Φ_{hg}, Φ_{PEG}, Φ_{Ab}, and Φ_{w}, denote the volume fractions of silicon, silicon oxide, hydrocarbon chains (belonging to both OTS and lipids), lipid head groups, PEG, antibodies, and water, respectively. The distance measured perpendicular to the surface is denoted with z, where $z = 0$ is arbitrarily defined as the interface between the lipid head groups and the aqueous medium accommodating the hydrated PEG brush and antibodies when applicable. By construction the sum of all volume fractions in the model amounts to unity at each z-position:

$$\sum_i \Phi_i(z) \equiv 1 \quad (4)$$

The volume fraction profiles are described with suitable functional forms determined by a set of adjustable parameters, following the procedure established in reference [37]. The only modification with respect to the original procedure is that lipid headgroups are treated explicitly in the present work (see Eq. 3), as motivated by our recent study in which this was found to significantly improve the fit quality [27]. In brief, silicon oxide, hydrocarbon chains, and lipid head groups are described as homogeneous layers with adjustable thickness and roughness parameters, the PEG brush has a parabolic shape with adjustable extension H_0 and maximal volume fraction Φ_0^{PEG}, and the antibody distribution is a homogeneous layer with adjustable center position, thickness, plateau-volume fraction, and gradual decays on both sides of the layer. An idealized (roughness-free), schematic illustration of the model is shown in Fig. 2. A unimodal Ab profile as presented in the figure was sufficient to reproduce the reflectivity curves for all systems except for the one discussed in the Results section, for which a bimodal Ab profile based on two rough slab representations had to be employed. The PEG amount per unit area in terms of an equivalent thickness,

$$D_{PEG} = \int \Phi_{PEG}(z)dz = N\sigma v_{EG} = Nfv_{EG}/A_{lip} \quad (5)$$

is not a free parameter but pre-determined by N, $\sigma = f/A_{lip}$, and the volume per ethylene glycol monomer $v_{EG} = 69$ Å^3 (ref. [27]). With that, H_0 is the only free parameter describing the PEG profile, while Φ_0^{PEG} follows from the normalization condition (Eq. 5). Since the conformation of the PEG brush in general can respond to antibody adsorption, two independent H_0 parameters are used, one before and one after incubation with the antibodies. Finally, water in the model fills all the space not occupied by the other chemical components, so that $\Phi_w(z)$ directly follows from Eq. 4.

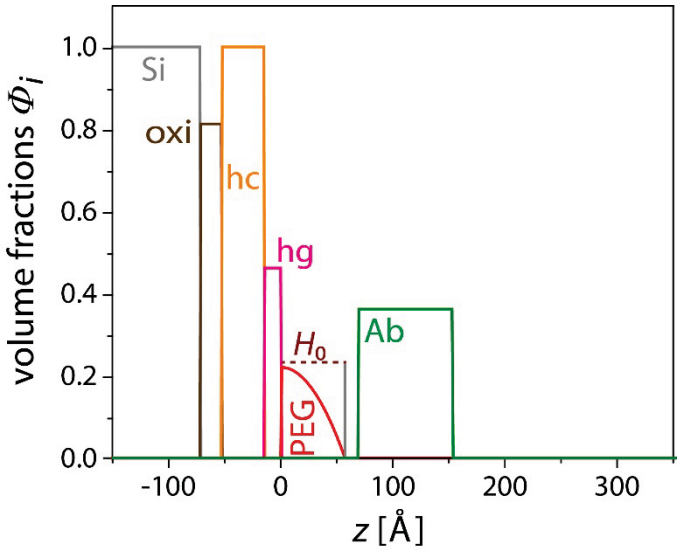

Figure 2: Schematic illustration and model description of the sample structure in terms of the volume fraction profiles $\Phi_i(z)$ of all chemical components: Silicon (Si), silicon oxide (oxi), hydrocarbon chains (hc), lipid head groups (hg), PEG, and antibodies (Ab). For the sake of clarity, interfacial roughness is neglected in this representation.

The set of model parameters with the best agreement with the experimental reflectivity data is obtained in the following way. Starting from initial parameter values specified in the Supporting Material, Eq. 3 is used to calculate for each sample its interfacial SLD profiles $\rho(z)$ corresponding to all measurement conditions, i.e. the same sample before and after protein adsorption and in each water contrast. In the next step, the corresponding theoretical reflectivity curves are calculated using dynamical reflection theory. For this purpose, the $\rho(z)$ profiles are discretized into hundreds of thin slabs of 1 Å thickness and of constant SLD. The q_z-dependent intensities are then calculated via application of Fresnel's reflection laws at each slab/slab interface using the iterative recipe of Parratt[51] and compared to the experimental data. In the last step, the parameters are varied until the best simultaneous agreement with all experimental reflectivity curves, characterized by the minimal chi-square deviation χ^2, is reached. Sets of volume fraction profiles obtained by this procedure for various samples are shown in Figs. 3, 5 and 6 and discussed below. As pointed out earlier[52], purely statistical parameter errors typically underestimate substantially the true parameter uncertainties. More meaningful error estimates approximately reflecting the robustness of the parameters with respect to the model are on the order of 10 % in the present study (see Tables 2-4 and Fig. 4).

Results and Discussion

The characteristics of the planar, solid-supported PEG brushes are summarized in Table 1. Polymerization degrees and grafting densities range between $22 \leq N \leq 455$ and $2.1 \cdot 10^{-4}$ Å^{-2} $\leq \sigma \leq$ $21 \cdot 10^{-4}$ Å^{-2}, respectively. The reduced brush density σ/σ_{OT} in terms of the overlap threshold $\sigma_{OT} = R_F^{-2}$, where $R_F = aN^{3/5}$ is the Flory radius and a = 4.1 Å is the linear dimension of an ethylene-glycol repeat unit[37]. The brushes were structurally characterized by NR in aqueous media before and after incubation with BB Abs. The results presented in the following do not necessarily apply to all biomedically-relevant PEG brushes, since those prepared by other procedures, such as *grafting-to*[53] and *grafting-from*[54], can have different densities ($\sigma/\sigma_{OT} > 10$) and considerable polydispersity. As the binding of the Abs is a physicochemically complex process, the results also cannot be generalized to Ab/PEG interactions under pH/ionic conditions that strongly deviate from those in the present work (see Methods section). Note also that specular NR averages over lateral sample heterogeneities. While considerable heterogeneity may occur for sparsely grafted brushes due to the PEG-lipids' in-plane mobility on longer time scales, the steric repulsion between PEG chains in the brush regime strongly promotes laterally homogeneous PEG-lipid distributions.

Sample structure prior to antibody adsorption

An exemplary set of volume fraction profiles, $\Phi_{Si}(z)$, $\Phi_{oxi}(z)$, $\Phi_{hc}(z)$, $\Phi_{hg}(z)$, $\Phi_{PEG}(z)$, and $\Phi_w(z)$ prior to antibody adsorption (PEG-lipid-114 at f = 0.01) is shown in Fig. 3A. The parameters characterizing the layer structure of the solid substrates to which the PEG brushes are anchored are consistent with earlier reports using the same or similar preparation protocols[27, 37, 52] and presented in detail in the supporting information. In brief, the thicknesses of the silicon oxide layer, the hydrocarbon chain layer, and the headgroup layer are obtained as d_{SiO2} = 22 ± 2 Å, d_{hc} = 40 ± 1 Å, and d_{hg} = 10 ± 4 Å, where the errors represent the standard deviation over all samples characterized. The extensions H_0 of the PEG brushes (see Fig. 2) can be determined with confidence only for dense-enough brushes ($D_{PEG} \gtrsim 5$ Å), where they are in satisfactory agreement with earlier studies (see Supporting Information).

BB vs. EB antibody adsorption to PEG brushes

In an earlier study[37] the structural characteristics of end-point-binding antibodies (EB Abs) to PEG brushes composed of PEG-lipid-114 were investigated for f = 0.01, f = 0.02, f = 0.05, and f = 0.1. In the

following, we discuss the results obtained with backbone-binding antibodies (BB Abs) under the same conditions and compare them with the EB Ab results. Fig. 3B exemplarily shows the volume fraction profiles of a brush formed by PEG-lipid-114 at $f = 0.01$ after BB Ab adsorption. As evident from the pronounced reflectivity change upon Ab adsorption (Fig. 1C), the Abs adsorb at a considerable density. The absence of nonspecific IgG Ab adsorption to the lipid surfaces was confirmed previously[37]. The Ab volume fraction profile $\Phi_{Ab}(z)$ extends over some 300 Å from the brush grafting surface at $z = 0$ and reaches up to $\Phi_{Ab}^{max} \approx 0.26$ (Fig. 3B). The figure also shows the distribution of EB Abs as obtained earlier for the same brush parameters. It is seen that the two distributions are significantly different regarding extension and maximal volume fraction. The differences between EB Ab and BB Ab distributions for all grafting densities can be characterized in terms of a number of quantities derived from the respective profiles $\Phi_{Ab}(z)$. They are summarized in Tables 2-4. Based on the adsorbed Ab amount per unit area in terms of an equivalent thickness,

$$D_{Ab} = \int \Phi_{Ab}(z)dz \,,$$

the area per adsorbed Ab follows as $A_{Ab} = v_{Ab}/D_{Ab}$, and the number of adsorbed Abs per PEG chain, in turn, as $n_{Ab} = \Sigma/A_{Ab}$. The adsorbed Ab mass per unit area, which is commonly reported in the literature on protein adsorption is $\Gamma_{Ab} = D_{Ab}m_{Ab}/v_{Ab}$, where m_{Ab} is the mass of one antibody-molecule, v_{Ab} is the volume of one antibody-molecule and $m_{Ab}/v_{Ab} = 1.4$ g/cm^3.

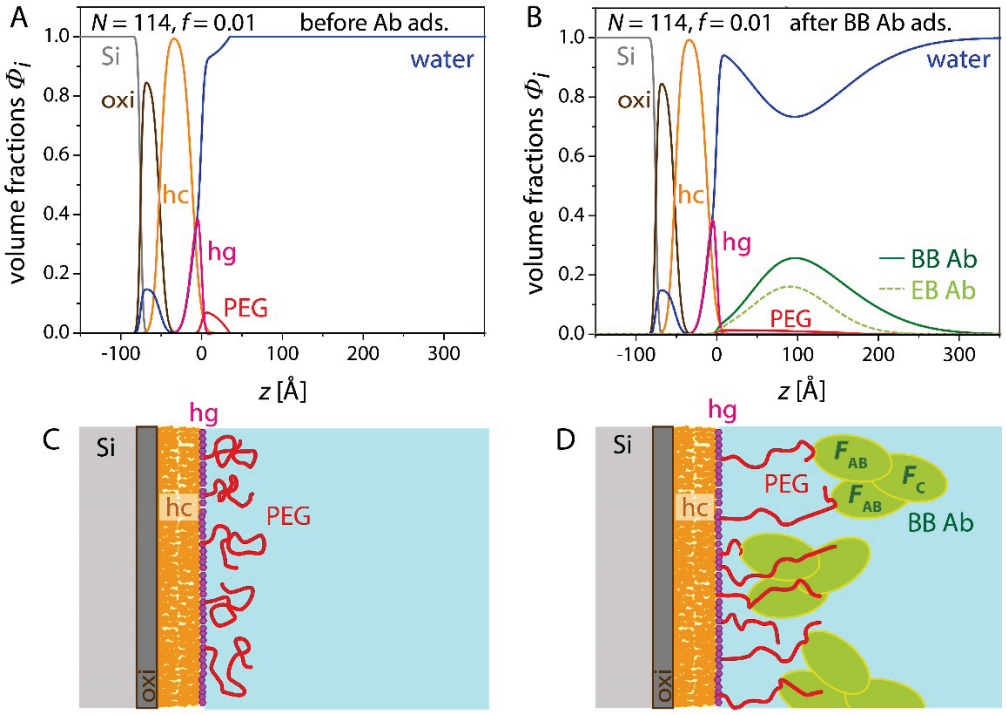

Figure 3: (A) Volume fraction profiles of silicon (Si), silicon oxide (oxi), hydrocarbon chains (hc), lipid head groups (hg), PEG, and water for a PEG brush with $N = 114$ and $f = 0.01$ prior to Ab adsorption. (B) Volume fraction profiles after BB Ab adsorption, showing also the Ab volume fraction profile. The dashed line indicates the volume fraction profile of EB Ab with respect to the grafting surface as obtained in an earlier study with the same brush parameters [37]. (C) Schematic drawing of the PEG brush prior to Ab adsorption. (D) Schematic drawing of the PEG brush after BB Ab adsorption.

Quantities characterizing the shape of the Ab profile are the maximal volume fraction $\Phi_{\mathrm{Ab}}^{\max}$, the center of mass (COM) position z_{Ab} of the antibody distribution with respect to the grafting density, $z_{Ab} = \int z\,\Phi_{Ab}(z)dz/D_{Ab}$, and the width w_{Ab} of the antibody distribution, with $w_{Ab}^2 = \int (z - z_{Ab})^2 \Phi_{Ab}(z)dz/D_{Ab}$. Fig. 4A shows Γ_{Ab} for BB Abs and EB Abs as a function of the grafting density σ. While for EB Abs Γ_{Ab} increases monotonically with σ, for BB Abs it exhibits non-monotonic behavior, with a maximum at comparatively low σ. At $\sigma = 2.1 \times 10^{-4}$ Å^{-2}, corresponding to $f = 0.01$, Γ_{Ab} is about twice higher for the BB Abs ($\Gamma_{\mathrm{Ab}} = 5.3$ mg/m^2) than for the EB Abs ($\Gamma_{\mathrm{Ab}} = 2.6$ mg/m^2), see Fig. 3B for the corresponding volume fraction profiles. With increasing σ, on the other hand, Γ_{Ab} for BB Abs decreases and reaches a plateau level significantly below Γ_{Ab} for the EB Abs. The crossover is roughly located between $\sigma = 5 \times 10^{-4}$ Å^{-2} and $\sigma = 10 \times 10^{-4}$ Å^{-2}. This behavior can be rationalized in the following way: at low brush grafting densities the maximum number of EB Ab per PEG chain is $n_{\mathrm{Ab}} = 1$ when monovalent binding is assumed and $n_{\mathrm{Ab}} = 0.5$ when divalent binding is assumed. The experimental value obtained for the lowest studied grafting density

(σ = 2.1 x 10^{-4} Å^{-2}, corresponding to f = 0.01) is n_{Ab} = 0.5 (see Fig. 4B and Table 3), suggesting that each Ab binds two PEG chains and therefore suggesting that Ab adsorption is diffusion-limited and occurs one-by-one with a slow time scale for the initial binding and a fast timescale for the second binding. For f = 0.01 the distance between grafting points can be spanned by two PEG chains, so that divalent binding is indeed possible. A transition from n_{Ab} = 0.5 to n_{Ab} = 1 should be observed for even lower grafting densities where this condition is no longer given, provided that the in-plane mobility of the PEG anchors is slow compared to the time scale of the adsorption. For the BB Abs we observe n_{Ab} ≈ 1, reflecting that multiple binding to each PEG chain is possible. At higher grafting densities Ab binding is limited by Ab crowding and the osmotic penalty, Πv_{ins}, imposed by the brush[27, 37], where $\Pi \approx k_B T/\xi^3$ is the osmotic pressure, $\xi \approx \sigma^{1/2}$ is the blob size, and $v_{ins} \leq v_{Ab}$ is the fraction of an Ab's volume inserted into the brush. This penalty must be considered higher for BB Abs than for EB Abs, because the former are believed to preferentially bind rather long portions of a PEG chain[36] and therefore on average insert more deeply into the brush upon binding. For dense brushes (N = 114, f = 0.1), the critical inserted volume was recently estimated as 10 nm^3 << v_{Ab} (ref. [27]), demonstrating that the osmotic penalty plays an important role in the present work. In summary, BB Abs can bind better than EB Abs at low σ, where binding is limited by the available binding sites, whereas EB Abs can bind better than BB Abs at high σ, where binding is limited by the osmotic penalty imposed by the brush.

BB Ab binding	D_{Ab} [Å]	A_{Ab} [Å^2]	Γ_{Ab} [mg/m^2]	z_{Ab} [Å]	w_{Ab} [Å]	Φ_{Ab}^{max}	n_{Ab}
PEG-lipid-22, f = 0.1	26	7100	3.6	93	42	0.24	0.07
PEG-lipid-114, f = 0.01	38	4700	5.3	119	60	0.26	0.98
PEG-lipid-114, f = 0.05	30	5800	4.3	138	63	0.20	0.16
PEG-lipid-114, f = 0.1	31	5600	4.4	168	102	0.17	0.08
PEG-lipid-455, f = 0.01	73	2500	10.3	285	116	0.22	1.92

Table 2: Characteristics of BB Ab adsorption to various PEG brushes in terms of Ab amount and mass per unit area, D_{Ab} and Γ_{Ab}, respectively, the area A_{Ab} per adsorbed Ab, the center of mass position z_{Ab} of the Ab volume fraction distribution, the width w_{Ab} of the distribution, the maximal Ab volume fraction Φ_{Ab}^{max}, and the number n_{Ab} of Ab per polymer chain. Errors are estimated as ≈ 10 % for all parameters (see main text).

EB Ab binding	D_{Ab} [Å]	A_{Ab} [Å^2]	Γ_{Ab} [mg/m^2]	z_{Ab} [Å]	w_{Ab} [Å]	Φ_{Ab}^{max}	n_{Ab}
PEG-lipid-114, f = 0.01	19	9500	2.6	96	45	0.16	0.50
PEG-lipid-114, f = 0.02	25	7200	3.4	128	40	0.24	0.33
PEG-lipid-114, f = 0.05	37	4300	5.1	143	40	0.32	0.20
PEG-lipid-114, f = 0.1	46	3900	6.3	165	44	0.35	0.12

Table 3: Characteristics of EB Ab adsorption to various PEG brushes in terms of Ab amount and mass per unit area, D_{Ab} and Γ_{Ab}, respectively, the area A_{Ab} per adsorbed Ab, the center of mass position z_{Ab} of the Ab volume

fraction distribution, the width w_{Ab} of the distribution, the maximal Ab volume fraction Φ_{Ab}^{max}, and the number n_{Ab} of Ab per polymer chain. Errors are estimated as ≈ 10 % for all parameters (see main text).

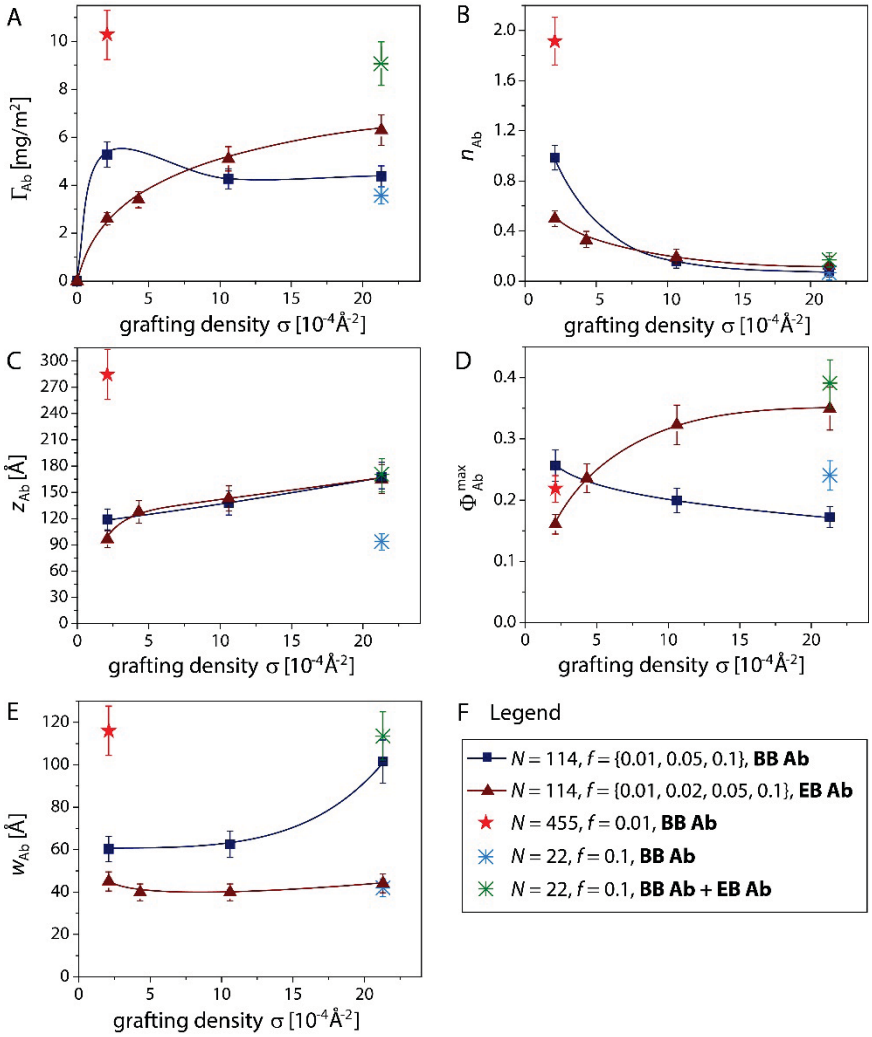

Figure 4: Characteristics of adsorbed Ab distributions as a function of the grafting density obtained for all systems investigated (Table 1). Solid lines are purely empirical and merely serve to guide the eye. (A) Ab mass per area Γ_{Ab}. (B) Number of adsorbed Ab per PEG chain. (C) Center of mass position, z_{ab}, of the distribution with respect to the brush grafting surface at $z = 0$. (D) Maximal antibody volume fraction Φ_{Ab}^{max} . (E) Width, w_{Ab}, of the distribution. (F) Legend.

The osmotic penalty can also be considered responsible for the displacement of the Ab distribution away from the grafting surface with increasing σ, as seen from the increase in the center-of-mass position z_{Ab} (Fig. 4C), which is essentially independent of the Ab specificity and approximately linear with σ. The maximal antibody volume fraction, Φ_{Ab}^{max}, is coupled to the adsorbed amount and therefore higher for BB Abs than for EB Abs at small σ (Fig. 4D), where BB Abs adsorb at higher densities. With increasing σ, however, Φ_{Ab}^{max} increases faster for the EB Abs than for the BB Abs, and

a cross-over occurs at around $\sigma \approx 5 \times 10^{-4}$ Å^{-2}. This behavior can be attributed to the more restricted binding mode of the EB Abs, which always bind to the polymer end-points, so that a more densely structured Ab layer with higher volume fraction is formed. In contrast, the BB Abs exhibit more variability in the binding position along the polymer backbone and, thus, form broader and less densely structured Ab layers. The same trend is seen in Fig. 4E, where the width of the Ab distribution, w_{Ab}, is shown as a function of σ: this width is higher for BB Abs than for EB Abs at all grafting densities.

EB and BB Abs both are IgG type Abs and have essentially the same generic physicochemical properties in terms of mass, volume, domain structure, and charge distribution. The selectivity for their respective binding motif is dominated solely by their binding pockets, which are small with respect to the entire Ab molecules. Generic (non-specific) interactions with the PEG brushes can therefore be considered approximately equal for the two Ab types. The Abs bind to the PEG chains while still being surrounded by aqueous medium at near-physiological salt, pH, and temperature conditions, so that no pronounced denaturation is expected on the time scale of the experiment. The affinities of the two Ab types for their respective binding motifs are reported to be comparable and at the order of 1 nM[36, 37]. In both cases, the binding is so strong that it is found to be irreversible on the time scale of the experiments even after rinsing with neat aqueous solutions. Selectivity to the terminal and main chain recognition has been previously confirmed[36] and is evidenced by the pronounced differences in the binding characteristics. The PEG Ab titers found in the human blood exhibit a large variety[36]. Under in-vivo conditions, Γ_{Ab} will therefore be variable, too, and typically lower than what is observed in the present work at a constant Ab concentration of 0.1 mg/mL.

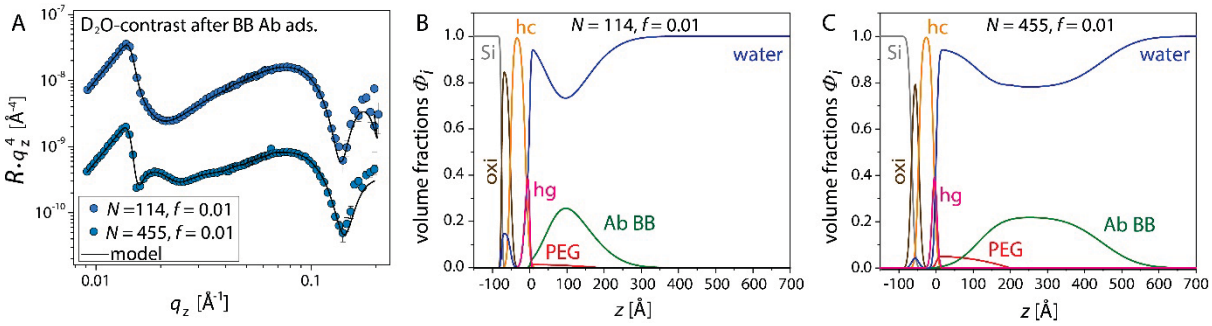

Figure 5: (A) Reflectivity curves in D_2O contrast of brushes with $N = 114$ (top) and $N = 455$ (bottom) at $f = 0.01$ after adsorption of BB Abs. Solid lines represent the simulated intensities corresponding to the best-matching parameters in the common model. Note that the analysis involves also reflectivity curves in other water contrasts (see Methods section). (B) Volume fraction profiles of silicon (Si), silicon oxide (oxi), hydrocarbon chains (hc), lipid head groups (hg), PEG, antibodies (Ab), and water after adsorption of BB Abs to the brush with $N = 114$. (C) Volume fraction profiles after adsorption of BB Abs to the brush with $N = 455$.

Influence of the polymerization degree

Up to here we have compared the adsorption of EB Abs and BB Abs to brushes of variable grafting density but constant polymerization degree N. In the following we discuss the influence of N for BB Abs. Figure 5A shows reflectivity curves in D_2O contrast after adsorption of BB Abs to brushes with $f = 0.01$ formed by polymers with different N, namely $N = 114$ and $N = 455$. The curves exhibit clear differences in the range between $q_z \approx 0.015$ Å^{-1} and $q_z \approx 0.05$ Å^{-1}. For $N = 455$, the emergence of two pronounced reflectivity minima, separated by only $\Delta q_z \approx 0.01$ Å^{-1}, indicates the formation of an extended protein layer extending the overall thickness of the interfacial region to $\approx 2\pi/\Delta q_z \approx 630$ Å. Solid lines in Fig. 5A represent the simulated intensities corresponding to the best-matching parameters in the common model. Panels B and C of Fig. 5 show the corresponding volume fraction profiles of all chemical components for $N = 114$ (panel B) and $N = 455$ (panel C), respectively. For $N = 455$ the protein distribution is indeed much broader ($w_{Ab} \approx 116$ Å, see Table 2 and Fig. 4E) than for $N = 144$ ($w_{Ab} \approx 60$ Å), indicating that BB Abs have a broader range of binding positions in a brush formed by longer polymers. The center of mass position of the Ab distribution for $N = 455$ ($z_{Ab} = 285$ Å, see Table 2 and Fig. 4C) is strongly shifted away from the grafting surface with respect to $N = 114$ ($z_{Ab} = 119$ Å). This can be interpreted as the combined effect of (i) the broader Ab distribution and (ii) the stronger osmotic penalty excluding Abs from a brush with higher density in terms of σ/σ_{OT} (see Table 1). The maximum Ab volume fraction is essentially unaffected by N. In line with the increased width at constant maximal Ab volume fraction, the overall adsorbed amount is

significantly higher for longer PEG chains. As seen in Fig. 4B, the number of bound Ab per PEG chain ($n_{Ab} \approx 2$) is approximately twice as large as for $N = 144$. At this point it should be noted that $n_{Ab} > 1$ is impossible by construction for EB Abs, but possible for BB Abs. Interestingly, n_{Ab} for BB Abs does not increase linearly with N, but to a significantly lower extent. This behavior can be attributed indirectly to the osmotic penalty introduced before: Abs binding to the brush outer edge are only partially inserted, while most of their volume is accommodated in the brush-free region. The osmotic penalty is thus minimized at the outer edge, and binding is more favorable than in the core regions of the brush. Increasing N at fixed σ merely increases the thickness of this core region, to which binding is less favorable, while the number of favorable binding sites at the outer edge remains largely constant.

The influence of N on Ab adsorption was also investigated at higher brush grafting densities but shorter chains. To this end, adsorption of BB Abs to brushes with $f = 0.1$ was compared between $N = 114$ and $N = 22$. The main motivation for the choice of chains as short as $N = 22$ was to see whether there is a lower limit of chain length to which the Abs can still bind. According to a recent study, the affinity of BB Abs of type IgG1 3.3 strongly decreases with decreasing PEG molecular weight[36]. Nonetheless, the reflectivity curves obtained in the present study evidence that substantial binding also occurs to brushes with $N = 22$, corresponding to a PEG molecular weight of 1000 Da. The reflectivity curve in D_2O after BB Ab adsorption is shown in Fig. 6A (top), and a comparison with the curve before adsorption is shown in the Supporting Information. In our previous work [37] we confirmed that IgG Abs do not adsorb to the bare grafting surfaces ($f = 0$). The present result demonstrates that BB Abs of type IgG1 3.3, in contrast to earlier claims effectively bind also to PEG chains as short as $N = 22$. Strikingly, the adsorbed amount per area Γ_{Ab} is not much lower for $N = 22$ than for $N = 144$, indicating that in a densely grafted brush the osmotic penalty is even more dominant and prevents the BB Abs from binding equally well along the entire brush height. In other words, the surface-effect identified already for the more sparsely grafted brushes (at $f = 0.01$) is even more pronounced for more densely grafted brushes. Turning to the characteristics of the BB Ab distribution for $N = 22$ (Fig. 6B and Table 2) we note that binding occurs close to the surface ($z_{Ab} = 93$ Å) in a very narrow and defined layer ($w_{Ab} = 42$ Å). This behavior can be interpreted as the consequence of a very restricted binding mode in which the Abs cope with the short chain: most of the chain is confined inside the binding pocket, so that the F_{AB} segments are pulled very close to the solid surface and the F_C segment faces the aqueous solution. This interpretation is also in excellent agreement with the maximal length of an IgG molecule of ≈ 16 nm [37], see Fig. 6B.

Sequential adsorption of BB Abs and EB Abs

Sequential adsorption of BB and EB Abs onto PEG brushes was investigated for the sample discussed in the previous paragraph ($N = 22$ at $f = 0.1$). For this purpose, after BB Ab adsorption and initial characterization (see Fig. 6B) the sample was incubated with EB Abs to allow for their adsorption to the brushes pre-loaded with BB Abs. The bottom curve in Fig. 6A shows the reflectivity in D_2O after the second incubation step (i.e., after incubation with EB Abs). It is clearly different from the reflectivity after incubation with the BB Abs only (top curve). The complete data set is shown in the Supporting Information. The emergence of pronounced reflectivity minima with a distance of only $\Delta q_z \approx 0.01$ Å^{-1} once more evidences the formation of a wide protein distribution. Solid lines in Fig. 6A represent the simulated intensities corresponding to the best-matching parameters in the common model. Panels B and C of Fig. 6 show the corresponding volume fraction profiles of all chemical components before and after the second incubation step. Reproducing the reflectivity curves after the second step to a satisfactory level required allowing for a more complex Ab distribution in the model, realized mathematically as two partially overlapping rough slabs (Footnote: Fit is still not perfect, but we did not want to further increase the model complexity to avoid overinterpretation of the data.). As immediately seen from the Ab profiles and condensed in the numbers in Table 4, substantial additional binding of EB Abs occurs onto the brush which is already pre-loaded with BB Abs. The overall amount per area increases from $\Gamma_{Ab} = 3.6$ mg/m^2 after BB Ab adsorption to $\Gamma_{Ab} = 9.1$ mg/m^2 after subsequent EB Ab adsorption. This result indicates that EB Abs can still bind to the polymer tails that are displayed by the pre-loaded brush and thus suggests that EB Ab binding does not require as long PEG sequences as BB Ab binding. Although we are in the position to identify the difference between the adsorbed amounts before and after the second incubation step (5.5 mg/m^2) to the EB Abs alone (Table 4), it is not possible to determine the individual profiles of BB Abs and EB Abs. This is because the two species have the same SLD, and one has to assume that the distribution of BB Abs is affected by the EB Ab binding, so that taking the difference in the distributions before and after the second adsorption step is not meaningful. However, disentangling the two distributions would be possible in principle by selective deuteration of one Ab type.

BB + EB Ab binding PEG-lipid-22, f = 0.1	D_{Ab} [Å]	A_{Ab} [Å^2]	Γ_{Ab} [mg/m^2]	n_{Ab}	z_{Ab} [Å]	w_{Ab} [Å]	Φ_{Ab}^{max}
Total BB + EB	65	2800	9.1	0.17	171	114	0.39
BB	26	7100	3.6	0.07	-	-	-
EB	39	4600	5.5	0.10	-	-	-

Table 4: Characteristics of BB Ab and EB Ab sequential adsorption to PEG brushes with N = 22 and f = 0.1 in terms of Ab amount and mass per unit area, D_{Ab} and Γ_{Ab}, respectively, the area A_{Ab} per adsorbed Ab, the center of mass position z_{Ab} of the Ab volume fraction distribution, the width w_{Ab} of the distribution, the maximal Ab volume fraction $\Phi_{Ab}^{\max}$, and the number n_{Ab} of Ab per polymer chain. Note that z_{Ab}, w_{Ab}, and $\Phi_{Ab}^{\max}$ are accessible only for the total (BB Ab + EB Ab) profile. Errors are estimated as ≈ 10 % for all parameters (see main text).

Influence of Ab binding on the brush conformation

Determining the response of the brush conformation to Ab adsorption is non-trivial. As pointed out above, only for dense-enough brushes is the sensitivity of the NR measurements high enough to determine their conformation after Ab binding with confidence. While the PEG conformation is hardly accessible for low PEG amounts, the contribution of PEG to the overall organic material is essentially negligible in these cases. The associated uncertainty in the Ab profiles is therefore minor. Note also that the Ab amounts are unaffected because the PEG amount is a fixed parameter. Dense brushes are expected to respond weakest to Ab adsorption and no significant general trend is indeed observed for these samples. For sparser brushes, significant conformational response to Ab binding is however expected. Insights into the brush conformation after Ab adsorption can be gained indirectly from the Ab volume fraction profiles. In certain cases, these profiles can only be explained by assuming significant elongation of the polymer chains out of the un-perturbed brush conformation. Namely, the extension of the Ab profiles away from the grafting surface in these cases is larger than the sum of the un-perturbed brush extension and the length of a stretched Ab (≈ 16 nm, see above). In fact, the Ab profile after sequential BB Ab and EB Ab binding (Fig. 6C) is so extended that it appears to be at odds with the assumption that all PEG chains remain fully anchored into the grafting surface even for fully extended PEG chains with contour length $L = Na$ ≈ 9 nm. One possible scenario is that some PEG-lipids are pulled out of the lipid monolayer by one FAB domain of an Ab which is bound to an anchored PEG-lipid with the other FAB domain. The PEG chains of these PEG-lipids are substantially displaced from the grafting surface by up to ≈ 20 nm, where they act as binding sites for additional Abs further away from the surface. This scenario obviously cannot occur for covalently surface-grafted PEG brushes.

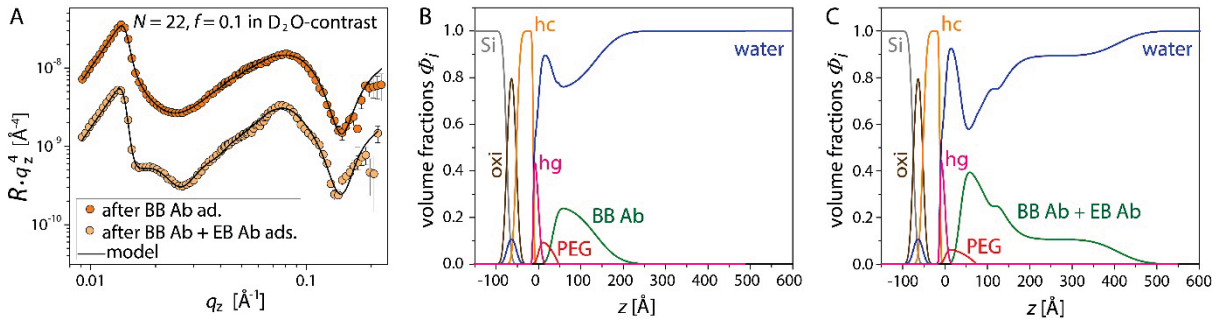

Figure 6: (A) Reflectivity curves in D_2O contrast of brushes with N = 22 at f = 0.1 after adsorption of BB Abs (top) and after subsequent adsorption of EB Ab after initial BB Ab adsorption. Solid lines represent the simulated intensities corresponding to the best-matching parameters in the common model. Note that the analysis involves also reflectivity curves in other water contrasts (see Methods section). (B) Volume fraction profiles of silicon (Si), silicon oxide (oxi), hydrocarbon chains (hc), lipid head groups (hg), PEG, antibodies (Ab), and water after adsorption of BB Abs. (C) Volume fraction profiles after subsequent adsorption of EB Ab after initial BB Ab adsorption.

Conclusions

We have used NR to comprehensively characterize on the structural level the adsorption of two Ab types to PEG brushes with well-defined grafting density σ and polymerization degree N. For all brush parameters investigated the adsorption of BB Abs exhibits structural features clearly different from those observed with EB Abs. Both the adsorbed Ab amount and the parameters characterizing the Ab volume fraction profiles have qualitatively different dependence on the grafting density for BB and EB Abs. The extent of Ab binding is substantial for all brush parameters investigated. Even for the densest brushes, the osmotic penalty is too weak to prevent specific binding at the brush outer edge. It thus appears unlikely that Ab adsorption can be prevented through variation of the parameters σ and N within a practically feasible range. The binding of EB Abs can in principle be prevented by end-modified PEG brushes which otherwise still have the character of a PEG brush. In contrast, BB Ab binding can only be prevented by dense chemical modifications all along the PEG chain, so that the binding motif is interrupted but at the same time the overall chemical nature of the brush is altered. Alternatively, PEG may be entirely replaced with chemically different polymers of similar behavior[55], for which Abs are less abundant in the human population. However, the abundance of Abs has been reported to increase with frequent exposure to the chemical motif[56]. Ultimately, the use of polymer brushes displaying biological motives, like phosphatidylcholines[57], may thus be a more sustainable route.

Associated content

Supporting information

Additional information on methods and results

Notes

The authors declare no competing financial interest.

Data Availability: The raw and processed data required to reproduce these findings are available to download from https://doi.ill.fr/10.5291/ILL-DATA.9-13-545 and https://doi.ill.fr/10.5291/ILL-DATA.9-13-648.

Acknowledgements

We thank Institut Laue-Langevin (ILL) for beam time allocation (dois: 10.5291/ILL-DATA.9-13-545 and 10.5291/ILL-DATA.9-13-648), the ILL/PSCM laboratories for support during sample preparation and pre-characterization, Laurianne Simon for insightful comments, and Richard A. Campbell and Yuri Gerelli for support during the beamtimes. Financial support by the Max Planck Society and by the German Research Foundation (DFG) via Emmy-Noether grant (SCHN 1396/1) is gratefully acknowledged. This article is dedicated to our friend and long-standing collaborator Avraham Halperin, who considerably contributed to the present work through his ideas and suggestions, but sadly passed away before the manuscript was written.

References

1. Immordino, M. L.; Dosio, F.; Cattel, L., Stealth liposomes: review of the basic science, rationale, and clinical applications, existing and potential. *International Journal of Nanomedicine* **2006,** 1, (3), 297-315.
2. Shi, J.; Xiao, Z.; Kamaly, N.; Farokhzad, O. C., Self-Assembled Targeted Nanoparticles: Evolution of Technologies and Bench to Bedside Translation. *Accounts of Chemical Research* **2011,** 44, (10), 1123-1134.
3. Shin, H.-S.; Park, K.; Kim, J. H.; Kim, J.-J.; Han, D. K.; Moon, M.-W.; Lee, K.-R.; Shin, J. H., Biocompatible PEG Grafting on DLC-coated Nitinol Alloy for Vascular Stents. *Journal of Bioactive and Compatible Polymers* **2009,** 24, (4), 316-328.
4. Pasut, G.; Veronese, F. M., State of the art in PEGylation: the great versatility achieved after forty years of research. *Journal of Controlled Release* **2012,** 161, (2), 461-472.
5. Elbert, D. L.; Hubbell, J. A., Surface Treatments of Polymers for Biocompatibility. *Annual Review of Materials Science* **1996,** 26, (1), 365-394.
6. Teramura, Y.; Iwata, H., Islet encapsulation with living cells for improvement of biocompatibility. *Biomaterials* **2009,** 30, (12), 2270-2275.
7. Bridges, A. W.; García, A. J., Anti-Inflammatory Polymeric Coatings for Implantable Biomaterials and Devices. *Journal of diabetes science and technology (Online)* **2008,** 2, (6), 984-994.
8. Li, S.; Henry, J. J. D., Nonthrombogenic approaches to cardiovascular bioengineering. *Annual review of biomedical engineering* **2011,** 13, 451-475.
9. Walkey, C. D.; Chan, W. C. W., Understanding and controlling the interaction of nanomaterials with proteins in a physiological environment. *Chemical Society Reviews* **2012,** 41, (7), 2780-2799.
10. Yu, M.; Urban, M. W., Polymeric Surfaces with Anticoagulant, Antifouling, and Antimicrobial Attributes. *Macromolecular Symposia* **2009,** 283–284, (1), 311-318.
11. Abuchowski, A.; McCoy, J. R.; Palczuk, N. C.; van Es, T.; Davis, F. F., Effect of covalent attachment of polyethylene glycol on immunogenicity and circulating life of bovine liver catalase. *Journal of Biological Chemistry* **1977,** 252, (11), 3582-6.
12. Abuchowski, A.; van Es, T.; Palczuk, N. C.; Davis, F. F., Alteration of immunological properties of bovine serum albumin by covalent attachment of polyethylene glycol. *Journal of Biological Chemistry* **1977,** 252, (11), 3578-81.
13. Merrill, E. W.; Salzman, E. W., Polyethylene oxide as a biomaterial. *ASAIO Journal* **1983,** 6, 60-64.
14. Veronese, F. M., *PEGylated Protein Drugs: Basic Science and Clinical Applications: Basic Science and Clinical Applications*. Springer: 2009.
15. Halperin, A., Polymer Brushes that Resist Adsorption of Model Proteins: Design Parameters. *Langmuir* **1999,** 15, 2525-2533.
16. Szleifer, I., Protein Adsorption on Surfaces with Grafted Polymers: A Theoretical Approach. *Biophys. J.* **1997,** 72, 595-612.
17. Jeon, S. I.; Andrade, J. D., Protein-surface interactions in the presence of polyethylene oxide: II. Effect of protein size. *Journal of colloid and interface science* **1991,** 142, (1), 159-166.
18. Jeon, S. I.; Lee, J. H.; Andrade, J. D.; De Gennes, P. G., Protein-surface interactions in the presence of polyethylene oxide: I. Simplified theory. *J. Colloid Interface Sci.* **1991,** 142, 149-158.
19. Currie, E. P. K.; van der Gucht, J.; Borisov, O. V.; Cohen Stuart, M. A., Stuffed brushes: theory and experiment. *Pure Appl. Chem.* **1999,** 71, 1227-1241.
20. Halperin, A.; Fragneto, G.; Schollier, A.; Sferrazza, M., Primary versus Ternary Adsorption of Proteins onto PEG Brushes. *Langmuir* **2007,** 23, 10603-10617.
21. Halperin, A.; Kroeger, M., Ternary Protein Adsorption onto Brushes: Strong versus Weak. *Langmuir* **2009,** 25, 11621-11634.
22. Chen, H.; Yuan, L.; Song, W.; Wu, Z.; Li, D., Biocompatible polymer materials: role of protein-surface interactions. *Progress in Polymer Science* **2008,** 33, (11), 1059-1087.

23. Abbott, N. L.; Blankschtein, D.; Hatton, T. A., Protein partitioning in two-phase aqueous polymer systems. 3. A neutron scattering investigation of the polymer solution structure and protein-polymer interactions. *Macromolecules* **1992,** 25, (15), 3932-3941.
24. Bloustine, J.; Virmani, T.; Thurston, G. M.; Fraden, S., Light scattering and phase behavior of lysozyme-poly (ethylene glycol) mixtures. *Physical review letters* **2006,** 96, (8), 087803.
25. Gon, S.; Fang, B.; Santore, M. M., Interaction of cationic proteins and polypeptides with biocompatible cationically-anchored PEG brushes. *Macromolecules* **2011,** 44, (20), 8161-8168.
26. Norde, W.; Gage, D., Interaction of Bovine Serum Albumin and Human Blood Plasma with PEO-Tethered Surfaces: Influence of PEO Chain Length, Grafting Density, and Temperature *Langmuir* **2004,** 20, 4162-4167.
27. Latza, V. M.; Rodriguez-Loureiro, I.; Kiesel, I.; Halperin, A.; Fragneto, G.; Schneck, E., Neutron Reflectometry Elucidates Protein Adsorption from Human Blood Serum onto PEG brushes. *Langmuir* **2017,** 33, (44), 12708-12718.
28. Currie, E. P. K.; Norde, W.; Cohen Stuart, M. A., Tethered polymer chains: surface chemistry and their impact on colloidal and surface properties. *Adv. Colloid Sci.* **2003,** 100-102, 205-265.
29. Harris, J. M., *Poly(Ethylene Glycol) Chemistry: Biotechnical and Biomedical Applications*. Plenum Press: New York, 2003.
30. Leckband, D.; Sheth, S.; Halperin, A., Grafted poly(ethylene oxide) brushes as nonfouling surface coatings. *Journal of Biomaterials Science, Polymer Edition* **1999,** 10, (10), 1125-1147.
31. Becker, A.; Schlichting, I.; Kabsch, W.; Schultz, S.; Wagner, A. F. V., Structure of peptide deformylase and identification of the substrate binding site. *Journal of Biological Chemistry* **1998,** 273, (19), 11413-11416.
32. Hasek, J., Poly (ethylene glycol) interactions with proteins. *Zeitschrift fur Kristallographie Supplements* **2006,** 2006, 613-618.
33. Armstrong, J. K., The occurrence, induction, specificity and potential effect of antibodies against poly (ethylene glycol). In *Pegylated protein drugs: Basic science and clinical applications*, Springer: 2009; pp 147-168.
34. Armstrong, J. K.; Hempel, G.; Koling, S.; Chan, L. S.; Fisher, T.; Meiselman, H. J.; Garratty, G., Antibody against poly (ethylene glycol) adversely affects PEGâ€asparaginase therapy in acute lymphoblastic leukemia patients. *Cancer* **2007,** 110, (1), 103-111.
35. Schellekens, H.; Hennink, W. E.; Brinks, V., The immunogenicity of polyethylene glycol: facts and fiction. *Pharmaceutical research* 30, (7), 1729-1734.
36. Chen, B.-M.; Su, Y.-C.; Chang, C.-J.; Burnouf, P.-A.; Chuang, K.-H.; Chen, C.-H.; Cheng, T.-L.; Chen, Y.-T.; Wu, J.-Y.; Roffler, S. R., Measurement of pre-existing IgG and IgM antibodies against polyethylene glycol in healthy individuals. *Analytical chemistry* **2016,** 88, (21), 10661-10666.
37. Schneck, E.; Berts, I.; Halperin, A.; Daillant, J.; Fragneto, G., Neutron reflectometry from poly (ethylene-glycol) brushes binding anti-PEG antibodies: Evidence of ternary adsorption. *Biomaterials* **2015,** 46, 95-104.
38. Riedel, T.; Riedelova-Reicheltova, Z.; Majek, P.; Rodriguez-Emmenegger, C.; Houska, M.; Dyr, J. E.; Brynda, E., Complete identification of proteins responsible for human blood plasma fouling on poly (ethylene glycol)-based surfaces. *Langmuir* **2013,** 29, (10), 3388-3397.
39. Hagiwara, T.; Nattawut, P.; Shibata, M.; Sakiyama, T., Monitoring of adsorption behaviors of bovine serum albumin onto a stainless steel surface by the quartz crystal microbalance based on admittance analysis. *Bioscience, Biotechnology, and Biochemistry* **2017,** 81, (4), 783-789.
40. Jin, J.; Jiang, W.; Yin, J.; Ji, X.; Stagnaro, P., Plasma Proteins Adsorption Mechanism on Polyethylene-Grafted Poly(ethylene glycol) Surface by Quartz Crystal Microbalance with Dissipation. *Langmuir* **2013,** 29, (22), 6624-6633.
41. Guzman, G.; Bhaway, S. M.; Nugay, T.; Vogt, B. D.; Cakmak, M., Transport-Limited Adsorption of Plasma Proteins on Bimodal Amphiphilic Polymer Co-Networks: Real-Time Studies by Spectroscopic Ellipsometry. *Langmuir* **2017,** 33, (11), 2900-2910.
42. Schneck, E.; Schollier, A.; Halperin, A.; Moulin, M.; Haertlein, M.; Sferrazza, M.; Fragneto, G., Neutron reflectometry elucidates density profiles of deuterated proteins adsorbed onto surfaces

displaying poly (ethylene glycol) brushes: evidence for primary adsorption. *Langmuir* **2013,** 29, (46), 14178-14187.
43. Yigit, C.; Kanduc, M.; Ballauff, M.; Dzubiella, J., Interaction of charged patchy protein models with like-charged polyelectrolyte brushes. *Langmuir* **2016,** 33, (1), 417-427.
44. Knop, K.; Hoogenboom, R.; Fischer, D.; Schubert, U. S., Poly (ethylene glycol) in drug delivery: pros and cons as well as potential alternatives. *Angewandte chemie international edition* **2010,** 49, (36), 6288-6308.
45. https://www.abcam.com/polyethylene-glycol-antibody-peg-b-47-ab51257.html
46. Su, Y.-C.; Chen, B.-M.; Chuang, K.-H.; Cheng, T.-L.; Roffler, S. R., Sensitive quantification of PEGylated compounds by second-generation anti-poly (ethylene glycol) monoclonal antibodies. *Bioconjugate chemistry* **2010,** 21, (7), 1264-1270.
47. Tamm, L.; McConnell, H. M., Supported phospholipid bilayers. *Biophys. J.* **1984,** 47, 105-113.
48. Hermelink, A.; Brezesinski, G., Do unsaturated phosphoinositides mix with ordered phosphadidylcholine model membranes? *Journal of lipid research* **2008,** 49, (9), 1918-1925.
49. Campbell, R. A.; Wacklin, H. P.; Sutton, I.; Cubitt, R.; Fragneto, G., FIGARO: The new horizontal neutron reflectometer at the ILL. *The European Physical Journal Plus* **2011,** 126, (11), 1-22.
50. Cubitt, R.; Fragneto, G., D17: the new reflectometer at the ILL. *Appl. Phys. A* **2002,** 74, S329-S331.
51. Parratt, L. G., Surface Studies of Solids by Total Reflection of X-Rays. *Phys. Rev* **1954,** 95, 359-369.
52. Rodriguez-Loureiro, I.; Scoppola, E.; Bertinetti, L.; Barbetta, A.; Fragneto, G.; Schneck, E., Neutron reflectometry yields distance-dependent structures of nanometric polymer brushes interacting across water. *Soft Matter* **2017,** 13, (34), 5767-5777.
53. Zdyrko, B.; Varshney, S. K.; Luzinov, I., Effect of molecular weight on synthesis and surface morphology of high-density poly (ethylene glycol) grafted layers. *Langmuir* **2004,** 20, (16), 6727-6735.
54. Fan, X.; Lin, L.; Dalsin, J. L.; Messersmith, P. B., Biomimetic anchor for surface-initiated polymerization from metal substrates. *Journal of the American Chemical Society* **2005,** 127, (45), 15843-15847.
55. Luxenhofer, R.; Han, Y.; Schulz, A.; Tong, J.; He, Z.; Kabanov, A. V.; Jordan, R., Poly (2-oxazoline) s as Polymer Therapeutics. *Macromolecular rapid communications* **2012,** 33, (19), 1613-1631.
56. Garay, R. P.; El-Gewely, R.; Armstrong, J. K.; Garratty, G.; Richette, P., Antibodies against polyethylene glycol in healthy subjects and in patients treated with PEG-conjugated agents. *Expert Opinion on Drug Delivery* **2012,** 9, (11), 1319-1323.
57. Schlenoff, J. B., Zwitteration: coating surfaces with zwitterionic functionality to reduce nonspecific adsorption. *Langmuir* **2014,** 30, (32), 9625-9636.

Neutron Reflectometry Elucidates Protein Adsorption from Human Blood Serum onto PEG brushes

Victoria M. Latza[a], Ignacio Rodriguez-Loureiro[a], Irena Kiesel[b,c], Avraham Halperin[d], Giovanna Fragneto[b], and Emanuel Schneck[a,*]

[a]Max Planck Institute of Colloids and Interfaces, Am Mühlenberg 1, 14476 Potsdam, Germany

[b]Institut Laue-Langevin, 71 avenue des Martyrs, 38042 Grenoble Cedex 9, France

[c]TU Dortmund University, August-Schmidt-Straße 4, 44227 Dortmund, Germany

[d]Univ. Grenoble Alpes, CNRS, LIPhy, 38000 Grenoble France

[*]Corresponding author: schneck@mpikg.mpg.de, Phone: +49-331567-9404, Fax: +49-331567-9402

Supporting information

Table of content

1.) Initial parameter values for the common model

Initial values for all parameters concerning the layered structure of the functionalized solid surface including the brush-grafting lipid monolayer were taken from the best-matching results obtained in a previous study [1]. The decay length Λ of the PEG brush was initially set to $\Lambda = H\sqrt{1-e^{-1}} \approx 0.8\,H$ (see main text), where *H* is the best-matching parabolic brush height obtained in the same study [1]. The stretching exponent *n* was initially set to 2, corresponding to a Gaussian distribution. Regarding the protein volume fraction profiles, various sets of initial parameters for z_k^{pro}, w_k^{pro}, and $\Phi_k^{\max}$ were tested. When they were taken from a suitable range, the parameter values during the fitting procedure converged to the values presented in the main text, for which the experimental data are well reproduced. In all other cases, the fitting procedure resulted in vanishing protein volume fraction profiles, for which the experimental data are poorly reproduced.

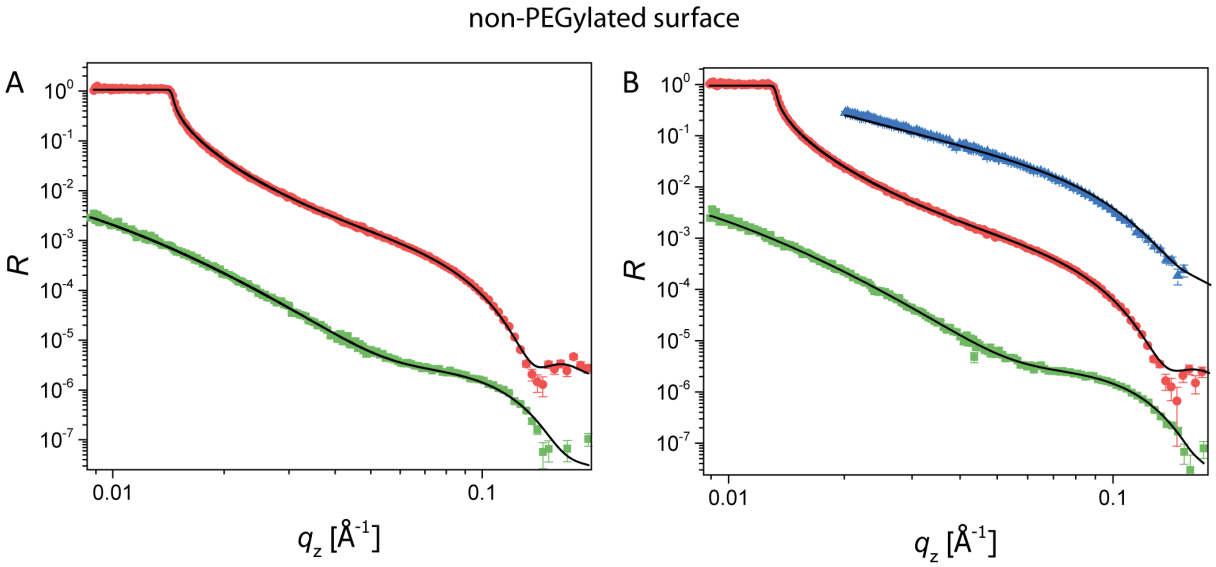

Figure S1: Set of reflectivity curves for non-PEGylated surfaces in various water contrasts. The solid lines indicate the simulated reflectivities corresponding to the best-matching model. (A) Reflectivity curves prior to contact with diluted serum in D_2O (top) and H_2O (bottom). (B) Reflectivity curves during contact with diluted serum in D_2O (middle), SMW (top), and H_2O (bottom). The curves are vertically shifted for clarity.

2.) Non-PEGylated surfaces in contact with dilute serum without rinsing

The reflectivity curves (Fig. S1) measured during exposure to diluted serum in three contrasts are again well reproduced with a model incorporating a single, narrow protein distribution in the headgroup region. The volume fraction profiles of proteins adsorbed to the non-PEGylated surface in presence of diluted serum (Fig. S2) are qualitatively similar to those obtained upon incubation in whole serum and subsequent rinsing.

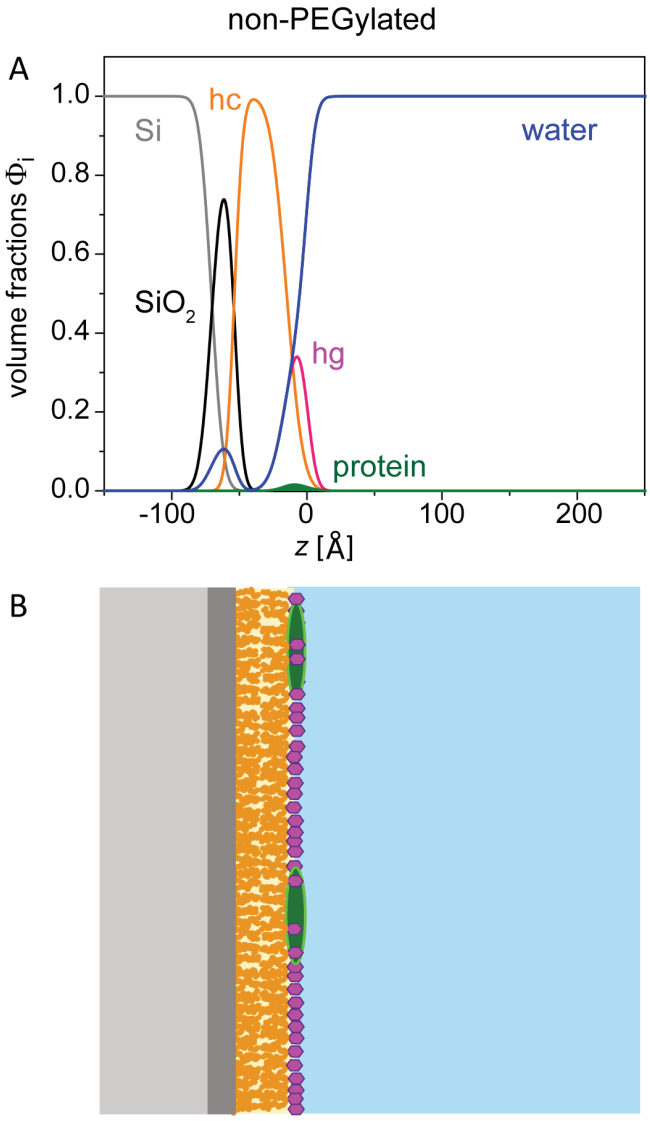

Figure S2: (A) The volume fraction profiles $\Phi(z)$ of all chemical components (Si, SiO_2, hydrocarbon chains, headgroups, PEG, protein, and water) for non-PEGylated surfaces during incubation with diluted human blood serum. The protein volume fraction distribution is unimodal. (B) Schematic illustration of the structures of non-PEGylated surfaces during incubation with dilute human blood serum, as suggested by the volume fraction profiles in panel B.

3.) PEGylated surfaces in contact with diluted serum without rinsing

Fig. S3 shows reflectivity curves in three contrasts of a PEGylated surface before and during exposure to 10 x diluted human serum together with the simulated reflectivities corresponding to the best-matching model allowing for simultaneous primary and ternary adsorption.

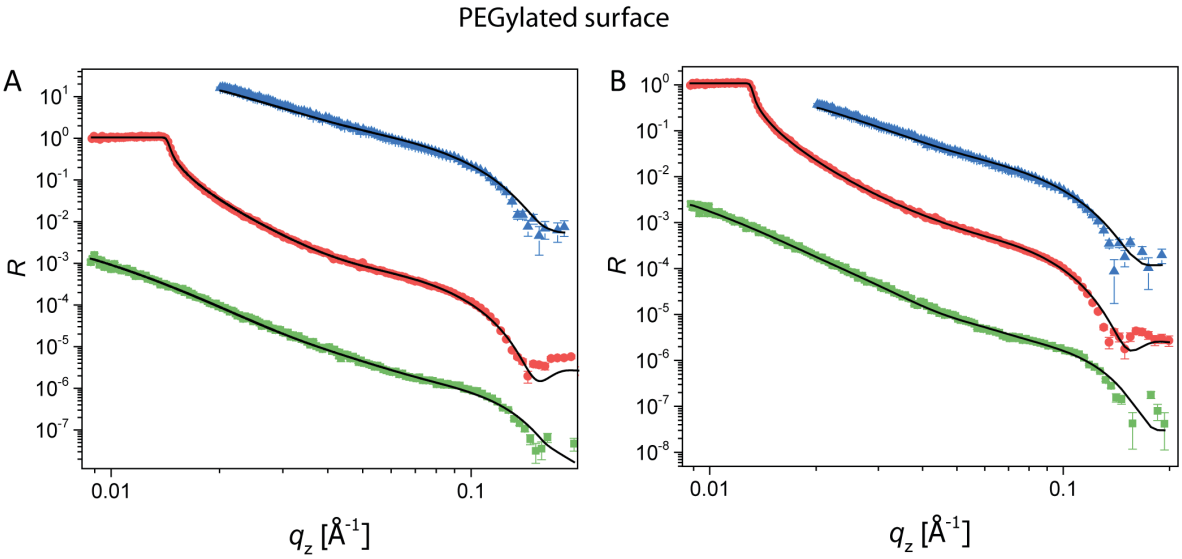

Figure S3: Set of reflectivity curves for a PEGylated surface in various water contrasts. The solid lines indicate the simulated reflectivities corresponding to the best-matching model. (A) Reflectivity curves prior to contact with 10 x diluted human serum in D_2O (middle), SMW (top), and H_2O (bottom). (B) Reflectivity curves during contact with dilute serum in D_2O (middle), SMW (top), and H_2O (bottom).

4.) Pressure/area isotherm of a DSPC/PEG-lipid mixture

Fig. S4 shows the influence of 10 mol% (f = 0.1) PEG-lipid on the pressure/area isotherm of DSPC at the air/water interface at room temperature. It is seen that the presence of the PEG chains leads to significant lateral repulsion between the molecules. Only at the lowest areas per lipid the steric repulsion between the hydrocarbon chains becomes dominant and the two curves converge again.

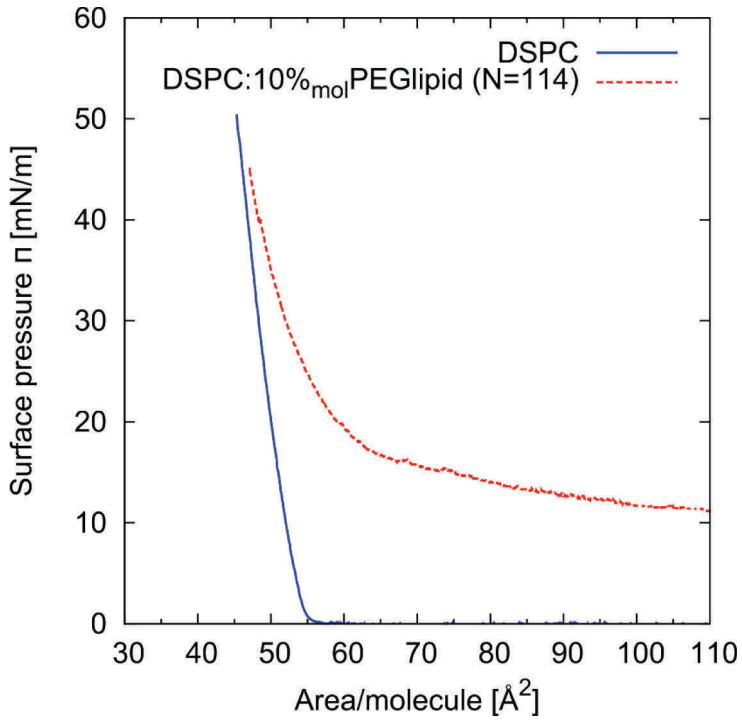

Figure S4: Pressure/area isotherms of DSPC with and without 10 mol% (f = 0.1) PEG-lipid at the air/water interface at room temperature.

5.) Comparison of various adsorption scenarios

Fig. S5 shows a comparison of various protein adsorption scenarios to phospholipid surfaces, differing only in the protein layer position with respect to the headgroup layer but not in the adsorbed amount. It is clearly seen that only the scenario in which the protein layer fully overlaps with the headgroup layer (see panel B) reproduces the experimental reflectivity data (see panel A) obtained after incubation with whole serum and subsequent rinsing.

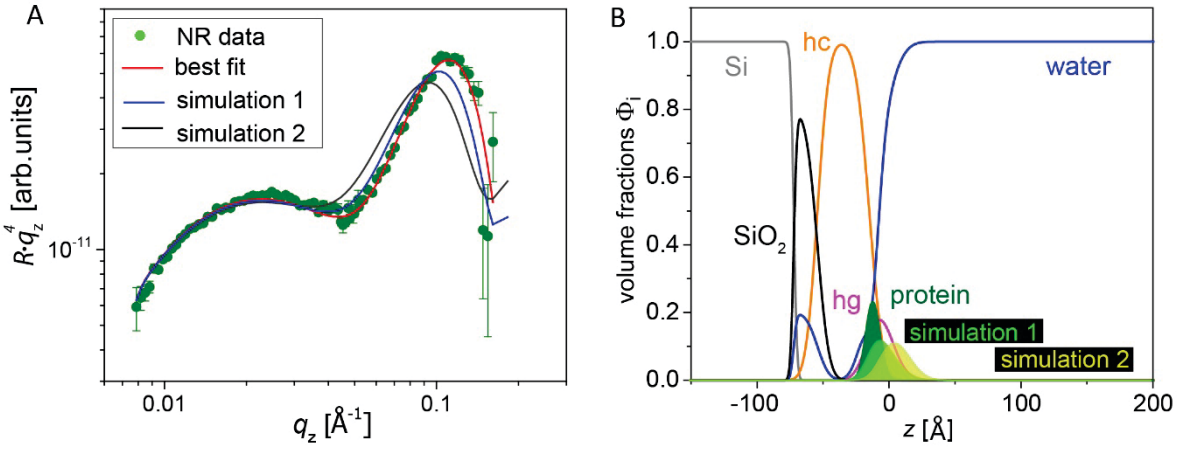

Figure S5: (A) Experimental reflectivity data (symbols) obtained after incubation of a non-PEGylated phospholipid surface with whole serum and subsequent rinsing. The solid lines represent the best-matching model and two alternative scenarios (simulations 1 and 2). (B) Volume fraction profiles according to the best-matching model together with two alternative scenarios of the protein profiles (simulations 1 and 2).

6.) Complete sets of reflectivity curves and fits obtained with non-PEGylated and PEGylated surfaces before and after incubation with whole serum and subsequent rinsing

Fig. S6 shows reflectivity curves in D_2O, 4MW, SMW, and H_2O contrasts of non-PEGylated and PEGylated surfaces before and after incubation with whole serum and subsequent rinsing, together with the simulated reflectivities corresponding to the best-matching models.

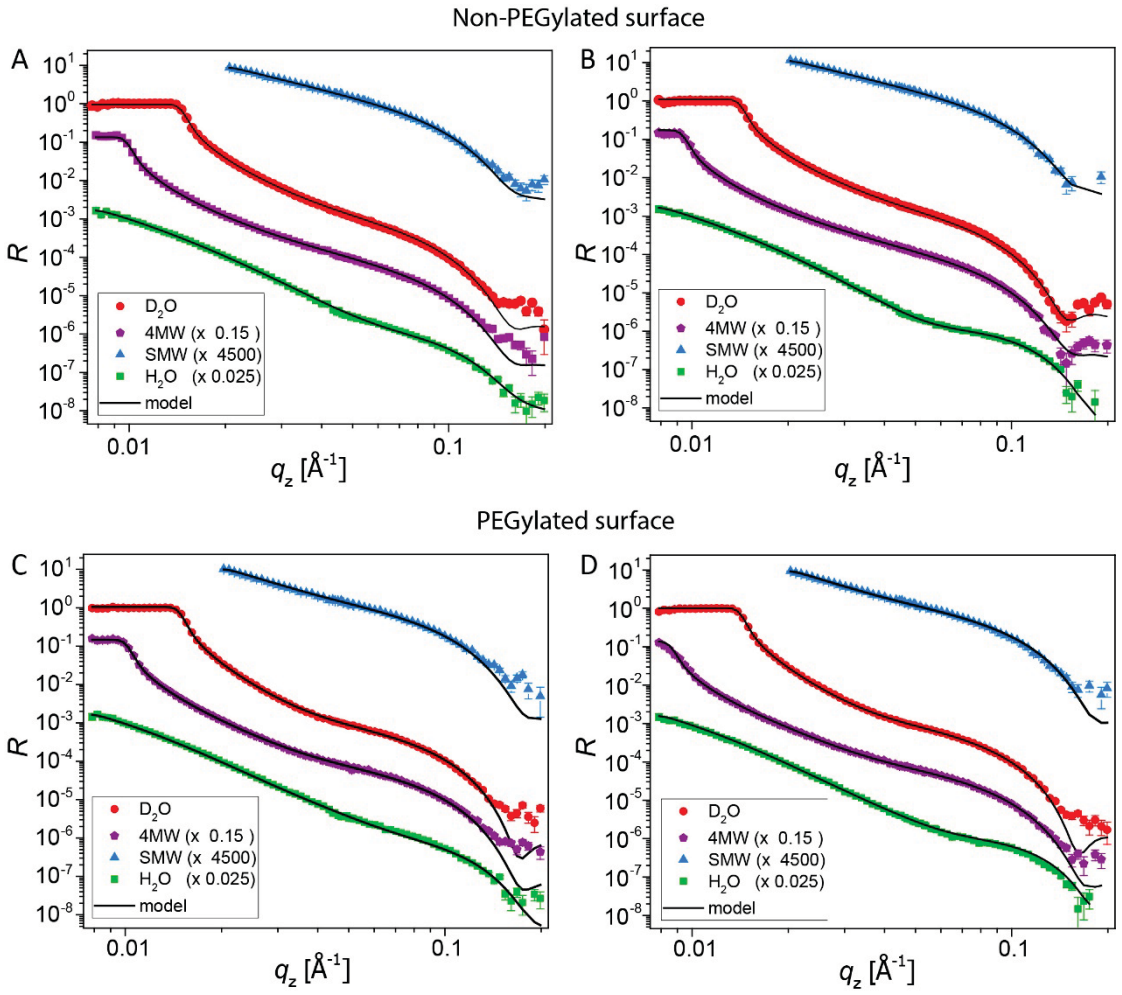

Figure S6: Reflectivity curves of non-PEGylated (top) and PEGylated (bottom) surfaces in D_2O, 4MW, SMW, and H_2O contrasts before (left) and after (right) incubation with whole serum and subsequent rinsing. The solid lines indicate the simulated reflectivities corresponding to the best-matching model.

7.) Influence of the enhanced statistical weighting of the H_2O contrast

Fig. S7 shows reflectivity curves in D_2O, SMW, and H_2O contrasts of a PEGylated surface before and during incubation with 10x diluted serum, together with the simulated reflectivities corresponding to the best-matching model obtained in reflectivity fits without enhanced H_2O weighting. Fig. S8 shows the corresponding volume fraction profiles. It is seen that the resulting profiles are largely consistent with those obtained with enhanced H_2O weighting (see main article).

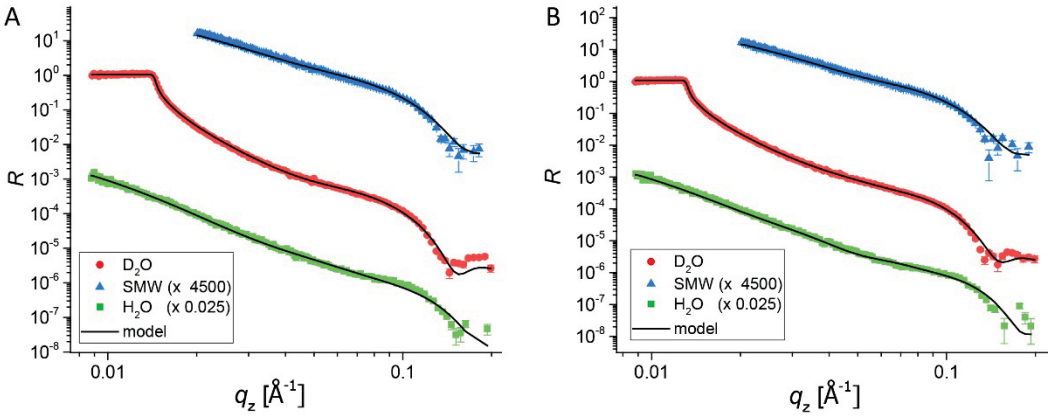

Figure S7: (A) Experimental reflectivity curves in various water contrasts (symbols) of a PEGylated surface before (left) and during (right) incubation with 10x diluted serum. The solid lines represent the best-matching model obtained in reflectivity fits without enhanced H_2O weighting.

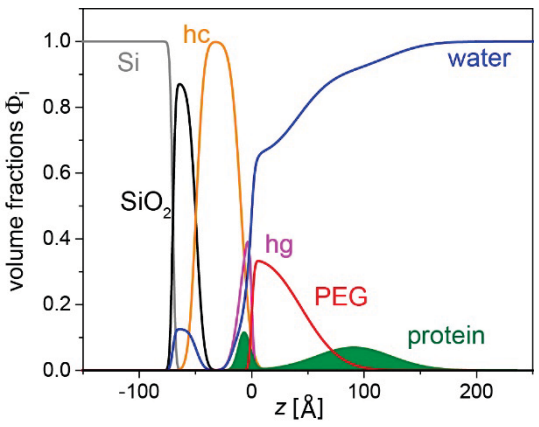

Figure S8: Volume fraction profiles of a PEGylated surface during incubation with 10x diluted serum deduced from a reflectivity fit without enhanced H_2O weighting.

8.) Comparison of models excluding and including ternary adsorption

Fig. S9 (right) shows reflectivity data obtained with a PEGylated surface during incubation with 10 times diluted serum in H_2O contrast. The data are smoothed using 5-point adjacent averaging. The solid lines indicate the simulated reflectivity curves according to the best-matching models excluding and including ternary adsorption. The comparison conveys the better match of the model including ternary adsorption, as it better captures the q_z-scaling of the intensity in the relevant q_z-range between low and intermediate q_z. Fig. S9 (left) shows the corresponding SLD profiles.

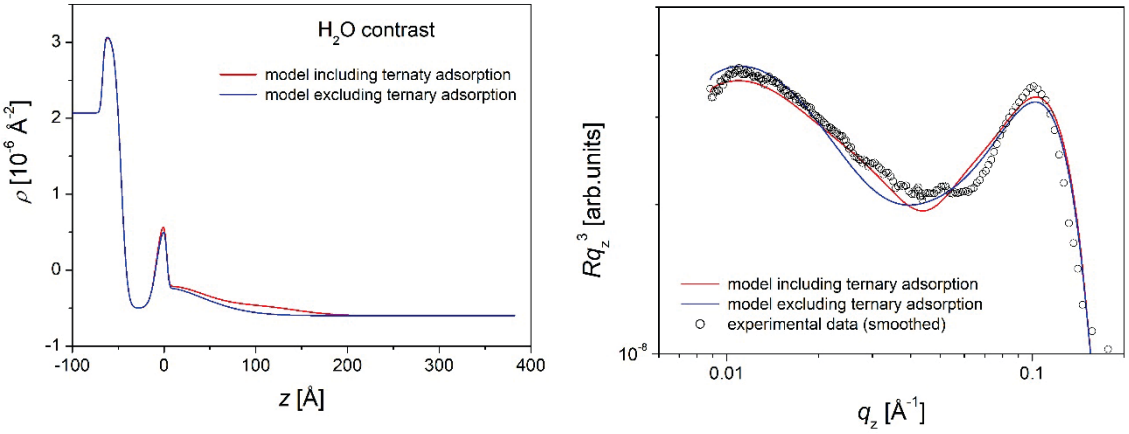

Figure S9: (left) SLD profiles in H_2O contrast according to the best-matching models excluding and including ternary adsorption. (right) Reflectivity data obtained with a PEGylated surface during incubation with 10x diluted serum in H_2O contrast. The data are smoothed using 5-point adjacent averaging. The solid lines indicate the simulated reflectivity curves according to the best-matching models excluding and including ternary adsorption.

References

1. Schneck, E.; Berts, I.; Halperin, A.; Daillant, J.; Fragneto, G. Neutron reflectometry from poly (ethylene-glycol) brushes binding anti-PEG antibodies: Evidence of ternary adsorption. *Biomaterials* **2015,** *46*, 95-104.

Manuscript III

Membrane adhesion via glycolipids occurs for abundant saccharide chemistries

Latza V. M., Demé B., Schneck E.

Membrane adhesion via glycolipids occurs for abundant saccharide chemistries

V. M. Latza, B. Demé, and E. Schneck

Keywords:
biological membranes, glycolipids, SAXS, WAXS, neutron diffraction, off-specular scattering

Running head: "Membrane adhesion via glycolipids"

Abstract: Membrane-bound oligosaccharides with specific chemistries are known to promote tight adhesion between adjacent membranes via the formation of weak saccharide bonds. However, in the literature one can find scattered evidence that other, more abundant saccharide chemistries exhibit similar behavior. Here, the influence of various glycolipids on the interaction between adjacent membranes is systematically investigated with the help of small- and wide-angle x-ray scattering (SAXS/WAXS) and complementary neutron diffraction (ND) experiments. Added electrostatic repulsion between the membrane surfaces is used to identify the formation of saccharide bonds and to challenge their stability against tensile stress. Some of the saccharide headgroup types investigated are able to bind adjacent membranes together, but this ability has no significant influence on the membrane bending rigidity. Our results indicate that glycolipid-mediated membrane adhesion is a highly abundant phenomenon and therefore potentially of great biological relevance.

Statement of Significance: Biological membranes can contain considerable amounts of glycolipids. However, surprisingly little is known about the influence of glycolipids on the interaction between neighboring membranes, apart from few special cases. Here, we find that various glycolipids with abundant types of saccharide headgroups are able to induce tight membrane adhesion even against repulsive forces, a phenomenon presumably playing important roles in cell biology.

1. Introduction

Biomembranes are vital components of all living organisms. They form the boundaries between the various compartments of cells and act as platforms for essential biochemical processes. But biomembranes do not only act alone, their functions being dependent on interactions with other membranes in their physiological environment. Membrane surfaces are formed by the headgroups of lipids and by membrane-bound saccharides, polypeptides, and other biomacromolecules (1). The interaction between membranes in their congested physiological surroundings is sensitive to this composition and affects structural organization and function of membrane systems like organelles, as well as membrane adhesion, vesicle release, or the formation of lamellar structures (2). Strikingly,

naturally stacked membrane systems like myelin sheaths (3) or photosynthetic membranes (thylakoids) in plants (4) contain high fractions of glycolipids. This correlation points towards a significant role of glycolipids in membrane adhesion. Indeed, early in-vitro experiments with thylakoid lipid extracts (5) and glycolipids with a di-galactose headgroup (*DGDG*) revealed spontaneous vesicle aggregation and membrane stack formation (6). Later on, the so-called hydration repulsion, i.e., the dehydrating pressure required to bring adjacent membranes to close proximity, was found to decay much more rapidly with the membrane separation for glycolipids (7, 8) than for commonly studied phospholipids with phosphatidylcholine (PC) headgroups (9). These results are in agreement with an earlier study by Marra, who found that the adhesion energies between glycolipid bilayers are up to six times higher than for PC lipid bilayers (10, 11). In contrast, Ricoul et al. reported that the addition of an uncharged glycolipid with a lactose headgroup appears to enhance the short-range repulsion between cationic surfactant lamellae (12). Wood et al. (13) investigated the interaction between PC lipid surfaces loaded with negatively charged glycolipids (sialo-gangliosides). Their results suggested repulsive saccharide interactions but favorable interactions between the saccharides and PC. Recently, Kanduč et al. quantitatively reproduced the interaction characteristics of glycolipid and PC lipid membranes in solvent-explicit atomistic molecular dynamics simulations (14). The study revealed that the repulsion mechanisms responsible for the comparatively longer hydration repulsion range of PC lipid membranes are inoperative for the glycolipid membranes. On the basis of an interplay between long-range van der Waals attraction and hydration repulsion (15, 16), the adhesion energy for the glycolipid was thus estimated to be enhanced by a factor of approximately six with respect to PC lipids (14), in excellent agreement with the results of Marra (10, 11). Within this picture, the tight cohesion between glycolipid membranes is rationalized solely on the basis of a shorter-ranged hydration repulsion. In other words, it does not explicitly invoke attraction between the saccharide groups belonging to the opposing membrane surfaces. Other studies have, however, demonstrated that already small fractions of glycolipids can induce pronounced cohesion between lipid membranes. For example, attractive forces were measured between lipid vesicles displaying low surface densities of membrane-bound *LewisX* (17), a trisaccharide motif known to be involved in cell adhesion processes during embryonic development (18). Later on, neutron diffraction (ND) on membrane multilayers showed that *LewisX* lipids effectively crosslink adjacent membranes via favorable carbohydrate-carbohydrate interactions (in the following termed “saccharide bonds”) even against repulsive membrane interactions (19). It was found that *LewisX* lipids lead to a strong confinement of the membrane separation around a value dictated by the lipids’ saccharide headgroups. However, in the literature one also finds indication that not only the specific trisaccharide motif *LewisX*, but also other motifs are able to crosslink membranes. Surprisingly strong attractive interactions were observed, for instance, for PC lipid membranes containing a glycolipid with a lactose disaccharide headgroup (N-hexadecanoyl-lactosylceramide, *LacCer-sat*) at ≈ 10 mol% (20). This finding is consistent with the observation that membrane-bound lactose has a similar effect on membrane adhesion as membrane-bound *LewisX* (17).

Here, we investigate how generic the phenomenon of membrane-crosslinking by glycolipids is, i.e., to what extent it really depends on the chemical details of the saccharide headgroups. For this purpose, we study the interaction of stacked phospholipid membranes (Fig. 1A) containing defined mole fractions of commercially-available glycolipids with various types of uncharged saccharide headgroups. The headgroups feature a systematic increase in their length from mono- to tetrasaccharides (see Fig. 1B) and comprise abundant monosaccharides (such as glucose and

galactose) as their building blocks. Moreover, the glycolipid types investigated somewhat reflect the abundance and biological relevance of glycolipids in various organisms: mono- and digalactosyl-diglyceride (*MGDG* and *DGDG,* comprising one or two galactose units, respectively) are the main constituents of the thylakoid membranes of chloroplasts (4). Psychosine (*Psyc*) also comprises a single galactose unit. This glycosphingolipid is a derivative of galctocerebroside and abundant in the central nervous system of vertebrates (3). Lactosylceramide (*Lac*) with a lactose headgroup is attributed to plentiful important functional roles in living cells, e.g. mediating the signal transduction pathway that leads to vascular endothelial cell proliferation (21-23). Ceramide-trihexoside (*Trihexo*) with a (galactose)-(galactose)-(glucose) headgroup is a glycosphingolipid involved in cellular signaling in mammals, where it acts as binding receptor for various toxins (24). Finally, ganglio-tetraosylceramide (*TetraG*) belongs to the asialo-gangliosides, a group of neutral glycosphingolipids and is known to be a receptor for certain bacteria and toxins (25). Its saccharide headgroup is composed of (galactose)-(N-acetyl-galactose)-(galactose)-(glucose) (26). Regarding the hydrocarbon chains of the investigated glycolipids, we generally distinguish between predominantly saturated chains and predominantly unsaturated chains, indicated in the following and in Fig. 1B with the suffices "*sat*" and "*unsat*", respectively. The influence of the glycolipids on the interaction between adjacent membranes is quantified with the help of small- and wide angle x-ray scattering (SAXS/WAXS), which yields the lamellar period of the multilayers. In order to test the stability the saccharide bonds against tensile stress, the membranes are further loaded with defined mole fractions of charged phospholipids inducing controlled electrostatic repulsion between the membrane surfaces. We find that some of the saccharide headgroup types investigated are able to bind adjacent membranes together. For monosaccharides, no such crosslinking is observed, likely because they are too small to protrude from the headgroup layer of the matrix lipids. Overall, our results indicate that glycolipid-mediated membrane adhesion is a highly abundant phenomenon, which is therefore potentially of great biological relevance.

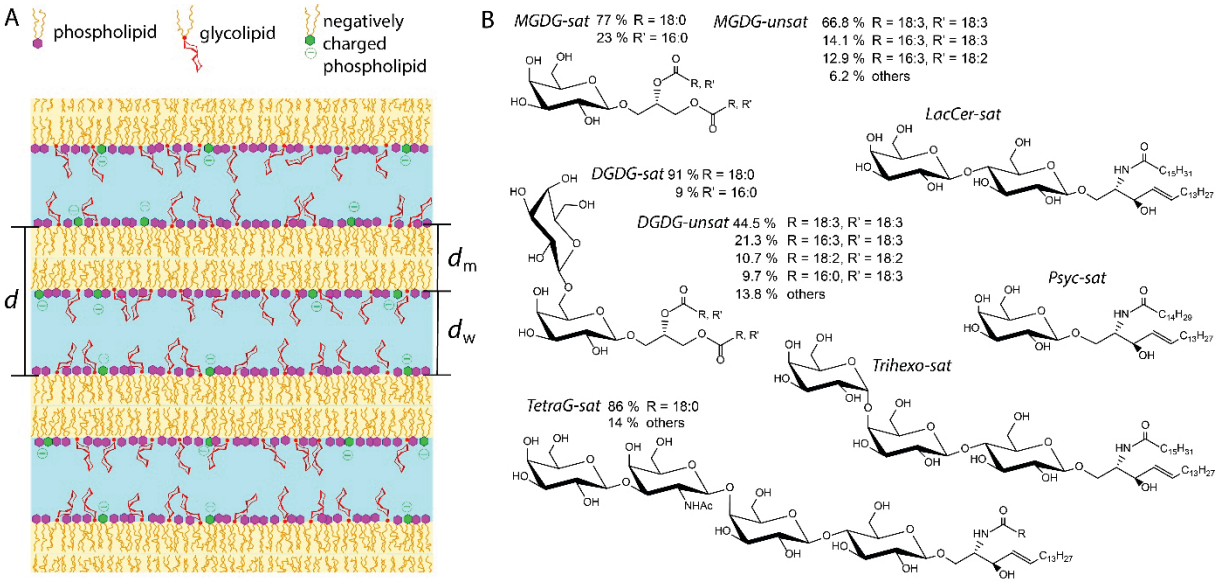

Figure 1: (A) Schematic illustration of phosphatidylcholine lipid membrane multilayers incorporating glycolipids and negatively charged phospholipids at various molar fractions. (B) Chemical structures of the glycolipids investigated: *LacCer-sat*, *MGDG-sat*, *MGDG-unsat*, *Psyc-sat*, *DGDG-sat*, *DGDG-unsat*, *Trihexo-sat*, and *TetraG-sat*.

2. Materials and methods

2.1. Chemicals

Unless stated otherwise the utilized chemicals were purchased from Sigma-Aldrich (St. Luis, MO, USA) and used without further purification. Ultrapure water was used for all purposes (MilliQ®-grade). The phospholipids 1,2-Dimyristoyl-*sn*-glycero-3-phosphocholine (DMPC), 1,2-Dipalmitoyl-*sn*-glycero-3-phosphocholine (DPPC), 1-Palmitoyl-2-oleoyl-*sn*-glycero-3-phosphocholine (POPC), 1,2-Dimyristoyl-*sn*-glycero-3-phospho-(1'-rac-glycerol) (Sodium Salt) (DMPG), 1,2-Dipalmitoyl-*sn*-glycero-3-phospho-(1'-rac-glycerol) (Sodium Salt) (DPPG), 1-Palmitoyl-2-oleoyl-*sn*-glycero-3-phospho-L-serine (Sodium Salt) (POPS) and the glycolipids Digalactosyl-diacylglycerol unsaturated (*DGDG-unsat*) and Monogalactosyl-diacylglycerol unsaturated (*MGDG-unsat*) were purchased from Avanti Polar Lipids (Alabaster, USA). The glycolipids Digalactosyl-diacylglycerol saturated (*DGDG-sat*), Monogalactosyl-diacylglycerol saturated (*MGDG-sat*), N-Pentadecanoyl-psychosine (*Psyc-sat*), N-Hexadecanoyl-lactosyl-ceramide (*LacCer-sat*), N-Hexadecanoyl-ceramide-trihexoside (*Trihexo-sat*), and Gangliotetraosyl-ceramide (*TetraG-sat*) were purchased from Matreya LLC. (State College, PA, USA). The chain-melting temperatures of the phospholipids used as matrix are summarized in Table 1.

Table 1: Phase transition temperatures of the phospholipids used in this study(27)

phospholipid	transition temperature (°C)
POPC	-2
POPS	14
DMPC	24
DMPG	23
DPPC	41
DPPG	41

2.2. Sample preparation

Before use, glassware was cleaned by 30 min immersion in chloroform, acetone, ethanol, water, and again ethanol, and finally dried with a stream of nitrogen or argon. Aqueous buffers (based on H_2O or D_2O) contained 100 mM NaCl and 5 mM HEPES and were adjusted to pH 7 by addition of 1 mM NaOH solution. Organic lipid solutions were prepared by weighing the lipid powder and adding solvent, resulting in a lipid concentration of 2 mg/mL. Phospholipids were dissolved in chloroform and glycolipids in chloroform/methanol mixtures (4:1 or 2:1 v/v). Mixed lipid solutions were prepared by mixing defined volumes of the respective single-component lipid solutions. The mixtures were then dried in their original glass containers with a nitrogen stream for at least 3 h and subsequently exposed to vacuum overnight. To prepare suspensions of multilamellar lipid aggregates, aqueous buffer was added to the dry lipid mixtures. The suspensions were then first bath sonicated for 7 min, heated to ≈ 50 °C for 1 h, and then stored at 5 °C. Before the transfer into the measurement capillaries for SAXS/WAXS, the samples were again bath sonicated for 15 min. Each capillary was filled with 100 μL suspension and stored at 5 °C overnight. For the preparation of solid-supported membrane multilayers, silicon wafers (size: 25 mm x 65 mm) were cleaned with the same protocol as the glassware. Shortly before deposition of the sample solution, the wafers were treated in an UV-ozone chamber for 20 min, in order to activate the surface. A 0.5 mL volume of a 2 mg/mL lipid organic solution was placed on the polished side of the chip on a petri dish. In order to generate a

homogenous multilayer covering most of the wafer surface, the petri dish was then manually rocked until all solvent was evaporated. The samples were then exposed to vacuum overnight to remove residual solvent and subsequently incubated for 3 h at 50 °C and high D_2O humidity ($h_{rel} \gtrsim 87$ % (28), achieved by addition of 40 μL of a 1 M $BaCl_2$-solution in D_2O to the bottom of the falcon tubes) for further annealing of the lamellar structures. Afterwards, they were stored in dry falcon tubes at 5 °C.

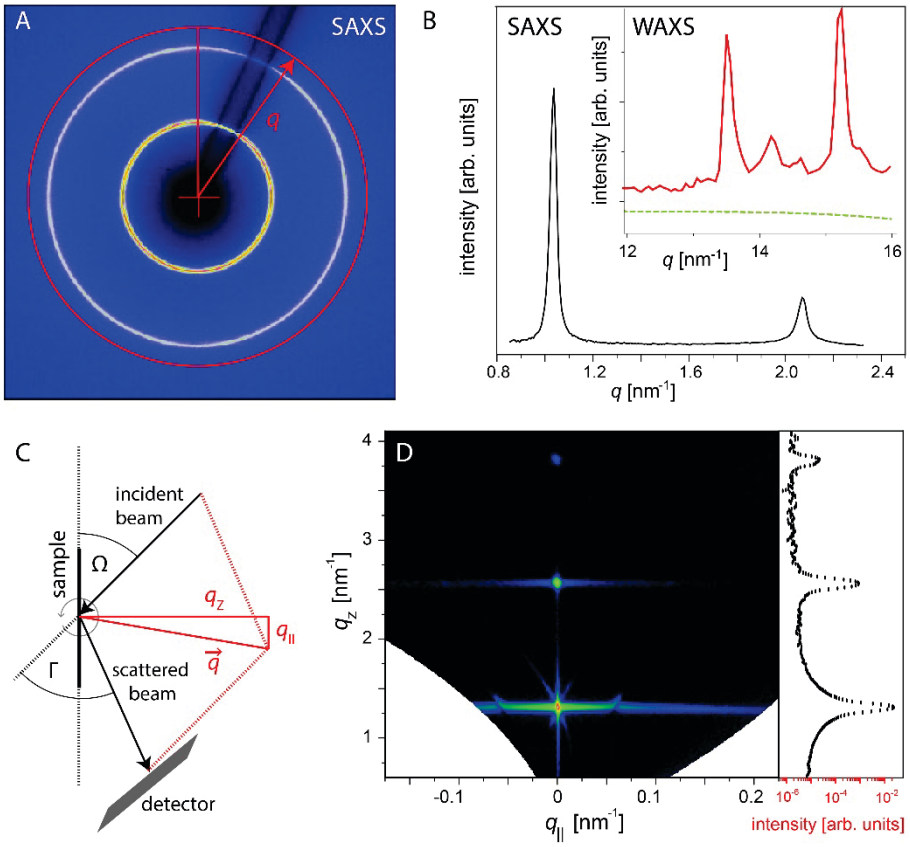

Figure 2: Small-angle x-ray scattering (SAXS) and neutron diffraction (ND) experiments (A) Representative 2D SAXS pattern featuring first and second order Bragg peaks in the form of concentric rings. (B) Radial plot of the integration in azimuthal direction of SAXS pattern with first and second order Bragg peaks. Inset: Wide-angle (WAXS) region exhibiting peaks only for exceptional samples in the chain-ordered $L_{\beta'}$-phase (here: *Psyc-sat* $f_{gly} = 1.0$ in DMPC; 50 °C; solid red curve). For typical samples in the fluid L_{α}-phase (here: *LacCer-sat* $f_{gly} = 0.1$ in DMPC; 50 °C; dashed green curve) no WAXS peaks are observed. (C) Schematic illustration of the experimental geometry for ND in top view. (D) Typical ND reciprocal space map, $S(q_z, q_{||})$, featuring three Bragg sheet orders (here: *DGDG-sat* $f_{gly} = 0.5$ in DMPC; 50 °C, $h_{rel} = 95$ %). Plot on the right: Specular intensity ($q_{||} \approx 0$) as a function of q_z.

2.3 Small angle and wide angle x-ray scattering (SAXS and WAXS)

Combined SAXS and WAXS measurements were performed at the µSpot beamline (29) at Synchrotron Bessy II (Helmholtz-Zentrum Berlin, Germany) with a beam energy of 15 keV corresponding to a wavelength of $\lambda = 0.0826$ nm. The beam was collimated with a set of pinholes with diameters of 100 µm and 150 µm, respectively. The x-ray scattering patterns were recorded with a position sensitive 2D-detector, either MarMosaic 225 (Rayonix Inc., Evanston, USA) or

Eiger X 9M (Dectris Ltd., Baden-Daetwil, Switzerland). The sample-to-detector distance was 480 mm. Measurements were conducted above the matrix lipid phase transition temperature (Table 1), either at 21 °C (for samples based on POPC) or 50 °C (for samples based on DMPC or DPPC). For this purpose, a home-made capillary holder with temperature control was used. The 2D scattering patterns obtained with the isotropically oriented multilamellar membrane aggregates (see Fig. 2A for an example) are radially symmetrical to good approximation (powder limit), and were thus integrated in azimuthal direction in order to obtain one-dimensional intensity profiles as a function of the magnitude q of the scattering vector (radial plot), $q = (4\pi/\lambda)\sin(\Gamma/2)$, associated with the scattering angle Γ. This procedure was performed with the software DPDAK (30), which also provides a precise q-axis calibration based on silver behenate ($CH_3(CH_2)_{20}COOAg$) as calibration standard. The intensity profiles $I(q)$ exhibit a number of Bragg peaks in the small angle range (see Fig. 2B), whose q-positions are related to the lamellar period d of the membrane multilayers according to Bragg's law, $q_{peak} = 2\pi n/d$, where n (= 1, 2, …) is the diffraction order. The precise peak positions were determined via Gaussian fits including an adjustable flat background. As shown in the inset of Fig. 2B, additional peaks in the wide angle region (at $q \approx 15$ nm^{-1}) occur for membranes in the chain-ordered $L_{\beta'}$-phase (31). Conversely, the absence of these peaks in most of the measurements confirms that the membranes investigated are in the fluid L_α-phase.

2.4 Neutron diffraction

Neutron diffraction (ND) measurements with solid-supported membrane multilayers were performed on the high-resolution diffractometer D16 at Institut Laue-Langevin (ILL, Grenoble, France). Figure 2C shows the geometry of the experiment in a view from the top. The incident beam with a wavelength of λ = 0.4518 nm hits the sample plane with an adjustable angle of incidence Ω, and is scattered into various directions at angles Γ with respect to the incident beam. For each Ω, the Γ-dependent intensity is recorded with a position-sensitive ^{3}He detector (MILAND) with a distance of 950 mm to the sample. By rotating the sample stage, and thus by stepwise variation of Ω, 2-dimensional maps of the intensity as a function of Γ and Ω are recorded. During this procedure, the intensity is normalized to the intensity of the incident beam (via an in-beam monitor), the detector channel sensitivity, and the illuminated sample area. Further details of the ND measurements are reported elsewhere (19). The angles Γ and Ω are associated with the reciprocal space coordinates q_z and $q_{||}$, i.e., the scattering vector components perpendicular and parallel to the sample plane, respectively, according to the geometrical relations $q_z = (2\pi/\lambda)[\sin(\Gamma - \Omega) + \sin(\Omega)]$ and $q_{||} = (2\pi/\lambda)[\cos(\Gamma - \Omega) - \cos(\Omega)]$, see Fig 2C. The main panel of Fig. 2D shows a typical reciprocal space map, i.e., a map of the intensity as a function of q_z and $q_{||}$, termed $S(q_z, q_{||})$ in the following. It features the characteristic horizontal "Bragg sheets" of planar membrane multilayers (32). While the scattering intensity along the specular line ($\Gamma = 2\Omega$, $q_{||} = 0$, see Fig. 2D right) contains information on the structure perpendicular to the surface (notably the lamellar periodicity as encoded in the Bragg peak positions and the scattering length density profile as encoded in the peak intensities), the diffuse scattering intensity ($\Gamma \neq 2\Omega$, $q_{||} \neq 0$) along the Bragg sheets additionally contains information on the in-plane structure, notably the membrane fluctuations in terms of their spatial self- and cross-correlation functions. Within the framework of a *Discrete Smectic Hamiltonian* of interacting multilayers, these correlation functions are in turn governed by the mechanical properties of the interacting membranes in terms of the membrane bending modulus κ and the inter-membrane

compression modulus *B* (33). As we have shown earlier, the experimentally obtained reciprocal space maps within this framework can be satisfactorily modeled solely based on the underlying mechanical parameters κ and *B*, and on an empirical cut-off parameter termed *R* (8, 19, 34). In practice, this procedure relies on the *kinematic approximation* (KA) of wave scattering, because application of the more accurate *distorted-wave Born approximation* (35) would require detailed additional knowledge of the sample structure, which is unavailable. As a consequence, our KA-based treatment, which is only valid wherever the intensity is weak compared to the incident beam, does not correctly capture the specular maximum of the first Bragg sheet, where this condition is typically violated. While in the past, we therefore ignored the first Bragg sheet and relied on the second one (8, 19, 34), we here combine information from the first two Bragg sheets (see Fig. 4): while the Caillé parameter

$$\eta = \pi k_B T / \left(2d^2 \sqrt{\kappa B / d}\right) \quad (1)$$

is obtained from the specular/diffuse scattering intensity ratio in the second Bragg sheet, the de Gennes parameter

$$\Lambda = \sqrt{\kappa / (Bd)} \quad (2)$$

is obtained from the decay of the off-specular intensity in the first Bragg sheet along $q_{||}$, excluding the specular intensity which violates the KA. The best-matching values of η, Λ, and *R* are then determined by their systematic variation in the model until the best agreement with the experimental data is achieved. Finally, the mechanical parameters are obtained by solving Eqs. 1 and 2 for κ and *B*.

ND measurements were conducted above the matrix lipid phase transition temperature (Table 1), either at 30 °C (for samples based on POPC) or 50 °C (for samples based on DMPC or DPPC). For measurements at controlled osmotic pressure, the beamline humidity chamber was used (36) providing simultaneous control of temperature and relative humidity (h_{rel}). The corresponding osmotic pressure is given as

$$\Pi = \frac{k_B T}{v_w} ln(h_{rel}), \quad (3)$$

where v_w = 0.03 nm^3 denotes the molecular volume of water and k_B is the Boltzmann constant. For measurements under bulk water conditions a “sandwich” cell, composed of two parallel chips was used (34). To achieve optimal scattering length density contrast, the samples were measured with D_2O vapor or in D_2O-based buffers.

3. Results and discussion

Fig. 1A schematically illustrates self-assembled multilayers of lipid membranes interacting in an aqueous environment. The membranes are composed of up to three lipid components with molar fractions *f*, where *f* = 1 corresponds to 100 mol%. Phosphatidylcholine (PC) lipids POPC, DMPC and DPPC are used as matrix with mole fraction $f_{PC} = 1 - f_{gly} - f_{neg}$ accommodating glycolipids (see Fig. 1B) with mole fraction $f_{gly} \in \{0, 0.1, 0.2, 0.5\}$ and negatively charged lipids (with phosphatidylserine (PS) or phosphatidylglycerol (PG) headgroups) with mole fraction $f_{neg} \in \{0, 0.01, 0.02, 0.05\}$. The negatively

charged lipids are introduced in order to exert defined repulsive electrostatic forces between neighboring membranes (see further below). For each glycolipid species the PC lipid and negatively charged lipid species were chosen to match the alkyl chain length of the glycolipid and the respective number and position of double bonds in the chain (see Table 2), in order to assure miscibility of all three lipid components.

Table 2: Investigated glycolipids together with the corresponding matrix lipids and negatively charged lipids (if applicable).

glycolipid	abbrev.	matrix lipid	neg. charged lipid
N-hexadecanoyl lactosyl-ceramide	*LacCer-sat*	DMPC	DMPG
N-Pentadecanoyl psychosine	*Psyc-sat*	DMPC	DMPG
Monogalactosyldiacylglycerol saturated	*MGDG-sat*	DMPC	DMPG
Monogalactosyldiacylglycerol unsaturated	*MGDG-unsat*	POPC	POPS
Digalactosyldiacylglycerol saturated	*DGDG-sat*	DMPC	DMPG
Digalactosyldiacylglycerol unsaturated	*DGDG-unsat*	POPC	POPS
N-hexadecanoyl-ceramide trishexoside	*Trihexo-sat*	DMPC	DMPG
Gangliotetraosyl-ceramide	*TetraG-sat*	DPPC	DPPG

The configuration illustrated in Fig. 1A equally applies to the multilayered membrane aggregates investigated by SAXS/WAXS and to the solid-supported aligned multilayers investigated by ND. The separation between the surfaces of neighboring membranes, i.e., the water layer thickness d_w, is encoded in the lamellar period d of the multilayers, according to $d = d_m + d_w$, where d_m denotes the membrane thickness.

The plots in Fig. 3 show d as a function of the glycolipid mole fraction for selected glycolipid types. The values of d are obtained from the q-positions of the Bragg peaks, as $d = 2n\pi/q_{peak}$, where n (= 1, 2, …) is the order of the peak (see Methods section). It should be noted that the lipid membranes are in the biologically relevant fluid L_α–phase, indicated by the absence of a chain-ordering peak in the WAXS region (31) (see Fig. 2B). When neglecting variations in the membrane thickness, a reduction in d upon addition of glycolipids indicates that the contribution of the glycolipids to the membrane interaction is attractive, while an increase indicates a repulsive contribution. Similarly, the observed increase in d upon addition of negatively charged lipids reflects their repulsive electrostatic contribution to the membrane interaction. For weakly charged surfaces in a monovalent electrolyte the pressure Π_{el} associated with the electrostatic repulsion is given as (37):

$$\Pi_{el}(d_w) \cong 2k_B T \rho_0 [\cosh(e\psi_m(d_w)/k_B T) - 1], \quad (4)$$

where ρ_0 is the number density of monovalent ions according to their bulk concentration of c_0 = 100 mM, e is the electron charge, and ψ_m is the electric potential at the midplane (i.e., the center of the water layer), which depends on the charge density of the surfaces (see SI) and is thus determined by f_{neg}. Note that the strength of the repulsion may be affected in general by charge regulation when the charged groups are protonable (38). The repulsion associated with the incorporation of negatively charged lipids is seen most prominently for interacting PC membranes without glycolipids (f_{gly} = 0, see Fig. 3), where d, and thus the membrane separation d_w, considerably

increases with increasing f_{neg}. The extent of this increase is governed by a subtle balance of interfacial forces acting between the membranes, namely van der Waals attraction on one side versus hydration repulsion (9, 39), undulation repulsion, and electrostatic repulsion on the other side (16). For DMPC bilayers with f_{neg} = 0.02 in 100 mM monovalent salt at d = 6.3 nm (see Fig. 3A), d_w = 2.8 nm (as follows from d_m = 3.5 nm (40)), and Eq. 4 yields $\Pi_{el} \approx 4 \cdot 10^3$ Pa, comparable to the hydration repulsion and the van der Waals attraction at the same separation, both on the order of $10^3 - 10^4$ Pa (41). It should be noted that when introducing charged lipids one strictly does not only introduce charge but may also induce other changes, albeit the former can be considered to be the dominant effect. Varying the electrostatic repulsion alternatively by variation of the salt concentration must be considered problematic because ions can influence the saccharide binding (42, 43) and lead to effective surface charges due to preferential interactions with PC lipids (19, 44) or glycolipids (45).

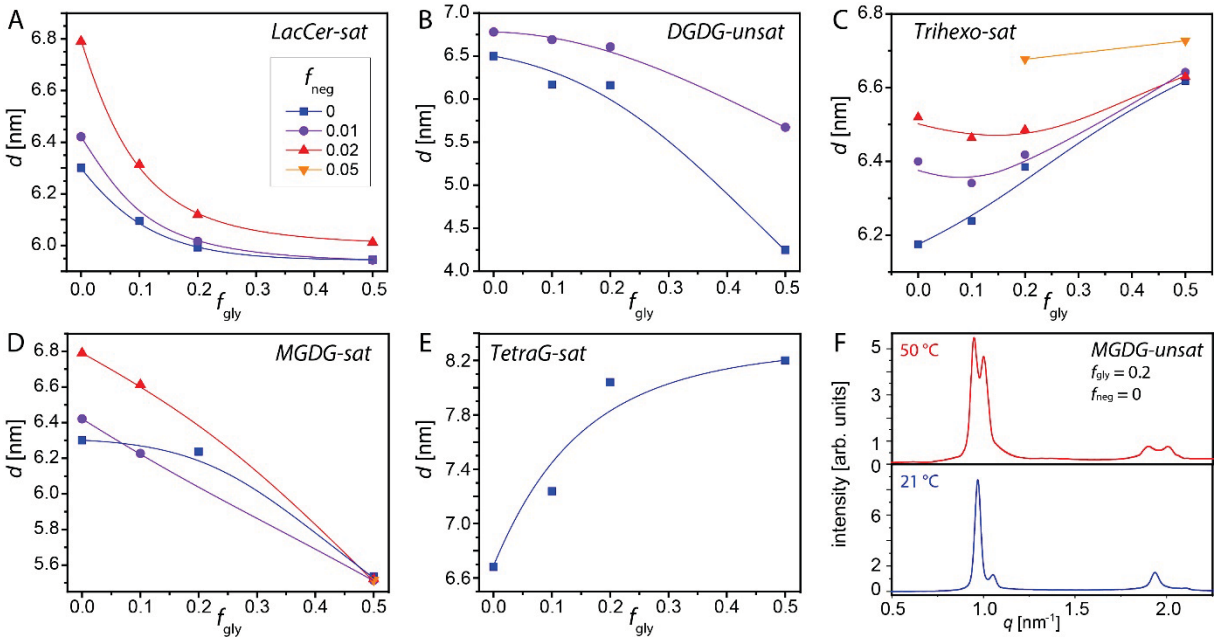

Figure 3: Lamellar periodicities d obtained by SAXS for of PC lipid membrane multilayers containing different fractions f_{gly} of glycolipids and f_{neg} of negatively charged lipids. (A) *LacCer-sat*, (B) *DGDG-unsat*, (C) *Trihexo-sat*, (D) *MGDG-sat*, and (E) *TetraG-sat.* Solid lines are guides to the eye. The measurements were conducted at 21 °C (B) or 50 °C (A, C, D, E). (F) Radial plots of the integration in azimuthal direction of the SAXS patterns of PC lipid membranes containing MGDG-unsat (f_{gly} = 0.2, f_{neg} = 0) at 21 °C (bottom) and 50 °C (top).

In the following, the influence of the glycolipid type and mole fraction on the interaction of PC lipid membranes is discussed. Fig. 3A shows $d(f_{gly})$ for DMPC membranes loaded with *LacCer-sat*, a glycolipid with a disaccharide headgroup (see Fig. 1B). In the absence of negatively-charged lipids (f_{neg} = 0), d assumes a value of ≈ 6.3 nm at f_{gly} = 0, in agreement with the literature (40). It decreases as a function of f_{gly} until it saturates at $d \approx$ 6.0 nm, a value that appears to be governed by this particular glycolipid. The f_{gly}-dependence of d is clearly non-linear: already low *LacCer-sat* fractions (f_{gly} = 0.1) lead to a considerable reduction in d, which suggests that the glycolipids are able to pull the membranes closer together. Even more strikingly, the impact of negatively-charged lipids (DMPG) on d diminishes systematically with increasing f_{gly}. While the pure phospholipid membranes

($f_{gly} = 0$) exhibit a response of as much as $\Delta d \approx 0.5$ nm to the incorporation of 2 mol% negatively-charged lipids ($f_{neg} = 0.02$), a much weaker response to the same level of electrostatic repulsion is observed when the membranes contain *LacCer-sat* ($\Delta d \approx 0.15$ nm at $f_{gly} = 0.2$; $\Delta d \approx 0.08$ nm at $f_{gly} = 0.5$). This result is very similar to what was reported earlier for the special *LewisX* trisaccharide motif (19) and clearly indicates that *LacCer-sat* glycolipids with disaccharide headgroups hold the membranes together, even against electrostatic repulsion. The remaining variability in *d* even under crosslinked conditions reflects that the lipid tails anchoring the saccharides into the bilayers are not entirely rigid but can be partially pulled out of the bilayers when subject to tensile forces. Moreover, the binding between two saccharides itself must be considered "diffuse", meaning that it can involve a number of different configurations with different "bond lengths" (46). In contrast, for a glycolipid with a different disaccharide headgroup (*DGDG-unsat.* incorporated in a POPC matrix, see Fig. 3B) there is no indication of such membrane crosslinking. Instead of observing a strong response of the periodicity already at low f_{gly}, followed by a saturation, pronounced changes only occur for high f_{gly} and without any indication of saturation. Moreover, the effect of negative charges remains pronounced even at high f_{gly}, in contrast to the case of LacCer-sat. The simplest explanation for this qualitatively different behavior is that the di-galactose headgroups of *DGDG-unsat* have a much weaker tendency to be engaged in homotypic inter-membrane "binding" than the lactose headgroups of *LacCer-sat*. Fig. 3C shows $d(f_{gly})$ for DMPC membranes loaded with *Trihexo-sat*, a glycolipid with a trisaccharide headgroup (see Fig. 1B). The overall behavior is similar to that of *LacCer-sat*, but the value at which *d* saturates for high f_{gly} ($d \approx 6.6$ nm), i.e., the membrane separation preferred by this saccharide headgroup, is larger than that of the pure PC membranes ($d \approx 6.2$ nm), which can be attributed to the bulkier trisaccharide headgroups. As in case of *LacCer-sat*, *d* becomes rather insensitive to electrostatic repulsion for sufficiently high glycolipid fractions. In fact, for $f_{gly} \geq 0.2$, the adjacent membranes are still stably crosslinked by *Trihexo-sat* even at comparatively high fractions of negatively-charged DMPG lipids ($f_{neg} = 0.05$), while for $f_{gly} \leq 0.1$ the multilamellar architecture is not stable against the considerable electrostatic repulsion and no lamellar periodicity can be specified. When comparing the chemistries of *LacCer-sat* and *Trihexo-sat* (which are both found to hold membranes together) with that of *DGDG-unsat* (which does not hold membranes together), one apparent difference is that the former two comprise a lactose motif, while the latter does not. This correlation may suggest that lactose strongly contributes to preferential interactions favoring homotypic saccharide contacts. In fact, lactose is much less water-soluble (≈ 19 g/dL) than other abundant disaccharides (47-49) like sucrose (≈ 200 g/dL), maltose (≈ 110 g/dL), or trehalose (≈ 70 g/dL), reflecting favorable lactose-lactose interactions in water, in line with the above hypothesis.

Coming back to Fig. 3, panel D shows $d(f_{gly})$ for DMPC membranes loaded with *MGDG-sat*, a glycolipid with a mono-galactose headgroup (see Fig. 1B). Independent of the fraction of negatively-charged lipids (DMPG), *d* decreases with increasing f_{gly} until it reaches a value of $d \approx 5.5$ nm at $f_{gly} = 0.5$. As in case of *DGDG-unsat*, the decrease is approximately linear with f_{gly} and does not exhibit any tendency of saturation. However, in contrast to *DGDG-unsat*, *d* for *MGDG-sat* is less sensitive to electrostatic repulsion for high f_{gly}. This may indicate that the mono-galactose headgroups of *MGDG-sat* in principle have the tendency to engage into homotypic membrane binding, but are sterically hindered for low f_{gly} because they are "buried" within the PC headgroup layer due to their compactness. This interpretation is corroborated by the observation that also other glycolipids with monosaccharide headgroups are unable to crosslink PC lipid membranes at low f_{gly} (for example *Psyc-sat*, see SI). Fig. 3E shows $d(f_{gly})$ for DPPC membranes loaded with *TetraG-sat*, a glycolipid with a linear

tetrasaccharide headgroup (see Fig. 1B). It is seen that d strongly increases with f_{gly}, first rapidly until it saturates at $d \approx 8.1$ nm. For these glycolipids with their comparatively bulky headgroups, steric repulsion appears to be dominating the membranes' equilibrium separation, while the influence of electrostatic repulsion via incorporation of negatively charged lipids ($f_{neg} \neq 0$) is insignificant (see Supporting Information). The f_{gly}-dependence of d is reminiscent of that of DPPC membranes loaded with *LewisX* lipids, whose headgroups are of similar bulkiness (19).

Finally, it should be noted that incorporation of glycolipids into PC lipid membranes can affect the lamellar periodicity d also in an indirect way, via their influence on the membrane thickness d_m (see Fig. 1A). This effect, which can be assumed to be approximately linear in f_{gly}, however, does not impede the conclusions drawn here, because it does not affect the response of d to electrostatic repulsion.

As exemplified in Fig. 3F for *MGDG-unsat* at $f_{gly} = 0.2$ and $f_{neg} = 0$, significant splitting of the SAXS Bragg peaks is observed in certain cases, indicating that phase separation into membrane multilayers with different lamellar periodicities occurs. This phase separation can be attributed to conflicting membrane separations preferred by the attraction-inducing membrane components (the glycolipids) and the more repulsive membrane components (the phospholipids). Interestingly, the separation is found predominantly for glycolipids with monosaccharide headgroups (*MGDG* and *Psyc*), which are unable to establish direct inter-bilayer-contacts under monophasic conditions, where they do not protrude from the headgroup layer of the PC lipid matrix (see above). This behavior is observed at low temperature (21 °C, Fig. 3F bottom) and high temperature (50 °C, Fig. 3F top). It is closely related to the results of earlier microscopy studies on solid-supported lipid membranes comprising lipopolymers inducing steric repulsion and biotin-lipids inducing strong binding via streptavidin, where the adhesion was found to be accompanied by lateral phase separation featuring domains of tight adhesion (50, 51). More recently, the adhesion of multicomponent membranes containing attraction-inducing and repulsion-inducing components was also studied theoretically (52). In that work it was shown that the segregation pattern depends on the strength of the repulsive component which opposes binding. In view of these experimental and theoretical reports we conclude that the observed phase separation constitutes additional evidence for the glycolipids' tendency to induce attraction between neighboring lipid membranes. Coming back to the SAXS data in Fig. 3F, the coexistence of two sets of Bragg peaks indicates that the different phases are aligned in registry in the multilayers. As proposed by Kollmitzer et al. (53), such behavior can result from the different strengths of hydration (14) and undulation forces in the glycolipid-rich and phospholipid-rich phases.

In order to explore to what extent the glycolipids' crosslinking abilities identified here by SAXS have their manifestation also with regard to the mechanical properties of interacting membranes, neutron diffraction (ND) on solid-supported membrane multilayers was carried out. In an earlier study (19) such measurements revealed a considerable influence of the density of *LewisX* lipids (see Section 1) on the inter-membrane compression modulus B (see Section 2.4), reflecting a rigidification through the formation of saccharide bonds. Fig. 4 shows the first two Bragg sheets recorded by ND with a system unable to form bonds (POPC membranes loaded with *DGDG-unsat* at $f_{gly} = 0.2$ and $f_{neg} = 0$, panel A) and with system able to form bonds (DMPC membranes loaded with *LacCer-sat* at $f_{gly} = 0.2$ and $f_{neg} = 0$, panel B). Plotted are the q_z-integrated Bragg sheet intensities [Footnote 1] as functions of $q_{||}$, featuring the respective central specular maxima symmetrically flanked by the slowly decaying diffuse scattering intensity. The latter is locally decorated with minima at conditions of high

absorption ($\Omega \approx 0$ and $\Omega \approx \Gamma$) and peaks arising from multiple scattering effects (19). Both data sets are from measurements at $h_{rel} = 95$ % (corresponding to a moderate dehydrating osmotic pressure of $\Pi \approx 8 \cdot 10^6$ Pa, see Eq. 3) and not from measurements under bulk water conditions, where the intensities of the second Bragg sheets were found to be too weak to be analyzed (see SI). Reason for these low intensities is a minimum in the membrane form factor, which essentially coincides with the position of second Bragg sheets due to near-identical thicknesses of the hydrogenous region (the alkyl chain layer) and the deuterated region (the hydrated headgroup layer). In fact, even under the slightly dehydrated conditions shown in Fig. 4, the information contained in the second Bragg sheets (primarily on the Caillé parameter, η) needed to be complemented with that of the first Bragg sheets (on the de Gennes parameter, Λ), as described in Section 2.4. The solid lines superimposed to the experimental data points represent simulated Bragg sheet intensities corresponding to the best-matching parameters η and Λ in the continuum-mechanical model simultaneously describing the first and second Bragg sheets. Absorption close to $\Omega \approx 0$ and $\Omega \approx \Gamma$ was modeled as described in the SI.

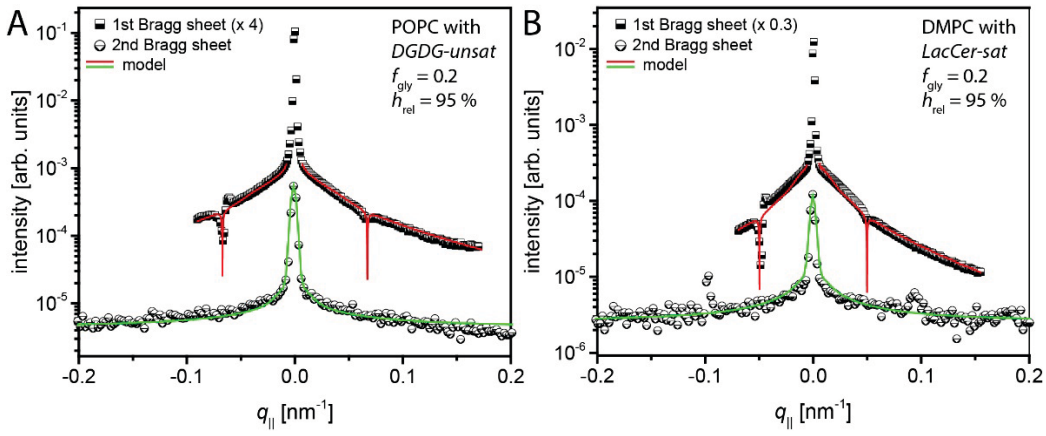

Figure 4: Intensities of the first and second Bragg sheets of (A) POPC membranes loaded with *DGDG-unsat* at $f_{gly} = 0.2$ and $f_{neg} = 0$ and (B) DMPC membranes loaded with *LacCer-sat* at $f_{gly} = 0.2$ and $f_{neg} = 0$, both at $h_{rel} = 95$ %. Solid lines: simulated intensities corresponding to the best-matching parameters η and Λ in the continuum-mechanical model (see main text).

The best-matching model parameters for both systems are summarized in Table 3, together with the mechanical parameters κ and B derived thereof according to Eqs. 1 and 2. For the membranes containing *DGDG-unsat* (unable to form saccharide bonds, see Fig. 3B) as well as for the membranes containing *LacCer-sat* (able to form saccharide bonds, see Fig. 3A) the obtained bending rigidities κ fall into the range of $\approx 10^{-19}$ J (or $\approx 25\ k_B T$), consistent with earlier reports on membranes in the fluid L_α phase (8, 19, 54, 55) and with the observation that κ is rather insensitive to the hydration level (8, 55). The similarity of the values obtained here with those reported earlier for glycolipid-free PC lipid membranes indicates that the saccharide headgroups at a lateral concentration of $f_{gly} = 0.2$ do not influence the bending rigidity much, in line with our earlier work on *LewisX* lipids (19). Moving on to the compression moduli B in Table 3 we notice that their values differ considerably between the two investigated membrane systems. Surprisingly, the value is higher for the system unable to form

saccharide bonds, in contrast to our earlier finding that *B* increases with increasing bond density, at least under bulk water conditions (19). This discrepancy suggests that under conditions of partial dehydration direct steric repulsion between the membrane surfaces rather than the bonds may be the dominant contribution to the compression modulus. Indeed, the moduli obtained here ($B \geq 3$ MPa) are much higher than those obtained previously under bulk water conditions (< 1 MPa) where the bonds were found to be the dominant contribution (19). Based on this notion we conclude that ND on membrane multilayers in general is a promising approach to quantify the effect of saccharide binding on membrane mechanical properties, in particular when information from two Bragg sheets is exploited as introduced here. However, the detailed analysis of mechanical parameters under bulk water conditions requires avoiding unfavorably-placed form factor minima. In the future this can be achieved by the use of chain deuterated (matrix) lipids in combination with light water (H_2O) or by the use of lipids with significantly longer or shorter tails.

Footnote 1: In practice, the integration is performed in Γ-direction (8, 19, 34).

Table 3: Best-matching parameters, as obtained by ND, of selected membrane multilayer systems containing glycolipids: Caillé parameter η; De Gennes parameter Λ; cut-off Radius *R* for the first two Bragg sheets (BS); membrane bending modulus κ; inter-membrane compression modulus *B* (see Methods Section for definitions).

Sample: *glycolipid*/phospholipid	h_{rel}	*T* [°C]	η	Λ [Å]	*R* [μm] for 1. BS/2. BS	κ [J]	κ [k_BT]	*B* [MPa]
DGDG-unsat/POPC, $f_{gly} = 0.2$; $f_{neg} = 0$	95 %	30	0.015	12	2.5 / 1.2	$1.1 \cdot 10^{-19}$	27	16
LacCer-sat/DMPC, $f_{gly} = 0.2$; $f_{neg} = 0$	95 %	50	0.029	25	1.1 / 1.1	$1.1 \cdot 10^{-19}$	25	3

4. Conclusions

With the help of x-ray and neutron scattering techniques we have studied the influence of various commercially-available glycolipids on the interaction between adjacent phospholipid bilayers, in order to test whether or not the glycolipids promote membrane adhesion via the formation of saccharide bonds. Some of the saccharide headgroup types investigated were found to be able to bind adjacent membranes together, even against repulsive forces generated by introducing defined fractions of negatively charged phospholipids. This finding indicates that glycolipid-mediated membrane adhesion is potentially highly abundant in biology and therefore merits further investigation in particular with regard to its biological role. In the present work, the cross-linking ability of glycolipids was not found to have any significant influence on the membrane bending rigidity. In certain cases, headgroup-driven phase separation into membrane multilayers with different lamellar periodicities occurs due to the conflicting membrane separations preferred by the glycolipids and the phospholipids.

Associated content

Supporting information

Acknowledgements

We thank Helmholtz-Zentrum-Berlin (HZB) and Institut Laue-Langevin (ILL) for beam time allocation (https://doi.ill.fr/10.5291/ILL-DATA.8-02-812), the ILL/PSCM laboratories for support during sample preparation and pre-characterization, Stefan Siegel and Chenghao Li for support during the SAXS experiments, Giuseppe Rosario Del Sorbo for support during the ND experiments and Thomas Weikl for insightful comments. Financial support by the Max Planck Society and by the German Research Foundation (DFG) via Emmy-Noether grant (SCHN 1396/1) is gratefully acknowledged.

References

1. Alberts, B., A. Johnson, J. Lewis, D. Morgan, M. Raff, K. Roberts, and P. Walter. 1983. Molecular Biology of the cell. Garland Science, United States.
2. Schneck, E. 2017. The Interaction between Soft Interfaces: Forces and Structural Aspects. 4(1):1600349.
3. Stoffel, W., and A. Bosio. 1997. Myelin glycolipids and their functions. Current Opinion in Neurobiology 7(5):654-661.
4. Boudière, L., M. Michaud, D. Petroutsos, F. Rébeillé, D. Falconet, O. Bastien, S. Roy, G. Finazzi, N. Rolland, and J. Jouhet. 2014. Glycerolipids in photosynthesis: composition, synthesis and trafficking. Biochimica et Biophysica Acta (BBA)-Bioenergetics 1837(4):470-480.
5. Ryrif, I. J., J. M. Anderson, and D. J. Goodchild. 1980. The Role of the Light-Harvesting Chlorophyll a/b -Protein Complex in Chloroplast Membrane Stacking. European Journal of Biochemistry 107(2):345-354.
6. Webb, M. S., and B. R. Green. 1990. Effects of neutral and anionic lipids on digalactosyldiacylglycerol vesicle aggregation. Biochimica et Biophysica Acta (BBA) - Biomembranes 1030(2):231-237.
7. Demé, B., C. Cataye, M. A. Block, E. Maréchal, and J. Jouhet. 2014. Contribution of galactoglycerolipids to the 3-dimensional architecture of thylakoids. The FASEB Journal 28(8):3373-3383.
8. Schneck, E., F. Rehfeldt, R. G. Oliveira, C. Gege, B. Demé, and M. Tanaka. 2008. Modulation of intermembrane interaction and bending rigidity of biomembrane models via carbohydrates investigated by specular and off-specular neutron scattering. Physical Review E 78(6):061924.
9. Parsegian, V. A., N. Fuller, and R. P. Rand. 1979. Measured work of deformation and repulsion of lecithin bilayers. Proceedings of the National Academy of Sciences 76(6):2750-2754.
10. Marra, J. 1985. Controlled deposition of lipid monolayers and bilayers onto mica and direct force measurements between galactolipid bilayers in aqueous solutions. Journal of Colloid and Interface Science 107(2):446-458.
11. Marra, J. 1986. Direct measurements of attractive Van der Waals and adhesion forces between uncharged lipid bilayers in aqueous solutions. Journal of Colloid and Interface Science 109(1):11-20.
12. Ricoul, F., M. Dubois, L. Belloni, T. Zemb, C. André-Barrès, and I. Rico-Lattes. 1998. Phase Equilibria and Equation of State of a Mixed Cationic Surfactant−Glycolipid Lamellar System. Langmuir 14(10):2645-2655.
13. Wood, J., P. Luckham, and R. Swart. 1993. Exploring the interactions between glycolipid bilayers. Colloids and Surfaces A: Physicochemical and Engineering Aspects 77(3):179-189.
14. Kanduč, M., A. Schlaich, A. H. de Vries, J. Jouhet, E. Maréchal, B. Demé, R. R. Netz, and E. Schneck. 2017. Tight cohesion between glycolipid membranes results from balanced water–headgroup interactions. Nature Communications 8:14899. Article.

15. Leontidis, E., A. Aroti, L. Belloni, M. Dubois, and T. Zemb. 2007. Effects of monovalent anions of the hofmeister series on DPPC lipid bilayers part II: modeling the perpendicular and lateral equation-of-state. Biophysical Journal 93:1591-1607.
16. Schlaich, A., B. Kowalik, M. Kanduc, E. Schneck, and R. R. Netz. 2015. Physical mechanisms of the interaction between lipid membranes in the aqueous environment. Physica A 418:105-125.
17. Gourier, C., F. Pincet, E. Perez, Y. Zhang, J.-M. Mallet, and P. J. G. J. Sinaÿ. 2004. Specific and non specific interactions involving LeXdeterminant quantified by lipid vesicle micromanipulation. 21(3):165-174. journal article.
18. Eggens, I., B. Fenderson, T. Toyokuni, B. Dean, M. Stroud, and S.-i. Hakamori. 1989. Specific interaction between Lex and Lex determinants. A possible basis for cell recognition in preimplantation embryos and in embryonal carcinoma cells. . Journal of Biological Chemistry 264(June 5).
19. Schneck, E., B. Demé, C. Gege, and M. Tanaka. 2011. Membrane Adhesion via Homophilic Saccharide-Saccharide Interactions Investigated by Neutron Scattering. Biophysical Journal 100(9):2151-2159.
20. Yu, Z. W., T. L. Calvert, and D. Leckband. 1998. Molecular Forces between Membranes Displaying Neutral Glycosphingolipids: Evidence for Carbohydrate Attraction. Biochemistry 37(6):1540-1550.
21. Chatterjee, S. 1991. Lactosylceramide stimulates aortic smooth muscle cell proliferation. Biochemical and Biophysical Research Communications 181(2):554-561.
22. Li, X.-M., M. M. Momsen, H. L. Brockman, and R. E. Brown. 2002. Lactosylceramide: Effect of Acyl Chain Structure on Phase Behavior and Molecular Packing. Biophysical Journal 83(3):1535-1546.
23. Sonnino, S., A. Prinetti, H. Nakayama, M. Yangida, H. Ogawa, and K. Iwabuchi. 2009. Role of very long fatty acid-containing glycosphingolipids in membrane organization and cell signaling: the model of lactosylceramide in neutrophils. Glycoconjugate Journal 26(6):615-621. journal article.
24. Ashkenazi, S., and T. G. Cleary. 1989. Rapid method to detect shiga toxin and shiga-like toxin I based on binding to globotriosyl ceramide (Gb3), their natural receptor. Journal of Clinical Microbiology 27(6):1145-1150.
25. Saiman, L., and A. Prince. 1993. Pseudomonas aeruginosa pili bind to asialoGM1 which is increased on the surface of cystic fibrosis epithelial cells. The Journal of Clinical Investigation 92(4):1875-1880.
26. Rondelli, V., P. Brocca, G. Fragneto, J. Daillant, C. Tringali, L. Cantu, and E. Del Favero. 2017. Membrane restructuring following in situ sialidase digestion of gangliosides: Complex model bilayers by synchrotron radiation reflectivity. Biochimica et Biophysica Acta (BBA) - Biomembranes 1859(5):845-851.
27. Silvius, J. R. 1982. Thermotropic phase transitions of pure lipids in model membranes and their modifications by membrane proteins. Lipid-protein interactions 2:239-281.
28. Rockland, L. B. 1960. Saturated Salt Solutions for Static Control of Relative Humidity between 5° and 40° C. Analytical Chemistry 32(10):1375-1376.
29. Paris, O., C. Li, S. Siegel, G. Weseloh, F. Emmerling, H. Riesemeier, A. Erko, and P. Fratzl. 2007. A new experimental station for simultaneous X-ray microbeam scanning for small- and wide-angle scattering and fluorescence at BESSY II. Journal of Applied Crystallography 40(s1):s466-s470.
30. Benecke, G., W. Wagermaier, C. Li, M. Schwartzkopf, G. Flucke, R. Hoerth, I. Zizak, M. Burghammer, E. Metwalli, P. Muller-Buschbaum, M. Trebbin, S. Forster, O. Paris, S. V. Roth, and P. Fratzl. 2014. A customizable software for fast reduction and analysis of large X-ray scattering data sets: applications of the new DPDAK package to small-angle X-ray scattering and grazing-incidence small-angle X-ray scattering. Journal of Applied Crystallography 47(5):1797-1803.

31. Mills, T. T., J. Huang, G. W. Feigenson, and J. F. Nagle. 2009. Effects of cholesterol and unsaturated DOPC lipid on chain packing of saturated gel-phase DPPC bilayers. Gen Physiol Biophys 28(2):126-139.
32. Salditt, T. 2005. Thermal fluctuations and stability of solid-supported lipid membranes. Journal of Physics: Condensed Matter 17(6):R287.
33. Lei, N., C. R. Safinya, and R. F. B. J. J. P. I. France. 1995. Discrete Harmonic Model for Stacked Membranes: Theory and Experiment. 5(8):1155-1163.
34. Schneck, E., R. G. Oliveira, F. Rehfeldt, B. Demé, K. Brandenburg, U. Seydel, and M. Tanaka. 2009. Mechanical properties of interacting lipopolysaccharide membranes from bacteria mutants studied by specular and off-specular neutron scattering. Physical Review E 80(4):041929.
35. Sinha, S. K., E. B. Sirota, Garoff, and H. B. Stanley. 1988. X-ray and neutron scattering from rough surfaces. Physical Review B 38(4):2297.
36. Gonthier, J., M. A. Barrett, O. Aguettaz, S. Baudoin, E. Bourgeat-Lami, B. Demé, N. Grimm, T. Hauß, K. Kiefer, and E. Lelièvre-Berna. 2019. BerILL: The ultimate humidity chamber for neutron scattering. Journal of Neutron Research 21(1-2):65-76.
37. Israelachvili, J. N. 2011. Intermolecular and surface forces. Academic press.
38. Majee, A., M. Bier, R. Blossey, and R. Podgornik. 2019. Charge regulation radically modifies electrostatics in membrane stacks. Physical Review E 100(5):050601.
39. Schneck, E., F. Sedlmeier, and R. R. Netz. 2012. Hydration repulsion between biomembranes results from an interplay of dehydration and depolarization. Proceedings of the National Academy of Sciences 109(36):14405-14409.
40. Lis, L. J., d. McAlister, N. Fuller, R. P. Rand, and V. A. Parsegian. 1982. Interactions between neutral phospholipid bilayer membranes. Biophysical Journal 37(3):657.
41. Demé, B., M. Dubois, and T. Zemb. 2002. Swelling of a lecithin lamellar phase induced by small carbohydrate solutes. Biophysical journal 82(1):215-225.
42. Geyer, A., C. Gege, and R. R. Schmidt. 1999. Carbohydrate-carbohydrate recognition between LewisX glycoconjugates. Angewandte Chemie International Edition 38(10):1466-1468.
43. Nodet, G., L. Poggi, D. Abergel, C. Gourmala, D. Dong, Y. Zhang, J.-M. Mallet, and G. Bodenhausen. 2007. Weak calcium-mediated interactions between Lewis X-related trisaccharides studied by NMR measurements of residual dipolar couplings. Journal of the American Chemical Society 129(29):9080-9085.
44. Lotan, O., L. Fink, A. Shemesh, C. Tamburu, and U. Raviv. 2016. Critical conditions for adsorption of calcium ions onto dipolar lipid membranes. The Journal of Physical Chemistry A 120(19):3390-3396.
45. Stefaniu, C., V. M. Latza, O. Gutowski, P. Fontaine, G. Brezesinski, and E. Schneck. 2019. Headgroup-Ordered Monolayers of Uncharged Glycolipids Exhibit Selective Interactions with Ions. The Journal of Physical Chemistry Letters 10(8):1684-1690.
46. Kav, B. 2019. Membrane adhesion mediated via lipid-anchored saccharides. PhD Thesis, University of Potsdam, Germany.
47. Higashiyama, T. 2002. Novel functions and applications of trehalose. Pure and applied Chemistry 74(7):1263-1269.
48. Machado, J. J. B., J. A. Coutinho, and E. A. Macedo. 2000. Solid-liquid equilibrium of alpha-lactose in ethanol/water. Fluid Phase Equilibria 173(1):121-134.
49. Mathlouthi, M., and P. Reiser. 2012. Sucrose: properties and applications. Springer Science & Business Media.
50. Albersdörfer, A., T. Feder, and E. Sackmann. 1997. Adhesion-induced domain formation by interplay of long-range repulsion and short-range attraction force: a model membrane study. Biophysical Journal 73(1):245-257.
51. Kloboucek, A., A. Behrisch, J. Faix, and E. Sackmann. 1999. Adhesion-induced receptor segregation and adhesion plaque formation: a model membrane study. Biophysical Journal 77(4):2311-2328.

52. Weikl, T. R., J. T. Groves, and R. Lipowsky. 2002. Pattern formation during adhesion of multicomponent membranes. EPL (Europhysics Letters) 59(6):916.
53. Kollmitzer, B., P. Heftberger, R. Podgornik, J. F. Nagle, and G. Pabst. 2015. Bending rigidities and interdomain forces in membranes with coexisting lipid domains. Biophysical Journal 108(12):2833-2842.
54. Dimova, R. 2014. Recent developments in the field of bending rigidity measurements on membranes. Advances in colloid and interface science 208:225-234.
55. Pan, J., S. Tristram-Nagle, N. Kucerka, and J. F. Nagle. 2008. Temperature dependence of structure, bending rigidity, and bilayer interactions of dioleoylphosphatidylcholine bilayers. Biophysical Journal 94(1):117-124.

Supporting References

#56. Israelachvili, J. N., Intermolecular and surface forces. Academic press: 2011
#57. NIST Center for Neutron Research, https://www.ncnr.nist.gov/resources/activation/

Membrane adhesion via glycolipids occurs for abundant saccharide chemistries

V. M. Latza, B. Demé, and E. Schneck

Supporting Information

1.) Electrostatic repulsion between charged surfaces in a monovalent electrolyte

For weakly charged surfaces in a monovalent electrolyte the pressure Π_{el} associated with the electrostatic repulsion is given as [1]:

$$\Pi_{el}(d_w) \cong 2k_BT\rho_0[\cosh(e\psi_m(d_w)/k_BT) - 1],$$

where ρ_0 is the number density of monovalent ions in the bulk, *e* is the electron charge, and ψ_m is the electric potential at the midplane (i.e., the center of the water layer). For sufficiently low charge densities (i.e., in the Debye-Hückel limit) and within the weak-overlap approximation, ψ_m is proportional to the surface electric potential ψ_0:

$$\psi_m(d_w) = 2\psi_0 e^{-\kappa d_w/2},$$

where

$$\kappa^{-1} = \sqrt{\frac{\varepsilon_0 \varepsilon k_B T}{2e^2\rho_0}}$$

is the Debye length and ψ_0 follows from the surface charge density σ according to the relation

$$\sigma^2 = 2\varepsilon\varepsilon_0 k_B T \sum_j \rho_0\left[\exp\left(-z_j e\psi_0/k_BT\right) - 1\right],$$

where $z_j = \pm 1$ is the charge number of the cations and anions, respectively.

2.) Lamellar periodicities obtained by SAXS for of DMPC membranes containing *Psyc-sat* and DMPG

Fig. S1 shows $d(f_{gly})$ for DMPC membranes loaded with *Psyc-sat*, a glycolipid with a mono-galactose headgroup. The lamellar periodicity decreases approximately linearly with increasing f_{gly}. The smallest value is $d \approx 6$ nm at $f_{gly} = 0.2$.

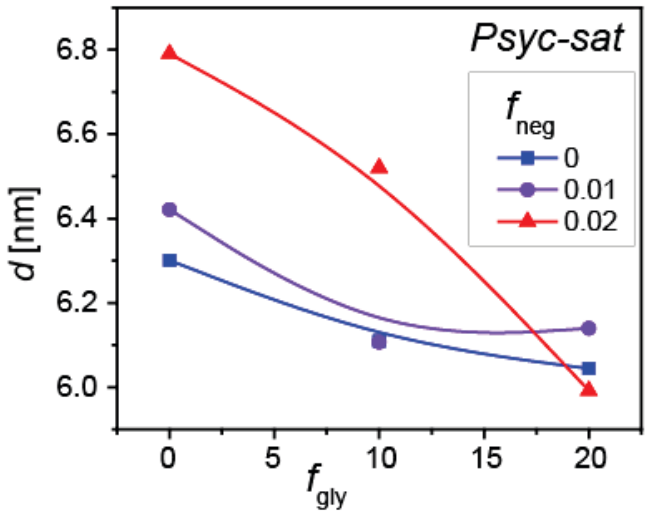

Figure S1: Lamellar periodicities *d* obtained by SAXS for DMPC lipid membrane multilayers containing various fractions f_{gly} of *Psyc-sat* and f_{neg} of the negatively charged lipid DMPG. The measurements were conducted at 50 °C. Solid lines are guides to the eye.

3.) Neutron diffraction (ND) measurements under bulk water conditions

The results of ND measurements of POPC membranes loaded with *DGDG-unsat* at $f_{gly} = 0.2$ and $f_{neg} = 0$, and of DMPC membranes loaded with *LacCer-sat* at $f_{gly} = 0.2$ and $f_{neg} = 0$ under bulk water conditions are summarized in Fig. S2. The intensities of the second Bragg sheets were found to be too weak to be analyzed.

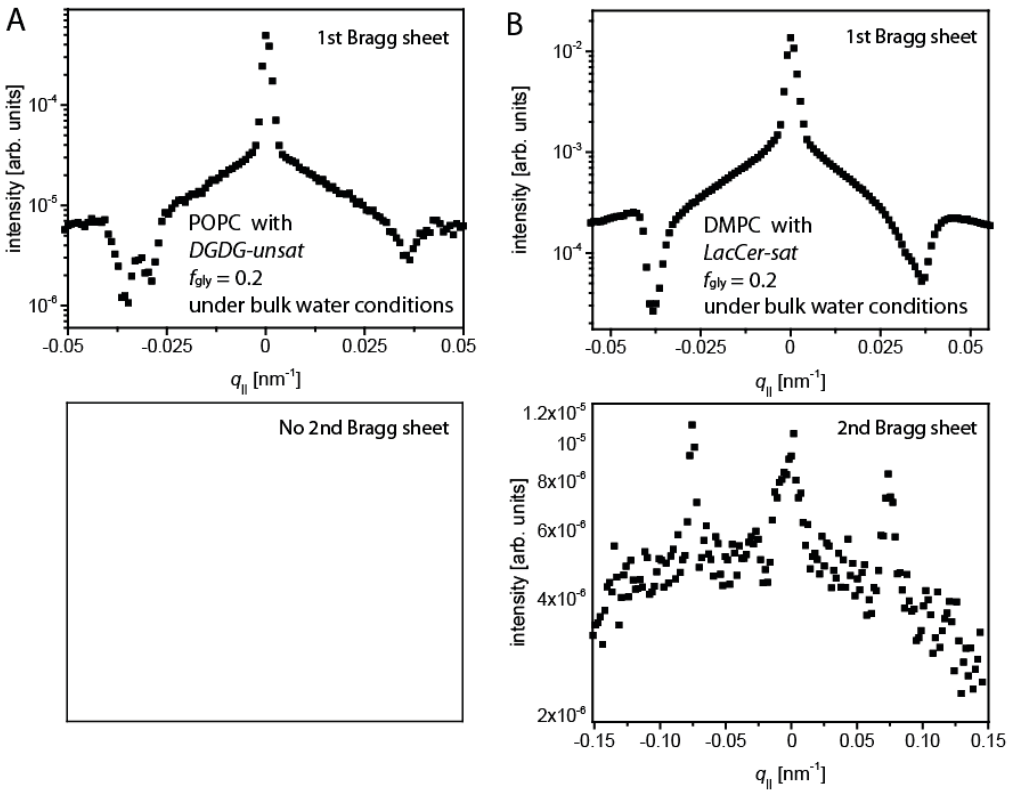

Figure S2: Intensities of the first (top) and second (bottom) Bragg sheets of (A) POPC membranes loaded with *DGDG-unsat* at $f_{gly} = 0.2$ and $f_{neg} = 0$ and (B) DMPC membranes loaded with *LacCer-sat* at $f_{gly} = 0.2$ and $f_{neg} = 0$, both under bulk water conditions.

4.) Accounting for absorption of the neutron beam in the modeled Bragg sheets

Close to the conditions $\Omega = O$ and $\Omega = \Gamma$ the incident and scattered neutron beams, respectively, travel essentially parallel to the sample plane and thus get strongly absorbed on the way through the sample. While crystalline silicon is practically transparent to neutrons on the length scales relevant for the present work, beam absorption through incoherent scattering by the lipid layer is considerable, because the lipids are hydrogenous, i.e., they contain light hydrogen (^{1}H). The attenuation coefficient for DMPC (chemical formula: $C_{36}H_{72}NO_8P$) at a mass density of 1 g cm^{-3} is $\mu \approx 5$ cm^{-1} at $\lambda = 4.518$ Å [2]. Hydrating D_2O has negligible contribution to absorption.

The average thickness of the lipid film on the silicon wafer is $h \approx 1$ µm, as follows from the deposited lipid amount (≈ 1 mg), their mass density (≈ 1 g cm^{-3}), as well as from the approximate extensions of the coated region in the direction parallel to the beam ($L_{||} \approx 2$ cm) and in the perpendicular direction ($L_{\perp} \approx 5$ cm). For each coated surface element along the direction of the beam ($0 \leq x \leq L_{||}$), the maximal path length is $s_{max}^{in}(x) = x$ for the incident beam and $s_{max}^{sc}(x) = L_{||} - x$ for the scattered beam. Depending on the angle of incidence, the actual path length is given as

$s_{in}(\Omega, x) = MIN\left(\left[s_{max}^{in}(x);\ h/\sin(|\Omega|)\right]\right)$ for the incident beam

and

$s_{sc}(\Omega, x) = MIN([s_{max}^{sc}(x);\ h/\sin(|\Omega - \Gamma|)])$ for the scattered beam

The overall attenuation by the sample on the way to the detector, represented as the transmission function $T(\Omega)$ thus follows as $T(\Omega) = T_{in}(\Omega) \cdot T_{sc}(\Omega)$, where

$$T_{in}(\Omega) = \frac{1}{L_{||}} \int_0^{L_{||}} e^{-\mu \cdot s_{in}(\Omega, x)} dx$$

$$T_{sc}(\Omega) = \frac{1}{L_{||}} \int_0^{L_{||}} e^{-\mu \cdot s_{sc}(\Omega, x)} dx$$

5.) Influence of negatively charged phospholipids in the interaction of phospholipid bilayers containing *TetraG-sat*

Fig. S3 shows $d(f_{gly})$ for DPPC membranes loaded with *TetraG-sat*, a glycolipid with a linear tetrasaccharide headgroup composed of (galactose)-(N-acetyl-galactose)-(galactose)-(glucose). There is a strong increase of d with f_{gly}., which is steep in the beginning until it reaches saturation. Incorporation of negatively charged lipids has no pronounced effect in the investigated range ($f_{neg} \leq 0.05$)

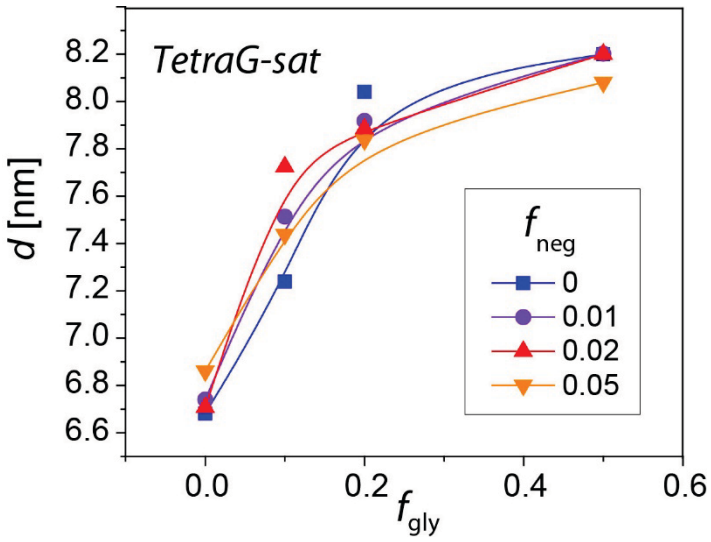

Figure S3: Lamellar periodicities d obtained by SAXS for DPPC lipid membrane multilayers containing various fractions f_{gly} of *TetraG-sat* and f_{neg} of the negatively charged lipid DPPG. The measurements were conducted at 50 °C. Solid lines are guides to the eye.

References

[1] Israelachvili, J. N., *Intermolecular and surface forces*. Academic press: 2011

[2] NIST Center for Neutron Research, https://www.ncnr.nist.gov/resources/activation/

II
Chemicals/Materials, sample preparation, and scattering techniques

1. *PEGylated* and non-*PEGylated* lipid surfaces for protein adsorption studies

1.1 Chemicals/materials

The utilized chemicals were purchased from Sigma Aldrich and used without further purification unless stated otherwise. The PEG brushes are composed of the phospholipid 1,2-distearoyl-*sn*-glycero-3-phosphocholine (DSPC) and of lipopolymers based on 1,2-distearoyl-*sn*-glycero-3-phosphoetanolamine (DSPE) comprising PEG polymers of various polymerization degrees *N* (*N* = 22, *N* = 114, or *N* = 455): DSPE-N-[methoxy(polyethylene glycol)-1000] (PEG-lipid-22), DSPE-N-[methoxy(polyethylene glycol)-5000] (PEG-lipid-114), or DSPE-N-[methoxy(polyethylene glycol)-20000] (PEG-lipid-455). The chemical structures of DSPC and the PEG-lipids are shown in Figure v. DSPC, PEG-lipid-22, and PEG-lipid-114 were purchased from Avanti Polar Lipids (Alabaster, USA) and PEG-lipid-455 from Nanocs (Boston, USA).

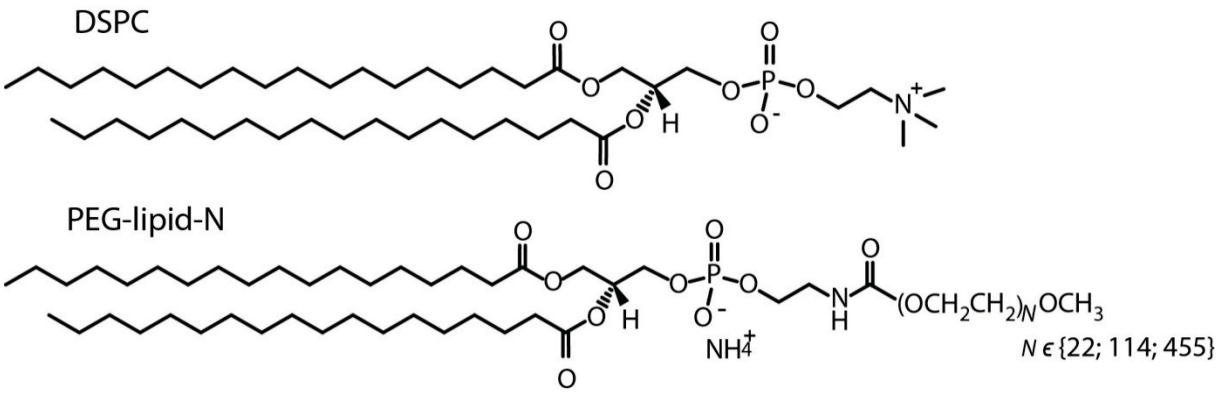

Figure v Chemical structure of sample constituents DSPC and PEG-lipid-*N*.

IgG1 3.3 anti-PEG monoclonal antibodies (Abs) with high affinity to the PEG backbone (backbone-binder Ab, BB Ab) were purchased from Institute of Biomedical Sciences, Academia Sinica (Taipei, Taiwan). IgG anti-PEG rabbit monoclonal Abs (clone ID: PEG-B-47) with high affinity to the methoxy end group (end-binder Ab, EB Ab) were purchased from Epitomics, Inc. (Burlingame, California, USA). Abs were shipped and stored in buffer solutions. Prior to the experiments the purchased Ab solutions were diluted with H_2O buffer solution yielding an overall concentration of 0.1 mg/mL. Human blood serum (HBS) was used either purely or tenfold diluted in aqueous buffer solutions. The buffer solutions were based on H_2O or D_2O or mixtures thereof for contrast variation, and contained 150 mM NaCl and 20 mM Tris at pH 7. Silicon single (111) crystal blocks, (size: 50 mm x 50 mm x 10 mm) polished on one large face and terminated with a thin layer of native silicon oxide (SiO_2), were purchased from Synchrotronix (Annemasse, France) and used as planar solid supports for the PEG brushes.

1.2 Sample preparation

Ultrapure water was used for all purposes (MilliQ®-grade). All glassware was cleaned beforehand by consecutively immersion into the following of solvents for 30 min: chloroform, acetone, ethanol, Milli Q water and ethanol. The glassware was dried with nitrogen afterwards. The silicon blocks were first immersed into the organic solvents chloroform, acetone, and ethanol. Afterwards they were dried with argon and treated in an UV-ozone chamber for 20 min, in order to activate the surface. (Note: the use of nitrogen or argon had no impact on the sample preparation, but was performed with respect of availability). The blocks were finally dehumidified in an oven at 50 °C for 30 min. The completely dry blocks were covalently functionalized in order to render their surfaces hydrophobic. For this purpose, they were placed in a freshly prepared 1 mM solution of anhydrous hexadecane and OTS (50 mL : 20 µL). Unbound, polymerized OTS was removed by rinsing with hexadecane and ethanol.

Table 1 Lipid surfaces displaying polymer brushes. Samples are described in terms of polymerization degree N, grafting density σ , area per polymer chain Σ, PEG amount D_{PEG}, mass per unit area Γ_{PEG}.

Sample	N	σ [10^{-4} Å^{-2}]	Σ [Å^2]	D_{PEG} [Å]	Γ_{PEG} [mg/m^2]
PEG-lipid-22, f = 0.1	22	21.3	470	3.2	0.34
PEG-lipid-114, f = 0.01	114	2.1	4700	1.7	0.18
PEG-lipid-114, f = 0.02	114	4.3	2350	3.3	0.35
PEG-lipid-114, f = 0.05	114	10.6	940	8.4	0.88
PEG-lipid-114, f = 0.1	114	21.3	470	16.7	1.77
PEG-lipid-455, f = 0.01	455	2.1	4700	6.7	0.71

Langmuir trough and Langmuir-Schaefer Deposition

The hydrophobic substrates were further functionalized with a phospholipid monolayers with attached PEG brushes via the Langmuir-Schaefer (LS) technique [105].

In the following the general working principle of a Langmuir trough is explained. Firstly, a solution of amphiphiles (here phospholipids) is spread evenly at the air-subphase interface of the Langmuir trough. The spreading solution consists of amphiphiles that are solubilized in a poorly water miscible solvent with high vapor pressure (here chloroform), evaporating fast in ambient conditions. Upon spreading on the aqueous subphase, the amphiphiles arrange on the interface while the solvent evaporates. The hydrophilic headgroups are in contact with the aqueous subphase, whereas the hydrophobic hydrocarbon tails stick out into the air (see Figure w A).

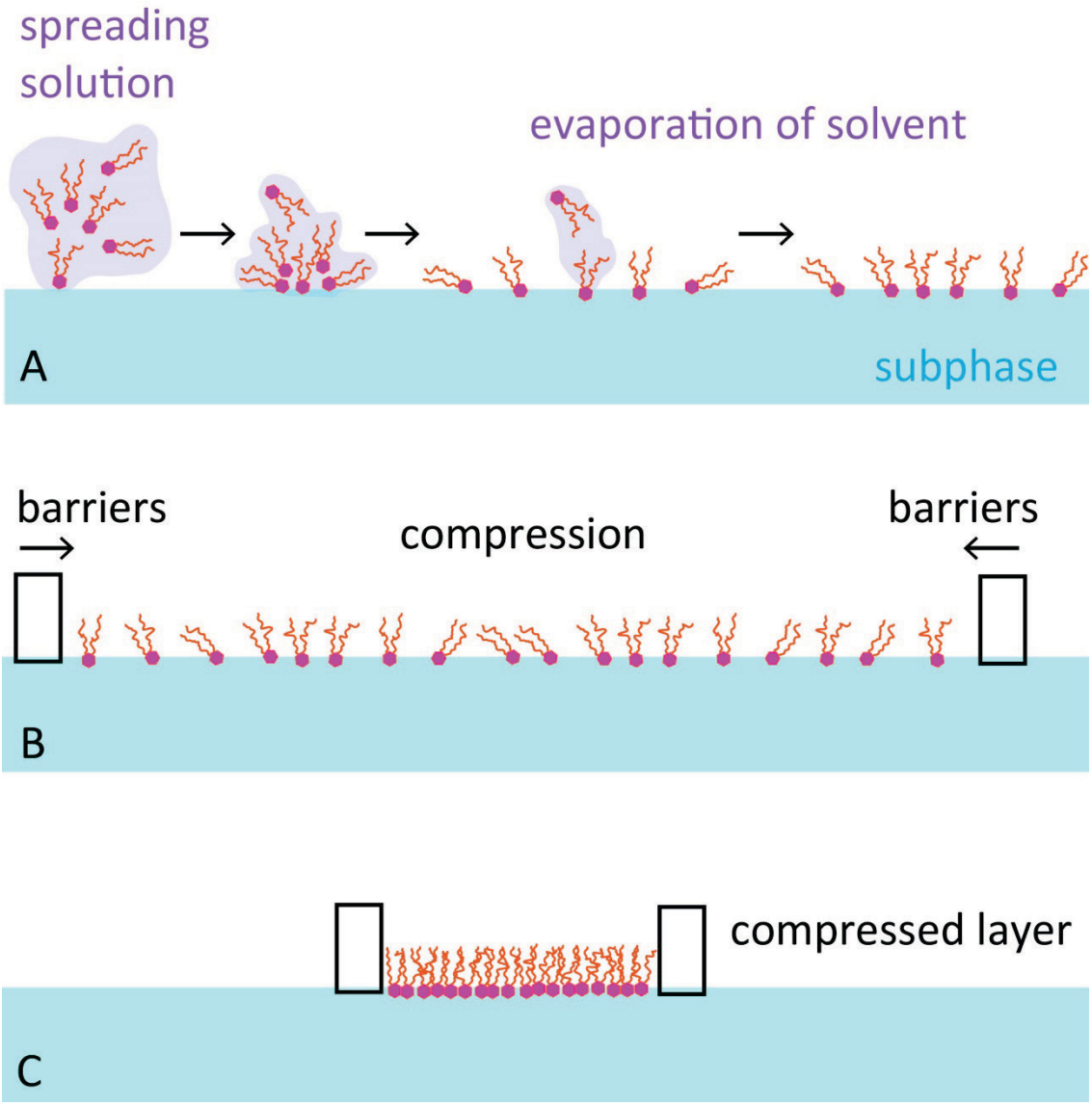

Figure w Scheme of basic working principle of a Langmuir-Blodgett trough. A) First, the solution containing an amphiphilic molecule is spread on the subphase. The solvent will evaporate immediately. B) In the second step, the barriers compress the molecules to a certain lateral pressure. C) A compressed layer at the wished final lateral pressure is obtained.

With the help of barriers the loosely spread lipids will be brought closer, in order to form a homogenous ordered monolayer (see Figure w B). A final lateral pressure of Π = 35 mN/m is used in order to form a homogenous dense lipid monolayer (see Figure w C).

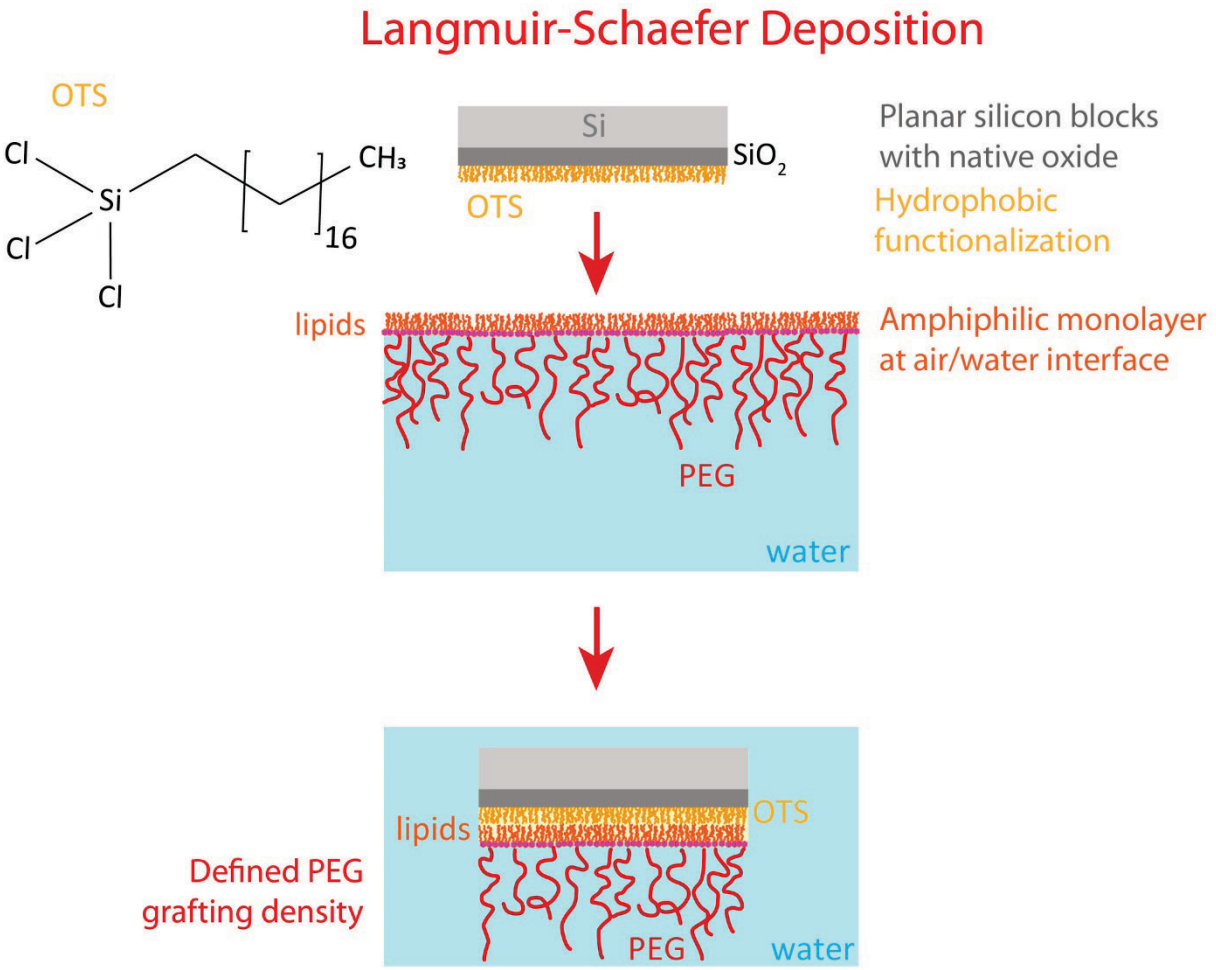

Figure x Langmuir-Schaefer deposition of amphiphilic monolayer on silicon substrate: The hydrophobized silicon block is moved slowly downwards until it reaches the air/subphase interface (of the Langmuir-Blodgett trough), where the lipids attach to the block. The block is moved further down until it is completely covered by the subphase.

In this thesis the produced monolayer consisted of mixtures of DSPC and PEG-lipid (PEG-lipid-22, PEG-lipid-114, or PEG-lipid-455) on a subphase of H_2O-buffer. The spreading solutions were prepared by solubilization of the components in chloroform at an overall concentration of 2 mg/mL. The PEG-lipid mole fractions f varied from f = 0.01 (1 mol% PEG-lipid) to f = 0.1 (10 mol% PEG-lipid). The monolayer was further transferred onto a hydrophobic block functionalized with OTS deploying the LS deposition (see Figure x). This means that the horizontally oriented and hydrophobized block is slowly moved downwards until it reaches the interface, where the lipids attach to the block. The block is moved further down until it is completely covered by the aqueous medium of the subphase, where the system is stabilized by the hydrophobic effect. Table 1 gives an overview about the samples.

2. Membrane multilayers for the study of membrane interactions

2.1 Chemicals/materials

The utilized chemicals were purchased from Sigma Aldrich and used without further purification unless stated otherwise. The utilized self-assembled multilayer membranes consisted of up to three lipid constituents (see Figure 20) with different molar fractions f, where $f = 1$ corresponds to 100 mol %.

The components were phosphatidylcholine (PC) lipids (1,2-Dimyristoyl-*sn*-glycero-3-phosphocholine (DMPC) or 1,2-Dipalmitoyl-*sn*-glycero-3-phosphocholine (DPPC) or 1-Palmitoyl-2-oleoyl-*sn*-glycero-3-phosphocholine (POPC)), serving as matrix lipid, negatively charged phospholipids with matching chain lengths (1,2-Dimyristoyl-*sn*-glycero-3-phospho-(1'-rac-glycerol) (Sodium Salt) (DMPG) or 1,2-Dipalmitoyl-*sn*-glycero-3-phospho-(1'-rac-glycerol) (Sodium Salt) (DPPG) or 1-Palmitoyl-2-oleoyl-*sn*-glycero-3-phospho-L-serine (Sodium Salt) (POPS)) (see Table 2) and glycolipids.

Table 2 List of utilized phospholipids and information of charge, manufacturer and solubility.

Phospholipid	Charge	Soluble in
DMPC	None	$CHCl_3$
DPPC	None	$CHCl_3$
POPC	None	$CHCl_3$
DMPG	Negative	$CHCl_3$
DPPG	Negative	$CHCl_3$
POPS	Negative	$CHCl_3$

The phospholipids and the glycolipids Digalactosyl-diacylglycerol unsaturated (*DGDG-unsat*) and Monogalactosyl-diacylglycerol unsaturated (*MGDG-unsat*) were purchased from Avanti Polar Lipids (Alabaster, USA) (see Table 2 and Table 3). The glycolipids Digalactosyl-diacylglycerol saturated (*DGDG-sat*), Monogalactosyl-diacylglycerol saturated (*MGDG-sat*), N-pentadecanoyl-psychosine (*Psyc-sat*), N-hexadecanoyl-lactosyl-ceramide (*LacCer-sat*), N-hexadecanoyl-ceramide-trihexoside (*Trihexo-sat*), and Gangliotetraosyl-ceramide (*TetraG-sat*) were purchased from Matreya LLC. (State College, PA, USA) (see Table 3). The chemical structures of the glycolipids are depicted in Figure y.

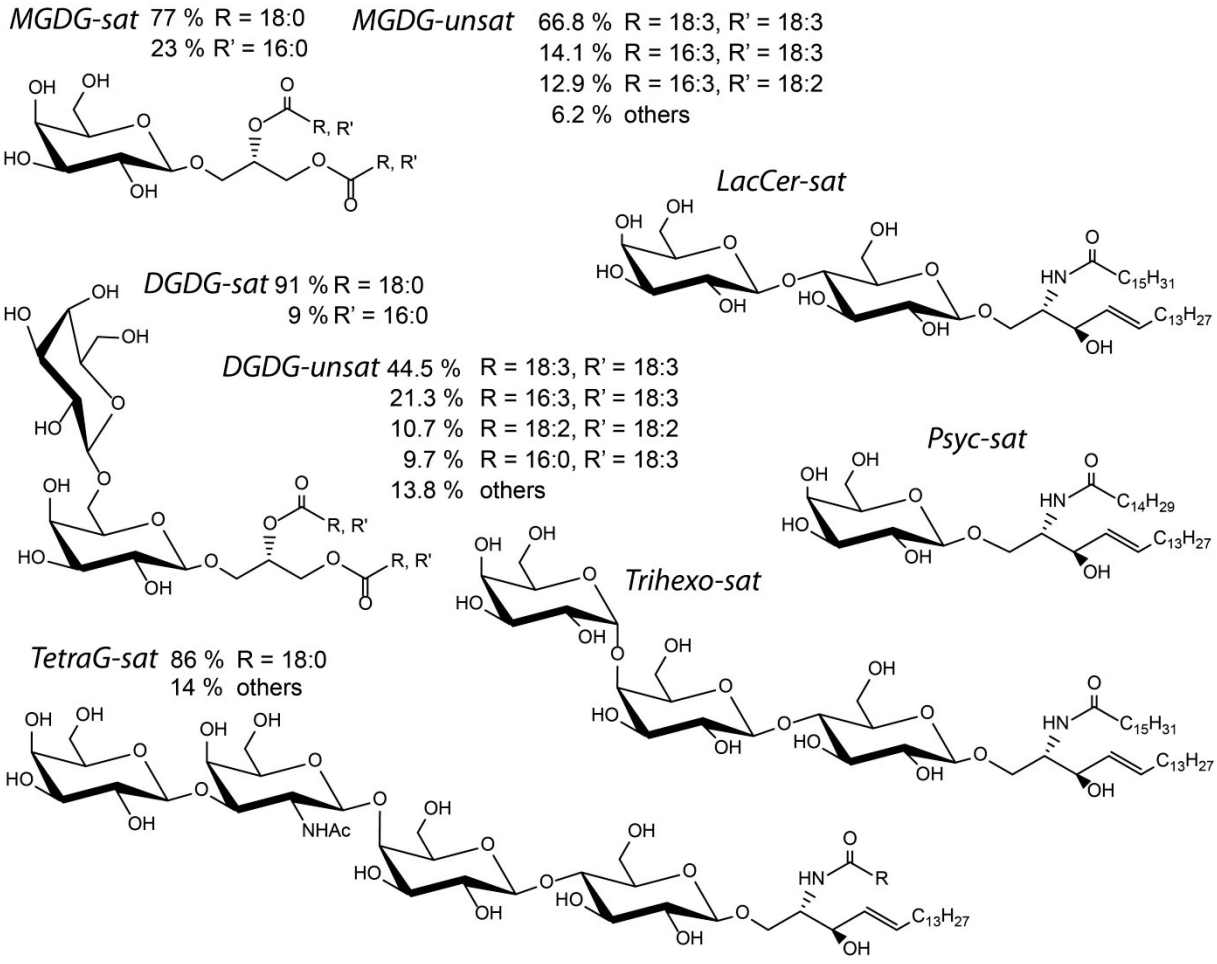

Figure y Chemical structure of utilized glycolipids: *MGDG-sat*, *DGDG-sat* and *–unsat*, *TetraG-sat*, *Psyc-sat*, *LacCer-sat* and *Trihexo-sat*.
Reprinted from [Latza, V.M., Demé B. Schneck E., *Membrane adhesion via glycolipids occurs for abundant saccharide chemistries.* Biophysical Journal, Manuscript submitted for publication.].

The samples were composed in the following way: Matrix-PC-lipids have a mole fraction of $f_{PC} = 1 - f_{gly} - f_{neg}$. The incorporated glycolipids mole fraction was varied (f_{gly} = 0, 0.1, 0.2, 0.5) together with the negatively charged lipid mole fraction (comprising phosphatidylserine (PS) or phosphatidylglycerol (PG) headgroups) (f_{neg} = 0, 0.01, 0.02, 0.05). Table 3 gives an overview about utilized samples.

Table 3 Overview of samples for membrane multilayers indicating corresponding matrix lipid and negatively charged lipid for the utilized glycolipids.

Glycolipid	*Abbreviation*	Soluble in $CHCl_3$/MeOH	Matrix-lipid	neg. lipid
DGDG unsaturated	*DGDG-unsat*	4:1 v/v	POPC	POPS
MGDG unsaturated	*MGDG-unsat*	4:1 v/v	POPC	POPS
N-hexadecanoyl lactosylceramide	*LacCer-sat*	2:1 v/v	DMPC	DMPG
N-pentadecanoyl psychosine	*Psyc-sat*	2:1 v/v	DMPC	DMPG
MGDG saturated	*MGDG-sat*	4:1 v/v	DMPC	DMPG
DGDG saturated	*DGDG-sat*	4:1 v/v	DMPC	DMPG
N-hexadecanoyl ceramide trishexoside	*Trihexo-sat*	2:1 v/v	DMPC	DMPG
Gangliotetraosylceramide	*TetraG-sat*	2:1 v/v	DPPC	DPPG

2.2 Preparation of membrane multilayers

Samples to study interactions between membranes were either multilamellar vesicles or solid-supported membrane multilayers. Ultrapure water was used for all purposes (MilliQ®-grade). All glassware was cleaned beforehand by successive immersion with the following solvents for 30 min: chloroform, acetone, ethanol, Milli Q water and ethanol. The glassware was dried with nitrogen afterwards. The stock-solutions of the pure lipids were prepared by weighing the lipid powder and adding solvent, resulting in a concentration of 2 mg/mL. Phospholipids were solubilized in chloroform (see Table 2) and glycolipids in chloroform/methanol mixtures (4:1 or 2:1 v/v) (see Table 3). Mixed lipid solutions were prepared by mixing defined volumes of the respective single-component lipid solutions. Therefore the exact volume of each single component was measured with *Hamilton* syringes.

2.2.1 Multilamellar vesicle samples for small and wide angle X-ray scattering

The ternary lipid mixtures were dried for at least 3 h and subsequent exposure to vacuum overnight to evaporate residual solvent. A 100 mM NaCl and 5 mM Hepes buffer solution based on D_2O or H_2O was set to a pH 7 by adding 1 mM NaOH in solution. To prepare suspensions of multilamellar lipid aggregates, aqueous buffer was added to the dry lipid mixtures and sonicated for 7 min. They stayed in the oven at around 50°C for 1 h and after cooling down to room temperature stored in the fridge at 5°C. Multilamellar vesicles were studied in capillaries out of borosilica glass (WJM-Glas, Berlin, Germany). Just before the transfer to the measurement capillaries for combined SAXS and WAXS the samples were sonicated for 15 min. Each borosilica capillary was filled with 100 μL of sample solution. The solution was moved to the end of the capillary by centrifugation (500 ppm for 1 min). The capillaries were stored at 5°C overnight. Just before the measurement the capillaries were kept at room temperature or at 50°C.

2.2.2 Solid-supported membrane multilayers for neutron diffraction

For the preparation of solid-supported membrane multilayers, single side polished silicon wafers Si(111) (Siegert Wafer, Aachen, Germany) having a size of 25 mm x 65 mm were cleaned with the already mentioned glassware cleaning procedure. They were dried with argon and kept at RT in falcon tubes. The wafers were treated in an UV-ozone chamber for 20 min just before the mixed lipid solution was deposited. A volume of 0.5 mL of a 2 mg/mL mixed lipid solution was applied on the polished face of the wafer placed on a petri dish. A homogenous multilayer that covers almost the entire surface was produced by swaying the petri dish until complete evaporation of solvent. Residual solvent was removed by overnight treatment in vacuum. Subsequent incubation followed for 3 h at 50 °C and high D_2O humidity ($h_{rel} \gtrsim 87$ %) [106], realised by placing 40 μL of a 1 M $BaCl_2$-solution in D_2O at the lowest point of the falcon tubes) in order to anneal the lipid membrane mulitlayers. Finally the samples they were kept at 5 °C in dry conditions in falcon tubes.

3. Scattering techniques

3.1 Neutron reflectometry

Neutron reflectometry (NR) probes the structure of planar samples perpendicular to the interface. It is a non-destructive method with high spatial resolution down to the sub-nanometer level. The probed length scale is nevertheless large compared to atomic structures, such that the description of matter as continuous media has proven useful [107]. Within this framework, the sample is described with a (position-dependent) refractive index *n*.

$$n = 1 - \delta + i\beta \tag{4}$$

$$where\ \delta = \frac{\lambda^2}{2\pi}\,\rho \tag{5}$$

$$and\ \beta = \frac{\lambda}{4\pi}\,\mu \tag{6}$$

where λ denotes the wavelength, ρ the scattering length density (SLD), and μ the adsorption coefficient;

The SLD depends on the nuclear composition of the medium:

$$\rho = \sum_j \rho_j b_j \tag{7}$$

where ρ_j denotes the number density of the nucleus j, b_j the coherent scattering length of the nucleus j (b_j values are known and tabulated [108]), and μ the absorption coefficient;

Since the SLD of a medium strongly depends on the nuclear composition, it is very different for hydrogenated and deuterated variants of molecules or materials thereof e.g. H_2O and D_2O. This fact is exploited by using contrast variation measurements. The SLD of the aqueous medium is varied by replacing H_2O with D_2O or defined H_2O/D_2O mixtures of known SLD. As one example, in H_2O contrast the hydrocarbonchains of the lipids are invisible in the measurement, because the SLDs of the contrast and the chains are similar. At the same time contributions from the other media of the sample are enhanced. In this thesis up to four contrasts are utilized: H_2O (ρ_w = -0.56 x 10^{-6} Å^{-2}), D_2O (ρ_w = 6.37 x 10^{-6} Å^{-2}), 4-matched water (4MW, ρ_w = 4.00 x 10^{-6} Å^{-2}), and water matching the SLD of the silicon substrate (SMW, ρ_w = 2.07 x 10^{-6} Å^{-2}).

Figure z depicts the experimental geometry of a reflectometry measurement. Specular scattering is utilized to obtain information on the out-of-plane structure along the z-axis of an oriented sample. In this case only the mirrored reflection is considered, where the incident angle θ equals the reflected angle θ (see Figure z).

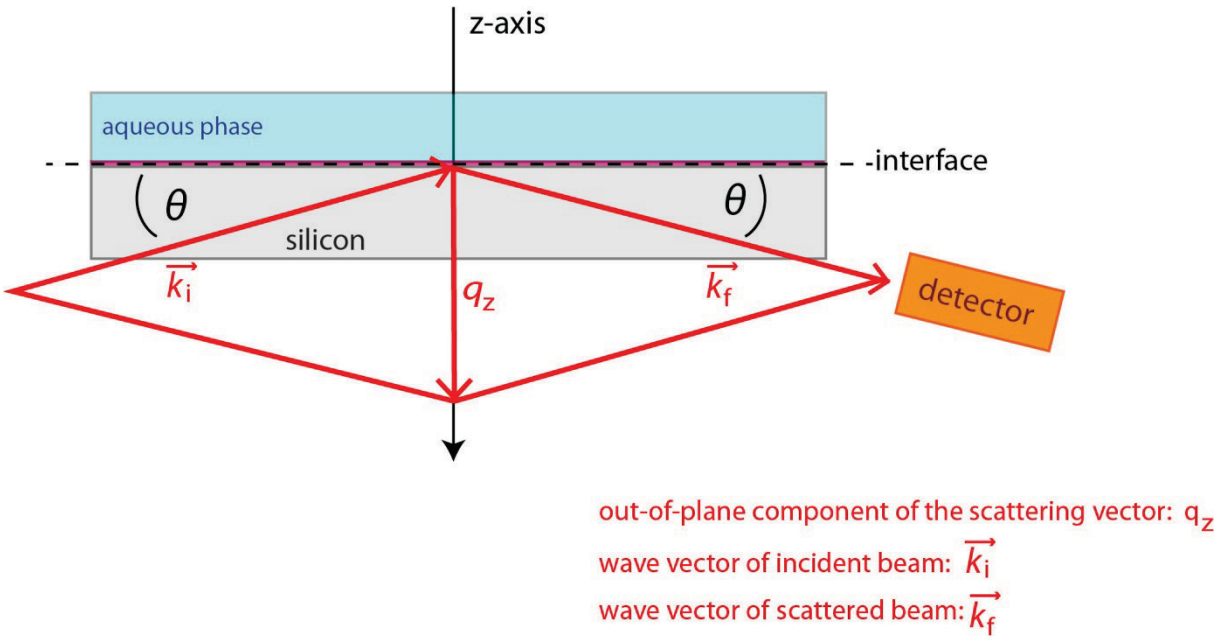

Figure z Scheme of experimental geometry or a reflectometry measurement.

In elastic scattering (as considered here) the length of the wave vector of the incident beam $\vec{k}_i$ and of the scattered beam $\vec{k}_f$ is conserved:

$$|\vec{k}_i| = |\vec{k}_f| = \frac{2\pi}{\lambda} \tag{8}$$

The scattering vector $\vec{q}$ is defined as: $\vec{q} = \vec{k_i} - \vec{k_f}$ (9)

For specular scattering, $\vec{q}$ has only an out-of-plane component, q_z.

Following from geometrical construction indicated with red lines in Figure z:

$$q_z = k_i^z - k_f^z = \frac{2\pi}{\lambda}(\sin\theta + \sin\theta) = \frac{4\pi}{\lambda}\sin\theta \tag{10}$$

Reflectometry in general measures the intensity of the reflected beam as a function of q_z. In practice q_z can be varied by variation of θ or λ, according to equation (10).

In this thesis, the samples (planar, solid-supported lipid-based surfaces with or without bound proteins) were measured in the so-called time-of-flight (TOF) mode. In this mode the neutron beam is pulsed and all wavelengths are used for the measurement (variation of λ). Neutrons of different wavelengths travel at different velocities and arrive on the detector at different time points (recalculation of the wavelength). For a given incident angle θ, the intensity on the detector therefore depends on time: I_θ (t) (see Figure aa). The wavelength λ of the neutron is then recalculated from its time of flight. Hence, wavelength-dependent intensities are deduced: I_θ (λ). Since each set of θ and λ encode a defined value of q_z (see equation (10)), q_z-dependent intensities are obtained in the final step (see Figure aa). The measurements for this thesis [50, 98] were conducted at two incident angles θ: θ_1 and θ_2. The use of all wavelengths at two different angles enlarges the q_z range and therefore reveals structural features at different length scales.

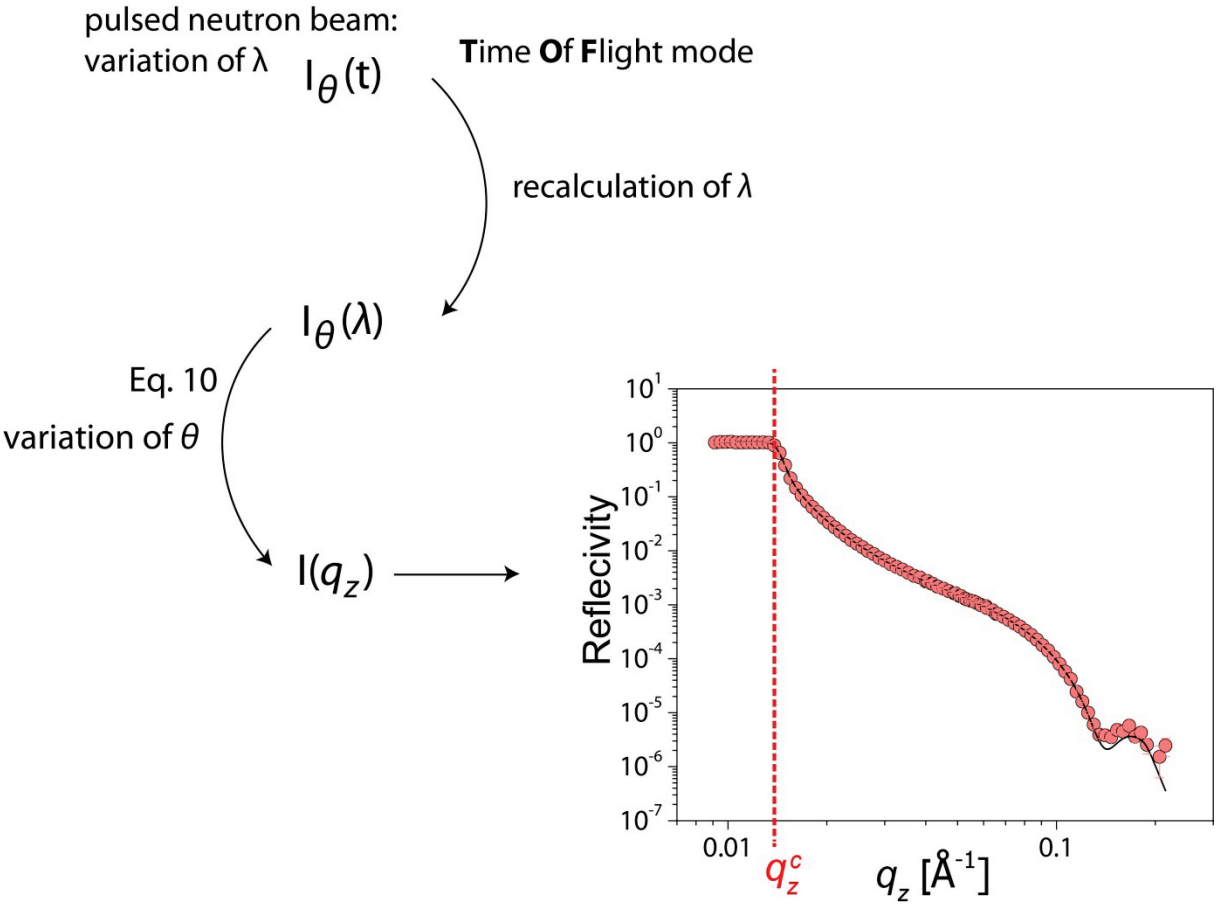

Figure aa Neutron reflectometry measurements were conducted in the so-called time-of-flight (TOF) mode: variation of λ. Neutrons of different wavelengths travel at different velocities and arrive on the detector at different time points (recalculation of the wavelength). For a given incident angle θ, the intensity on the detector therefore depends on time: I_θ (t). The wavelength λ of the neutron is then recalculated from its time of flight. Hence, wavelength-dependent intensities are deduced: I_θ (λ). Since each set of θ and λ encode a defined value of q_z (see equation (10)), q_z-dependent intensities are obtained in the final step.

The following paragraph will explain how a reflectivity curve from an interface depends on the interfacial SLD profile. The simplest case is an ideal interface between two media with homogenous SLD, where a discrete SLD jump is observed.

An ideal interface between 2 homogenous media 0 and 1 and an incident beam, coming from medium 0, which is scattered at the interface of the 2 media, is considered (see Figure bb).

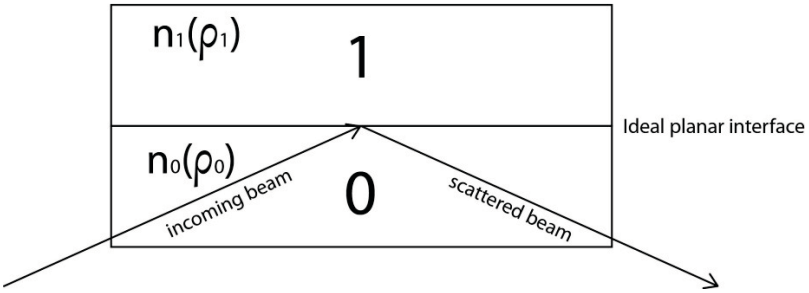

Figure bb Scheme of an ideal planar interface between 2 homogenous media 0 and 1. The incident beam is coming from medium 0 is scattered at the interface of media 0 and 1.
Adapted by permission from Rightslink: [Springer eBook] [Generic and Specific Roles of Saccharides at Cell and Bacteria Surfaces, Schneck E.] [Springer Nature] (2011)

Here, the wave vector in z direction in each medium k_j^z is defined by q_z and the refractive indices of both media (note: absorption contributions are neglected):

$$k_j^z = \sqrt{\left(\frac{q_z}{2}\right)^2 + 4\pi\rho_j} \tag{11}$$

The amplitudes of the refracted and transmitted waves are defined via the Fresnel amplitude reflection coefficients:

$$r_{0,1}^F = \frac{k_0^z - k_1^z}{k_0^z + k_1^z} \tag{12}$$

The specular reflectivity R is defined as the ratio between the reflected intensity I_f and the incident intensity I_i, which equals the absolute square of the complex Fresnel amplitude reflection coefficient:

$$R(q_z) := \frac{I_f}{I_i} = \left|r_{0,1}^F\right|^2 \tag{13}$$

when considering equations (11) to (13), $R = 1$ for $q_z < q_z^c$ (critical value), when $\rho_1 > \rho_0$.

q_z^c is defined as: $q_z^c \cong \sqrt{16\pi(\rho_1 - \rho_0)}$ (14)

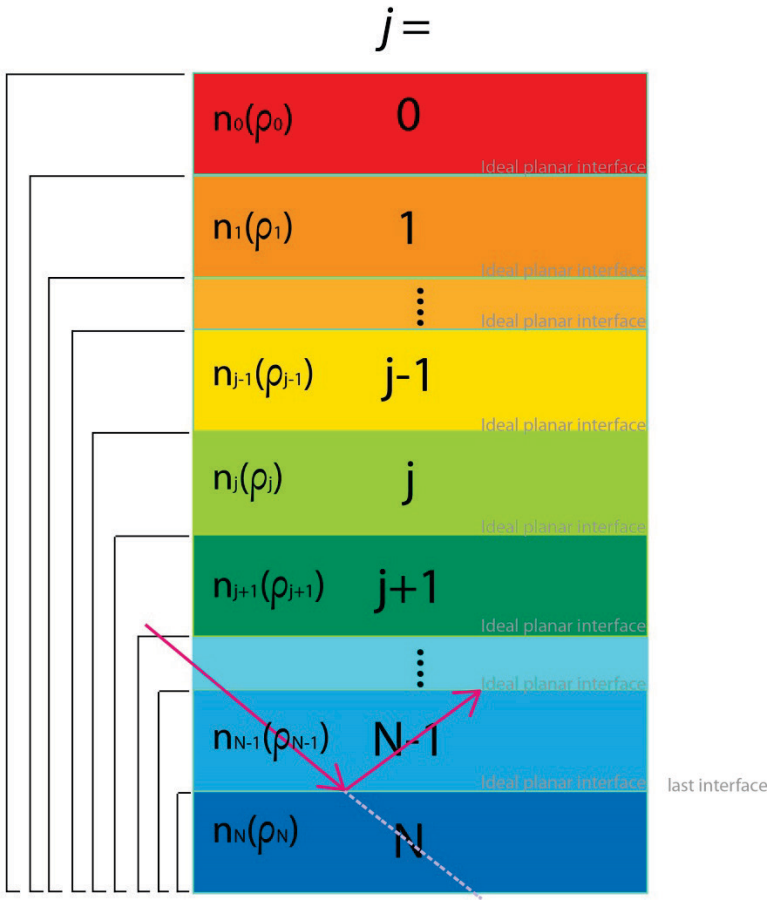

Figure cc Model with *N*+1 media, from medium 0 to medium N. In the most general case medium *j* is considered, being far from medium 0 or *N*.
Adapted by permission from Rightslink: [Springer eBook] [Generic and Specific Roles of Saccharides at Cell and Bacteria Surfaces, Schneck E.] [Springer Nature] (2011)

If we now consider a model with *N* stratified interfaces (see Figure cc), where we have multiple layers of different media, the reflectivity *R* can be determined by the following formalism, introduced by Parratt [109].

The Fresnel amplitude reflection coefficients for each sublayer *j* in this system are (see Equation (12)):

$$r_{j,j+1}^{F} = \frac{k_j^z - k_{j+1}^z}{k_j^z + k_{j+1}^z} \tag{15}$$

With these expressions the effective reflection coefficient $r_{0,N}$ of the entire system composed of *N* media can be deduced. The calculation starts recursively from the last interface between medium *N*-

1 and *N*. This is illustrated in Figure cc, where the beam is coming from above. Only the last interface has no further contributions from other interfaces (dashed line in Figure cc).

$$r_{N-1,N} = r^F_{N-1,N} \tag{16}$$

For all the other interfaces, contributions from lower interfaces have to be taken into account. So e.g. for the effective reflection coefficient $r_{N\text{-}2,N}$, the interface between medium *N*-2 and *N*-1, the contribution from the interface between medium *N*-1 and *N* has to be considered. This procedure leads to the following recursive expression [110]:

$$r_{j,N} = \frac{r^F_{j,j+1} + r_{j+1,N} \cdot e^{2ik^z_{j+1}d_{j+1}}}{1 + r^F_{j,j+1} \cdot r_{j+1,N} \cdot e^{2ik^z_{j+1}d_{j+1}}} \tag{17}$$

$$d_j = z_{j+1} - z_j \tag{18}$$

with $j \in N-1, N-2, \ldots, 1, 0$ and where j denotes the thickness of the medium;

The reflectivity R of the full set of interfaces is then obtained as $R(q_z) = \left|r_{0,N}\right|^2$ (19)

Above, it was stated how the theoretical reflectivity for a given SLD profile with the help of discretization is obtained and how the theoretical reflectivity can be compared with the experimental data. The SLD profiles of the examined samples are composed of the volume fraction profiles of the chemically different components (see equation (7)). Modeling of these profiles is described in the publications [50, 98] in great detail and is therefore not explained further.

3.2 Small and wide angle x-ray scattering

Combined small and wide angle x-ray scattering (SAXS/WAXS) measurements yield information of sample architectures at various length scales. WAXS gives insight into comparatively smaller structures, with length scales ranging from sub Å to a few Å, whereas SAXS uncovers comparatively larger structures in the sub-nm to 100 nm range. The scattering signal arises from spatial variations in the electron density.

The basic concept behind x-ray diffraction is the elastic scattering of an electromagnetic wave by the electrons present in the sample. In other words this technique probes the electron density distribution of matter. In general there are two types of scattering effects: i) inelastic scattering, where the scattered radiation has a different wavelength than the incident beam (Compton scattering) and ii) elastic scattering, where the scattered beam has the same wavelength λ (Rayleigh or Thomson scattering). In the case of elastic scattering the length of the wave vector $\vec{k}$ is conserved (see Equation (8)). The scattered radiation is detected by a 2D-detector (see e.g. Figure i and Figure j A). When the incident beam hits the sample, it is scattered with a scattering angle *Γ* with respect to the incident direction. These scattering processes show a very distinct interference pattern such as shown in Figure i and Figure j A., which stems from planar, periodic structures. This regular distribution of matter can be described in terms of their relative distance, also called lattice spacing *d*. High intensities are detected for angles at which waves interfere constructively. This occurs for path length differences of different waves of $n\lambda$, where n is an integer. This leads to Bragg's law, which describes the conditions for the intensity maxima for a periodic structured sample:

$$2 \cdot d \cdot sin\,\theta = n \cdot \lambda \text{ or} \qquad (20)$$
$$\theta = arcsin\left(\frac{n\lambda}{2d}\right)$$

Here, θ denotes the angle of incidence and equals $\frac{\Gamma}{2}$. The intensity maxima are called Bragg peaks. Depending on the angular range where they occur, they contain information on periodic structures in a sample on the scale of individual atoms (WAXS) or molecular arrangements on the nano- to mesoscale (SAXS).[111]

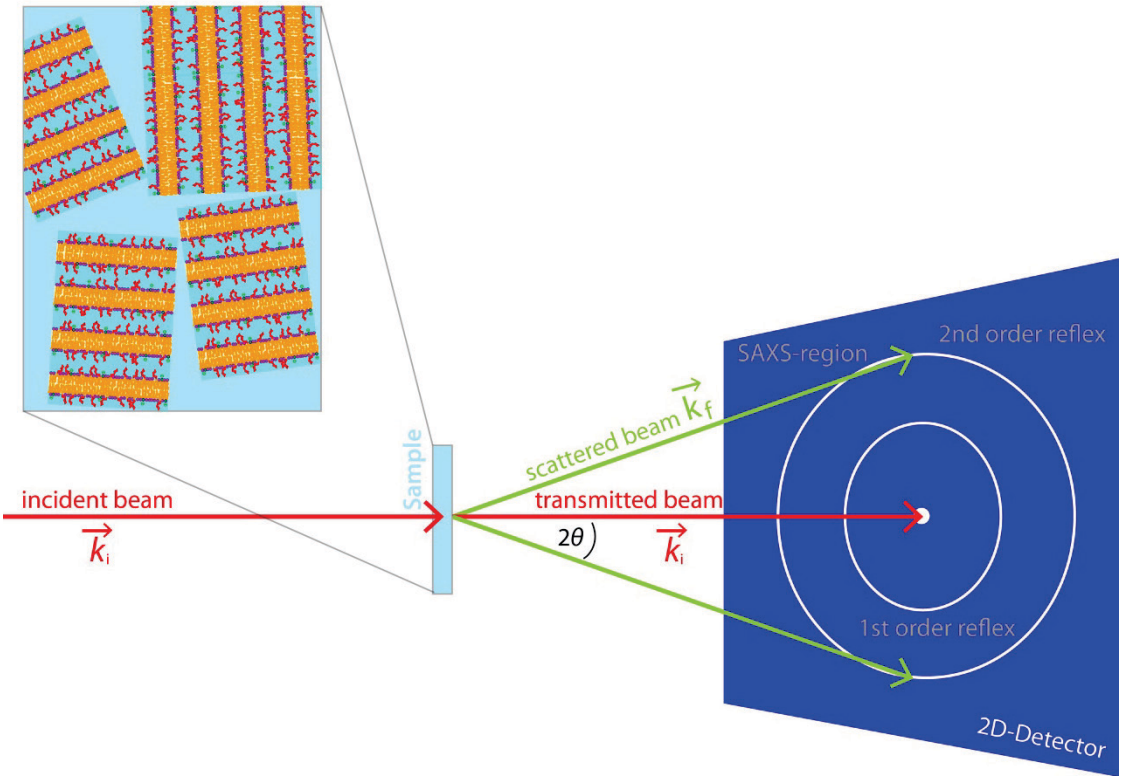

Figure i: Schematic drawing of the general setup of the experiment. The incident beam, defined by the wave vector $\overrightarrow{k_\iota}$, hits the sample and is scattered with an angle 2θ with respect to the transmitted beam (defined by the wave vector $\overrightarrow{k_\iota}$). The length of the wave vector $\overrightarrow{k_\iota}$ is conserved. 2D x-ray scattering patterns are obtained.

The scattering vector $\vec{q}$ is the difference between the scattered and the incident wave vectors, $\overrightarrow{k_f}$ and $\overrightarrow{k_\iota}$, respectively (see Equation (9)). Its magnitude $q = |\vec{q}|$ depends on the scattering angle and the wavelength, $q = \frac{4\pi}{\lambda} \cdot sin\theta$. The q-position of a Bragg peak is directly linked to the associated periodicity d as $q = \frac{2\pi}{d}$. In this generalized representation of Bragg's law, the wavelength conveniently drops out.

When measuring powder samples with isotropically oriented structures, the Bragg peaks are detected in form of concentric ring-shaped intensity-distributions. This is schematically illustrated in Figure i. A sample displaying a huge amount of small periodic structures, that are randomly oriented in space, leads to a 2D pattern with concentric rings. The order stems from the path length differences of different waves $n\lambda$. In contrast, single-crystalline samples show distinct spots on the 2D patterns.

The investigated multilamellar membrane aggregates in aqueous medium show concentric rings in the SAXS region (Figure j). Therefore, on the molecular scale, the multilayer aggregates are periodically arranged, but do not have a predominant orientation (see also Figure i, sketch of the sample). In the WAXS region, giving information on the scale of atoms, concentric rings are measured when lipids were in the oriented L_{β}-phase and no signal when lipids were in the fluid L_{α}-phase (see Figure j B) The concentric rings were radially integrated to obtain 1D intensity profiles as a function of the magnitude q of the scattering vector (see Figure j B). Figure j A shows the inner and the outer limit of the radial integration.

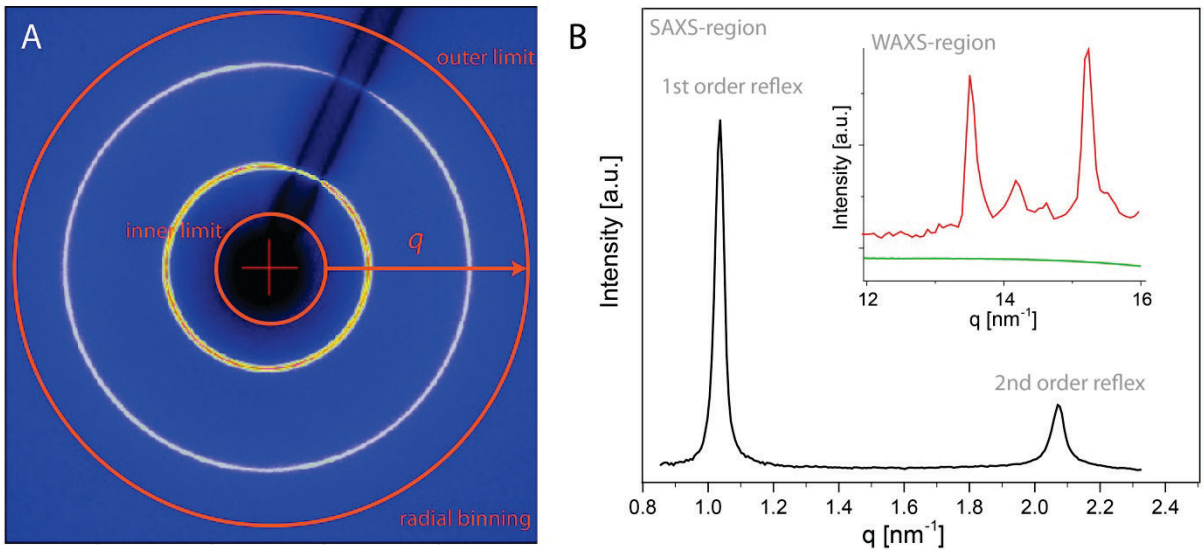

Figure j A) Representative 2D x-ray scattering pattern with first and second order reflexes in the SAXS region. The red arrow is indicating the binning of all pixels with the same radial distance. The inner and outer red circles mark the inner and outer binning limits of the SAXS signal. The red cross indicates the calibrated geometrical center of the beam. B) Integrated radial intensity profile over q [nm^{-1}] in relevant SAXS region from 0.8 nm^{-1} – 2.4 nm^{-1}. Inset relevant WAXS region from 12 nm^{-1} – 16 nm^{-1}.

3.3 Neutron diffraction

3.3.1 Specular and off-specular scattering

During a scattering experiment with an oriented sample the incident beam with a wave vector $\overrightarrow{k_i}$ is impinging the sample with the incident angle θ_i. The scattering geometry of the experiment is shown in Figure k. Waves are scattered into directions θ_f with respect to the incident direction. The scattered beam under consideration is defined by the wave vector $\overrightarrow{k_f}$. Here, elastic scattering with conservation of the length of the wave vector (see Equation (8)) is described. The scattering vector is defined in Equation (9).

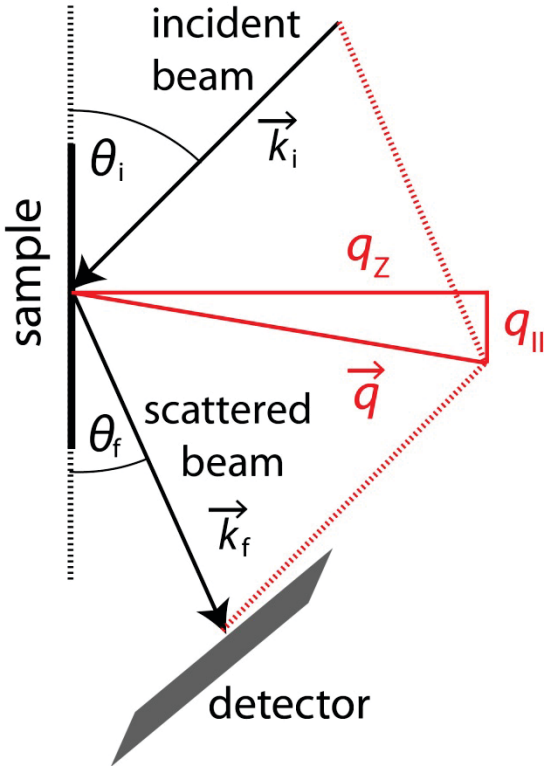

Figure k Schematic illustration of the geometry of a scattering experiment (specular and off-specular) from above. The incident beam (defined by the wave vector $\overrightarrow{\boldsymbol{k_i}}$) hits the sample with an incident angle $\boldsymbol{\theta_i}$, and is scattered. The scattered beam is defined by the wave vector $\overrightarrow{\boldsymbol{k_f}}$. The length of $\overrightarrow{\boldsymbol{k_i}}$ is conserved. The scattering vector $\vec{\boldsymbol{q}}$ has two components: the in-plane component q_{II} and the out-of-plane component q_z.

The scattering vector can be separated into an out-of-plane component q_z and an in-plane component q_{II}, which are the reciprocal space coordinates and follow from geometrical considerations (see Figure k):

$$q_z = k_f^z - k_i^z = \frac{2\pi}{\lambda}\left(sin\theta_f + sin\theta_i\right) \tag{21}$$

and

$$q_{II} = k_f^{II} - k_i^{II} = \frac{2\pi}{\lambda}\left(cos\theta_f - cos\theta_i\right) \tag{22}$$

For off-specular scattering the angle of the incident beam and of the scattered beam with respect to the sample plane are not equal ($\theta_f \neq \theta_i$) whereas specular scattering is characterized by $\theta_f = \theta_i$ and $q_{II} = 0$.

Neutron diffraction (ND) probes the structure of a planar sample with lamellar membrane architecture. Information on the structure perpendicular to the surface is accessible via specular scattering ($q_{II} = 0$): The lamellar periodicity is encoded in the Bragg peak positions and the SLD profile is obtained from the peak intensities. In the case of membrane multilayers, investigated in this thesis, the off-specular scattering (also referred to as diffuse scattering) (where $q_{II} \neq 0$) offers information on the in-plane structure, namely the fluctuations of the membrane with regard to the particular aspect of their spatial self- and cross-correlation functions [84, 91, 112].

The off-specular scattering is caused by the topological roughness of the interface. When considering the off-specular intensity from stratified interfaces the topological roughness is correlated. Generally the way how the features of the diffuse scattering intensity relate to those of the specular scattering intensity is determined by cross-correlation functions. Bending and compression moduli, which are mechanical properties characterizing single membranes, are described by these correlation functions [103, 104]. The out-of-plane displacement of the topological roughness (defined by the coordinate *x*) caused by thermal fluctuations is shown schematically in Figure l. At any time point, the displacement of each membrane segment from the average *z*-position of the membrane is described by an increment $u_n(x)$.

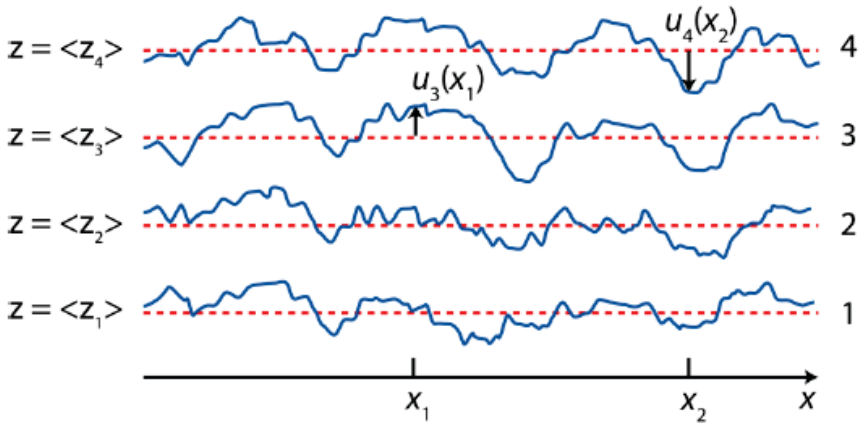

Figure l Parametrization of a set of four (numbered 1 to 4) rough layers of interfaces. The displacements (blue line) of the average *z*-position (red dashed line) of a set of four rough layers are shown as a function of time (*x*). At different time points e.g. x_1 and x_2 the displacement of the membrane is described by an increment of $u_3(x_1)$ and $u_4(x_2)$ respectively.
Reprinted by permission from Rightslink: [Springer eBook] [Generic and Specific Roles of Saccharides at Cell and Bacteria Surfaces, Schneck E.] [Springer Nature] (2011)

3.3.2 Sample environments for neutron diffraction under vapor or bulk water conditions

3.3.2.1 Humidity chamber

In order to measure solid-supported membrane multilayers at defined temperature and humidity the ILL D16 humidity chamber was used (see Figure m). It is made out of two compartments that are thermally insulated but connected for water exchange: The sample chamber and the water reservoir, filled with D_2O. The relative humidity (h_{rel}) in the chamber is determined by the relation of the vapor pressures ($p(T)$) at the temperature of the water reservoir (T_{res}) and at the sample chamber (T_s):

$$h_{rel}\ (T_{res}) = p\ (T_{res})/\ p(T_s) \tag{23}$$

There are two thermostats controlling T_s and T_{res} independently, allowing the regulation of both sample temperature and relative humidity at the same time.

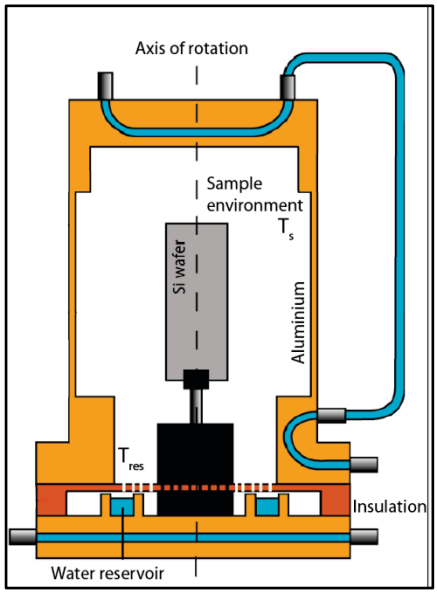

Figure m Schematic illustration of the humidity chamber used for neutron scattering experiments. The two main compartments, the sample chamber and the water reservoir, are thermally insulated and separated, but the exchange of vapor is possible. This allows the regulation of sample temperature and relative humidity.
Reprinted by permission from Rightslink: [Springer eBook] [Generic and Specific Roles of Saccharides at Cell and Bacteria Surfaces, Schneck E.] [Springer Nature] (2011)

The settings for T_{res} and resulting relative humidity (h_{rel}) for the samples are presented in the following table:

T_s	T_{res}	h_{rel}
30 °C	21.4 °C	60 %
30 °C	27.2 °C	85 %
30 °C	29.0 °C	95 %
50 °C	40.1 °C	60 %
50 °C	46.8 °C	85 %
50 °C	49.0 °C	95 %

Table 4 Settings for the temperature of the reservoir T_{res} in order to achieve T_s of 30 °C or 50 °C at the sample for different relative humidities (h_{rel}).

3.3.2.2 Liquid cell

Bulk water conditions were achieved by sandwiching two silicon chips: one chip was placed on another chip of the same dimension. The polished side of the chip, where the planar multilayers of membranes are deposited, is facing the rough side of the second chip (see Figure n). By adding spacers in form of small pieces of a glass slide (thickness 0.1 mm) water is trapped in between the wafers as soon as the sandwich is in contact with the D_2O buffer reservoir by capillary forces (see Figure 35). The design of this liquid cell was first used in the context of interacting membranes [112]. For the measurement this liquid cell was mounted in the humidity chamber (see previous chapter) using a defined temperature and h_{rel} above 95 % in order to avoid evaporation of water. The chip containing the sample was oriented towards the incident beam.

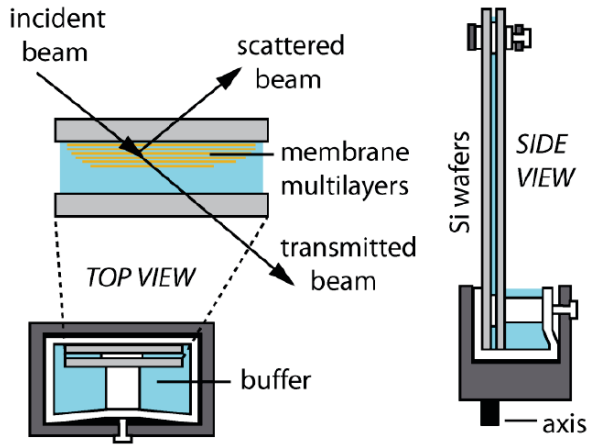

Figure n Schematic illustration of the liquid cell, developed for studies on interacting membranes[112]. The solid-support containing the membrane multilayers is mounted onto a second solid support and clamped on the top and bottom. The sandwich is mounted into a reservoir filled with aqueous medium and is subsequently immersed in a 0.1 mm thick layer by capillary forces. The incident beam impinges the sample through the solid support. Reprinted by permission from Rightslink: [Springer eBook] [Generic and Specific Roles of Saccharides at Cell and Bacteria Surfaces, Schneck E.] [Springer Nature] (2011)

III Literature

1. Urry, L.A., et al., *Campbell biology*. 2017.
2. Lipowski, R., *Vesicles And Biomembranes*, in *Encyclopedia of Applied Physics*. 1998, Wiley.
3. Elbert, D.L. and J.A. Hubbell, *Surface Treatments of Polymers for Biocompatibility.* Annu. Rev. Mater. Sci., 1996. **26**: p. 365-394.
4. Immordino, M.L., F. Dosio, and L. Cattel, *Stealth liposomes: review of the basic science, rationale, and clinical applications, existing and potential.* International Journal of Nanomedicine, 2006. **1**(3): p. 297-315.
5. Shi, J., et al., *Self-assembled targeted nanoparticles: evolution of technologies and bench to bedside translation.* Accounts of chemical research, 2011. **44**(10): p. 1123-1134.
6. Shin, H.-S., et al., *Biocompatible PEG Grafting on DLC-coated Nitinol Alloy for Vascular Stents.* Journal of Bioactive and Compatible Polymers, 2009. **24**(4): p. 316-328.
7. Teramura, Y. and H. Iwata, *Islet encapsulation with living cells for improvement of biocompatibility.* Biomaterials, 2009. **30**(12): p. 2270-2275.
8. *Structure and Dynamics of Membranes*. 1st ed, ed. R. Lipowski and E. Sackmann. Vol. 1A. 1995: Elsevier.
9. Fruijtier-Pölloth, C., *Safety assessment on polyethylene glycols (PEGs) and their derivatives as used in cosmetic products.* Toxicology, 2005. **214**(1): p. 1-38.
10. Pasut, G. and F.M. Veronese, *State of the art in PEGylation: the great versatility achieved after forty years of research.* Journal of Controlled Release, 2012. **161**(2): p. 461-472.
11. Bridges, A.W. and A.J. García, *Anti-Inflammatory Polymeric Coatings for Implantable Biomaterials and Devices.* Journal of diabetes science and technology (Online), 2008. **2**(6): p. 984-994.
12. Li, S. and J.J.D. Henry, *Nonthrombogenic approaches to cardiovascular bioengineering.* Annual review of biomedical engineering, 2011. **13**: p. 451-475.
13. Walkey, C.D. and W.C.W. Chan, *Understanding and controlling the interaction of nanomaterials with proteins in a physiological environment.* Chemical Society Reviews, 2012. **41**(7): p. 2780-2799.
14. Yu, M. and M.W. Urban, *Polymeric Surfaces with Anticoagulant, Antifouling, and Antimicrobial Attributes.* Macromolecular Symposia, 2009. **283–284**(1): p. 311-318.
15. Abuchowski, A., et al., *Effect of covalent attachment of polyethylene glycol on immunogenicity and circulating life of bovine liver catalase.* Journal of Biological Chemistry, 1977. **252**(11): p. 3582-6.
16. Abuchowski, A., et al., *Alteration of immunological properties of bovine serum albumin by covalent attachment of polyethylene glycol.* Journal of Biological Chemistry, 1977. **252**(11): p. 3578-81.
17. Merrill, E.W. and E.W. Salzman, *Polyethylene oxide as a biomaterial.* ASAIO Journal, 1983. **6**: p. 60-64.
18. Veronese, F.M., *PEGylated Protein Drugs: Basic Science and Clinical Applications: Basic Science and Clinical Applications*. 2009: Springer.
19. Williams, D.F., *The Williams dictionary of biomaterials*. 1999: Liverpool University Press.
20. Armstrong, J.K., *The occurrence, induction, specificity and potential effect of antibodies against poly (ethylene glycol)*, in *Pegylated protein drugs: Basic science and clinical applications*. 2009, Springer. p. 147-168.
21. Armstrong, J.K., et al., *Antibody against poly (ethylene glycol) adversely affects PEG-asparaginase therapy in acute lymphoblastic leukemia patients.* Cancer, 2007. **110**(1): p. 103-111.
22. Schellekens, H., W.E. Hennink, and V. Brinks, *The Immunogenicity of Polyethylene Glycol: Facts and Fiction.* Pharmaceutical Research, 2013. **30**(7): p. 1729-1734.
23. Becker, A., et al., *Structure of peptide deformylase and identification of the substrate binding site.* Journal of Biological Chemistry, 1998. **273**(19): p. 11413-11416.
24. Hasek, J., *Poly (ethylene glycol) interactions with proteins.* Zeitschrift fur Kristallographie Supplements, 2006. **2006**: p. 613-618.

25. Nanjappa, V., et al., *Plasma Proteome Database as a resource for proteomics research: 2014 update.* Nucleic Acids Research, 2014. **42**(Database issue): p. D959-D965.
26. Chen, H., et al., *Biocompatible polymer materials: Role of protein–surface interactions.* Progress in Polymer Science, 2008. **33**(11): p. 1059-1087.
27. Chen, B.-M., et al., *Measurement of pre-existing IgG and IgM antibodies against polyethylene glycol in healthy individuals.* Analytical chemistry, 2016. **88**(21): p. 10661-10666.
28. Schneck, E., et al., *Neutron reflectometry from poly (ethylene-glycol) brushes binding anti-PEG antibodies: Evidence of ternary adsorption.* Biomaterials, 2015. **46**: p. 95-104.
29. Israelachvili, J.N., *Intermolecular and Surface Forces*. 2 ed. 1991, London,UK: Academic Press Inc.
30. Boudière, L., et al., *Glycerolipids in photosynthesis: Composition, synthesis and trafficking.* Biochimica et Biophysica Acta (BBA) - Bioenergetics, 2014. **1837**(4): p. 470-480.
31. Stoffel, W. and A. Bosio, *Myelin glycolipids and their functions.* Current Opinion in Neurobiology, 1997. **7**(5): p. 654-661.
32. Halperin, A., *Polymer Brushes that Resist Adsorption of Model Proteins: Design Parameters.* Langmuir, 1999. **15**: p. 2525-2533.
33. Szleifer, I., *Protein Adsorption on Surfaces with Grafted Polymers: A Theoretical Approach.* Biophys. J., 1997. **72**: p. 595-612.
34. Jeon, S.I. and J.D. Andrade, *Protein-surface interactions in the presence of polyethylene oxide: II. Effect of protein size.* Journal of colloid and interface science, 1991. **142**(1): p. 159-166.
35. Jeon, S.I., et al., *Protein-surface interactions in the presence of polyethylene oxide: I. Simplified theory.* J. Colloid Interface Sci., 1991. **142**: p. 149-158.
36. Currie, E.P.K., et al., *Stuffed brushes: theory and experiment.* Pure Appl. Chem., 1999. **71**: p. 1227-1241.
37. Halperin, A., et al., *Primary versus Ternary Adsorption of Proteins onto PEG Brushes.* Langmuir, 2007. **23**: p. 10603-10617.
38. Halperin, A. and M. Kroeger, *Ternary Protein Adsorption onto Brushes: Strong versus Weak.* Langmuir, 2009. **25**: p. 11621-11634.
39. Currie, E.P.K., W. Norde, and M.A. Cohen Stuart, *Tethered polymer chains: surface chemistry and their impact on colloidal and surface properties.* Adv. Colloid Sci., 2003. **100-102**: p. 205-265.
40. Harris, J.M., *Poly(Ethylene Glycol) Chemistry: Biotechnical and Biomedical Applications*. 2003, New York: Plenum Press.
41. Abbott, N.L., D. Blankschtein, and T.A. Hatton, *Protein partitioning in two-phase aqueous polymer systems. 3. A neutron scattering investigation of the polymer solution structure and protein-polymer interactions.* Macromolecules, 1992. **25**(15): p. 3932-3941.
42. Bloustine, J., et al., *Light scattering and phase behavior of lysozyme-poly (ethylene glycol) mixtures.* Physical review letters, 2006. **96**(8): p. 087803.
43. Gon, S., B. Fang, and M.M. Santore, *Interaction of cationic proteins and polypeptides with biocompatible cationically-anchored PEG brushes.* Macromolecules, 2011. **44**(20): p. 8161-8168.
44. Leckband, D., S. Sheth, and A. Halperin, *Grafted poly(ethylene oxide) brushes as nonfouling surface coatings.* Journal of Biomaterials Science, Polymer Edition, 1999. **10**(10): p. 1125-1147.
45. Vroman, L., et al., *Interaction of high molecular weight kininogen, factor XII, and fibrinogen in plasma at interfaces.* Blood, 1980. **55**(1): p. 156-159.
46. Riedel, T., et al., *Complete Identification of Proteins Responsible for Human Blood Plasma Fouling on Poly(ethylene glycol)-Based Surfaces.* Langmuir, 2013. **29**(10): p. 3388-3397.
47. Schöttler, S., et al., *Protein adsorption is required for stealth effect of poly(ethylene glycol)- and poly(phosphoester)-coated nanocarriers.* Nature Nanotechnology, 2016. **11**: p. 372.

48. Walkey, C.D., et al., *Nanoparticle Size and Surface Chemistry Determine Serum Protein Adsorption and Macrophage Uptake.* Journal of the American Chemical Society, 2012. **134**(4): p. 2139-2147.
49. Pitt, J.J., *Principles and applications of liquid chromatography-mass spectrometry in clinical biochemistry.* The Clinical biochemist. Reviews, 2009. **30**(1): p. 19-34.
50. Latza, V.M., et al., *Neutron Reflectometry Elucidates Protein Adsorption from Human Blood Serum onto PEG Brushes.* Langmuir, 2017. **33**(44): p. 12708-12718.
51. Homola, J., et al., *Spectral surface plasmon resonance biosensor for detection of staphylococcal enterotoxin B in milk.* International Journal of Food Microbiology, 2002. **75**(1): p. 61-69.
52. Liedberg, B., I. Lundström, and E. Stenberg, *Principles of biosensing with an extended coupling matrix and surface plasmon resonance.* Sensors and Actuators B: Chemical, 1993. **11**(1): p. 63-72.
53. Green, R.J., et al., *Surface plasmon resonance for real time in situ analysis of protein adsorption to polymer surfaces.* Biomaterials, 1997. **18**(5): p. 405-413.
54. Pavey, K.D. and C.J. Olliff, *SPR analysis of the total reduction of protein adsorption to surfaces coated with mixtures of long- and short-chain polyethylene oxide block copolymers.* Biomaterials, 1999. **20**(9): p. 885-890.
55. Jin, J., et al., *Plasma Proteins Adsorption Mechanism on Polyethylene-Grafted Poly(ethylene glycol) Surface by Quartz Crystal Microbalance with Dissipation.* Langmuir, 2013. **29**(22): p. 6624-6633.
56. Hagiwara, T., et al., *Monitoring of adsorption behaviors of bovine serum albumin onto a stainless steel surface by the quartz crystal microbalance based on admittance analysis.* Bioscience, Biotechnology, and Biochemistry, 2017. **81**(4): p. 783-789.
57. Tanaka, M., et al., *Study on kinetics of early stage protein adsorption on poly(2-methoxyethylacrylate) (PMEA) surface.* Colloids and Surfaces A: Physicochemical and Engineering Aspects, 2002. **203**(1): p. 195-204.
58. Glasmästar, K., et al., *Protein adsorption on supported phospholipid bilayers.* Journal of colloid and interface science, 2002. **246**(1): p. 40-47.
59. Molino, P.J., et al., *Fibronectin and Bovine Serum Albumin Adsorption and Conformational Dynamics on Inherently Conducting Polymers: A QCM-D Study.* Langmuir, 2012. **28**(22): p. 8433-8445.
60. Nagasawa, D., et al., *Role of Interfacial Water in Protein Adsorption onto Polymer Brushes as Studied by SFG Spectroscopy and QCM.* The Journal of Physical Chemistry C, 2015. **119**(30): p. 17193-17201.
61. Höök, F., et al., *A comparative study of protein adsorption on titanium oxide surfaces using in situ ellipsometry, optical waveguide lightmode spectroscopy, and quartz crystal microbalance/dissipation.* Colloids and Surfaces B: Biointerfaces, 2002. **24**(2): p. 155-170.
62. Azzam R.M.A., B.N.M., *Ellipsometry and polarized light*. 3rd ed. 1992, North Holland: Elsevier Science Publishers.
63. Guzman, G., et al., *Transport-Limited Adsorption of Plasma Proteins on Bimodal Amphiphilic Polymer Co-Networks: Real-Time Studies by Spectroscopic Ellipsometry.* Langmuir, 2017. **33**(11): p. 2900-2910.
64. Elwing, H., *Protein absorption and ellipsometry in biomaterial research.* Biomaterials, 1998. **19**(4): p. 397-406.
65. Gölander, C.-G. and E. Kiss, *Protein adsorption on functionalized and ESCA-characterized polymer films studied by ellipsometry.* Journal of Colloid and Interface Science, 1988. **121**(1): p. 240-253.
66. Malmsten, M., *Ellipsometry studies of the effects of surface hydrophobicity on protein adsorption.* Colloids and Surfaces B: Biointerfaces, 1995. **3**(5): p. 297-308.
67. Rennie, A.R., et al., *Structure of a cationic surfactant layer at the silica-water interface.* Langmuir, 1990. **6**(5): p. 1031-1034.

68. Fragneto, G., et al., *Structure of Monolayers of Tetraethylene Glycol Monododecyl Ether Adsorbed on Self-Assembled Monolayers on Silicon: A Neutron Reflectivity Study.* Langmuir, 1996. **12**(2): p. 477-486.
69. Fragneto, G., et al., *Neutron Reflection from Hexadecyltrimethylammonium Bromide Adsorbed on Smooth and Rough Silicon Surfaces.* Langmuir, 1996. **12**(25): p. 6036-6043.
70. Brouette, N., et al., *Protein adsorption properties of OEG monolayers and dense PNIPAM brushes probed by neutron reflectivity.* The European Physical Journal Special Topics, 2012. **213**(1): p. 343-353.
71. Brouette, N., et al., *A neutron reflection study of adsorbed deuterated myoglobin layers on hydrophobic surfaces.* Journal of Colloid and Interface Science, 2013. **390**(1): p. 114-120.
72. Schneck, E., et al., *Neutron Reflectometry Elucidates Density Profiles of Deuterated Proteins Adsorbed onto Surfaces Displaying Poly(ethylene glycol) Brushes: Evidence for Primary Adsorption.* Langmuir, 2013. **29**(46): p. 14178-14187.
73. Evans, E. and D. Needham, *Physics of Amphiphilic Layers*. Springer Proceedings in Physics, ed. J. Meunier, D. Langevin, and N. Boccara. Vol. 21. 1987, Berlin: Springer.
74. Demé, B., M. Dubois, and T. Zemb, *Swelling of a lecithin lamellar phase induced by small carbohydrate solutes.* Biophys. J., 2002. **82**(1): p. 215-225.
75. Demé, B., et al., *Effect of carbohydrates on the swelling of a lyotropic lamellar phase.* J. Phys. Chem., 1996. **100**: p. 3828â€“3838.
76. LeNeveu, D.M., R.P. Rand, and V.A. Parsegian, *Measurements of forces between lecithin bilayers.* Nature, 1976. **259**: p. 601-603.
77. Lis, L.J., et al., *Interactions between Neutral Phospholipid Bilayer Membranes.* Biophys. J., 1982. **37**: p. 657-666.
78. Helfrich, W., *Steric interaction of fluid membranes in multilayer systems.* Z. Naturforsch., 1978. **33a**: p. 305-315.
79. Helfrich, W., *Lyotropic lamellar phases.* J. Phys. Condens. Matter, 1994. **6**: p. A79.
80. Bachmann, M., H. Kleinert, and A. Pelster, *Fluctuation pressure of a stack of membranes.* Phys. Rev. E, 2001. **63**: p. 051709.
81. Ryrif, I.J., J.M. Anderson, and D.J. Goodchild, *The Role of the Light-Harvesting Chlorophyll a/b -Protein Complex in Chloroplast Membrane Stacking.* European Journal of Biochemistry, 1980. **107**(2): p. 345-354.
82. Webb, M.S. and B.R. Green, *Effects of neutral and anionic lipids on digalactosyldiacylglycerol vesicle aggregation.* Biochimica et Biophysica Acta (BBA) - Biomembranes, 1990. **1030**(2): p. 231-237.
83. Demé, B., et al., *Contribution of galactoglycerolipids to the 3-dimensional architecture of thylakoids.* The FASEB Journal, 2014. **28**(8): p. 3373-3383.
84. Schneck, E., et al., *Modulation of Inter-Membrane Interaction and Bending Rigidity of Biomembrane Models via Carbohydrates Investigated by Specular and Off-Specular Neutron Scattering.* Phys. Rev. E, 2008. **78**: p. 061924.
85. Parsegian, V.A., N. Fuller, and R.P. Rand, *Measured Work of Deformation and Repulsion of Lecithin Bilayers.* Proc. Natl. Acad. Sci. USA, 1979. **76**(6): p. 2750-2754.
86. Kanduč, M., et al., *Tight cohesion between glycolipid membranes results from balanced water–headgroup interactions.* Nature Communications, 2017. **8**: p. 14899.
87. Leontidis, E., et al., *Effects of monovalent anions of the hofmeister series on DPPC lipid bilayers part II: modeling the perpendicular and lateral equation-of-state.* Biophysical Journal, 2007. **93**: p. 1591-1607.
88. Schlaich, A., et al., *Physical mechanisms of the interaction between lipid membranes in the aqueous environment.* Physica A, 2015. **418**: p. 105-125.
89. Gourier, C., et al., *Specific and non specific interactions involving LeXdeterminant quantified by lipid vesicle micromanipulation.* 2004. **21**(3): p. 165-174.

90. Eggens, I., et al., *Specific interaction between Lex and Lex determinants. A possible basis for cell recognition in preimplantation embryos and in embryonal carcinoma cells. .* Journal of Biological Chemistry, 1989. **264**(June 5).
91. Schneck, E., et al., *Membrane Adhesion via Homophilic Saccharide-Saccharide Interactions Investigated by Neutron Scattering.* Biophys. J., 2011. **100**: p. 2151.
92. Yu, Z.W., T.L. Calvert, and D. Leckband, *Molecular Forces between Membranes Displaying Neutral Glycosphingolipids: Evidence for Carbohydrate Attraction.* Biochemistry, 1998. **37**(6): p. 1540-1550.
93. Israelachvili, J.N. and G.E. Adams, *Measurement of Forces between Two Mica Surfaces in Aqueous Electrolyte Solutions in the Range 0-100nm.* J. Chem. Soc., Faraday Trans. 1, 1978. **74**: p. 975-1001.
94. Orozco-Alcaraz, R. and T.L. Kuhl, *Interaction Forces between DPPC Bilayers on Glass.* Langmuir, 2013. **29**(1): p. 337-343.
95. Aroti, A., et al., *Effects of Monovalent Anions of the Hofmeister Series on DPPC Lipid Bilayers Part I: Swelling and In-Plane Equations of State.* Biophysical Journal, 2007. **93**(5): p. 1580-1590.
96. Janeway, C.A., et al., *Immunobiology.* 2001.
97. Roux, K.H., *Immunoglobulin structure and function as revealed by electron microscopy.* International Archives of Allergy and Immunology, 1999. **120**(2): p. 85-99.
98. Latza, V.M., et al., *End Point Versus Backbone Specificity Governs Characteristics of Antibody Binding to Poly(ethylene glycol) Brushes.* Langmuir, 2018. **34**(46): p. 13946-13955.
99. Lin, W., et al., *Poly-phosphocholinated Liposomes Form Stable Superlubrication Vectors.* Langmuir, 2019. **35**(18): p. 6048-6054.
100. Machado, J.J.B., J.A. Coutinho, and E.A. Macedo, *Solid-liquid equilibrium of alpha-lactose in ethanol/water.* Fluid Phase Equilibria, 2000. **173**(1): p. 121-134.
101. Mathlouthi, M. and P. Reiser, *Sucrose: properties and applications*. 2012: Springer Science & Business Media.
102. Higashiyama, T., *Novel functions and applications of trehalose.* Pure and applied Chemistry, 2002. **74**(7): p. 1263-1269.
103. Salditt, T., *Thermal fluctuations and stability of solid-supported lipid membranes.* J. Phys. Cond. Matt., 2005. **17**(6): p. R287-R314.
104. Lei, N., C.R. Safinya, and R.F. Bruinsma, *Discrete Harmonic Model for Stacked Membranes - Theory and Experiment.* Journal de Physique II, 1995. **5**(8): p. 1155-1163.
105. Tamm, L. and H.M. McConnell, *Supported phospholipid bilayers.* Biophys. J., 1984. **47**: p. 105-113.
106. Rockland, L.B., *Saturated Salt Solutions for Static Control of Relative Humidity between 5° and 40° C.* Analytical Chemistry, 1960. **32**(10): p. 1375-1376.
107. Russell, T.P., *X-ray and neutron reflectivity for the investigation of polymers.* Materials Science Reports, 1990. **5**(4): p. 171-271.
108. Sears, V.F., *Neutron scattering lengths and cross sections.* Neutron News, 1992. **3**(3): p. 26-37.
109. Parratt, L.G., *Surface Studies of Solids by Total Reflection of X-Rays.* Physical Review, 1954. **95**(2): p. 359-369.
110. Schneck, E., *Generic and Specific Roles of Saccharides at Cell and Bacteria Surfaces*. Springer Theses. 2011, Berlin, Heidelberg: Springer.
111. Stangl, J., et al., *Nanobeam X-Ray scattering*, in *Nanobeam X-Ray scattering*. 2014, Wiley-VCH: Weinheim, Germany.
112. Schneck, E., et al., *Mechanical properties of interacting lipopolysaccharide membranes from bacteria mutants studied by specular and off-specular neutron scattering.* Phys. Rev. E, 2009. **80**: p. 041929.